

Endocardial Activation Mapping of Human Atrial Fibrillation

Thesis submitted for the degree of

Doctor of Philosophy
Imperial College London

By

Ian Edward Mann

2020

Department of Myocardial Function
Imperial College London
Hammersmith Hospital
London W12 0NN

Acknowledgements

This thesis would not have been possible without the help and incredible support from so many, and the Clinical Research Training Fellowship Grant awarded by the British Heart Foundation. Special thanks goes to my supervisors, Professor Prapa Kanagaratnam, Dr Nick Linton and Dr Norman Qureshi. I will take the wise words from Prapa – “Prioritise everything” – and apply them to all aspects of life! I am so grateful for their inspiration and guidance through the past 3 years.

I would like to make a special acknowledgement to Nick Linton. It would not have been possible to undertake any of this research without the countless hours of Matlab coding he invested in to RETRO-Mapping, and the constant advice, support and encouragement – Thank you. The support from Norman is also greatly appreciated. Thank you for guiding me through many of the key stages, and the multiple troubleshooting sessions.

I would also like to thank everyone that was involved in this research, including the patients that kindly consented to take part. During the course of this research, I have been fortunate to have such strong support from the clinical team at Hammersmith Hospital, especially – Zach Whinnett, Mike Koa-Wing, Wyn Davies, Michael Fudge, Elaine Lim, Rob Edwards and Ian Wright. I frequently populated the lists of Mike, Zach and Wyn with research cases, and drove Michael, Elaine and Ian mad by asking them to constantly switch everything over from Carto to Precision. I am so grateful for their patience.

My deepest thanks goes to my family and friends for their unshakeable support and spurring me on. I would not be where I am today without my amazing parents and sisters. I also want to thank my brother-in-law Simon, for his statistical assistance, and solid research advice. Particular thanks goes to my dear friend Pav, for her constant de-stressing chats and support! The biggest thank you goes to Jason, who became my husband during this process. You have been there throughout everything, motivated me to keep going, and listened to my ramblings about AF to the point that you probably know more about it than most cardiologists! I couldn't have done this without you at my side.

Declaration

I declare that this thesis was conducted and written by myself under the supervision of Professor Prapa Kanagaratnam, Dr Nick Linton and Dr Norman Qureshi. Computational code for RETRO-Mapping was written by Dr Nick Linton. Some of the test data used for development of the code was provided by Dr Norman Qureshi. The work included is my own unless otherwise stated.

Copyright Declaration

The copyright of this thesis rests with the author. Unless otherwise indicated, its contents are licensed under a Creative Commons Attribution – Non Commercial 4.0 International Licence (CC BY-NC).

Under this licence, you may copy and redistribute the material in any medium or format. You may also create and distribute modified versions of the work. This is on the condition that: you credit the author and do not use it, or any derivative works, for a commercial purpose.

When reusing or sharing this work, ensure you make the licence terms clear to others by naming the licence and linking to the licence text. Where a work has been adapted, you should indicate that the work has been changed and describe those changes.

Please seek permission from the copyright holder for uses of this work that are not included in this licence or permitted under UK Copyright Law.

Abstract

Successful ablation of arrhythmias depends upon interpretation of the mechanism. However, in persistent atrial fibrillation (AF) ablation is currently directed towards the mechanism that initiates paroxysmal AF. We sought to address the hypothesis that atrial activation patterns during persistent AF may help determine the underlying mechanism.

Activation mapping of AF wavefronts is labor intensive and often restricted to short time segments in limited atrial locations. RETRO-Mapping was developed to identify uniform wavefronts that occur during AF, and summate all wavefront vectors on to an orbital plot. Uniform wavefronts were mapped using RETRO-Mapping during sinus rhythm, atrial tachycardia, and atrial fibrillation, and validated against detailed manual analysis of the same wavefronts with conventional isochronal mapping. RETRO-Mapping was found to have comparable accuracy to isochronal mapping.

RETRO-Mapping was then used to investigate atrial activation patterns during persistent AF. Atrial activation patterns demonstrated evidence of spatiotemporal stability over long time periods. Orbital plots created at different time points in the same location remained unchanged. Together with this important discovery, both fractionation and bipolar voltage were also demonstrated to express stability over time. Spatiotemporal stability during persistent AF enables sequential mapping as an acceptable technique. This property also allowed the development of a method for displaying sequentially mapped locations on a single map – RETRO-Choropleth Map. These findings go against the multiple wavelet hypothesis with random activation.

Having gained insights in to these stable activation patterns, extensive analysis was undertaken to identify the presence of focal activation. Focal activations were identified during persistent AF. RETRO-Mapping was used to show that adjacent activation patterns were not related to focal activations.

Lastly, the effect of pulmonary vein isolation (PVI) was studied by mapping atrial activation patterns before and after PVI. RETRO-Mapping showed that PVI leads to increased organisation of AF in most patients, supporting a mechanistic role of the pulmonary veins in persistent AF.

In conclusion, a new technique has been developed and validated for automated activation mapping of persistent AF. These techniques could be used to guide additional ablation strategies beyond PVI for patients with persistent AF.

Abbreviations

AF – atrial fibrillation

AT – atrial tachycardia

CFAE – complex fractionated atrial electrogram

CL – cycle length

CS – coronary sinus

EP – electrophysiology

EGM – electrogram

GP – ganglionic plexus

GUI – graphical user interface

HFS – high frequency stimulation

LA – left atrium

LAA – left atrial appendage

LAT – local activation time

LGE-CMRI – late-gadolinium enhanced cardiac magnetic resonance imaging

PV – pulmonary vein

PVI – pulmonary vein isolation

RA – right atrium

RETRO-AD – RETRO-Automated Direction

RETRO-Mapping – Representation of Electrical Tracking or Origin Mapping

RETRO-PM – RETRO-Propagation Map

SVC – superior vena cava

TCL – tachycardia cycle length

Awards and Publications arising from this work

Prizes

2nd Place Featured Poster Prize, European Cardiac Arrhythmia Society, Paris, 2018.

Ian Mann, Nick Linton, Szabolcs Nagy, Norman Qureshi, Mike Koa-Wing, Phang Boon Lim, Zachary Whinnett, D. Wyn Davies, David Lefroy, Darrel Francis, Nicholas Peters, Prapa Kanagaratnam. RETRO-MAPPING: A novel 5D mapping method for atrial fibrillation shows spatiotemporal stability.

1st Place Featured Poster Prize, NHLI Post Graduate Research Day, London, 2017.

Ian Mann, Nick Linton, Szabolcs Nagy, Norman Qureshi, Mike Koa-Wing, Phang Boon Lim, Zachary Whinnett, D. Wyn Davies, David Lefroy, Darrel Francis, Nicholas Peters, Prapa Kanagaratnam. A New Mapping Technique for Atrial Fibrillation shows frequent Focal and Uniform Activations.

Publications

Ian Mann, Clare Coyle, Norman Qureshi, Szabolcs Z Nagy, Michael Koa-Wing, Phang Boon Lim, Darrel P Francis, Zachary Whinnett, Nicholas S Peters, Prapa Kanagaratnam, Nick W F Linton. Evaluation of a new algorithm for tracking activation during atrial fibrillation using multipolar catheters in humans. *Journal of Cardiovascular Electrophysiology*. 2019;1-11. DOI: 10.1111/jce.14033.

Ian Mann, Belinda Sandler, Nick Linton and Prapa Kanagaratnam. Drivers of Atrial Fibrillation: Theoretical Considerations and Practical Concerns. *Arrhythmia & Electrophysiology Review*. 2018;7(1):49–54. DOI: 10.15420/aer.2017.40.3.

Nick W F Linton, **Ian Mann**, Yuriy Alexandrov, Norman Qureshi, Michael Koa-Wing, Zachary Whinnett, Phang Boon Lim, Vishal Luther, Markus B Sikkell, D Wyn Davies, Darrel P Francis,

Nicholas S. Peters, Prapa Kanagaratnam. RETRO-Mapping: Initial Experience with Computerized Wavefront Direction Tracking to create Atrial Choropleth Maps of Activation during Atrial Fibrillation. (Submitted for peer review)

Ian Mann, Nick W F Linton, Clare Coyle, James P Howard, Michael Fudge, Elaine Lim, Norman Qureshi, Michael Koa-Wing, Zachary Whinnett, Phang Boon Lim, D Wyn Davies, Nicholas S Peters, Darrel P Francis, Prapa Kanagaratnam. RETRO-MAPPING: A new 5D mapping method shows activation patterns during persistent atrial fibrillation are not random. (Submitted for peer review)

Abstracts

Ian Mann, Nick Linton, Clare Coyle, Norman Qureshi, Mike Koa-Wing, Phang Boon Lim, Zachary Whinnett, D. Wyn Davies, Darrel Francis, Nicholas S Peters, Prapa Kanagaratnam. RETRO-Mapping: A 5-dimensional framework for mapping wavefronts during AF reveals mechanistic insight with both focal activation and stable vectors. Oral Abstract Session, Heart Rhythm Congress, Birmingham, October 2019.

Clare Coyle, **Ian Mann**, Nicholas Linton, Ji-jian Chow, Norman Qureshi, Michael Koa-Wing, Zachary Whinnett, Phang Boon Lim, Darrel P Francis, Nicholas S Peters, Prapa Kanagaratnam. Use of a novel algorithm 'RETRO-Mapping' to map focal activation in persistent atrial fibrillation. Oral Abstract Session, European Cardiac Arrhythmia Society, Paris, April 2019.

Ian Mann, Nick Linton, Clare Coyle, Norman Qureshi, Mike Koa-Wing, Phang Boon Lim, Zachary Whinnett, D. Wyn Davies, Darrel Francis, Nicholas S Peters, Prapa Kanagaratnam. Persistent atrial fibrillation mapping using 5D-RETRO-Mapping reveal the AF substrate has stable components. *Europace* 2018;20(suppl_4):iv27;doi.org/10.1093/europace/euy201.006.

Nagy S, von Maydell A, **Mann I**, Afonso V, Kim S, Linton N, Lefroy D, Whinnett Z, Davies W, Ng FS, Koa-Wing M, Kanagaratnam P, Peters NS, Qureshi N, Lim PB. A novel automated cycle

length algorithm allows rapid panoramic assessment of cycle length in the persistent AF substrate. *Europace*. 2018;20(suppl_1):i217-i217. DOI: 10.1093/europace/euy015.632.

Nagy S, Kim S, **Mann I**, Linton N, Lefroy D, Whinnett Z, Davies W, Ng FS, Koa-Wing M, Kanagaratnam P, Peters NS, Qureshi N, Lim PB. Global AF voltage is reduced with pulmonary vein isolation in persistent AF. *EP Europace*, Volume 20, Issue suppl_4, October 2018, Pages iv47–iv48. DOI: 10.1093/europace/euy205.046.

Ian Mann, Nick Linton, Norman Qureshi, Mike Koa-Wing, Wyn Davies, Zach Whinnett, Phang Boon Lim, David Lefroy, Darrel Francis, Nicholas S Peters, Prapa Kanagaratnam. A new mapping technique for atrial fibrillation shows frequent focal and uniform activations. *Europace*. 2017;19(suppl_1):i37-i37. DOI: 10.1093/europace/eux283.080.

Ian Mann, Nick Linton, Norman Qureshi, Mike Koa-Wing, Wyn Davies, Zach Whinnett, Phang Boon Lim, David Lefroy, Darrel Francis, Nicholas S Peters, Prapa Kanagaratnam. A new method for mapping persistent atrial fibrillation shows spatiotemporal stability. Atrial Signals Conference, Valencia, October 2017.

Ian Mann, Nick Linton, Norman Qureshi, Mike Koa-Wing, Wyn Davies, Zach Whinnett, Phang Boon Lim, David Lefroy, Darrel Francis, Nicholas Peters, Prapa Kanagaratnam. A novel approach to activation mapping of atrial fibrillation shows frequent focal and uniform activations. Atrial Signals Conference, Valencia, October 2017.

Ian Mann, Norman Qureshi, Phang Boon Lim, Vishal Luther, Markus Sikkel, Zachary Whinnett, D. Wyn Davies, Nicholas Peters, Prapa Kanagaratnam, and Nick Linton. Rapid Mapping of Uniform Wavefront is Feasible During Atrial Fibrillation and Demonstrates Preferential Directions of Activation. *Heart Rhythm*. 2016;13(5):S1547-5271.

Sikkel MB, B Sandler, PB Lim, L Malcolm-Lawes, **I Mann**, V Luther, S Sohaib, F Ng, I Wright, N Qureshi, K Leong, M Koa-Wing, Z Whinnett, DW Davies, N Peters, N Linton, P Kanagaratnam. Ectopy-Triggering Ganglionated Plexus Sites May Be An Alternative Target For Atrial Fibrillation Ablation. *Heart Rhythm*. 2016; 13(5): S1-S688.

Table of Contents

1 Introduction.....	20
1.1 Introduction.....	21
1.2 Mechanisms of Atrial Fibrillation	21
1.2.1 The Critical Mass Theory of Atrial Fibrillation	21
1.2.2 Re-entry and Multiple Wavelets.....	22
1.2.3 The Double Layer Hypothesis	28
1.2.4 Focal Sources	29
1.2.5 Rotors as drivers of atrial fibrillation.....	30
1.2.6 Autonomic Function Initiating AF.....	36
1.3 Left Atrial Substrate in AF.....	37
1.3.1 Non-invasive Assessment	38
1.3.2 Invasive Assessment.....	39
1.3.3 Left Atria Myofiber Architecture	39
1.4 Alternative Ablation Targets	40
1.4.1 Complex Fractionated Atrial Electrograms	41
1.4.2 Spectral Analysis.....	43
1.5 Induced and Spontaneous Atrial Fibrillation.....	44
1.6 Activation Mapping	45
1.6.1 Determining Local Activation Time	45
1.6.2 Isochronal Mapping.....	45
1.7 Recording Cardiac Electrograms	46
1.7.1 Unipolar Electrograms.....	47
1.7.2 Bipolar Electrograms	48
1.7.3 Filtering.....	50
1.8 Chaos Theory.....	50
1.9 Hypothesis.....	51
1.10 Scope of this thesis.....	52
2 Methodology	54
2.1 Introduction.....	55

2.2	Patient studies	55
2.2.1	Patient selection	55
2.2.2	System setup and electrogram recording	55
2.2.3	Acquisition of bipolar electrograms	56
2.3	Accessing data	58
2.3.1	Exporting data from Ensite Precision	58
2.4	Endocardial electroanatomical mapping during atrial fibrillation	58
2.4.1	Bipolar Voltage Maps	58
2.4.2	Complex Fractionated Atrial Electrogram Maps	59
2.4.3	Isochronal Maps	60
2.5	Development of a new signal processing algorithm to map human atrial fibrillation: Representation of Electrical Tracking on an Orbital Map (RETRO-Map).....	61
2.5.1	Tracking Wavefronts.....	61
2.5.2	Automation of Wavefront Tracking.....	62
2.5.3	Choropleth Maps.....	63
2.6	Conclusion	64

3 Development and validation of a new mapping technique...65

3.1	Introduction.....	66
3.2	Methods	67
3.2.1	Patient Selection and Procedural Technique	67
3.2.2	Data Collection and Export.....	67
3.2.3	Algorithm Development	68
3.2.4	Automation of Wavefront Tracking.....	73
3.2.5	Isochronal Map Construction	74
3.2.6	Validation of RETRO-Mapping.....	74
3.2.7	Statistical Analysis	76
3.3	Results	76
3.3.1	Assessment of Algorithms applied to Atrial Fibrillation.....	77
3.3.2	RETRO-Mapping Algorithm Validation in Sinus Rhythm and Atrial Tachycardia.....	79
3.3.3	Algorithm Validation during Atrial Fibrillation	80
3.3.4	Manual and Automated Orbital Plots	87
3.4	Discussion	88
3.5	Limitations.....	91

3.6	Conclusion	92
-----	------------------	----

4 Mechanistic Insights from Mapping Persistent Atrial Fibrillation

.....		93
4.1	Introduction.....	94
4.2	Methods	94
4.2.1	Patient selection	95
4.2.2	Design modifications of RETRO-Mapping.....	97
4.2.3	Optimal mapping duration	98
4.2.4	Developing Analysis Techniques.....	98
4.2.5	Statistical analysis.....	101
4.3	Results	102
4.3.1	Optimal mapping duration	102
4.3.2	Percentage match in activation patterns during persistent AF	103
4.3.3	Temporal stability of CFAE _{mean}	107
4.3.4	Temporal stability of mean bipolar voltage	108
4.3.5	Relationship between low percentage match and CFAE _{mean} stability 109	
4.3.6	Correlation between CFAE _{mean} and mean bipolar voltage	110
4.3.7	The Effect of Amiodarone on CFAE _{mean} and Mean Voltage: A Sub-analysis 112	
4.3.8	Organisation characteristics of persistent AF.....	114
4.3.9	Correlation between CFAE _{mean} and R50	118
4.3.10	Correlation between CFAE _{mean} and Shannon entropy	119
4.4	Discussion	119
4.5	Limitations	124
4.6	Conclusion	125

5 Focal Activation during Persistent Atrial Fibrillation..... 126

5.1	Introduction.....	127
5.2	Methods	128
5.2.1	Patient selection	128
5.2.2	Characterising Atrial Activation Patterns	129

5.2.3	Additional tools for analysis	130
5.2.4	Myofiber Architecture	131
5.2.5	Statistical analysis	131
5.3	Results	132
5.3.1	Wavefront characteristics during persistent AF	132
5.3.2	Focal Activations and Conventional Markers of Atrial Substrate ...	135
5.3.3	Focal Activations and Novel Markers of Atrial Substrate.....	137
5.3.4	Choropleth Maps	139
5.3.5	Effect of Amiodarone on Focal Activation.....	141
5.3.6	Effect of Duration of Persistent Atrial Fibrillation on Focal Activation	141
5.3.7	Atlas of Myofiber Architecture with Choropleth Maps.....	143
5.4	Discussion	144
5.5	Limitations	146
5.6	Conclusion	146

6 The Effect of Ablation on Atrial Activation Patterns during Persistent Atrial Fibrillation..... 148

6.1	Introduction.....	149
6.2	Methods	151
6.2.1	Patient selection	151
6.2.2	Live Data Export.....	152
6.2.3	Choropleth Maps	153
6.2.4	Data analysis techniques	153
6.2.5	Statistical Analysis	154
6.3	Results	154
6.3.1	Baseline Percentage Match	154
6.3.2	Organising effects of ablation	155
6.3.3	Correlation between R50 and dominant directions.....	164
6.3.4	Differences between induced and spontaneous persistent AF	165
6.3.5	Effect of previous ablation	168
6.3.6	Workflow for online RETRO-Mapping	170
6.4	Discussion	171
6.5	Limitations	175
6.6	Conclusion	175

7	Conclusions and Future Work	176
7.1	Introduction.....	177
7.2	Original Contributions	177
7.2.1	Activation Mapping of Atrial Fibrillation	177
7.2.2	Spatiotemporal Stability of Atrial Fibrillation.....	178
7.2.3	Tools to Quantify Activation Characteristics	179
7.3	Implications of the research.....	180
7.4	Future directions	181
7.5	Conclusion	182
8	References	183

Supplemental Video Data:

Movie 3-1, Movie 3-2, Movie 5-1.

List of Figures

Figure 1-1 Ring preparation cut from the Cassiopea jellyfish.	22
Figure 1-2 Schematic diagram of atrial flutter and atrial fibrillation.....	23
Figure 1-3 Isochronal activation map of atrial fibrillation.	25
Figure 1-4 Classification criteria of atrial fibrillation mapping	26
Figure 1-5 Activation maps of atrial fibrillation.....	27
Figure 1-6 Schematic diagram of a rotor.	31
Figure 1-7 Schematic diagram of leading circle re-entry.....	32
Figure 1-8 Optical mapping of a rotor.	33
Figure 1-9 FIRM Mapping.....	33
Figure 1-10 Non-invasive rotor mapping using CardioInsight.	34
Figure 1-11 Myofiber orientation.	40
Figure 1-12 Spectral analysis.	44
Figure 1-13 Unipolar electrogram.....	48
Figure 1-14 Bipolar electrogram.	49
Figure 1-15 The effect of fibrosis on the bipolar electrogram.	49
Figure 2-1 Graphical user interface on Ensite Precision.....	57
Figure 2-2 Electrogram acquisition over 8 seconds for mean voltage.	59
Figure 2-3 Electrogram acquisition over 8 seconds for CFAEmean.....	60
Figure 2-4 Isochronal map of a uniform wavefront.....	61
Figure 2-5 Graphical user interface of RETRO-Mapping.....	62
Figure 2-6 Assignment of direction of uniform wavefronts.	64
Figure 3-1 3-Dimensional dynamic mapping of a uniform wavefront.	68
Figure 3-2 Continuous moving dots map.....	69
Figure 3-3 Time-shifting electrograms.....	70
Figure 3-4 Electrode positions and midpoints.....	71
Figure 3-5 Validating techniques of RETRO-Mapping.	73
Figure 3-6 Assignment of activation direction.....	76

Figure 3-7 Continuous mapping of 2 seconds of AF.	81
Figure 3-8 Examples of activation patterns during AF.....	83
Figure 3-9 Good correlation between mapping modalities.	85
Figure 3-10 Poor correlation between mapping modalities.	86
Figure 3-11 Bland-Altman plot of wavefront directions.....	87
Figure 3-12 Manual and automated orbital plots.	88
Figure 4-1 Multiple AFocusII location shadows in Ensite Precision.....	96
Figure 4-2 Updated GUI for RETRO-Mapping.	98
Figure 4-3 Percentage match in activation.....	99
Figure 4-4 Percentage match for 10 second data increments.	103
Figure 4-5 Percentage match for datasets A and B.	104
Figure 4-6 Qualitative and quantitative comparison of orbital plots.....	106
Figure 4-7 Bland-Altman of CFAEmean for datasets A and B.....	107
Figure 4-8 Bland-Altman for mean voltage for datasets A and B.....	108
Figure 4-9 CFAEmean outliers.....	110
Figure 4-10 Correlation between CFAEmean and voltage.	111
Figure 4-11 Effect of amiodarone on voltage.....	113
Figure 4-12 Effect of amiodarone on CFAEmean.....	114
Figure 4-13 Bland-Altman for Shannon entropy of datasets A and B.	115
Figure 4-14 Orbital plots and Shannon entropy.	116
Figure 4-15 Bland-Altman plot of R50 for datasets A and B.....	117
Figure 4-16 Correlation between Shannon entropy and R50.....	118
Figure 4-17 Correlation between CFAEmean and R50.	118
Figure 4-16 Correlation between Shannon entropy and CFAEmean.	119
Figure 5-1 Theoretical model of a ‘focal driver’ mechanism for AF.....	128
Figure 5-2 Examples of wavefront types on RETRO-Propagation Maps.	133
Figure 5-3 Frequency of focal activations.....	135
Figure 5-4 CFAEmean area with and without focal activation.....	136
Figure 5-5 Voltage area with and without focal activation.....	137

Figure 5-6 Correlation between R50 and focal activation.....	138
Figure 5-7 The effect of focal activations on dominant directions.....	139
Figure 5-8 Choropleth maps for 18 patients.....	140
Figure 5-9 The effect of amiodarone on focal activations.....	141
Figure 5-10 The effect of AF duration on focal activations	142
Figure 5-11 Correlation between duration of AF and focal activations.	142
Figure 5-12 Choropleth map with myofiber orientation.	143
Figure 6-1 Baseline percentage match	154
Figure 6-2 Left atrial appenage cycle length before and after PVI.....	155
Figure 6-3 R50 before and after PVI.	156
Figure 6-4 Change in R50 after PVI in each patient.	157
Figure 6-5 Correlation between LAA cycle length and R50.	158
Figure 6-6 Choropleth map during AF.	160
Figure 6-7 LAT map during macro re-entry.	161
Figure 6-8 LAT and choropleth map during macro re-entry.....	162
Figure 6-9 Dominant directions before and after PVI.	163
Figure 6-10 Change in dominant directions before and after PVI.....	164
Figure 6-11 Correlation between R50 and dominant directions.....	165
Figure 6-12 Effect of PVI on R50 for induced and spontaneous AF.....	166
Figure 6-13 Effect of PVI on dominant directions for induced and spontaneous AF. ...	167
Figure 6-14 Baseline percentage match for induced and spontaneous AF.....	168
Figure 6-15 Differences between previous PVI and no previous PVI.	170

List of Tables

Table 3-1 Patient demographics and characteristics.....	77
Table 4-1 Patient demographics and characteristics.....	96
Table 4-2 Optimal mapping duration.....	103
Table 4-3 Delayed mapping.	105
Table 4-4 Correlation between CFAEmean and voltage.....	112
Table 5-1 Patient demographics and characteristics.....	129
Table 5-2 Frequency of focal activation per patient.....	134
Table 6-1 Patients demographics and characteristics.	152
Table 6-2 Changes in LAA cycle length and R50 with PVI.....	159

1 Introduction

1.1	Introduction.....	21
1.2	Mechanisms of Atrial Fibrillation	21
1.2.1	The Critical Mass Theory of Atrial Fibrillation	21
1.2.2	Re-entry and Multiple Wavelets.....	22
1.2.3	The Double Layer Hypothesis	28
1.2.4	Focal Sources	29
1.2.5	Rotors as drivers of atrial fibrillation.....	30
1.2.6	Autonomic Function Initiating AF.....	36
1.3	Left Atrial Substrate in AF.....	37
1.3.1	Non-invasive Assessment	38
1.3.2	Invasive Assessment.....	39
1.3.3	Left Atria Myofiber Architecture	39
1.4	Alternative Ablation Targets	40
1.4.1	Complex Fractionated Atrial Electrograms	41
1.4.2	Spectral Analysis.....	43
1.5	Induced and Spontaneous Atrial Fibrillation.....	44
1.6	Activation Mapping	45
1.6.1	Determining Local Activation Time	45
1.6.2	Isochronal Mapping.....	45
1.7	Recording Cardiac Electrograms	46
1.7.1	Unipolar Electrograms.....	47
1.7.2	Bipolar Electrograms	48
1.7.3	Filtering.....	50
1.8	Chaos Theory.....	50
1.9	Hypothesis.....	51
1.10	Scope of this thesis.....	52

1.1 Introduction

Atrial fibrillation (AF) is the most common arrhythmia encountered in clinical practice. Regardless of age, there is a prevalence within the UK of around 1%. This prevalence increases sharply in the elderly population, to a prevalence of around 10%.^{1, 2} There are significant associations with morbidity and mortality, with consequent health economic implications.

At present, the direct cost of AF approximates to 1% of the total healthcare spending in the UK. Patients suffering with AF have between a 10-40% chance of hospitalisation each year. Furthermore, around 20-30% of all strokes are due to AF, while other complications such as left ventricular dysfunction, decreased quality of life, depression, cognitive decline and vascular dementia remain strongly associated. AF is also independently associated with a 1.5-fold increased risk of all-cause mortality in men, and 2-fold increased risk in women.³⁻⁵

Catheter ablation procedures form an important part of the treatment strategy for patients with AF, as either an alternative to, or alongside pharmacological therapy. Since the important discovery of focal ectopy from the pulmonary veins (PVs) initiating AF⁶, other mechanistic insights have not resulted in any significant or reproducible improvement in procedural outcome.^{7, 8} As such, antral pulmonary vein isolation (PVI) forms the basis of all conventional catheter ablation procedures. This involves encirclement of the pulmonary veins with ablation lesions, resulting in their electrical isolation from the body of the left atrium.

Despite approximately 100 years of attempts at understanding mechanisms responsible for maintaining AF, they remain poorly defined. Mapping activation during AF is notoriously challenging, however it may hold key mechanistic information. The chaotic activation patterns observed during AF are significant challenges when attempting to map AF. New tools are required in order to better understand the mechanisms resulting in human persistent AF.

1.2 Mechanisms of Atrial Fibrillation

1.2.1 The Critical Mass Theory of Atrial Fibrillation

While watching the exposed fibrillating atrium of an animal heart, in 1914 Garrey described chaotic activity, with contractions that did not appear to be dependent on one another.⁹ He also noted that large mammalian ventricles would fibrillate with relative ease, while those of smaller mammals would either spontaneously stop fibrillating, or not fibrillate at all.

Following these observations he cut fibrillating tissue into four equal parts and found that fibrillation continued, but a critical muscle mass was required.

1.2.2 Re-entry and Multiple Wavelets

Predating the observations made by Garrey, insightful experiments utilising the contractile bell of the rhizostomous Scyphomedusa (jellyfish) *Cassiopea xamachana*, and ventricular rings cut from turtles were conducted by Mayer (Figure 1-1).¹⁰ Combining the appropriate combinations of electrical pulses, wavefronts could propagate indefinitely in preparation. He also observed that simultaneous induction of two wavefronts from the same location could progress in opposite directions. However, wavefront collision resulted in their extinction, rather than indefinite propagation.

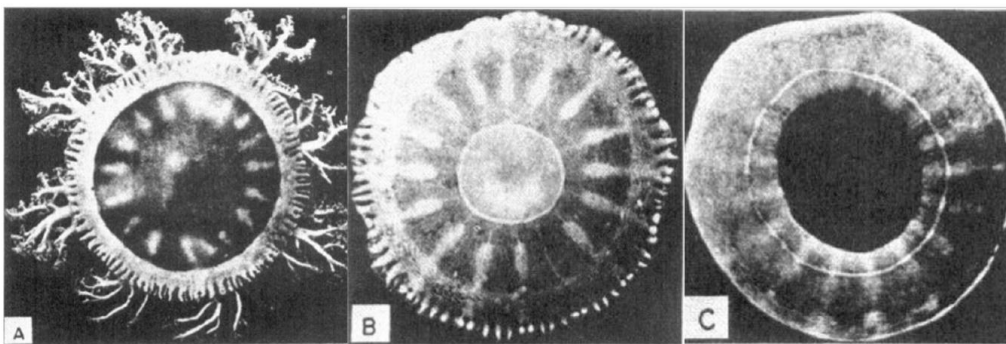


Figure 1-1. Ring preparation cut from the rhizostomous Scyphomedusa *Cassiopea xamachana*. The intact jellyfish (A) has its arm and stomach removed (B) before removal of the centre to create a ring preparation (C). Adapted from Mayer AG.¹⁰

In subsequent work, Garrey was the first to suggest that AF was caused by circus movement re-entry.¹¹ This was contrary to the popular alternative mechanistic theory involving multiple discharging foci, suggest by others. During these experiments, he simultaneously presented evidence against a focal source. He induced circus movement with a single stimulus in a ring preparation, and observed that the contractile impulse travelled in a ring-like circuit to repeatedly involve a given region after completion of each circuit. Following this, he cut the tissue in to pieces, such that only a single piece contained the original site/foci of stimulation. In doing so, this provided evidence against a focal source, as *“only one of the pieces can contain the original hypothetical tachysystolic pacemaker”*.

Ralf Mines conducted a series of experiments, corroborating the findings of Garrey. These defined the fundamental principles that govern the laws of re-entry¹², which include:

1. The requirement of unidirectional block for initiation of a re-entrant circuit
2. A refractory period in which tissue cannot be excited
3. Slowing in conduction rate with an increased rate of stimulation and shortened refractory period
4. Re-entrant circuit dependence upon the conduction rate, refractory period duration, and length of the muscle path

In 1921, Lewis *et al.* hypothesised that re-entry around anatomical structures, or functional re-entry around an unexcitable core due to functional block may be potential drivers of AF, in the mother wave hypothesis.¹³ This model was based on a meandering central or “mother wave” moving in multiple directions and giving rise to daughter waves whose conduction properties are determined by local tissue properties. This was supported by evidence from the surface electrocardiogram showing minor changes in the electrical axis of the fibrillatory deflections in patients with AF. Lewis incorporated these findings, along with the concepts of Garrey and Mines to describe the mechanisms of both atrial flutter and fibrillation. This later went on to become known as the ‘circus movement hypothesis of re-entry’ (Figure 1-2).^{14, 15}

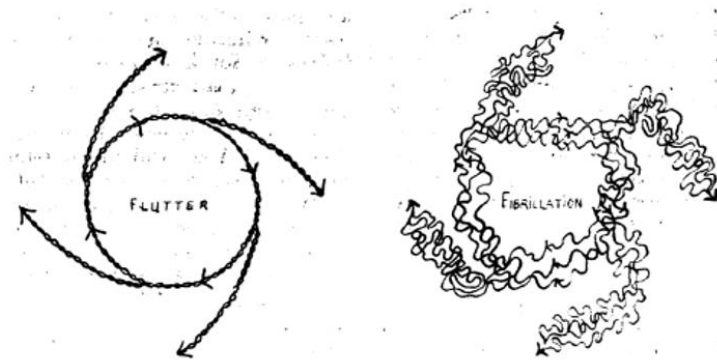


Figure 1-2. Schematic diagram of atrial flutter (left) and atrial fibrillation (right). There is re-entry around a central area in both, however the course is variable in AF. Adapted from Lewis *et al.*¹³

While AF could be induced with high rate pacing in animal models, these episodes would not persist beyond a few seconds. Moe therefore developed a canine model which enabled AF to be sustained for much longer periods of time. This model involved the use of

simultaneous vagal nerve stimulation to shorten the atrial refractory period, while pacing from the right atrial appendage.¹⁶ During AF, the appendage was excluded with a clamp. Upon discontinuation of atrial appendage pacing, the appendage was no longer in AF, however the rest of the atrium continued to fibrillate, suggesting the original foci was not required to sustain AF. This suggested that despite AF having originated from a single foci, it was independent of the ongoing high rate of discharge to sustain AF. Moe concluded that re-entry was the most likely mechanism for atrial fibrillation, with grossly irregular wavefronts becoming fractionated and producing independent, randomly wandering daughter wavelets as offspring. This became the multiple wavelet hypothesis for atrial fibrillation.

Moe realised that while supporting re-entry as a major mechanism of AF, irregular activation of the atria could be the result of several factors. These include a single rapidly discharging focus, multiple discharging foci, or rapidly circulating circus movement. Due to the challenges of testing this in living tissue, Moe undertook computational modelling where the theoretical substrate had a variable repolarisation time and conduction velocity according to the level of tissue excitability.¹⁷ Following initiation of electrical activity in this model, it remained self-sustaining with activity resembling fibrillation. An estimate of 23-40 electrical wavelets, re-entering random regions of the substrate was determined to be required in order to sustain fibrillation. This model also illustrated that re-entrant circuits could be generated without an anatomical obstacle and added support for the multiple wavelet hypothesis. Interestingly, Lee *et al.* re-studied Moe's canine vagal nerve stimulation model of atrial fibrillation some 50 years later, proposing that multiple foci are responsible for driving AF, rejecting the multiple wavelet hypothesis.¹⁸

With the advent of mapping technology, Allessie *et al.* corroborated Moe's findings in a series of elegant studies by placing micro-electrodes on rabbit atria. They demonstrated that re-entrant circuits could be independent of an anatomical substrate. From this, the "leading-circle" concept of re-entry was proposed, where functional circuits could operate anywhere in the heart under the right local conditions. Initiation of re-entry was found to be dependent of the inhomogeneity in atrial fibre refractoriness in close proximity to one another, and the activation wavefront continually emitting wavefronts centrally to produce and sustain a refractory core.¹⁹⁻²²

Subsequent detailed studies by Allessie were conducted on Langendorff-perfused canine hearts using epicardial multi-electrode arrays.²³ Continuous beat-to-beat variations in

activation pattern including functional turning, collision, fractionation and extinction in functional lines of block were mapped and described (Figure 1-3). Rather than the 23-40 wavelets required to maintain AF as proposed by Moe¹⁷, the critical number of wavelets suggested by Allesie was just 3 to 6.²³

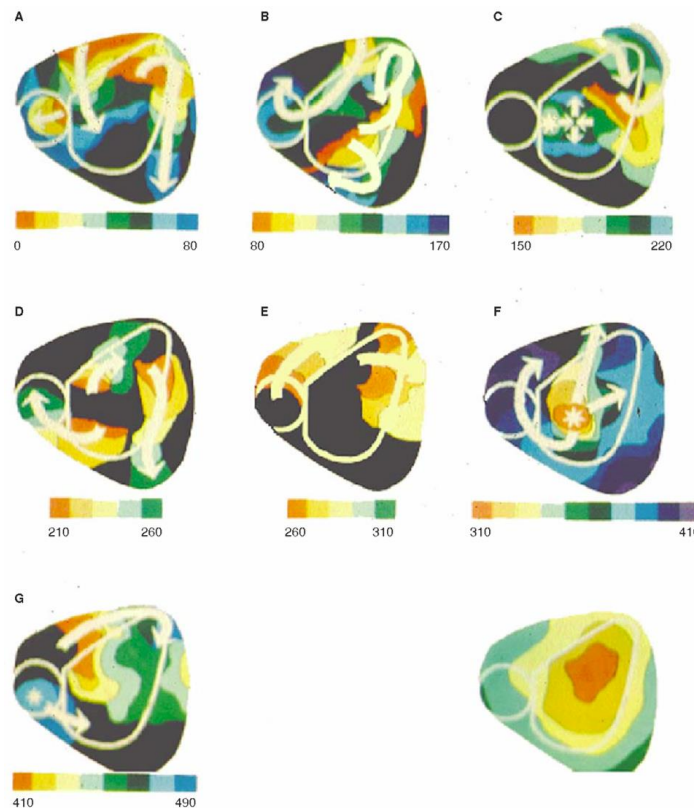


Figure 1-3. Isochronal activation maps of 0.5 seconds (from A to G) of AF in the right atrium of isolated canine hearts. A colour spectrum is applied to the map, with each colour representing 10ms. The right lower image shows an example of a sinus rhythm activation pattern for comparison. Focal activations resulting from epicardial-endocardial breakthrough are seen in panels C, F and G (marked with an asterisks). Reproduced from Allesie *et al.*²³

The potential benefit of multi-electrode mapping during cardiac surgery in humans was first described by Canavan.²⁴ Atrial activation patterns were recorded from 156 epicardial electrodes during sinus rhythm, atrial pacing and reciprocating tachycardia. This group went on to study electrically induced AF in patients undergoing surgery for Wolf-Parkinson-White (WPW) syndrome.²⁵ Once again, the complex activation patterns of multiple wavelets, fragmenting, colliding and propagating in variable directions was observed. Although re-

entrant circuits involving anatomical obstacles such as the pulmonary and caval veins were present, there was further confirmation of circuits existing in the absence of structural obstacles.

Further work in a similar patient population by Konings *et al.*²⁶ showed different degrees of disorganised activation patterns. This ranged from predominantly planar activation, to those with completely disorganised activation. A classification system was developed to identify 3 different types of AF based on their degree of disorganisation (Figure 1-4). In addition, they described a small number of “new” wavelets appearing to originate from the free wall of the right atrium. These focal activations were thought to be the result of epicardial breakthrough due to the frequent presence of a small r wave on the unipolar signal at the earliest site of activation, rather than a true focal source. These events were infrequent, and the dominant mechanism for sustaining AF was concluded to be multiple re-entrant wavelets.²⁷

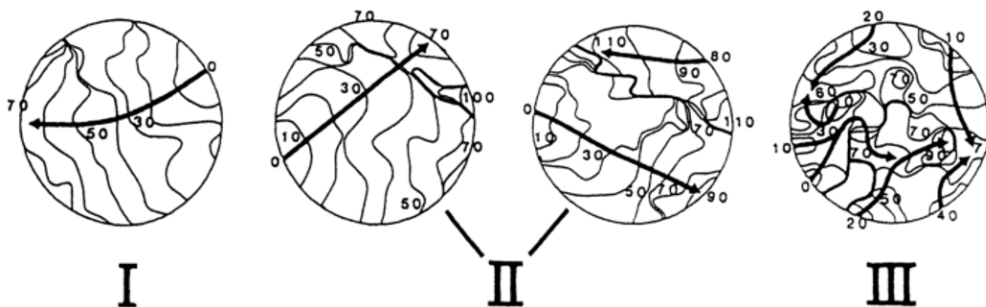


Figure 1-4. Classification criteria of AF mapping. (Left to right) Type I is characterised by single uniform wavefronts. During Type II, single non-uniform wavefronts, or two wavelets are present. Type III is characterised by three or more wavelets with multiple areas of slow conduction and arcs of conduction block. Reproduced from Konings *et al.*²⁷

The detailed mapping studies of Konings *et al.* provided insight in to the activation patterns that occur during AF. However, even for those with experience in this type of mapping, interpretation is challenging. In addition, separate maps are required to display the activation of AF rather than on one single map, making the technique cumbersome (Figure 1-5).

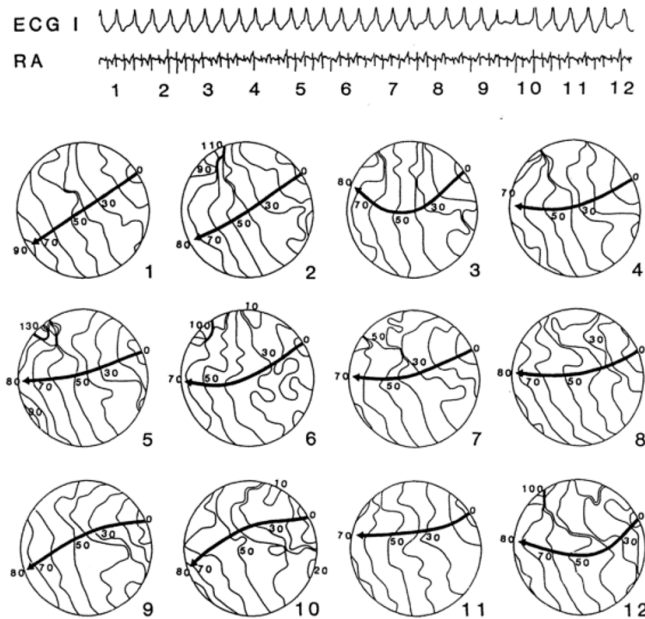


Figure 1-5. Activation maps are displayed for 12 consecutive seconds of electrically induced AF. A surface ECG is displayed at the top, with a right atrial (RA) unipolar electrogram directly below. Each second has been annotated along the RA unipolar electrogram strip, with the corresponding activation maps numbered, and displayed below. Reproduced from Konings *et al.*²⁷

Around the same time, Schuessler *et al.* described activation patterns in a canine model of induced AF.²⁸ With increasing concentrations of acetylcholine they observed a decrease in atrial refractory period, and eventual sustained fibrillation induced. In accordance with the multiple wavelet hypothesis, as the refractory period decreases, both the number and instability of re-entrant circuits should increase. As predicted, this was observed for non-sustained rapid repetitive responses, with activation sequence maps revealing multiple re-entrant circuits. However, with further shortening of the refractory period at higher acetylcholine concentrations, the trend did not continue. Instead, the re-entry “*stabilized to a small, single, relatively stable re-entrant circuit,*” independent of anatomic obstacles. The same group further challenged Moe’s hypothesis by demonstrating that re-entry is able to occur in a three-dimensional manner due to the connecting transmural muscle fibres between epi- and endocardium during epicardial electrode mapping in canine atria.²⁹

1.2.3 The Double Layer Hypothesis

It is important to recognise that mapping either the epicardial or endocardial surface will present two-dimensional data, ignoring the transmural conduction which might be interpreted as focal activation. Bi-atrial high-density unipolar mapping of the epicardium has revealed frequent epicardial breakthrough of waves propagating in deeper layers in the so-called 'double-layer hypothesis'. De Groot *et al.* describe the observation of small r waves in unipolar electrogram recordings, suggesting that this supports breakthrough rather than a true focal mechanism resulting from automatic cellular discharge.³⁰ Although this alone is not proof of breakthrough, they used a number of other metrics to support their concept. A wavemapping approach was used to identify individual fibrillation waves. This defines the starting point of the first fibrillation wave as the earliest activated site in the mapping area. The shortest time difference with the neighbouring 8 electrode is then calculated. If the time difference was $\leq 12\text{ms}$, the electrode activation was attributed to that wave. In case of a time difference $>12\text{ms}$, the electrode was annotated as the starting point of a new wave. Four criteria were required for the classification of epicardial breakthrough; the epicardial breakthrough site had to be activated earlier than all surrounding electrodes, located at least 2 electrodes from the mapping array border, and not obscured by large QRS complexes or artefact. Lastly, a time delay of $>40\text{ms}$ between the site of epicardial breakthrough and lateral border of another wave was required, otherwise the wave was attributed to discontinuous conduction from the lateral boundary of that wave.

This elegant mapping study by De Groot *et al.*³⁰ does suggest some compelling evidence for the existence of a 'double layer hypothesis'. However, it remains challenging to understand how a small r wave from a unipolar electrogram can definitively be assigned to that of transmural activity. The complexities of interpreting electrogram morphology during AF means that this deflection may merely be the result of wavefront collision or far-field signal. Furthermore, the measurement of 'the smallest time delay' between epicardial and endocardial signal may be difficult to interpret without the use of a reliable fiducial signal due to myocardial anisotropy. Lastly, a wavefront was deemed to reflect transmural conduction if it was present within a 4mm distance and $<15\text{ms}$ before the origin of the focal wave based on normal atrial conduction properties. It is rare that patients with atrial fibrillation have normal atria, and therefore the likelihood of having normal conduction properties would seem doubtful in this patient population. Simultaneous mapping of the endo- and epicardial

surface has suggested asynchronous activation between the two layers, promoting maintenance of AF by replacing fibrillation waves that die out with breakthrough from the opposite side.³¹ This has important implications as limited and focal ablation is unlikely to result in termination of AF due to the multiple potential breakthrough sites, and may explain the high recurrence rates of AF after ablation of focal and rotational drivers.

1.2.4 Focal Sources

Defining a source as 'focal' is controversial, as the interpretation of this nomenclature for many is synonymous with an arrhythmia that results from a discrete collection of myocardial cells at its origin, such as a focal automatic atrial tachycardia. Within the AF literature, both rotors and complex fractionated atrial electrograms (CFAEs) are sometimes referred to as focal sources. This is confusing, as mechanistically they are completely different, although a 'localised' ablative strategy would be applied to both. Furthermore, defining something as a 'driver' can also be open to debate. For the purposes of this thesis, a focal source will be considered to be a localised source, where activity propagates outward from its earliest point of activation in all directions. It will not make inference on the underlying mechanism, unless specifically referred to under its accepted name and associated mechanism. It may be considered that all localised sources have the potential to be a driver.

Rothberger and Winterberg first hypothesised that AF was the result of a single electrical focus in 1909.³² The persuasive evidence from Lewis for a re-entrant mechanism resulted in little further support for a focal driver mechanism until the 1940s. In a series of experiments, Scherf suggested that AF was the result of an ectopic focus.³³ In one study he injected aconitine into canine atria, leading to rapid excitation with the appearance of AF. When he undertook local cooling of the area the arrhythmia terminated but restarted on discontinuation of cooling. Importantly, in his observations he stated that the wavefront interacted with islands of refractory tissue causing weaving and interweaving contraction, characteristic of fibrillation as it entered the larger mass of auricular muscle. He concluded that AF was caused by a rapid stimulus rather than re-entry. Consequently, he reported that the re-entry waves of excitation were a concomitant feature of AF rather than its cause.

While some groups have failed to demonstrate repetitive focal activation as the mechanism driving AF^{25, 27}, Harada *et al.* demonstrated regular and repetitive activation originating in the left atrium in 10 patients with chronic AF undergoing isolated mitral valve

surgery.³⁴ Interestingly, they found activation in the right atrium to be chaotic, and suggested that the left atrium was driving the AF. Jais *et al.* described a small series of 9 patients with paroxysmal AF in which the surface ECG pattern of AF was the result of focal rapidly firing activity, exhibiting a consistent and centrifugal pattern of activation. All patients underwent limited focal radiofrequency ablation with elimination of the foci and subsequent non-inducibility of AF.³⁵ The following year, in 1998, Haissaguerre *et al.* made the important discovery of focal ectopy from PVs initiating AF.⁶ This has been central in both advancing our understanding of AF, and identifying a treatment target. It is on the basis of this finding that pulmonary vein isolation currently forms the mainstay of conventional ablation procedures.

While a subset of patients achieve success from PVI in treatment of AF, others remain in AF despite the veins being electrically isolated indicating that this is not the only mechanism. As a result, the challenge of identifying targets for ablation beyond the pulmonary veins has remained.

1.2.5 Rotors as drivers of atrial fibrillation

Rotors are a specific type of localised functional re-entrant circuit. They possess a central core of extreme wavefront curvature, such that it results in very slow conduction at the core. The extreme wavefront curvature increases as conduction slows towards the central core, where a small curved excitable gap is present between the wavefront head and tail. The central core (or re-entrant phase singularity) from which the spiral wave is emitted is termed a 'rotor'. The wavefront pivots around this unexcited but excitable tissue (Figure 1-6).³⁶

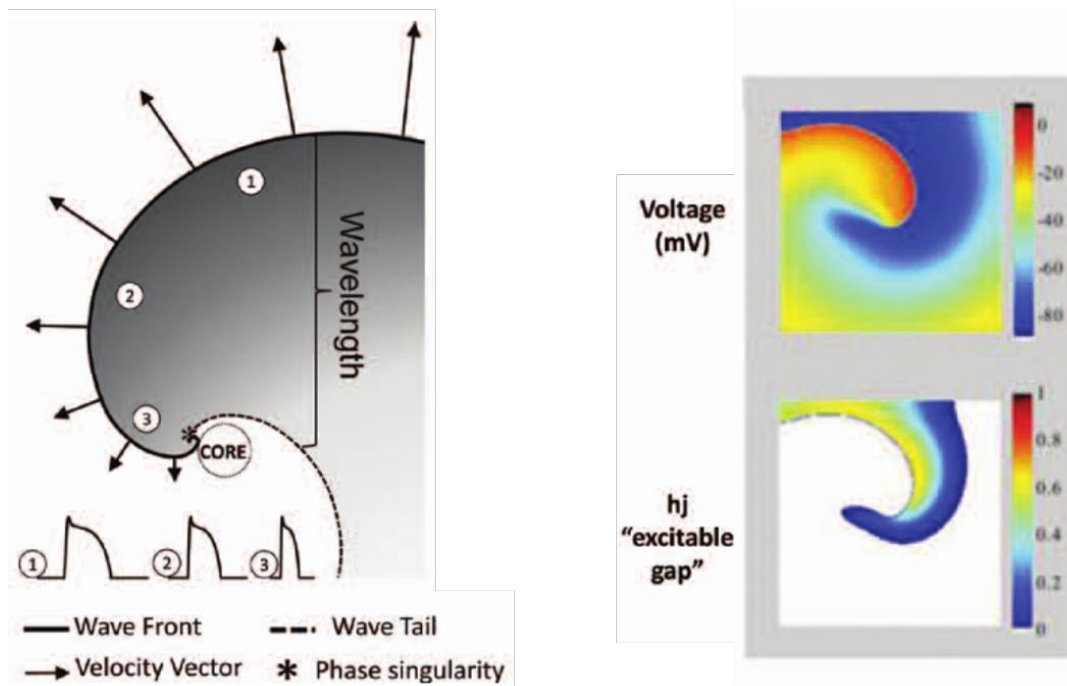


Figure 1-6. (Left) Schematic diagram of a rotor. (1 to 3) Conduction velocity decreases (black arrows) and action potential duration shortens, which shortens the wavelength with increasing proximity to the rotor core. (Right, top) The transmembrane voltage distribution of a rotor is displayed during simulated model. (Right, bottom) The corresponding excitable gap during rotor re-entry. Adapted from Pandit *et al.*³⁷

Although there appear to be similarities between leading circle re-entry and rotors, there are fundamental differences. Importantly, there is complete refractoriness at the core during leading circle re-entry. This is the result of continuous centripetal invasion creating a ring of excitation around a functionally unexcitable obstacle (Figure 1-7). This prevents movement of the rotational circuit, and instead anchors it to a location for as long as it continues. Conversely, rotors are able to meander as they pivot around an unexcited, but excitable core.

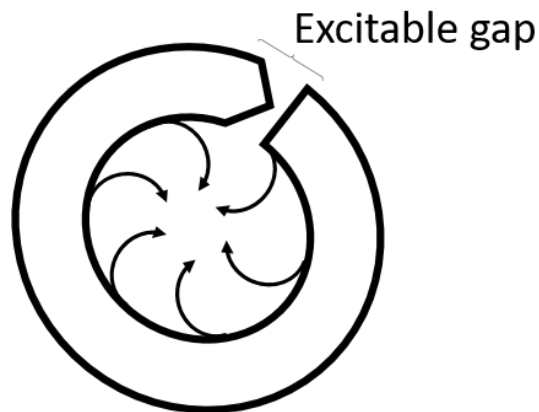


Figure 1-7. Schematic diagram of leading circle re-entry around a functional obstacle. Centripetal activation (curved arrows) invade the core to create a refractory centre.

Despite recent popularity in this field of research, rotors are not a new concept. Seminal work by Winfree in canine ventricular myocardium demonstrated spiral waves rotating around a phase singularity.³⁸ In 1992, with the use of optical mapping Davidenko demonstrated cardiac fibrillation in animal myocardium where spiral waves could be non-stationary, shifting the position of the phase singularity, as well as stationary by anchoring to anatomical structures.³⁹ The idea that one or a number of localised rotors may drive AF holds important therapeutic implications as targets for catheter ablation. Complex computational algorithms have been developed which afford investigators important insight in to the patterns of activation in human AF.

Mapping Rotors

The Jalife group have published extensively on their optical mapping studies in the Langendorff-perfused ovine model of acetylcholine induced AF.⁴⁰⁻⁴² They have demonstrated sustained rotors during AF, predominantly on the posterior LA wall, but also on the anterior wall of the left atrial appendage.

Optical mapping is a technique that was established over 40 years ago and enabled the characterisation of wavefront propagation with resolution capabilities below the level of millimetres.⁴³ More recently, simultaneous use of voltage-sensitive dyes have enabled the 3-dimensional behaviour of rotors to be observed. This technique is limited in its use within humans due to the toxicity of voltage-sensitive dyes (Figure 1-8).

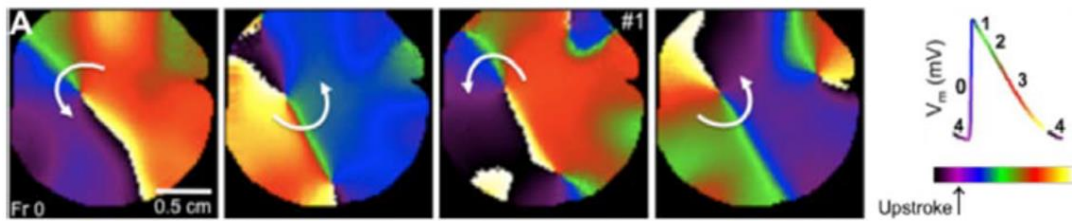


Figure 1-8. Sequential images (left to right) of optical mapping showing a rotor pivoting around its phase singularity. Adapted from Quintanilla *et al.*³⁶

Bi-atrial endocardial mapping using multi-spline basket catheters and a proprietary computational algorithm have been undertaken in Focal Impulse and Rotor Mapping (FIRM) by Narayan *et al.* In this approach, phase analysis has shown the presence of a small number of rotors in more or less fixed locations (Figure 1-9).⁴⁴

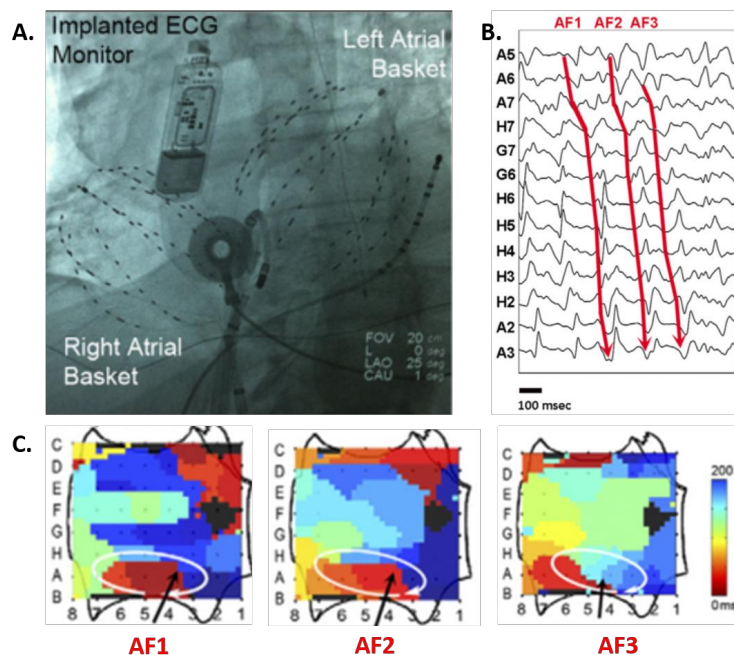


Figure 1-9. (A.) Fluoroscopic image of two, 64-pole basket catheters in each atrium. A decapolar catheter is positioned in the coronary sinus, and a map catheter in the left atrium. An implantable ECG monitor is also seen. (B.) FIRM post-processed and filtered electrograms show sequential activation over the course of the rotor (AF1 to AF3), with the corresponding FIRM map (C.). Adapted from Narayan *et al.*⁴⁵

Employing a completely different mapping modality, which applies a complex algorithm of inverse-solution based analysis of body surface electrogram data, Haissaguerre *et al.* have also identified rotors using CardiInsight. Instead, they have observed them to be transient and migratory with a tendency to cluster around fibrotic zones (Figure 1-10). Furthermore, median rotor duration was 2.6 rotations⁴⁶, in contrast to several minutes as observed by Narayan *et al.*⁴⁴

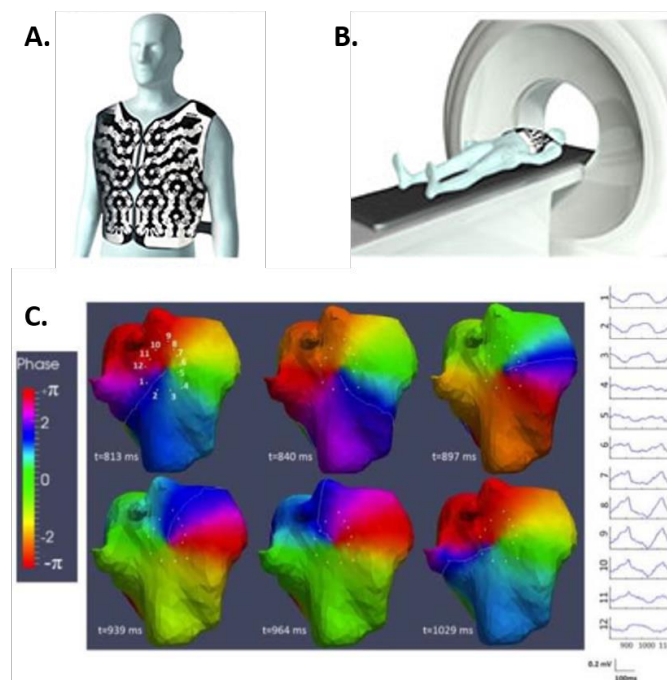


Figure 1-10. Non-invasive rotor mapping using CardiInsight. (A) A vest containing 252 electrodes is worn by the patient. (B) A CT scan is done to determine the relationship of each electrode to the CT geometry of the cardiac chambers. (C) Phase maps display the activation pattern. In this example, a rotor pivots around its phase singularity. Adapted from Haissaguerre *et al.*⁴⁷

Ablating Rotors

The importance of rotors in arrhythmia maintenance has been suggested by limited ablation of localised regions resulting in termination of AF. In the CONFIRM trial, the acute efficacy endpoint of AF termination or $\geq 10\%$ consistent slowing of AF CL was achieved in 86%, with AF termination in 56% after a mean of 4.3 ± 6.3 min of FIRM ablation at the primary source.⁴⁴ This limited ablation success was not the case with the AFACART study⁴⁸, where mean RF time for driver-only ablation resulting in AF termination was 46 ± 28 minutes despite a mean of

only 4.9 ± 1 driver sites mapped per patient. It therefore seems surprising that RF ablation times are so long, despite rotors being localised sources. One possible explanation may be that the proposed source areas are in the order of cm^2 , and the choice of ablation area wider and operator dependent. They did however report AF termination in 64% of patients undergoing 'driver only' ablation. Despite this, evidence suggesting rotors possibly being transient and migratory does not explain why focal ablation should result in termination of AF.^{44, 49}

Initial high success rates were achieved from FIRM guided catheter ablation⁴⁴, but other groups were unable to achieve comparable success rates.⁸ If focal drivers such as rotors were spatiotemporally stable, it would be expected that focal ablation would consistently result in successful treatment of AF. Evidence that focal sources are stable is also challenged by the recent double-layer hypothesis demonstrating endocardial-epicardial dissociation where multiple different breakthrough locations are possible.³¹ With this hypothesis it is understandable why a focal ablative strategy would fail, and may in part contribute to the low procedural success rates.

In the largest series of source focal source ablation, Miller et al.⁵⁰ undertook FIRM guided ablation in 170 consecutive patients, including patients with PAF (37%), persistent AF (31%) and long-standing persistent AF (32%). 43% of these patients had undergone at least one prior ablation for AF. In combination with PVI, they achieved 87% freedom from AF after a single FIRM procedure at 1 year. They concluded that higher rates procedural success could be obtained with FIRM-guided ablation to those of PVI alone, supporting localised sources as a mechanism for AF, and corroborating the findings of CONFIRM.

If the maintenance of AF is related to a hierarchical (focal sources) rather than non-hierarchical (multiple wavelet) mechanism, it may be possible to explain why persistent AF has been terminated with relatively localised ablation. Narayan's groups have undertaken computational modelling⁵¹ suggesting a possible explanation. They simulated spiral wave re-entry in monodomain 2-dimensional myocyte sheets. Ablation lesions were applied, with models confirming that localised ablation may anchor re-entry, resulting in organised tachycardias. The ablation results in an excitable gap, which can be invaded by fibrillatory waves, which collide and rapidly terminate spiral re-entry. Targeted ablation may also terminate spiral waves by connecting lesions to large non-conducting obstacles, such as large areas or scar or an anatomic orifice.

There is disagreement as to whether rotors are stable or migratory. If rotors primarily localise at borders of fibrotic regions, it may be more appropriate to target these regions of scar, rather than the rotors themselves. However, extent of delayed enhanced-MRI (DE-MRI) abnormalities have been frequently show to far exceed driver domains, and the micro-fibrosis that anchored drivers in optical studies was beyond the resolution of clinical scanners.⁵² Distinction between ‘culprit’ and ‘bystander’ regions would likely be required if this approach was to be successful.

1.2.6 Autonomic Function Initiating AF

Animal models have often needed autonomic stimulation to maintain induced AF.^{16, 53, 24} Consequently, the autonomic nervous system has been assumed to be important in human AF pathogenesis. The description of ‘vagal symptoms’ and changes in heart rate variability prior to AF initiation has been presented as circumstantial evidence. Richly innervated areas on the epicardial surface of the left atrium have been identified around the pulmonary veins, known as ganglionated plexi (GP). The GP sites are located at the four PV atrial junctions and are highly innervated with both adrenergic and cholinergic nerve fibres. These sites form part of the epicardial neural network, which comprises multiple ganglia with interconnecting neurons and axons, including sensory fibres and sympathetic and parasympathetic efferents.⁵⁴ During the delivery of radiofrequency energy during catheter ablation for AF, an increase in dispersion of AF cycle length has been observed with vagal responses.⁵⁵ The increase in dispersion may promote wavefront fragmentation into multiple, smaller wavelets – a potential mechanism that sustains AF.¹⁶

Direct stimulation of GP sites has been shown to initiate PV ectopy and induce AF.⁵⁶ Canine studies of PV sleeve preparations have shown action potential shortening, and triggered firing in the adjacent PVs but not the atrial myocardium in response to GP stimulation.⁵⁷ This indicates that PVs appear to be the main effectors of GP stimulation. A well described method of functionally locating GP sites is to stimulate the left atrium with high output – high frequency stimulation (HFS)⁵⁸ – over a presumed GP. If there is direct contact, a bradycardic AV nodal response can be elicited. Our group has used this technique to show autonomic modification of the AF substrate by demonstrating changes in AF cycle lengths both near and distant from the site of stimulation.⁵⁶

With evidence of PV ectopy being triggered by stimulation of GP sites, Katritsis *et al.* investigated the effect of empirical GP ablation based on known anatomical sites in addition to PVI, and found it to be superior to outcomes of PVI alone.⁵⁹ The same group went on to investigate the effect of GP ablation alone in AF, although they found this strategy to be less effective than either PVI alone, or in combination with GP ablation. However, formal evidence of autonomic modification was not presented, as the study did not use a functional method to confirm GP sites or a change after ablation.⁶⁰

There are two methods described for locating GP sites that include continuous high frequency stimulation (HFS) and synchronised HFS, with impulses delivered within the local refractory period, and the subsequent response observed. Continuous HFS locates GP sites by identifying AV nodal effects such as bradycardia and pauses. Synchronised HFS aims to identify the sites that trigger AF.⁶¹ There are studies that have used these techniques in a limited capacity to demonstrate the autonomic network in the human LA, and the feasibility to ablate these effects from the endocardium.⁴⁰ Most studies have inferred a role for GP sites based on presumed anatomical co-localisation with little direct evidence of effect.⁶² In arrhythmias where there is a clear anatomical circuit, there is no need to target the autonomic stimuli as there is a clear substrate to ablate. In AF the stimuli and substrate appear to span a large part of the left atrial anatomy and therefore the autonomic stimuli may actually represent a 'more targeted' approach.

1.3 Left Atrial Substrate in AF

It was recognised early on that AF could be induced with relative ease. However, maintaining AF was only made possible under certain circumstances, such as vagal nerve stimulation.²⁴ This suggested that specific electrophysiological conditions were required in order to perpetuate AF. Structural and electrical remodelling have been implicated in the facilitation of AF.

Structural remodelling is characterised by atrial enlargement and myocardial fibrosis, and has been shown to correlate with outcome from catheter ablation.⁶³ Similarly, atrial electrophysiological properties governed by ion channels, exchangers and pumps can be transformed as a result of atrial remodelling, thereby facilitating AF continuation. Surrogate markers of electrical remodelling can be studied, manifesting as reduced voltage and

fractionated electrograms, while the structural changes can be determined with detailed imaging modalities.

1.3.1 Non-invasive Assessment

Fibrosis has been attributed with mechanistic importance in AF. Whether cause or effect, it has frequently been observed in this patient group. Late-gadolinium enhanced cardiac magnetic resonance imaging (LGE-CMRI) has been utilised by several groups for the quantification of atrial fibrosis. Although a technically challenging technique, the degree of atrial fibrosis has been shown to be higher with AF persistence and the presence of more AF risk factors.⁶⁴ Furthermore, atrial fibrosis demonstrated by LGE-CMRI has been independently associated with AF recurrence in patients undergoing catheter ablation for AF.⁶³

The electrical manifestations of fibrosis are sometimes, but not exclusively seen during catheter ablation as regions of low-voltage and slowed conduction. There are challenges when using voltage as a surrogate marker for fibrosis. While some areas are low voltage during AF, they have been demonstrated to have increased voltage at the same site during sinus or paced rhythm.^{65,66} This is important as areas of low voltage measured during AF may not truly identify regions of abnormal atrial substrate.

High resolution contrast enhanced MRI has been integrated with transmural optical mapping.⁵² Conduction was found to occur in preferential micro-anatomic tracks via fibrotically insulated pectinate muscles and intramural myocardial bundles, such that re-entry was established. Radiofrequency ablation at primary re-entrant driver regions resulted in either termination of AF, continuation of AF with a new re-entrant driver established in a different location, or macro-re-entry around the ablation lesion. This suggested the importance of the atrial micro-architecture in the maintenance of AF. The same group went on to hypothesise that human AF is maintained by a limited number of spatially stable microanatomic re-entrant, but temporally competing sources.⁶⁷ Haissaguerre *et al.* reported a tendency for rotors to cluster around fibrotic zones.⁴⁶ Some have raised the question of whether homogenisation of low voltage regions from sinus rhythm maps to eradicate all potential channels and drivers supporting the arrhythmia is warranted.⁶⁸ However, this risks damage to significant regions of atrial myocardium that may not even be implicated in arrhythmia maintenance. This approach would be ineffective should CFAE sites be driving AF, where an inverse relationship between fractionated electrograms and atrial fibrosis has been

demonstrated. Up to 90% of continuous CFAE sites occur in locations that have either patchy or no late gadolinium enhancement on MRI.⁶⁹

1.3.2 Invasive Assessment

Endocardial voltage is frequently used during catheter ablation procedures as a surrogate marker of fibrosis or 'scar'. Studies of persistent AF in humans and canine models have shown histopathological changes with fibrotic infiltration^{70, 71}, while there is evidence that low voltage areas predict poor outcome from catheter ablation.⁷²

The constant variability in bipolar electrogram amplitude during AF makes accurate assessment of voltage challenging. It has been shown that mean peak-to-peak bipolar voltage maps during AF require an 8 second sampling window before spatial stability is achieved.⁷³ Despite this, it is not clear if these maps are reproducible over time. Others have attempted to overcome electrogram variability during AF by creating voltage maps during sinus rhythm. Bipolar voltage has been shown to be higher in patients with paroxysmal than persistent AF, during sinus rhythm and AF.⁷⁴ However, by cardioverting patients to sinus rhythm, the opportunity for mapping potential drivers of AF is lost.

Adopting an individualised approach, Rolf *et al.* undertook atrial substrate modification in low-voltage areas.⁶⁸ Following circumferential PVI, voltage maps were created during sinus rhythm for patients with paroxysmal and persistent AF. Low voltage areas were defined as being <0.5mV. Based on this criteria, low-voltage areas were more commonly identified in the left atrial roof, anterior septum, and posterior wall. Fewer patients with paroxysmal AF were found to have low-voltage areas than patients with persistent AF (10% and 35%, respectively), although there was no improved arrhythmia free survival with substrate modification.

1.3.3 Left Atria Myofiber Architecture

The relationship between left atrial structural pathways and electrical function during persistent AF has not been fully characterised. Wavefronts with preferential activation direction have been demonstrated during re-entrant arrhythmias, and structural determinants suggested to be implicated.⁷⁵ Electrical conduction from the PVs has also been correlated with anatomic features in canine atria.⁷⁶ Similarly, the branching sites of the crista terminalis and pectinate muscles of the right atrium have been linked to causation of breakdown of wave propagation into fibrillatory conduction.⁷⁷

Until recently, myofiber orientation has been determined by destructive sectioning with visually observed tracings or photography. More recently a technique has been developed which allows the myofiber architecture of the human left atrium to be imaged using diffusion tensor magnetic resonance imaging (DTMRI) at the submillimetre level.⁷⁸ This has allowed an unprecedented insight in to the structure of the LA. This technique has been used by Pashakhanloo *et al.* to image the entire intact human heart of 8 specimens *ex vivo*. On average, the MRI scan time was approximately 50 hours per specimen using a 3T clinical scanner. They observed the existence of a LA coordinate system in 7 of the 8 specimens based on the PV origins, where major fibre bundles run in the same orientation (Figure 1-11). Similar observations of fibre orientation had been made in the 1960s using dissection and visual tracings of the PVs of 16 post mortem hearts.⁷⁹ Therefore, a detailed understanding of the LA structure, down to the level of myofiber orientation might be beneficial in understanding the mechanisms responsible for maintenance of persistent AF and possible ablation strategies.

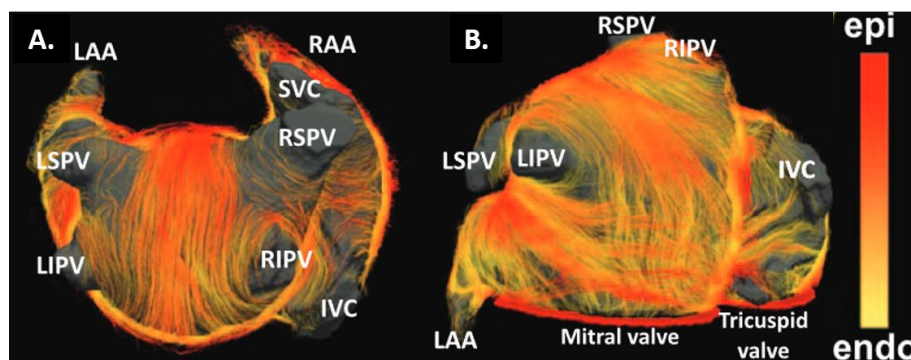


Figure 1-11. Atrial geometry and myofiber orientation have been defined by DTMRI. (A) A posterior view of the roof and posterior wall, and (B) inferior and left lateral view are shown. Colour coding is applied to identify the local distance of the myofiber to the endocardial shell; the epicardial layer is red, and the endocardial later is yellow. Adapted from Pashakhanloo *et al.*⁷⁸

1.4 Alternative Ablation Targets

Catheter ablation is less effective for persistent AF (AF duration lasting more than 7 days) compared to paroxysmal AF (AF duration lasting less than 7 days, with spontaneous reversion to sinus rhythm).⁸⁰ This is presumably due to the progressive structural, electrical, and mechanical changes associated with an increasing duration of AF. Furthermore, ablative strategy in persistent AF often has limited scientific justification, and is largely empirically

based. Techniques commonly include linear ablation, and targeting of fractionated electrograms; neither of which has any demonstrable incremental benefit in maintaining sinus rhythm.⁷

Recent attention has been heavily focused on the identification and ablation of focal sources. Use of novel tools to identify focal sources have been hampered either by dye toxicity in humans with optical mapping techniques, or complex mathematical algorithms using phase analysis to infer activation, rather than actually mapping true activation. Despite this, there has been some initial success with acutely terminating persistent AF during ablation of 'rotors' identified by Focal Impulse and Rotor Modulation (FIRM) mapping.^{45,49} FIRM guided ablation has suffered from a lack of reproducibility in the hands of others, with poor outcomes in long term maintenance of sinus rhythm.⁸ Similarly, termination of persistent AF has been demonstrated with ablation of CFAEs⁸¹⁻⁸³, suggesting that they contain either focal triggers or micro re-entrant circuits. The reproducibility of this technique has also proven challenging.^{7,}

81

In contrast to many modern theories for maintenance of AF, the multiple wavelet hypothesis⁵³ has still not been scientifically rejected. It seems somewhat hasty to suggest novel mechanistic theory when one is yet to prove or disprove a hypothesis dating back half a century. Recent support for the multiple wavelet hypothesis came from detailed activation mapping studies²⁷ and the observation of endo-epicardial dissociation³¹ demonstrating multiple self-perpetuating and randomly propagating wavelets. These studies have been reliant on more traditional activation mapping during AF.

1.4.1 Complex Fractionated Atrial Electrograms

CFAE ablation was based on the assumption that areas of myocardium with such electrical activity may be acting as drivers of persistent AF. Identifying which were true drivers of AF was challenging. Ablation of some CFAEs resulted in prolongation of the AF cycle length suggesting their importance in contributing as a driver, while others had no effect on cycle length at all.

Early studies by Konings *et al.*²⁶ showed that CFAEs observed during intraoperative mapping in human AF were mainly in areas of slow conduction and/or regions of functional block where wavelets pivot. They were thought to represent either continuous re-entry of fibrillation, or areas where multiple different wavelets enter the same area. In 121 patients,

Nademanee *et al.*⁸⁴ used electroanatomical mapping to tag and ablate CFAEs. They identified specific regions that were more likely to contain CFAEs, successfully ablating 115 of the 121 patients to sinus rhythm, without the need for external cardioversion. Despite these encouraging results, others have not been able to replicate this. Oral *et al.* undertook solely CFAE ablation in 100 patients with persistent AF, reporting only 33% of patients maintaining sinus rhythm off medical therapy at a mean follow-up time of 14 months.⁸⁵ Furthermore, the BOCA study suggest that not only did adjunctive CFAE ablation confer no additional benefit in maintaining sinus rhythm, but it significantly increased the incidence of both organised atrial tachycardia, and gap-related macro-re-entrant flutter.⁸⁶

Most recently, the STAR-AF II trial reported no additional benefit of CFAE ablation in addition to PVI for patients with persistent AF.⁷ The variability in definition of CFAE may in part be responsible for the large disparity in results from catheter ablation, or the variability of operator experience with CFAE ablation. While some have defined CFAEs based on only simple visual descriptions⁸⁴, others have produced a more comprehensive visual classification system⁸⁷, or characterisation using automated algorithms.⁸⁸ There are certainly observations that support CFAE ablation resulting in acute organisation of AF, and in some cases termination. However, there are no consistently reproducible data that prove long-term adjunctive benefit.

A recent meta-analysis of the efficacy of driver-guided catheter ablation for AF has demonstrated mixed results. A variety of different driver guided ablation strategies were used, including CFAE, FIRM, and high frequency source ablation. Four studies within the meta-analysis suggested increased single-procedure freedom from AF/AT at ≥ 1 year (RR 1.34, 95% CI 1.05-1.70; P = 0.02).^{44, 89-91} However, after excluding cases of driver-guided ablation without PVI this was no longer significant (RR 1.41, 95% CI 0.96-2.08; P = 0.08).

Four studies also reported a higher proportion of acute AF termination with driver-guided ablation compared to controls (pooled RR 2.08, 95% CI 1.43-3.05; P <0.0001).^{44, 89, 91, 92} This increased to a RR 2.90 (95% CI 1.152-5.55, P = 0.001) after excluding patients undergoing driver-guided ablation without concomitant PVI.^{44, 89, 92} Although this is promising, the meta-analysis included primarily nonrandomised studies of moderate quality, making results difficult to interpret. Interestingly, the only two full randomised controlled trials^{89, 92} in the meta-analysis, did show greater acute AF termination with driver-guided ablation. Atienza *et al.*⁸⁹ found that driver-guided ablation was non-inferior to PVI in achieving freedom

from AT/AF at 12 months in patients with PAF, however there was no benefit when combined with PVI in patients with persistent AF. In contrast, Lin et al.⁹² reported greater freedom from AF/AT at 17.7 ± 8.2 months in patients that had undergone PVI with driver-guided ablation, rather than PVI with CFAE ablation.

Current electroanatomical mapping systems have incorporated algorithms to map fractionation. There has been uncertainty over the stability of CFAEs, and no clear consensus on the optimal amount of time for data acquisition. The CFAE mapping algorithm in CARTO produces CFAE mean maps from data acquired over a period of 2.5 seconds, while Ensite Precision allows the user to determine the duration which can range from 1 to 8 seconds. CFAE mean is defined as the average time duration between consecutive deflections during a specific time period at a recording site. A study by Stiles *et al.*⁸⁸ reported that at least 5 seconds of electrogram data acquisition was required to accurately characterise CFAE sites. Shorter durations resulted in unacceptable error rates which could lead to misinterpretation and inappropriate ablation.

1.4.2 Spectral Analysis

The heterogeneous nature of CFAE sites prompted alternative methods for identification of high-frequency activation. Targeting of high-frequency activation is based on the assumption that they represent either localised re-entry or focal sources. Analysis of electrograms within the frequency domain is thought to distil information on local activation which is too challenging to interpret in the time domain, as it is with CFAEs.

For analysis of electrograms within the frequency domain to be made possible, the Fourier transform is applied (Figure 1-12). This transform decomposes continuous signals to a sum of weighted sinusoidal functions. Doing so allows the frequency of the largest peak in the spectrum to be identified – the dominant frequency (DF) – which is used as a surrogate for the average activation rate at that location.

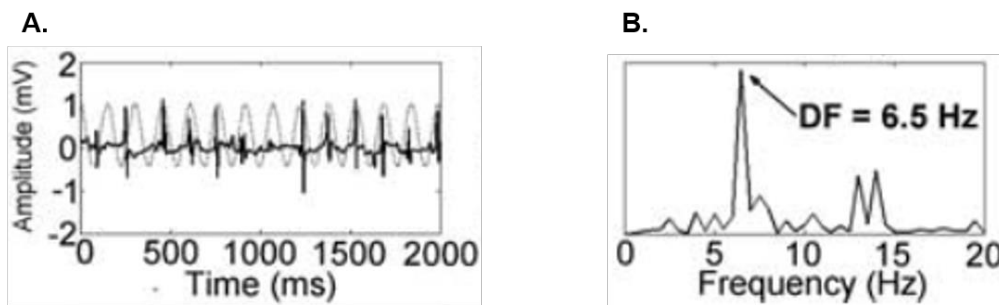


Figure 1-12. (A) Bipolar electrograms are displayed in the time domain before undergoing analysis with the Fourier transform. Following spectral analysis (B), the frequency distribution is appreciated, with the tallest peak representative of the dominant frequency. Adapted from Ng *et al.*⁹³

Spectral analysis in paroxysmal AF has demonstrated that high dominant frequency sites co-localise with PV junctions.⁹⁴ Furthermore, a gradient has been identified from the left to right atria, indicating drivers within the left atrium.⁹⁵ However, in persistent AF the distribution of sites with high dominant frequency is more widespread, with locations predominantly beyond the pulmonary veins.⁹⁴ Targeting sites of high dominant frequency has suffered a similar fate to CFAE ablation, with variable reported outcomes with regard to its benefit.⁹⁶ This may be related to incorrect interpretation of locations with apparently high dominant frequency that are actually the result of wavefront collision. Furthermore, there is debate surrounding the spatiotemporal stability of dominant frequency locations,⁹⁷ limiting its clinical application.

1.5 Induced and Spontaneous Atrial Fibrillation

It is likely that there are significant differences between induced and spontaneous AF. These two distinct groups have been studied to extrapolate and explain the electrophysiologic changes that further promote AF.^{98,99} Further research has identified differences surrounding the complexity of atrial activation patterns and organisation characteristics.^{27, 100}

Using a canine model, Sih *et al.*¹⁰⁰ identified major differences between acutely induced AF and a chronic pacing induced model of AF. The LA of dogs in the chronic AF group had a significantly shorter LA cycle length (mean CL over 10 seconds) compared to the RA. In dogs with induced AF, there was no significant difference between the LA and RA cycle length. Activation mapping of the LA also showed predominantly repetitive broad wavefronts of

activation in induced AF, and more complex activation in chronic AF dogs. However, induced AF episodes was only required to last 15 seconds in order to be acceptable for analysis. Furthermore, data was analysed after exclusion of just 2 seconds following AF induction, and 2 seconds before AF termination. Immediately following AF induction, it is common to see organised wavefronts that can persist for several seconds.¹⁰¹ Similarly, increased organisation is frequently seen significantly longer than 2 seconds prior to spontaneous termination of AF. It is therefore conceivable that the waiting time before mapping was insufficient. Additionally data too close to the time of spontaneous AF termination was included. This would have a significant impact on organisation characteristics of the wavefronts observed during mapping. Interestingly, other groups have not observed consistent differences between the left and right atria during induced AF in humans.²⁷

1.6 Activation Mapping

1.6.1 Determining Local Activation Time

Identifying the point of local activation is not a trivial task. This is made significantly more challenging during AF. In normal homogeneous myocardial tissue, the first peak of a bipolar electrogram is a reasonable approximation of activation time at the electrode pair. For the unipolar electrogram, the maximum negative slope is a good indicator of local activation.¹⁰² The unipolar and bipolar electrogram is further discussed in Section 1.7.

During AF, double potentials and fractionated electrograms present greater challenges regarding the correct electrogram component to define as local activation. Double potentials occur at sites of slow conduction or conduction block, where electrical activity is recorded from both sides of the line. Fractionated electrograms result from regions with heterogeneous conduction properties, such as fibrosis. Regions of fibrosis result in a reduced electrogram amplitude, which compounds the challenge of correct identification of local activation time (LAT).

1.6.2 Isochronal Mapping

Isochronal mapping is conventionally applied to rhythms with a regular cycle length. Electrograms are recorded from multiple different location across the cardiac surface. Each electrogram is assigned with a relative LAT to a fixed reference signal (also referred to as a fiducial signal). This is either a surface ECG component, or electrogram that is related to the

chamber being mapped. Electrograms with a similar LAT are grouped according to their relative timings, and assigned a colour to enable visual interpretation of activation times.

In situations where there is a regular cycle length, the relative timing of electrograms collected across the cardiac surface can be used to infer the activation pattern. Its application for mapping AF is precluded by the constant cycle length variability. However, it is possible to create isochronal maps for individual uniform wavefronts (see Chapter 2). For an isochronal map to be created, and correctly interpreted, a number of steps are involved¹⁰³:

1. Stability of the catheter, and good electrode contact.
2. Appropriate choice of reference: It is conventional that when mapping the atria or ventricles, a reference related to that chamber is used. This reference must also be spatially stable as it is being used to identify the relative timings of points collected.
3. Sufficient density of points: The colour projection on to the anatomical shell involved interpolation between the points of data collection. The extent of interpolation is user defined, however it is important to recognise that the colouring extends beyond the boundaries of the location at which the electrogram recording was made. If interpolation is not appropriately set, the map may not be a true reflection of activation.
4. Appropriate assignment of LAT: The correct electrogram component must be identified, and also the LAT correctly assigned within the complex.

The Window of Interest

The purpose of a window of interest is to ensure that electrograms from the same beat of tachycardia are compared. Typically, a window of interest is set at 90% of the tachycardia cycle length. It is only possible to set a single window of interest for each map, and relies upon the variability in cycle length of the tachycardia being no more than approximately ± 20 ms. In many atrial tachycardias, for example, there is a repeating sequence of electrograms with a relatively consistent cycle length. Cycle length variability underpins the main obstacle to isochronal mapping during AF.

1.7 Recording Cardiac Electrograms

The intracardiac electrogram is used by clinical electrophysiologists as a signal for timing local electrical events, determining wavefront propagation direction, and morphologically as a

surrogate marker of the underlying endocardial substrate. Electrograms are generated by small potential differences that result from transmembrane ion flux throughout the myocardial action potential. These potential differences can be measured by unipolar and bipolar configurations, from electrodes conventionally between 1-4mm in diameter, and variable inter-electrode spacing. The advent of multipolar mapping catheters has greatly increased the amount of information that we can collect, however the interpretation of these electrograms is fundamental to understanding arrhythmias.

1.7.1 Unipolar Electrograms

Unipolar recordings are obtained by measuring the potential difference between an intracardiac exploring electrode, and a second electrode distant from the heart; the indifferent electrode. Wilson's central terminal is frequently used as the indifferent electrode. It is formed by connecting the left and right arms, and left leg electrodes through high impedance resistors. This can result in unacceptable electrical noise, which can be reduced by selecting an alternative indifferent electrode, such as an intravascular electrode remote from the heart.¹⁰⁴

As a wavefront propagates towards the exploring electrode, a positive electrogram deflection is formed. Once the wavefront reaches the exploring electrode and begins to travel away, a steep negative deflection occurs (Figure 1-13). The maximum negative slope ($-dV/dt$) approximates to the local arrival of the wavefront directly under the exploring electrode. This is the LAT annotation point.

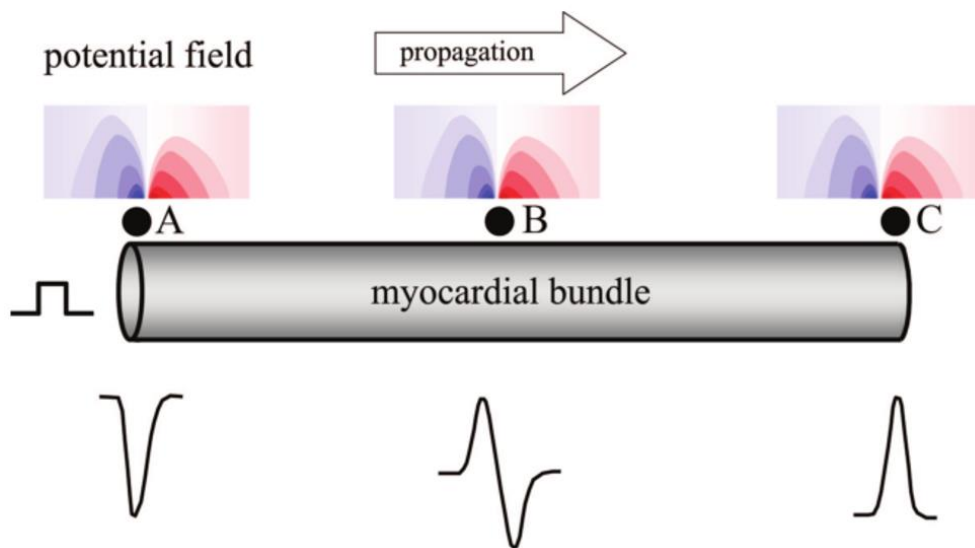


Figure 1-13. Unipolar electrogram created by a wavefront propagating across a myocardial bundle. Activation starts at the left (A) reflected by a negative electrogram with a QS morphology. A biphasic electrogram is created (B) as the wavefront propagates towards, and subsequently away from the electrode. As it continues towards the right (C) there is a positive deflection. Colour maps are displayed above which show the potential field generated by the wavefront. Reproduced from de Bakker *et al.*¹⁰⁵

The unipolar electrogram morphology can be exploited to gain additional information. When an electrogram has a QS morphology it can be used to identify the location of focal tachycardias, and accessory pathway localisation during anterograde conduction.¹⁰⁴

The unipolar configuration does have its disadvantage, as it contains far-field signal generated by myocardial tissue remote to the exploring electrode. Electrical interference can usually be easily mitigated by selecting an alternative indifferent electrode, as previously described.

1.7.2 Bipolar Electrograms

Bipolar recordings are made from a pair of electrodes located on the same catheter, exploring the region of interest.¹⁰⁶ It has better spatial resolution than unipolar recordings, and can be improved by using narrowly spaced electrodes. The bipolar electrogram is formed by the summation of the potential from the positive and negative input. The far-field signal is largely subtracted out, with only local signal remaining.

In normal homogeneous tissue, the initial peak of a bipolar electrogram coincides with LAT beneath the recording electrode pair (Figure 1-14).

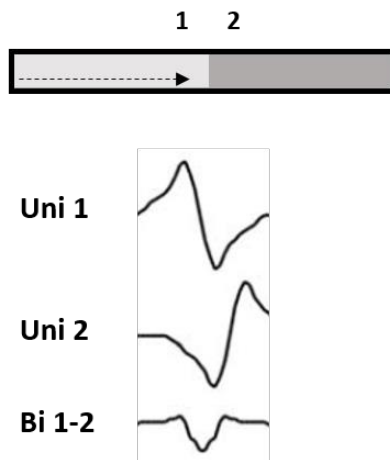


Figure 1-14. Schematic diagram of a bipolar electrogram recording with corresponding unipolar electrograms. Electrode positions are numbered 1 and 2. As the wavefront propagates from left to right (arrow) a delay between the two unipolar electrograms (Uni 1 and Uni 2) is apparent, due to the time difference in the signal arriving at the electrodes. Uni 2 is an inversion of Uni 1 due to the wavefront direction. Addition of the two unipolar signals results in the bipolar signal (Bi 1-2), and removal of far-field signal. Adapted from Stevenson *et al.*¹⁰²

In other situations, additional information about the underlying substrate can be gained, although assignment of LAT can be more difficult (Figure 1-15).

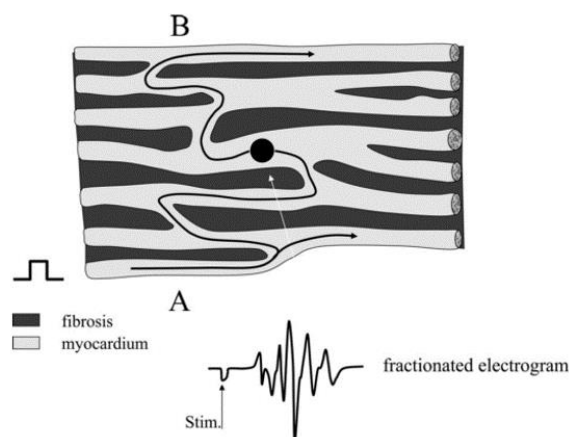


Figure 1-15. Schematic diagram of the effect of fibrosis on the bipolar electrogram. A stimulation at position A begins a wavefront of activation. The wavefront takes a meandering pathway towards its destination (B) due to the effects of fibrosis slowing conduction. The resulting electrogram shows fractionation due to the course of the wavefront. Reproduced from de Bakker *et al.*¹⁰⁵

1.7.3 Filtering

To emphasise components of the electrogram that correspond to activation, filtering is applied. Different types of filter can be applied, which include high pass, low pass, band pass, and notch filters.

A high pass filter eliminates components below a given frequency, while a low pass filter eliminated components above a given frequency. A band pass filter restricts the frequency by setting an upper and lower limit, retaining only the frequencies between this range. In some specific situations, it may be desirable to eliminate a specific frequency. A notch filter is applied for this purpose. The most common notch filter to be applied is for the elimination of mains electrical interference (50Hz).

Intracardiac bipolar signals are typically filtered with a high pass filter of 30-50Hz, and a low pass filter of 250-300Hz. In contrast, unipolar signals are filtered with a high pass filter of 1-2Hz, and a low pass filter of 300Hz.

1.8 Chaos Theory

Chaos theory is an area of mathematics that focuses on highly sensitive dynamical systems. It is a relatively new area due to its heavy reliance on significant computational power. Chaos has the outward appearance of apparent randomness, however there are in fact underlying, repetitive patterns. We are surrounded by natural chaotic systems in our everyday lives, such as road traffic and climate. AF is frequently described as being completely random, with support offered by the multiple wavelet theory.⁵³ However, if the electrical activation patterns are a manifestation of an underlying stable mechanism, they may possess features consistent with chaotic behaviour. Understanding the mechanisms responsible for chaotic behaviour in a system is important, as it is possible that by altering the underlying mechanism, we can eliminate undesirable chaos. Chaos theory has been applied to many chaotic systems that we depend on, such as weather forecasts.

Weather systems can seemingly be random, as it results from multiple different parameters and conditions that depend on one another, similar to AF. Atmospheric convection results from temperature differences in the atmosphere. The different rates at which Earth's temperatures change within dry and moist air result in instability. During the day, air mixing expands the atmospheric boundary layer height – the lowest part of the atmosphere. This results in increased winds, cloud development, and decreases the

temperature to which air must be cooled to become saturated with water. Subsequently, moist convection leads to thunderstorms responsible for severe weather changes. Without understanding of these underlying mechanisms, changes in weather conditions can have the appearance of completely random behaviour rather than chaotic behaviour.

Edward Lorenz developed a mathematical model for atmospheric convection.¹⁰⁷ This enabled weather to be predicted for short durations ahead, revealing that although weather appears chaotic, it is not random. The effect of small rounding errors within calculations from initial conditions become more divergent over longer periods, making distant predictions less accurate. This is frequently referred to as the 'butterfly effect' or 'deterministic chaos'; i.e. a small change in one place (a butterfly flapping its wings in China) of a deterministic nonlinear system will result in a large change elsewhere (a hurricane in London).

The question of whether cardiac fibrillation – atrial or ventricular – is chaotic has been investigated, but with mixed results.^{108, 109} However, the mathematical equations representing the spatiotemporal phenomena are more complex than purely temporal behaviour. Garfinkle *et al.* used an ouabain-epinephrine-induced arrhythmia model in rabbit ventricular septum preparations to study deterministic chaos.¹¹⁰ With a custom program to detect action potentials, they recorded time intervals between spontaneous activations. An indicator of the existence of deterministic chaos was the presence of preferred directions of approach and departure. It is possible that this exists during AF, however there are no mapping systems at present that enable automated mapping of atrial activation patterns during AF. We are therefore reliant at present on manual analysis, which limits the amount of data that can be analysed. It is likely that much longer recordings of AF are required to decipher the presence or absence of chaotic behaviour. This holds important consequences, with the possibility of developing a catheter ablation technique targeted towards the key interactions resulting in the apparently random activation patterns of AF.

1.9 Hypothesis

This thesis sets out to address the hypothesis that activation during human persistent AF is not random, but is determined by the underlying mechanism. This was investigated by initially developing a new AF activation mapping technique, with subsequent evaluation of these complex activation patterns.

1.10 Scope of this thesis

In this chapter, historic and contemporary mechanisms of AF are reviewed, alongside current methods for mapping activation and surrogate markers of underlying atrial substrate. This has identified the following key issues that form the basis for the work in this thesis.

- Develop a new method to track uniform activation during atrial fibrillation without the need for a window of interest, with comparable accuracy to that of carefully adjusted manual isochronal maps.
- Avoid the need for manual assignment of local activation times.
- Display data and electrograms in a manageable way for the user to interpret.
- Determine spatiotemporal characteristics of persistent AF.
- Characterise activation patterns and types of wavefront during persistent AF.
- Create a prototype and potential workflow for analysis of clinical cases.

Atrial activation patterns were studied by using conventional multielectrode catheters to collect endocardial bipolar electrogram data from humans that were undergoing clinically indicated procedures. The methods used are described in detail in Chapter 2.

Although studies have been conducted in order to map activation during AF, they have historically been for short durations in limited regions due to the labor intensive manual analysis techniques. A stepwise approach was adopted for the development of an automated technique suitable for activation mapping during AF. Chapter 3 sets out the development and validation of this novel activation mapping technique.

In Chapter 4, the mapping technique is applied to data collected from humans during persistent AF. Data was collected from the same location at different times to determine the spatiotemporal characteristics of persistent AF. This led to the discovery that atrial activation patterns during persistent AF are not random, but display stability over time. This important discovery suggests that a sequential mapping technique employing a roving multipolar catheter is feasible.

Other research groups have demonstrated focal sources during persistent AF. On this basis, mapped locations were screened for evidence of focal activation in Chapter 5. The locations of focal activations were reviewed to investigate their relationship to AF activation maps, and new techniques developed to quantify the degree of organisation. No relationship

between focal activation location and activation pattern was identified, underlining the complexities of the mechanisms maintaining persistent AF.

Having demonstrated the absence of a relationship between focal activation and atrial activation patterns during persistent AF, the effect of PVI on activation maps was studied in Chapter 6. The only consistently demonstrable mechanism for AF has been pulmonary vein ectopy. It stands that one would expect activation maps to change following PVI, should the PVs be mechanistically important in persistent AF. Indeed, activation maps following PVI displayed increased wavefront coherence, confirming the role for PVI in the treatment of AF.

2 Methodology

2.1	Introduction.....	55
2.2	Patient studies.....	55
2.2.1	Patient selection.....	55
2.2.2	System setup and electrogram recording.....	55
2.2.3	Acquisition of bipolar electrograms.....	56
2.3	Accessing data.....	58
2.3.1	Exporting data from Ensite Precision.....	58
2.4	Endocardial electroanatomical mapping during atrial fibrillation.....	58
2.4.1	Bipolar Voltage Maps.....	58
2.4.2	Complex Fractionated Atrial Electrogram Maps.....	59
2.4.3	Isochronal Maps.....	60
2.5	Development of a new signal processing algorithm to map human atrial fibrillation: Representation of Electrical Tracking on an Orbital Map (RETRO-Map).....	61
2.5.1	Tracking Wavefronts.....	61
2.5.2	Automation of Wavefront Tracking.....	62
2.5.3	Choropleth Maps.....	63
2.6	Conclusion.....	64

2.1 Introduction

The first part of this chapter describes the methods used for collection of clinical data. Following this, there is a brief description of the methods used to develop custom software to map activation during atrial fibrillation. The purpose of this research was to develop a tool that removes the requirement for the laborious manual analysis techniques observed in historical AF mapping literature. This will allow longer durations of AF over larger surface areas to be mapped, with the aim of gaining mechanistic insight.

2.2 Patient studies

2.2.1 Patient selection

Patients with a history of symptomatic atrial fibrillation that were undergoing clinically indicated procedures were recruited (in accordance with published guidance from the AHA/ACC/HRS/ESC). The study was approved by the Local Research Ethics Committee, and written informed consent obtained from all patients.

2.2.2 System setup and electrogram recording

Procedures were performed in a catheter laboratory routinely used for clinical electrophysiology procedures. All procedures were conducted in the post-absorptive state under general anaesthesia, with appropriate patient monitoring. Following general anaesthesia, all patients underwent trans-oesophageal echocardiography (TOE) to exclude left atrial appendage thrombus. TOE was also used to assist with transseptal puncture. A deflectable decapolar catheter (Inquiry™, St Jude Medical, St Paul, MN, USA) was positioned in the coronary sinus as a spatial reference, for recording of electrograms, and pacing if required.

A single transseptal puncture was made using a Brokenbrough needle via an SLO sheath under fluoroscopic guidance. Unfractionated heparin was administered after transseptal puncture, and an activated clotting time of around 300 was maintained throughout the procedure.

Data was collected using the Ensite Velocity cardiac mapping system (Abbott, Chicago, Illinois, USA. Formerly St Jude Medical, St Paul, MN, USA) between 3/3/2016 and 12/10/2016 date. An updated version of this mapping system was released following this date, and all subsequent data was collected using Ensite Precision. For the purposes of this thesis,

reference will only be made to Ensite Precision, which will include data collected from both software versions.

Following transseptal access, left atrial and pulmonary venous geometry were collected using a roving 20-pole spiral double loop catheter (Inquiry™, AFocusII™, Abbott/St Jude Medical; 4mm inter-electrode spacing, 20mm fixed loop diameter) via the SLO sheath. Ablation was undertaken at the operator's discretion, and in accordance with the clinical requirements for each patient, using the TactiCath™ catheter (Quartz, Abbott/St Jude Medical) via a deflectable long sheath (Agilis™ NXT Steerable Introducer, Abbott/St Jude Medical).

2.2.3 Acquisition of bipolar electrograms

The AFocusII catheter was chosen because of its double loop configuration. Other spiral shaped catheters (e.g. Lasso Catheter, Biosense Webster, California, USA) lack electrodes central to the mapping field, as they are primarily designed to be used for mapping pulmonary vein signals. The AFocusII has superior coverage of the mapping area central to the catheter, due to its central electrode. The shaft of the catheter is also in a centralised position, which allows the catheter to be placed on the endocardial surface 'en face' with relative ease (Figure 2-1).

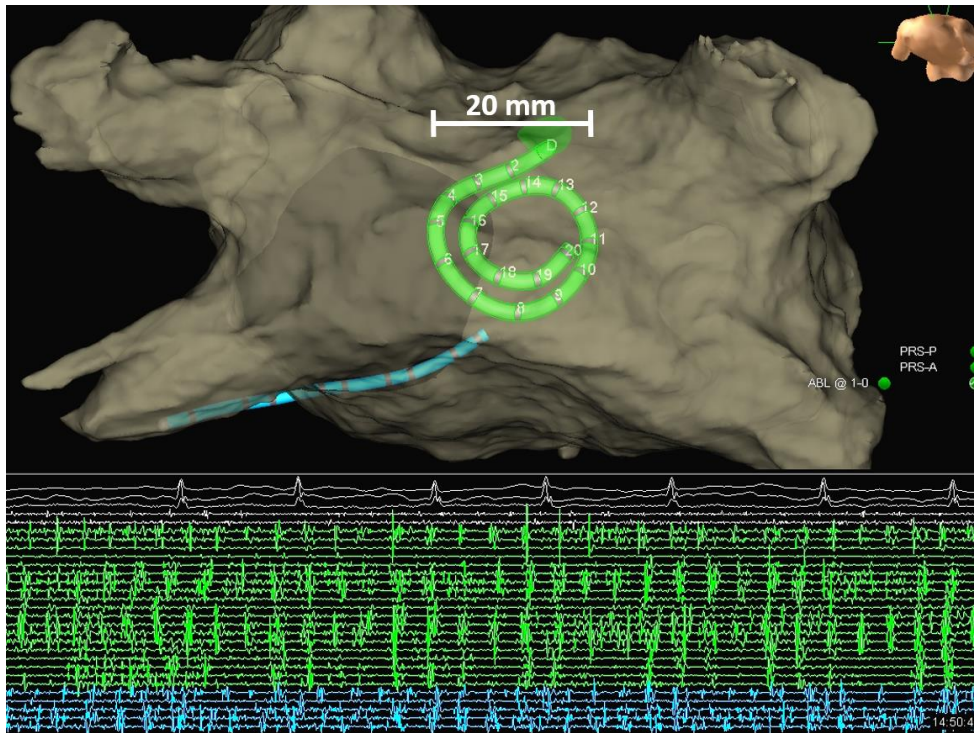


Figure 2-1. Graphical user interface for Ensite Precision. A shadow of the spiral shaped AFocusII catheter is shown in the middle of the posterior wall of the left atrial geometry. The decapolar catheter is positioned in the coronary sinus. Bipolar electrograms are displayed below from the AFocusII (green), decapolar catheter (blue) and TactiCath ablation catheter (white), with three surface ECG leads directly above (white).

The AFocusII multipolar catheter was used to acquire intracardiac bipolar electrogram data in all cases. Ensite Precision allows bipolar data to be recorded from multipolar catheters in two bipolar configurations:

1. Paired bipoles, using electrodes 1-2, 3-4, 5-6, and so on
2. All bipoles, using electrodes 1-2, 2-3, 3-4, and so on.

The ‘all bipoles’ setting was used to allow 19 simultaneous bipoles to be recorded in each location, thereby maximising data points and resolution.

Electrograms were recorded from the AFocusII by holding the catheter in a stable left atrial position for 30 seconds in each location to create each ‘data segment’ for analysis. The recording position of each data segment was documented by projecting a catheter shadow

on to the left atrial geometry surface. Following this, the catheter was moved to a different location and the process repeated.

2.3 Accessing data

2.3.1 Exporting data from Ensite Precision

Following completion of each clinical procedure, data was exported for offline analysis with custom software. Data segments consist of electrode location and bipolar electrogram data for each recording position. The relative positions of electrodes from a multipolar catheter are represented as a matrix of x , y , and z coordinates in Ensite Precision. These coordinates are spatiotemporally relative to one another and have a sampling frequency of 1034.5Hz. Bipolar intracardiac electrograms were band-pass filtered at 30-500Hz during clinical procedures. A 'raw', unfiltered data file of bipolar electrograms is exported from Ensite Precision for offline analysis using custom software.

2.4 Endocardial electroanatomical mapping during atrial fibrillation

2.4.1 Bipolar Voltage Maps

Based on previous studies¹¹¹, mean peak-to-peak voltage maps become stable with an 8 second sampling time. The constant variability in electrogram amplitude means that shorter durations are not an accurate representation of mean voltage. A dedicated platform with a research version of Ensite Precision (version 5.2R) was used to create mean peak-to-peak bipolar voltage maps from an 8 second sampling window in each recording location (Figure 2-2). This function is not available on the clinical version of the mapping system. The first 8 seconds of each data segment was used to produce the voltage map for each location mapped.

The following settings were applied to the atrial bipolar electrograms acquired using the AFocusII catheter for mean peak-to-peak voltage: EGM width <10ms, to avoid detecting far-field electrograms; EGM refractory period 50ms; peak-to-peak sensitivity 0.08mV, to avoid sensing noise; interpolation set to 10mm and interior projection 5mm, as surrogate markers to exclude insufficient electrode contact.

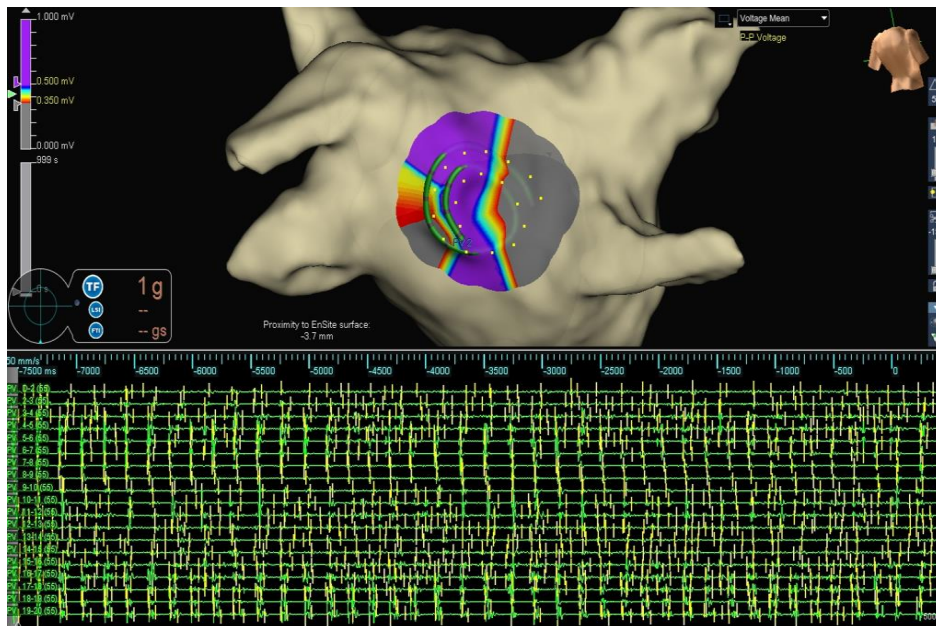


Figure 2-2. Electrograms are acquired to create an 8-second mean peak-to-peak bipolar voltage map. The AFocusII position is shadowed on the mid posterior wall of the left atrial geometry during acquisition of electrograms for each data segment. Eight seconds of electrogram data are displayed below (green). Electrograms are annotated with yellow markers in accordance with the pre-set criteria previously described. The mean voltage is visually displayed by assignment of a colour spectrum.

2.4.2 Complex Fractionated Atrial Electrogram Maps

A standard algorithm available on the clinical version of Ensite Precision was used to create CFAE maps. The mean interval between the multiple deflections over an 8 second period of time (CFAE_{mean}) was calculated for each mapped location, and a colour map of the CFAE_{mean} projected on to the LA geometry (Figure 2-3). Areas of CFAE were defined based on previous research as sites with a CFAE_{mean} of 80-120ms.⁸⁴ The following settings were applied to the CFAE_{mean} tool: CL 80-120ms, defining the typical CFAE range; EGM width <10ms; EGM refractory period 50ms; peak-to-peak sensitivity 0.08mV; interpolation set to 10mm and interior projection 5mm.

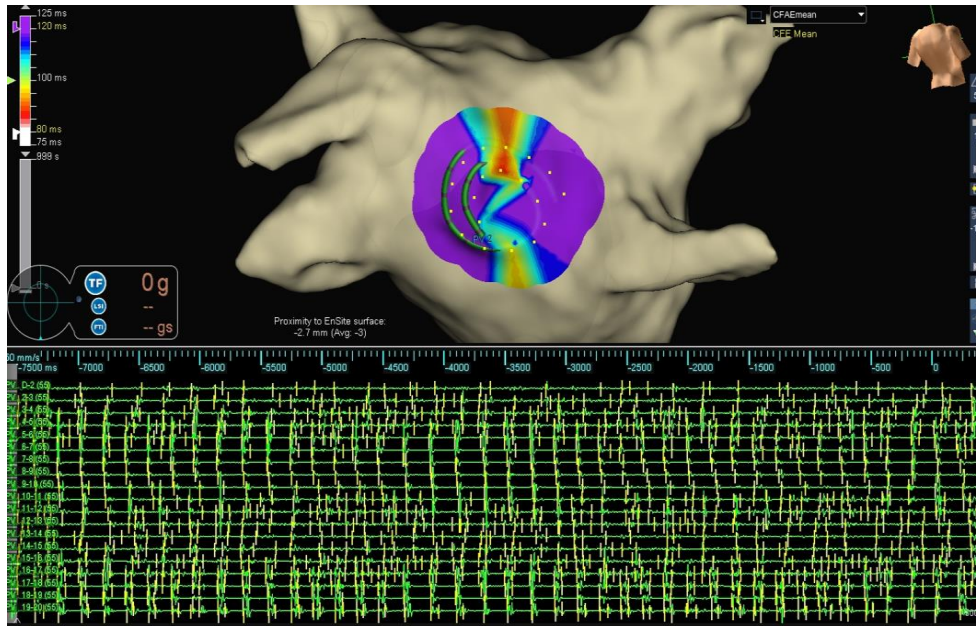


Figure 2-3. Electrograms are acquired to create an 8-second CFAEmean map. The AFocusII position is shadowed on the mid posterior wall of the left atrial geometry during acquisition of electrograms for each data segment. Eight seconds of electrogram data are displayed below (green). Electrograms are annotated with yellow markers in accordance with the pre-set criteria previously described. The CFAEmean is visually displayed by assignment of a colour spectrum.

2.4.3 Isochronal Maps

This technique is typically reserved for mapping activation across a cardiac surface during rhythms with a regular cycle length. The constant variation in cycle length and electrogram amplitude during AF precludes its use in the conventional sense. Although it is not practically convenient, it is possible to create an isochronal map using Ensite Precision during AF. This was done to validate the activation sequence observed with RETRO-Mapping against a recognised and established technique.

In each validation example, a wavefront was identified using RETRO-Mapping. The same wavefront was identified in Ensite Precision. A window of interest was manually set to include only the electrograms from that single wavefront. LAT was assigned to each electrogram using a validated algorithm (first deflection) incorporated on the Ensite Precision mapping system (Figure 2-4).

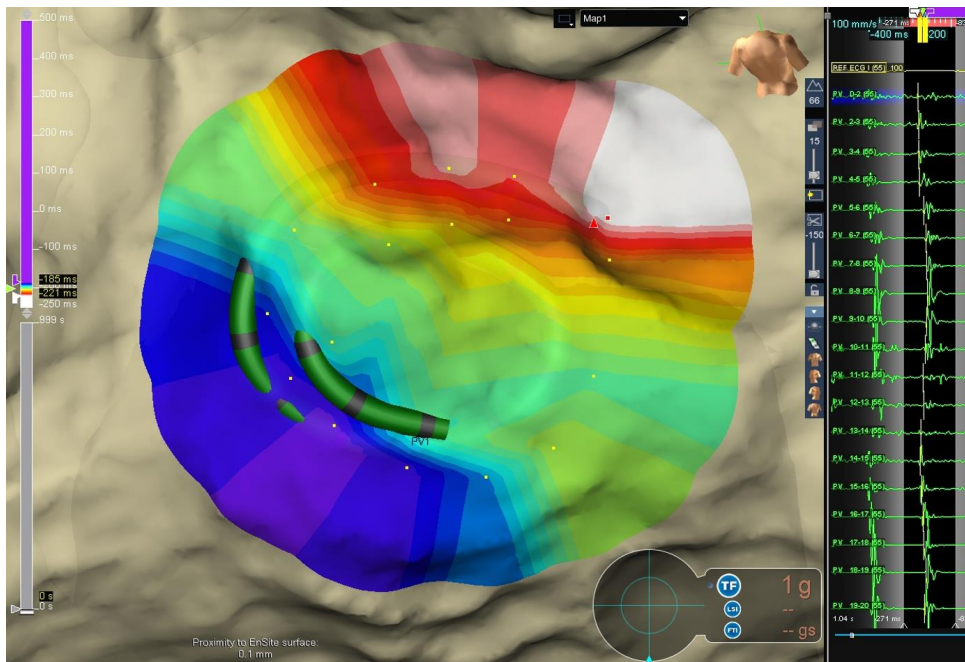


Figure 2-4. Isochronal map of a uniform wavefront during AF. Electrograms are acquired during AF, and the AFocusII catheter position shadowed on the left atrial geometry. A window of interest has been set around a single wavefront (electrograms to the right). LAT is marked on the bipolar electrograms in yellow in accordance with the pre-set criteria previously described. The activation sequence is visually displayed by assignment of a colour spectrum. White is assigned to the earliest activation, moving through the colour spectrum to purple which is the latest activation time.

2.5 Development of a new signal processing algorithm to map human atrial fibrillation: Representation of Electrical Tracking or Origin Mapping (RETRO-Mapping)

The RETRO-Mapping algorithm underwent systematic stages of validation. This is described in detail in the relevant chapter (see Chapter 3).

2.5.1 Tracking Wavefronts

A custom platform (RETRO-Mapping) was developed to post-process large amounts of data that have been acquired during atrial fibrillation. Data was acquired using a commercially available electroanatomical mapping system – Ensite Precision – from multiple locations of the left atrium with the AFocusII multipolar catheter.

Software for RETRO-Mapping has been designed with the specific intention to identify uniform wavefronts that occur during atrial fibrillation (see Chapter 3 for detailed

explanation). Data from each recording location is exported from Ensite Precision for analysis in RETRO-Mapping. The frequency of mean activation is identified in each direction and displayed on an orbital plot.

A graphical user interface (GUI) has been developed to show a 2-dimensional representation of the AFocusII catheter. Electrodes that are not activated are displayed on a green background, while the activating wavefront is represented by a colour change to purple (Figure 2-5). The change in colour is to aid in visualisation of electrical activation only, and does not provide information on repolarisation characteristics. The user is able to corroborate the activation patterns observed in the GUI with the intracardiac electrograms displayed alongside. Activation can be played back at different speeds, defined by the user. This type of map is referred to as a RETRO-Propagation Map (RETRO-PM).

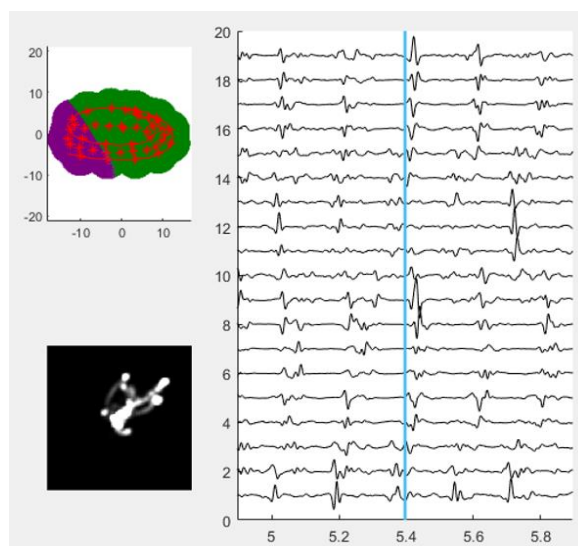


Figure 2-5. GUI of RETRO-Mapping. (Right) Bipolar electrograms collected using the AFocusII in Ensite Precision are displayed in the GUI. A timing line (blue) enables the relative timing of electrograms to be easily appreciated. (Top left) The AFocusII catheter is displayed as a red spiral. Non-activated electrodes are displayed on a green background, and activated electrodes are assigned purple (RETRO-Propagation Map). (Lower left) A white dot moves from the centre of the plot in the direction of mean wavefront activation in the wavefront vector plot.

2.5.2 Automation of Wavefront Tracking

Custom software was written to enable automated tracking of wavefronts. The space underlying the AFocusII catheter is triangulated to produce a fine 2-dimensional grid. As

activating wavefronts pass across the catheter, the activation direction of the triangulated segments can be used to identify the mean activation direction of that wavefront. A display window shows a plot with a dot moving in the direction of mean activation (Figure 2-5). The distance the dot moves from the centre of the plot is related to the uniformity of the wavefront – the further the dot moves from the centre of the plot, the more uniform the wavefront. This is referred to as the wavefront RETRO-Automated Direction (RETRO-AD), where the average wavefront direction in the catheter locality can be assigned, and magnitude (distance the dot moves) represents the uniformity.

A constant record of wavefront vectors is retained by the custom software. This data is displayed on an orbital plot to allow a summary of all activation from a mapped location to be appreciated. The orbital plots produced from RETRO-AD were validated against orbital plots produced from manually assigned activation directions.

2.5.3 Choropleth Maps

Following offline analysis using RETRO-Mapping, a choropleth map was produced for each patient. A choropleth map is typically a map used to display geographical data using differences in colour, shading or symbols to indicate values of a specific measure, enabling all regions to be compared and viewed simultaneously on a single map.

Each analysed data segment is displayed on an orbital plot. By re-projecting the orbital plots for all mapping location on to the Ensite Precision LA geometry, activation patterns of neighbouring locations can be appreciated (Figure 2-6).

Data that has been analysed using RETRO-Mapping, and displayed as a choropleth map, is referred to as a RETRO-Choropleth Map.

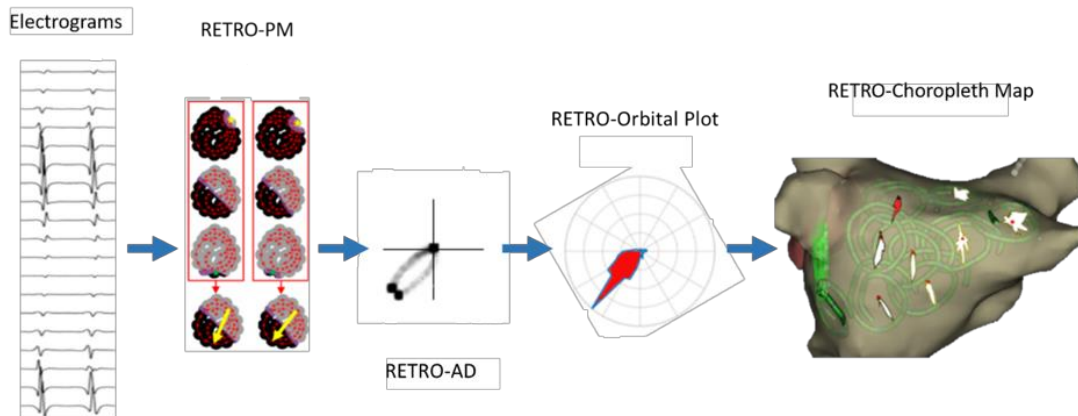


Figure 2-6. Assignment of direction of uniform wavefronts. (Left to right) Exported bipolar electrograms from an AFocusII catheter are displayed distal (top) to proximal (bottom). Graphical representation of the AFocusII catheter (red spiral) with 2 consecutive uniform wavefronts. Colour coding is applied to the catheter as the activating wavefront (grey) propagates. The earliest (yellow star) and latest activating (green star) electrodes have been marked and a yellow arrow manually applied to assign the direction of activation on the RETRO-PM (RETRO-Propagation Map). An automated plot identifies the mean wavefront direction in the RETRO-Automated Direction (RETRO-AD) of the same uniform wavefronts. The black dot (colour inverted to aid visualisation) moves from the centre to the magnitude of uniformity. A continuous record of all areas the dot has moved is used to create a summative image on an orbital plot. Each orbital plot is projected on to the left atrial geometry to build a RETRO-Choropleth Map.

2.6 Conclusion

The methods involved in this research have been outlined in this chapter. Further and more detailed explanations of these methods are provided in the following relevant chapters.

3 Development and validation of a new mapping technique

3.1	Introduction.....	66
3.2	Methods	67
3.2.1	Patient Selection and Procedural Technique	67
3.2.2	Data Collection and Export.....	67
3.2.3	Algorithm Development	68
3.2.4	Automation of Wavefront Tracking.....	73
3.2.5	Isochronal Map Construction	74
3.2.6	Validation of RETRO-Mapping.....	74
3.2.7	Statistical Analysis	76
3.3	Results	76
3.3.1	Assessment of Algorithms applied to Atrial Fibrillation.....	77
3.3.2	RETRO-Mapping Algorithm Validation in Sinus Rhythm and Atrial Tachycardia.....	79
3.3.3	Algorithm Validation during Atrial Fibrillation	80
3.3.4	Manual and Automated Orbital Plots	87
3.4	Discussion	88
3.5	Limitations.....	91
3.6	Conclusion	92

3.1 Introduction

The following work has been published.¹¹² This has been reorganised to include the appendices within the text, and additional data and discussion.

Activation during AF is difficult to map due to the varying cycle lengths and electrogram morphology. However, mapping studies in canine atria, and later in humans^{27, 34, 113-115}, have advanced our understanding of the electrical activation patterns that occur. Many of the studies that have attempted LAT mapping of AF have done so using laborious manual annotation, or relied upon extremely high density electrode arrays that cannot be used during ablation procedures.^{27, 34, 114, 115} This has led researchers to seek alternative, surrogate markers of activation. These have included CFAE mapping^{84,7}, dominant frequency analysis¹¹⁶, and phase analysis.^{117,8}

Ripple Map is a commercially available mapping tool that was developed to overcome the limitations of isochronal mapping during atrial tachycardia. Other groups have applied this mapping technique to map activation during AF.^{118, 119} However, the rapidly varying activation sequences during AF make it difficult to identify wavefronts and activation patterns using this approach. Using custom software, a number of permutations were tested to overcome the challenges of being able to produce a method to track activation without a fiducial signal, and visual interpretation once it was possible to map activation (see Section 3.3.3). During these studies it was apparent that the electrograms from multipolar catheters can be cross-referenced against each other. Using this principle, RETRO-Mapping is a new mapping technique that has been developed and tested to automatically determine wavefronts on a multipolar catheter.

The initial development stages were conducted during sinus rhythm and atrial tachycardia, which have reliable uniform wavefronts. The algorithm was subsequently applied to track uniform wavefronts during persistent AF. A number of validation steps were carried out, including manual analysis of wavefronts and their bipolar electrograms, construction of isochronal maps, and qualitative assessment.

3.2 Methods

3.2.1 Patient Selection and Procedural Technique

Patients with a history of symptomatic AF that were undergoing clinically indicated procedures were recruited. The study was approved by the Local Research Ethics Committee for Imperial College Healthcare NHS Trust, and written informed consent obtained from all patients.

Clinical demographics, and parameters including duration of persistent AF, left atrial size, and anti-arrhythmic medication were recorded (Table 3-1). AF was induced in patients that presented in sinus rhythm on the day of their procedure, but whom data collection during AF was required (for induction protocol, See 3.3.2). Mapping was undertaken during sinus rhythm, atrial tachycardia, and atrial fibrillation for algorithm validation purposes.

All procedures were performed in the post-absorptive state under general anaesthesia. Trans-oesophageal echocardiography was performed in all patients to exclude left atrial appendage (LAA) thrombus, and to assist with transseptal puncture. A deflectable decapolar catheter (Inquiry™, St Jude Medical, St Paul, MN, USA) was positioned in the coronary sinus as a spatial reference, for recording electrograms, and pacing if required. A single transseptal puncture was done using a Brokenbrough needle via an SL-0 sheath. Unfractionated heparin was administered after transseptal puncture. An activated clotting time of around 300 seconds was maintained throughout the procedure.

The Ensite Precision cardiac mapping system was used to collect left atrial and pulmonary venous geometry, using the AFocusII catheter via an SL-0 sheath. Following research data collection using the AFocusII, catheter ablation was undertaken according to the clinical requirements for each patient.

3.2.2 Data Collection and Export

The AFocusII was held in multiple stable recording positions on the left atrial posterior wall for 30 seconds in each location to produce each data segment. The posterior wall was targeted due to the relative ease of obtaining good contact on all electrodes of the catheter.

Data was collected during sinus rhythm, AT, and during AF. AF was induced with burst pacing from the mid coronary sinus, starting with a cycle length of 300ms and reducing by 20ms until AF induction. A waiting time of 2 minutes was observed to ensure self-perpetuation and stabilisation of AF.

Following data collection and procedural completion, data were exported for offline processing.

3.2.3 Algorithm Development

Data collected was used to develop a custom Matlab algorithm capable of tracking uniform wavefront propagation (Matlab R2015b, MathWorks, Inc., Natick, MA, USA). Exported bipolar electrograms were bandpass filtered 10-250Hz to remove noise and baseline artefact. A number of algorithms and techniques were developed and tested to track and display activation during AF. Numerous challenges were encountered during this phase, and are presented in chronological order.

Ripple Mapping Atrial Fibrillation

Ripple Mapping was developed for mapping regular cycle length tachycardias.¹¹⁸ Ripple Mapping does not rely on a fiducial signal, and does not require annotation of local activation time. A dynamic bar is used to represent the voltage-time relationship of the bipolar electrogram. Ripple Mapping was applied to bipolar data collected during AF from a single location in which the catheter had been held in a stable position, and played back at different speeds to identify wavefronts.

Dynamic Mesh

Wavefront propagation was initially displayed by showing the bipolar voltage-time relationship as a dynamic bar on the geometry surface. A blue mesh was superimposed over the dynamic bars from the catheter to create a 3-dimensional dynamic landscape as activation passed across the catheter (Figure 3-1, and Movie 3-1).

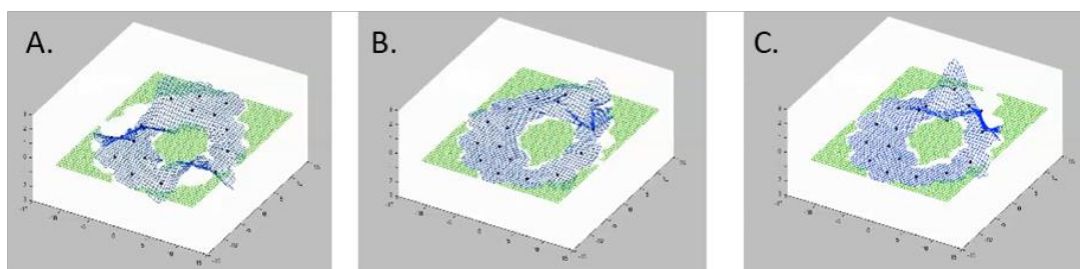


Figure 3-1. Three consecutive time-segments (moving from A-C) of a uniform wavefront passing across an AFocusII catheter during AF. The blue mesh moves in time with local activation. This is more clearly seen in Movie 3-1.

The 30 second recording of the dynamic mesh from a location was viewed so that the direction of uniform wavefronts could be observed. The most dominant direction of uniform wavefront activation was manually determined, and a second map generated by placing a patch of continuously moving dots on to the 3-dimensional left atrial geometry in the location in which the data had been collected. The direction of dot movement was manually determined by the operator (Figure 3-2). Multiple different patch locations were superimposed on to the left atrial geometry.

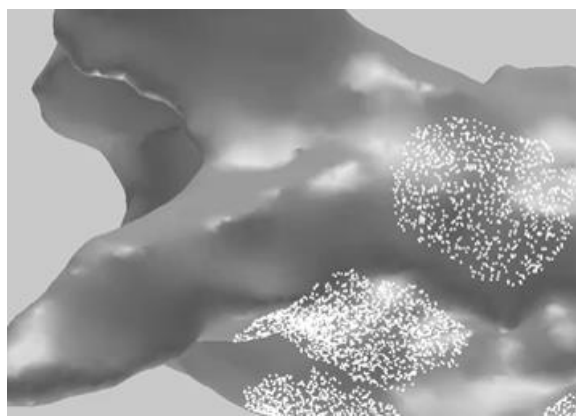


Figure 3-2. Multiple dots are displayed on the LA geometry from different mapping locations. The dots constantly move in the mean direction of activation at a fixed speed.

Cross-correlation of Electrograms

In uniform activation of homogeneous tissue, electrograms from adjacent poles will have similar morphology but a small difference in timing. Adjacent electrograms are compared by the algorithm. This is done by applying a time-shift to these electrograms and quantifying the degree of similarity, to find the time delay that produces the best match (Figure 3-3). Using this windowed cross-correlation method, the relative timings were used to create and display the wavefront propagation.

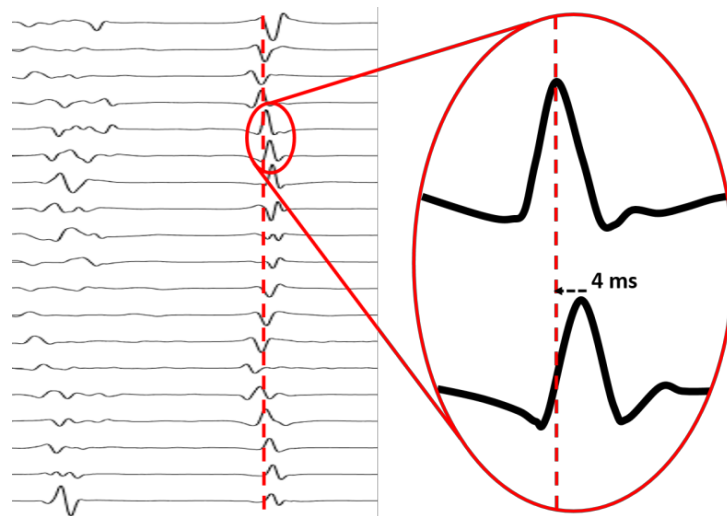


Figure 3-3. Time-shifting electrograms. Bipolar electrograms from a uniform wavefront during AF are displayed as they pass across the AFocusII catheter. A timing line (broken red line) shows the relative timings of electrograms. (Magnified electrograms) By shifting the lower electrogram back 4 milliseconds, there is a clear match in similarity of electrogram morphology to its neighbouring electrogram. This relative timing can be used to construct a display showing a propagating wavefront.

Each data segment corresponds to voltage and position information from the 20 poles of the AFocusII catheter. We used bipolar voltage between successive poles ($egm_1=V_2-V_1$, $egm_2=V_3-V_2$, $egm_3=V_4-V_3$, etc.) in order to reduce far-field signal from ventricular activation. The location of each midpoint between neighboring electrodes (p_1, p_2, p_3 etc.) corresponds to the position of each bipolar electrogram, as illustrated in Figure 3-4. For the purposes of analysis, the positions of the electrodes are interpolated onto the best-fit plane. Using a standard Delaunay triangulation algorithm, they are then triangulated and where two positions are connected by an edge, the corresponding electrograms are compared.

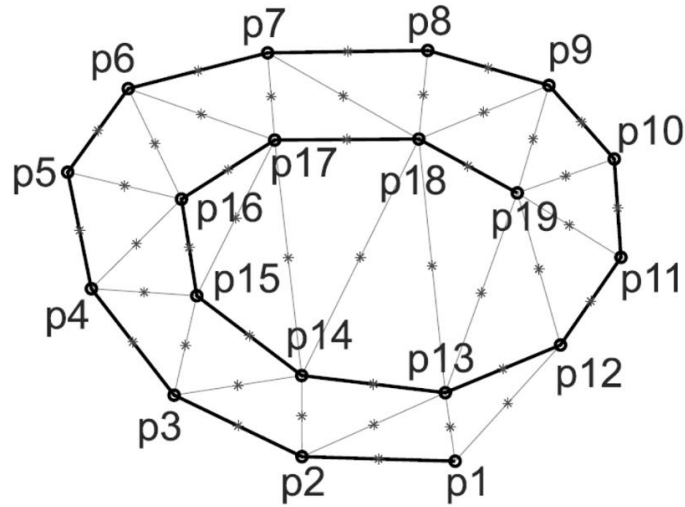


Figure 3-4. The position of the midpoint between consecutive electrodes is shown after interpolation onto the best-fit plane. The midpoint between electrode 1 and electrode 2 on the catheter is p1, corresponding to the position of the bipolar electrogram measured between these electrodes. These positions are triangulated (grey lines). The triangulation forms the basis for comparing spatially neighboring electrograms. For example, the electrogram at p1 will be compared with the electrograms corresponding to p2, p13, and p12. Asterisks are drawn at the midpoint of each edge that is used for comparison.

The comparison algorithm is a windowed cross-correlation. The 'windowing' involves weighting of the data so that the algorithm only compares data near to the time of interest (Figure 3-3). Cross-correlation is a signal processing method that provides a measure of similarity between two data series. The equation used is:

$$R_{i,j}(t,\Delta) = \sum_{k=-n}^n \left\{ egm_i \left(t - \frac{\Delta}{2} + k \right) \cdot W(k) \cdot egm_j \left(t - \frac{\Delta}{2} + k \right) \cdot W(k) \right\} \quad \text{Eq [1]}$$

where $R_{i,j}(t,\Delta)$ is the magnitude of the cross-correlation, i and j are the electrogram numbers, t is time (expressed as sample number), Δ is the offset (expressed as a number of samples) between the two electrograms, egm_i and egm_j , $W(k)$ is a Kaiser window with Kaiser parameter 3 and a total width of $2n+1$.

Next the local maxima in $R_{i,j}(t,\Delta)$ are determined and accepted if they exceed a threshold. At each local maximum, $R_{egm_1, egm_2}^{max}(t_{max}, \Delta_{max})$, the relative timing of egm_1 and egm_2 is given by Δ_{max} :

$$T_{egm_2} - T_{egm_1} = \Delta_{max} \quad \text{Eq [2]}$$

Approximate timing of activation can be determined as follows:

$$T_{egm_1} = t_{max} - \frac{\Delta_{max}}{2} \quad \text{Eq [3]}$$

$$T_{egm_2} = t_{max} + \frac{\Delta_{max}}{2} \quad \text{Eq [4]}$$

In order to avoid 'double counting' we assume that the tissue cannot depolarize more than once in a 50ms period (this might be refined in the future with more complex models that include action potential restitution information). The activation wavefront is interpolated onto a uniformly spaced grid with spatial smoothing and then displayed on the Propagation Map – RETRO-PM.

A window was developed to display the propagation of activating wavefronts across a representation of the multipolar catheter. A grey colour is assigned to the activating wavefront. When the electrodes are non-activated, the background is black. The return of the grey activating wavefront to black is to aid wavefront visualisation only, and does not give information on repolarisation data. Over the developmental course of this display, different colours were applied. This propagation map is referred to as the RETRO-PM. Exported bipolar electrograms are simultaneously displayed so that the user can ensure that the RETRO-PM is an accurate representation of the corresponding electrograms. The RETRO-PM can also be played back at different speeds determined by the user (Figure 3-5, A-B).

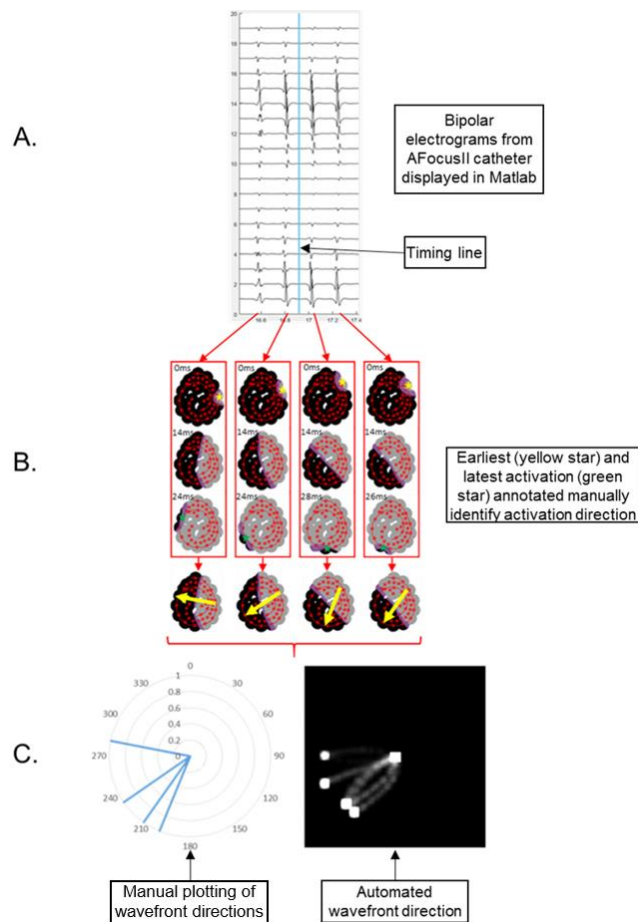


Figure 3-5. (A) Bipolar electrograms of 4 uniform wavefronts during AF have been collected with the AFocusII catheter. (B) RETRO-PM for each of the 4 uniform wavefronts are displayed. The grey activating wavefront passes across the 2-dimensional representation of the spiral shaped AFocusII catheter (red spiral). The earliest (yellow star) and latest (green star) activated electrode have been marked. A yellow arrow has been placed on the RETRO-PM to show the direction of activation. (C) The manually assigned activation direction of each wavefront is displayed on an orbital plot (left). The same wavefronts have been analysed using the automated RETRO-AD (right). The dot moves in the direction of mean activation.

3.2.4 Automation of Wavefront Tracking

As a wavefront propagates across the triangulated 2-dimensional grid, the mean activation direction perpendicular to that wavefront can be calculated. A display window was created to show a dot moving from the centre of a plot (RETRO-AD), based on the direction of mean activation obtained from the RETRO-PM. The distance the dot moves from the centre of the plot relates to the uniformity of that wavefront – the more uniform the wavefront, the further

the dot moves from the centre (Figure 3-5, C). A constant record of the wavefront directions that have been tracked is retained by the custom software. This automated assignment of activation direction using the RETRO-AD is used to summate the data from a mapping location on a single orbital plot.

3.2.5 Isochronal Map Construction

Isochronal maps were constructed using a validated algorithm available on the clinical version of Ensite Precision. A window of interest was set manually so that it includes only the bipolar electrograms of a single wavefront, while other wavefronts are excluded. LAT was assigned to electrograms using the first deflection algorithm. Isochronal maps were created for each wavefront using two different methods (See Results, Figure 3-8):

1. Automated isochronal – No adjustment of LAT assignment allowed
2. Manual isochronal – Adjustment of LAT allowed according to the operator's discretion

The number of electrograms requiring manual adjustment of LAT was documented. LAT annotation was only documented as being manually adjusted if it resulted in a change in the overall activation sequence order, or if an entirely different electrogram component was annotated (i.e. the upward instead of downward deflection of an electrogram). Minor manual adjustments of electrogram annotation points that did not fulfil these criteria were not counted as being manually adjusted. Isochronal maps were all produced by an independent operator that was blinded to the RETRO-PM.

3.2.6 Validation of RETRO-Mapping

The RETRO-Mapping algorithm was validated in 4 stages:

1. Manual analysis was done by playing through each data segment to identify uniform wavefronts on the RETRO-PM. Activation direction was assigned by manually identifying the earliest and latest electrodes to be activated from the RETRO-PM. Where more than one neighbouring electrode was activated earliest or latest simultaneously, the midpoint between the most lateral boundaries was identified as the point of activation. The activation direction was simultaneously measured for the same wavefront in the RETRO-AD plot for direct comparison (Figure 3-6).
2. Isochronal maps were constructed using Ensite Precision for each of the wavefronts analysed in validation stage 1 by assigning a window of interest manually to include only the electrograms from that single wavefront. The isochronal maps were created

using the built-in first deflection algorithm (automated isochronal). The same wavefront was also used to create a second isochronal map in Ensite Precision in which the operator could manually adjust any of the automated annotation points at their discretion (manual isochronal). Not all automated isochronal maps required manual adjustment. These isochronal maps were validated against the RETRO-PM and RETRO-AD maps. For planar activation wavefronts, the direction was taken using the vector from the earliest to the latest electrogram. The two types of isochronal map were produced to identify whether an automated algorithm and manual adjustment of signal annotation are of similar accuracy - there being no true gold standard approach.

3. A variety of previously described wavefront activation patterns have been described. Isochronal maps, constructed in Ensite Precision by the two different methods previously described (manual and automated isochronal), were used to validate these different activation patterns observed during persistent AF using RETRO-Mapping. Three of each activation pattern were identified from the RETRO-PM, and isochronal maps constructed for each wavefront. Maps were interpreted by a single operator that was blinded to the RETRO-PM for each wavefront (See Results, Figure 3-8).
4. A qualitative assessment of non-uniform wavefront activations was made. Where the wavefront did not have a linear propagation, electrograms were inspected and wavefront patterns were inspected for sequences that have previously been described in the AF Mapping literature.^{27, 34, 114}

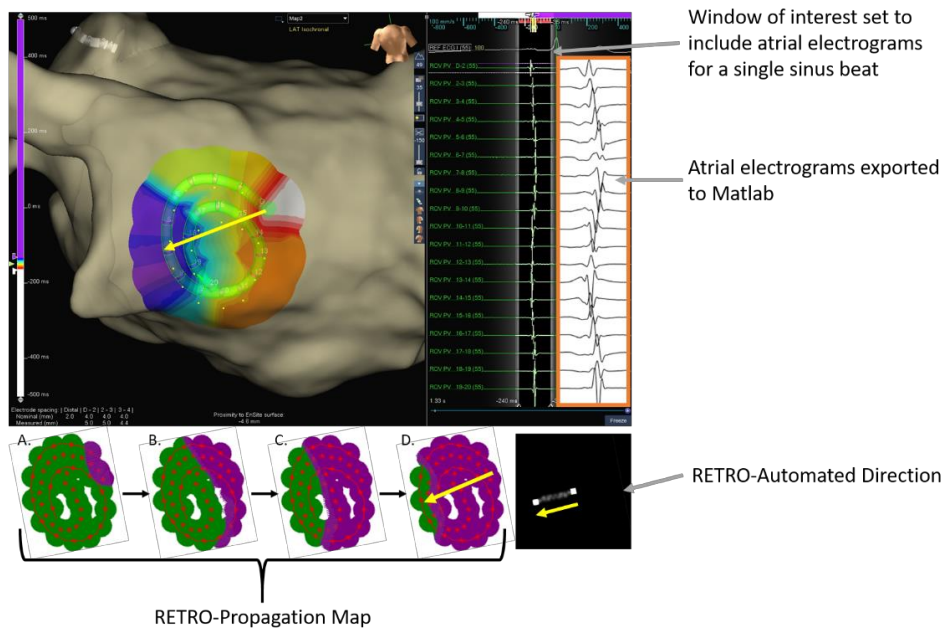


Figure 3-6. Assignment of activation direction. The AFocusII catheter has been held in a stable position on the posterior left atrium near the left lower pulmonary vein. A window of interest has been set to include only the atrial electrograms from a single sinus beat. A yellow marker on each electrogram identifies the point at which the activation time has been annotated. The same exported bipolar electrograms, as viewed in the custom software are displayed alongside those seen in Ensight Precision. An isochronal map shows uniform activation moving from the earliest (white) to latest (purple) area of activation for the displayed atrial activation pattern. Four consecutive images (moving from A-D) along the bottom show the RETRO-Propagation Map of the same beat using the custom algorithm. The AFocusII catheter is displayed in red. The activating wavefront (purple) can be seen to propagate across the catheter. The non-activated regions are displayed in green. The RETRO-Automated Direction is shown at the bottom right. The white dot moves from the centre of the plot towards the periphery in the mean direction of activation. A yellow arrow has been placed on the isochronal map, RETRO-PM, and RETRO-AD to show the direction of activation.

3.2.7 Statistical Analysis

Results were expressed as mean \pm SD (degrees). Bland-Altman analysis was used to visualise the reproducibility of measurements between RETRO-PM and RETRO-AD, and this was quantified by the limits of agreement.

3.3 Results

Data was collected from 33 different recording location in 16 patients (10 during AF, 3 in sinus rhythm, and 3 in atrial tachycardia). Patient demographics and characteristics are displayed in Table 3-1.

Case	Age	Gender	LA size (mm)	Medications	Persistent AF Duration (months)	Previous ablation	Previous Cardioversion
1	57	M	44	Bisoprolol	N/A Paroxysmal	No	No
2	50	M	44	Flecainide	N/A Paroxysmal	No	No
3	59	M	38	Bisoprolol	N/A Paroxysmal	No	No
4	63	M	48	Bisoprolol	N/A Atrial Tachycardia	PVI	No
5	44	M	49	Bisoprolol	N/A Atrial Tachycardia	PVI, roof, mitral	Yes
6	69	M	46	Bisoprolol	N/A Atrial Tachycardia	PVI, roof, mitral	Yes
7*	56	M	45	Amiodarone	36	No	Yes
8	35	M	32	Bisoprolol, Flecainide	6	PVI, redo PVI	Yes
9*	53	M	47	Bisoprolol	24	Cryo PVI, redo PVI + CTI	Yes
10	67	M	41	Flecainide	48	CTI	Yes
11	64	M	40	Bisoprolol	5	No	Yes
12	58	F	43	Bisoprolol	8	No	Yes
13*	72	M	51	Amiodarone	18	No	Yes
14	59	M	39	Bisoprolol	7	No	Yes
15	61	M	43	Bisoprolol, Amiodarone	34	No	Yes
16	69	M	45	Bisoprolol	6	No	Yes

Table 3-1. Details of the cases recruited for algorithm development and validation. Sinus rhythm data was collected from case 1-3, and atrial tachycardia data from case 4-6. *AF was induced on the day of the procedure.

3.3.1 Assessment of Algorithms applied to Atrial Fibrillation

During atrial fibrillation, periods of intermitted organised activation were interspersed with disorganised activation. A number of challenges were encountered when applying different algorithms and visual interfaces to track uniform activation during AF.

Ripple Mapping

Offline analysis of bipolar electrograms using the Ripple Map algorithm was challenging to interpret, despite playing back recorded data at different speeds. The significant variability in amplitude of bipolar electrograms during AF resulted in constant low level movement of bars. This was distracting and hampered visualisation of uniform wavefronts. There is no interpolation of electrograms with Ripple Map, resulting in insufficient numbers of bars moving up and down to allow clear identification of wavefronts.

Dynamic Mesh

In order to try and overcome the problem of insufficient numbers of bars moving, and visually filter out the low level movement of bars, a blue mesh was superimposed over the dynamic ripple bars. This created a 3-dimensional dynamic landscape as activation passed across the catheter (Figure 3-1, and Movie 3-1). This improved clarity of wavefront propagation, although visual interpretation remained challenging. In part, this was attributed to the 3-dimensional projection of chaotic activation being overwhelming, although it was now possible to identify intermittent uniform wavefronts.

The movements of the dynamic mesh could be viewed for a single location over the period of data collection. Uniform wavefronts could be identified intermittently. For some mapped locations, a single uniform wavefront direction was identified and occurred intermittently throughout the mapping period. In many instances the uniform wavefronts occurred in multiple different directions. The observation of these uniform wavefront directions was used to create the 2-dimensional map of continuously moving dots. The direction that the dots move was determined by the operator. In situations where a single uniform wavefront direction was observed, programming the direction of moving dots and superimposing them on to the 3-dimensional geometry enabled the predominant direction of uniform activation to be observed. Where multiple different uniform wavefront directions occurred, this type of mapping failed. It was not possible to display dots continuously moving in multiple different directions for the same location. Additionally, identification of uniform wavefronts using this method required the playback speed to be slowed down. This resulted in time consuming manual analysis which was highly subjective.

Cross-correlation of Electrograms

Intermittent wavefronts with uniform activation, interspersed with disorganised activation were clearly observed during AF using windowed cross-correlation of electrograms to create a propagation map (RETRO-PM). Triangulation assisted with the point density, allowing less interpolation when constructing the propagation map.

By assigning a colour change to displaying wavefront propagation, it helped to draw attention to the areas of electrical activity. For additional clarity, the bipolar electrograms could be visualised alongside. From initial observational analysis, there was good

correlation between the propagation map and sequence of bipolar electrograms. More detailed analysis of this technique was undertaken and is presented below.

3.3.2 RETRO-Mapping Algorithm Validation in Sinus Rhythm and Atrial Tachycardia

Having identified windowed cross-correlation as a suitable technique to track activation during AF, a series of validation steps were undertaken. A comparison of the automated isochronal and manually adjusted isochronal maps was undertaken. The number of electrograms requiring manual adjustment of LAT was documented. LAT annotation was only documented as being manually adjusted if it resulted in a change in the activation sequence order, or if a different part of the electrogram component was annotated (e.g. the down-stroke instead of the upstroke). Minor manual adjustments of signal annotation points that did not fulfil these criteria were not counted as being manually adjusted. The number of electrograms requiring manual adjustment of LAT was documented.

Data from sinus rhythm (Patient 1-3) and atrial tachycardia (Patient 4-6) were used for the validation of RETRO-Mapping during regular activation. Five sequential beats at the start of the recorded data segments underwent detailed analysis alongside isochronal maps produced using conventional techniques in Ensite Precision.

Automated isochronal electrogram annotation was adjusted for 26/285 sinus electrograms, and 22/285 atrial tachycardia electrograms when constructing the manually adjusted isochronal maps. For some electrograms, the automated algorithm assigned an 'unconfirmed local activation time', displayed in Ensite Precision as a dashed purple annotated line. The number of electrograms with unconfirmed annotation points was 5/285 sinus beat electrograms, and 9/285 AT beat electrograms. Of these unconfirmed annotation points, they were manually adjusted in 4/5 sinus electrograms, and 3/9 AT electrograms, while the remainder were confirmed without manual adjustment.

Although there is no true 'gold standard' for activation mapping, wavefront direction assigned from manual isochronal maps was defined as the 'gold standard' for the purposes of this validation step. For sinus rhythm wavefronts, the difference (mean \pm SD, degrees) compared to manual isochronal map activation direction was: 1.6 ± 7.3 for automated isochronal maps; -0.4 ± 5.7 for RETRO-PM; and 3.9 ± 3.2 for RETRO-AD. For AT wavefronts the difference compared to manual isochronal map activation direction was; -3.5 ± 10.5 degrees

for automated isochronal maps, -0.8 ± 5.7 degrees for RETRO-PM, and -0.3 ± 4.6 degrees RETRO-AD.

3.3.3 Algorithm Validation during Atrial Fibrillation

The longest mapping duration in a single location was 90 seconds. By viewing the RETRO-PM and making static images, it is possible to reproduce maps similar to those derived from conventional isochronal maps, but without the need for setting a time window (Figure 3-7). A video clip of the typical activation patterns observed during persistent AF can be seen in Movie clip 3-2.

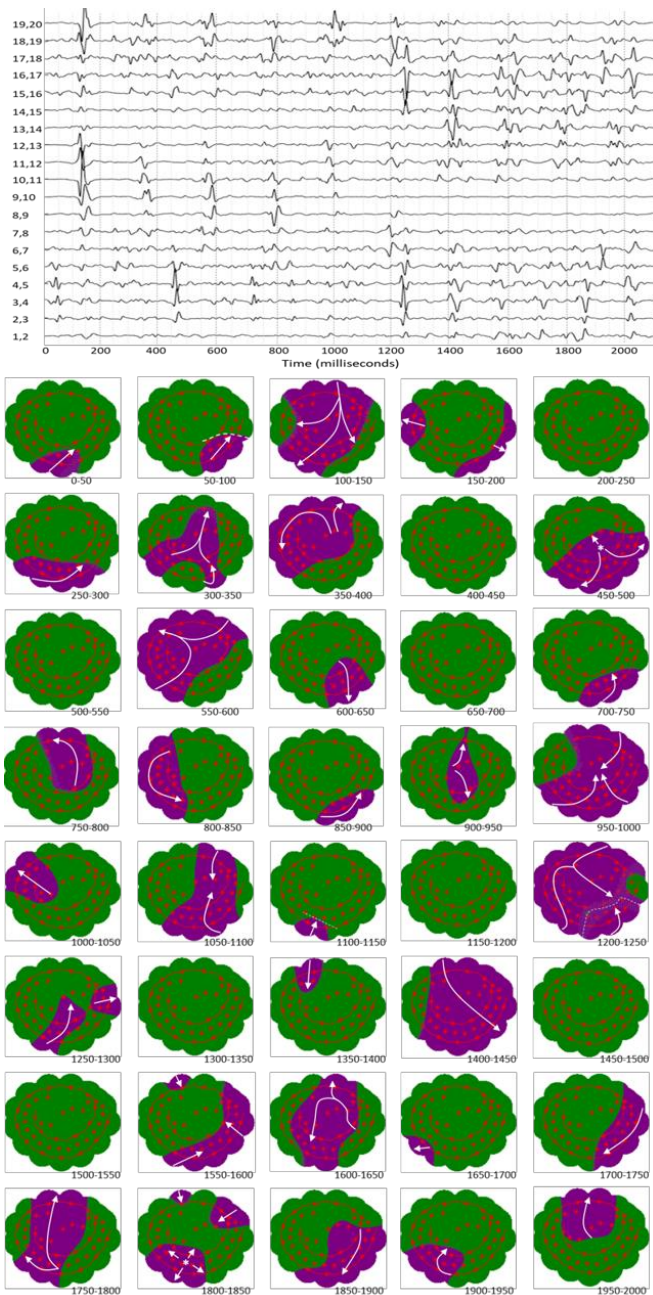


Figure 3-7. Continuous mapping of 2 seconds from a 90 second data segment of AF. Bipolar electrograms recorded from the AFocusII catheter held in a stable position in the left atrium are displayed above. Each broken grey line transecting the electrograms represents a 50ms interval which relates to the activation displayed in each static map in the panel below. The AFocusII catheter is displayed in red on a background of non-activated electrodes in green. The activating wavefront is shown in purple. White arrows show the activation directions during each mapped time period. Broken lines on the static maps indicate regions of collision or block. The white asterisks on the static maps identify activation starting from a focus within the catheter mapping region and spreading out towards its periphery.

Qualitative assessment of the RETRO-PM viewer demonstrated the presence of uniform wavefronts in all data segments. These were interspersed with disorganised activity and a variety of activation patterns that have previously been described by other groups. All of the following were observed: uniform wavefronts; focal activations; rotational waves; turning waves; wavefront collisions. Three examples of each pattern were identified from the RETRO-PM. These same wavefronts were used to generate isochronal maps in Ensite Precision using the automated and manually adjusted methods (Figure 3-8).

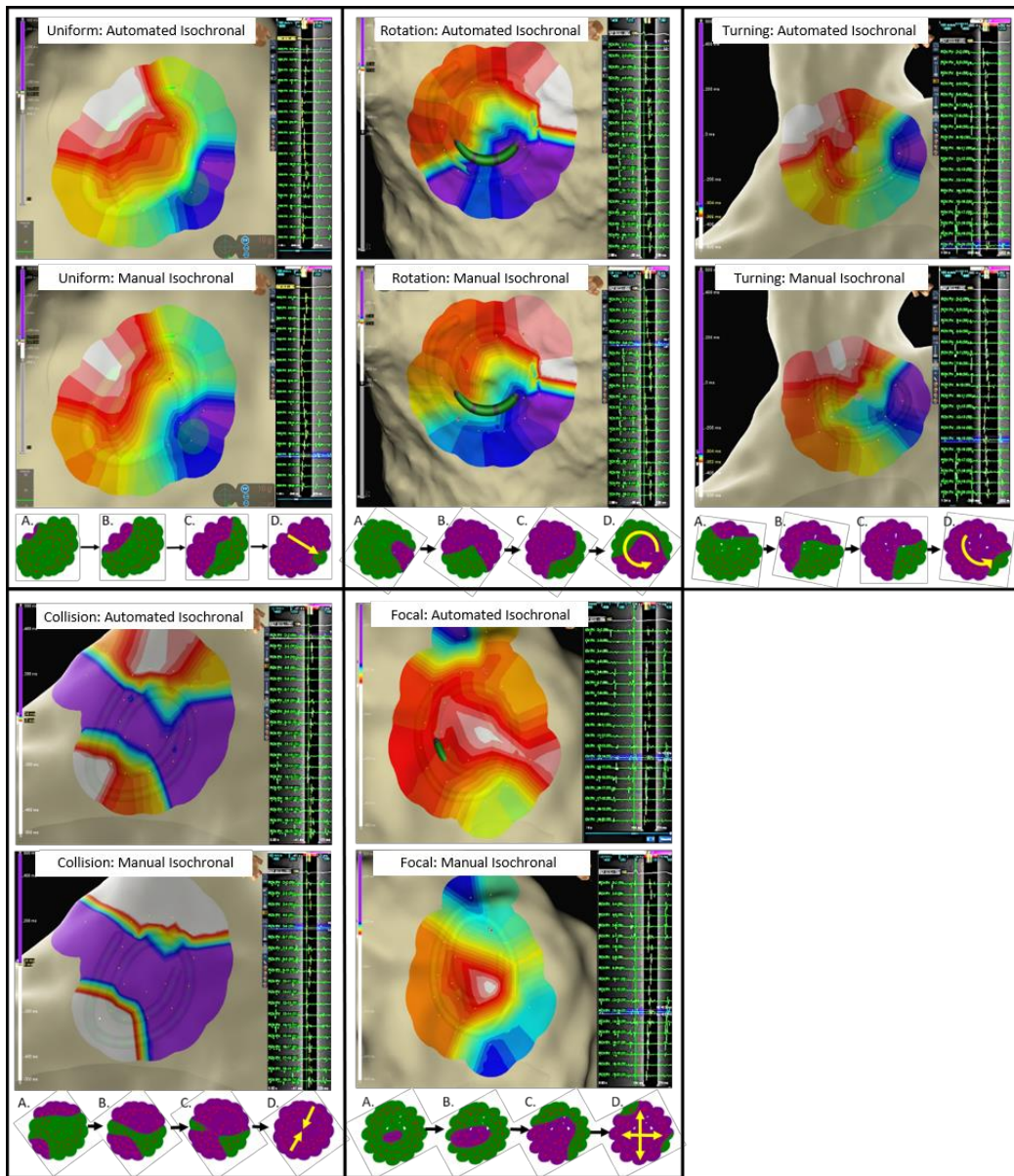


Figure 3-8. Example of the different patterns of activation observed during atrial fibrillation including a uniform wavefront, rotational activation, turning wavefront, wavefront collision, and focal activation identified during manual analysis of atrial fibrillation. For each activation pattern there are two isochronal maps; an automated isochronal constructed using the first deflection setting (top), and a manual isochronal with manual adjustment of annotated signals (bottom). Earliest activation is white, and latest activation is purple. The window of interest has been set so that it includes only the atrial signals for a single wavefront. Along the bottom of each activation pattern are RETRO-PM for the same atrial signals that have been analysed using the custom software. Four consecutive static images (moving from A-D) along the bottom show the RETRO-PM of the same wavefront using the custom algorithm. The AFocusII (red) is displayed. The activating wavefront (purple) can be seen to propagate across the catheter, and the non-activated regions displayed in green.

Automated isochronal electrogram annotation was adjusted for 64/285 electrograms when constructing the manual isochronal maps; 14/57 uniform wavefront electrograms, 9/57 rotational wavefront electrograms, 16/57 turning wavefront electrograms, 11/57 collision wavefront electrograms and 14/57 focal activation electrograms. The number of electrograms with unconfirmed annotation points was 39/285 electrograms in total; 12/57 uniform wavefronts, 6/57 rotational wavefronts, 8/57 turning wavefronts, 7/57 collision wavefronts and 6/57 focal activations. Adjustment of the unconfirmed electrogram annotation points was done in 4/12 uniform wavefront electrograms, 3/6 rotational wavefront electrograms, 5/8 turning wavefront electrograms, 3/7 collision wavefront electrograms and 3/6 focal activation electrograms.

A comparative assessment was made of the activation directions assigned by the different measurement techniques. For uniform wavefronts the difference (mean \pm SD, degrees) compared to manual isochronal map activation direction was: 6.3 ± 8.5 for automated isochronal maps; 1 ± 6.9 for RETRO-PM; and 2 ± 6.6 for RETRO-AD. For turning wavefronts the difference compared to manual isochronal map activation direction was: 21 ± 19.5 for automated isochronal maps; -2.3 ± 8.6 for RETRO-PM; and 0.7 ± 8.1 for RETRO-AD. Collision wavefronts were analysed by drawing a line between the two earliest points of activation and identifying the activation direction from one of the two early activation sites for each wavefront. There is no RETRO-AD data due to the colliding wavefronts 'cancelling out' activation from opposing directions. For collision wavefronts the difference compared to manual isochronal map activation direction was: -0.3 ± 3.1 for automated isochronal maps; and -4.3 ± 3.8 for RETRO-PM. Rotational wavefronts and focal activation patterns all showed the same pattern of activation when qualitatively compared.

Qualitative comparison of three different techniques to map the same wavefront was made. This included the automated isochronal map, manual isochronal map and RETRO-PM. This revealed agreement between all 3 maps in 2/3 uniform wavefronts, 3/3 rotational wavefronts, 2/3 turning wavefronts, 1/3 collision wavefronts and 2/3 focal activations. When comparing the manual isochronal map with the RETRO-PM, there was strong agreement between all 3/3 maps in uniform wavefronts, rotational wavefronts, turning wavefronts, collision wavefronts and focal activations. All instances of disagreement between all 3 maps were the result of the automated isochronal maps. An example of the maps with strongest and weakest agreement between the 3 maps is displayed (Figure 3-9 and 3-10).

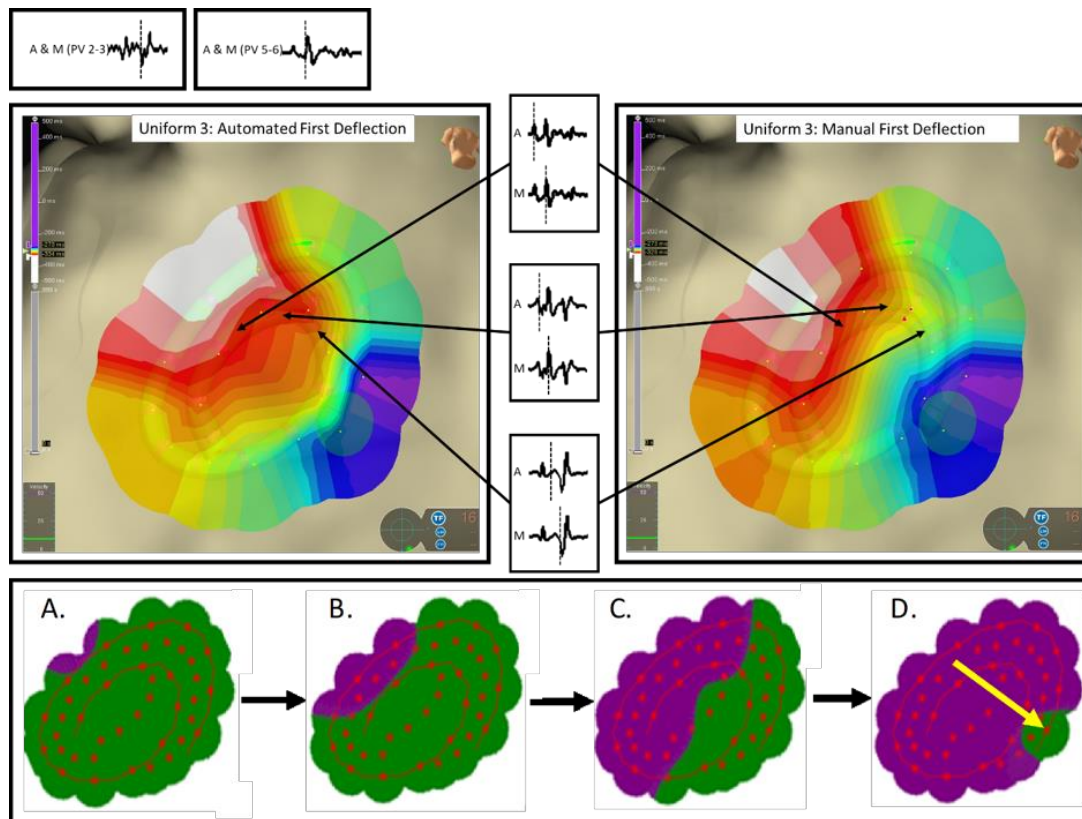


Figure 3-9. Example of the best correlation between maps constructed using automated isochronal, manual isochronal and RETRO-PM. The isochronal maps as viewed in Ensite Precision show the AFocusII catheter held in a stable position on the posterior left atrium with activation moving in the same direction in both the automated (left) and manual (right) isochronal maps. Activation moves from earliest (white) to latest (purple) with the same activation pattern. Three electrograms are displayed between the two isochronal maps showing the signal annotation points that were adjusted between the two maps. A dashed line through each electrogram identifies the signal annotation point made in the automated isochronal map (electrogram labelled A), and manual isochronal map (electrogram labelled M). Two bipolar electrogram signals from electrodes 2-3 and 5-6 on the AFocusII are displayed (top left) that were unconfirmed in the automated isochronal map. These two electrogram annotation points were confirmed only and not adjusted. All other electrograms that were not adjusted are not displayed. The bottom panel displays the RETRO-PM (moving from A-D) using the custom software of the same wavefront analysed in the isochronal maps. The AFocusII (red) is displayed. The activating wavefront (purple) can be seen to propagate across the catheter, and the non-activated regions displayed in green. A yellow arrow shows the activation direction of the wavefront.

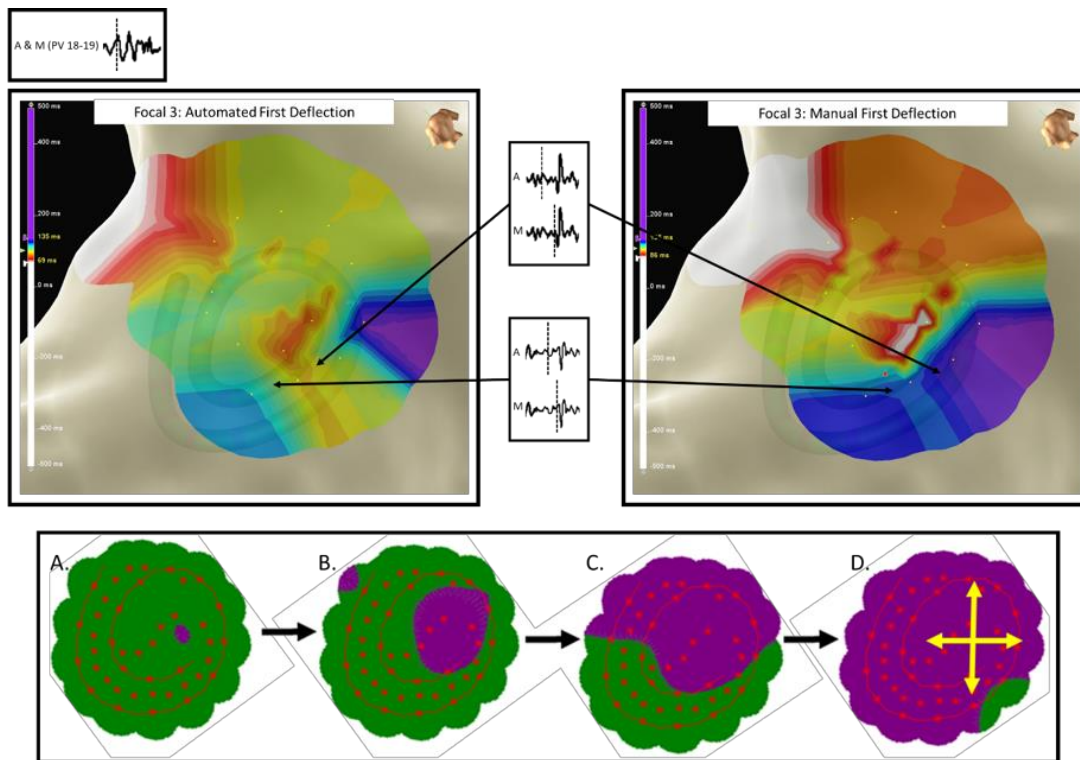


Figure 3-10. Example of the worst correlation between maps constructed using automated isochronal, manual isochronal and RETRO-PM. The isochronal maps as viewed in Ensite Precision shows the AFocusII catheter held in a stable position on the posterior left atrium. Activation moves from earliest (white) to latest (purple). Although there are similarities between the automated (left) and manual (right) isochronal maps, the appearance of the automated isochronal map more closely resembles that of uniform activation. The adjustment of just two electrogram annotation points (electrograms displayed between the two isochronal maps) to the correct location reveals the focal activation. A dashed line through each electrogram identifies the signal annotation point made in the automated isochronal map (electrogram labelled A), and manual isochronal map (electrogram labelled M). In this example there is an area of focal activation (central catheter) along with a uniform wavefront beginning near the distal electrode of the AFocusII catheter. A bipolar electrogram signal form electrodes 18-19 on the AFocusII is displayed (top left) that was unconfirmed in the automated isochronal map. This electrogram annotation point were confirmed only and not adjusted. All other electrograms that were not adjusted are not displayed. The bottom panel displays the RETRO-PM (moving from A-D) using the custom software of the same wavefront analysed in the isochronal maps. The AFocusII (red) is displayed. The activating wavefront (purple) can be seen to propagate across the catheter, and the non-activated regions displayed in green. A yellow arrow shows the activation direction of the wavefront. The activation pattern of the RETRO-PM more closely resembles that of the manual isochronal map.

Twenty-seven data segments of 30 seconds from 10 patients were manually analysed for uniform wavefronts during AF. All uniform wavefronts were assigned an activation

direction from the RETRO-PM and the RETRO-AD for direct comparison. In total, 1373 wavefront showing directional uniformity were observed. During AF, the RETRO-AD underestimated the activation direction (Bland-Altman mean difference: -0.1 degrees; limits of agreement: -8.0 to 8.3; 95% CI -0.4 to 0.2; ($r = 0.01$) $R^2 = <0.005$), although this was not statistically significant ($P = 0.77$) (Figure 3-11).

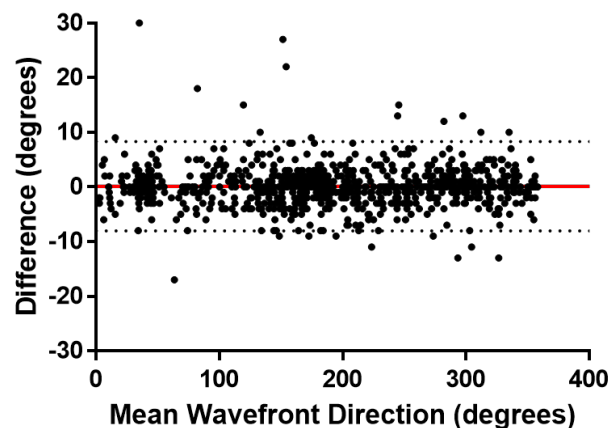


Figure 3-11. Bland-Altman plot showing agreement between wavefront directions assigned from the RETRO-PM and RETRO-AD during AF. The middle line (red) indicates the mean difference between the two measurement techniques (-0.1 degrees). Broken lines above and below indicate upper and lower limits of agreement (-8.0 to 8.3 degrees).

3.3.4 Manual and Automated Orbital Plots

Orbital plots were produced as a method to display multiple wavefronts from a single location on one map. Part of the problem of applying conventional mapping techniques to AF mapping, is that each wavefront has to be displayed on a separate map. Initially, the number and direction of all uniform wavefronts from a data segment were displayed in an orbital plot that was manually created. The validated RETRO-AD algorithm was subsequently applied to the same data segments, using the directional data to produce an ‘automated’ orbital plot.

Fifteen data segments from 4 patients underwent manual and automated orbital plot construction for qualitative comparison. When comparing the two orbital plots for each location, in all instances there was a strong similarity between the manual and automated activation patterns. Activation patterns ranged from having predominantly all of the uniform activation in a single direction – almost resembling that of an atrial tachycardia – to having

relatively few uniform wavefronts occurring in all directions. This is more clearly displayed in Figure 3-12.

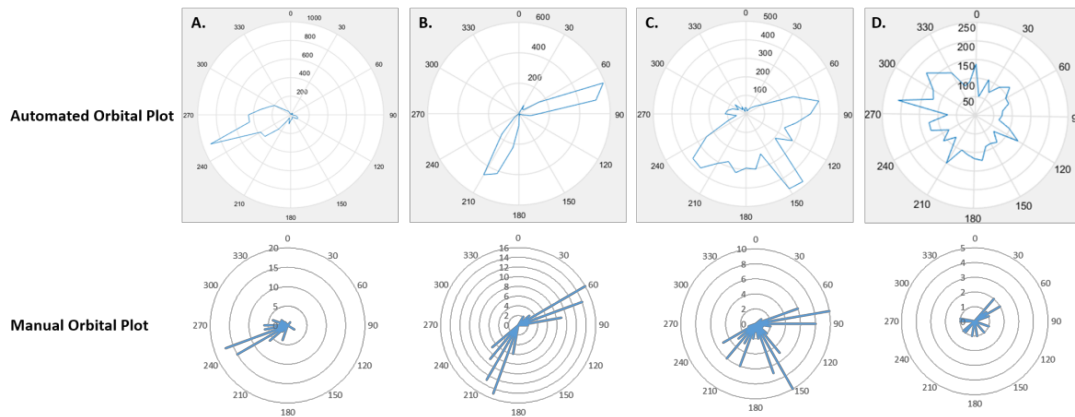


Figure 3-12. Orbital plots constructed from wavefront direction assigned by RETRO-AD (top row – Automated Orbital Plot) to produce an automated orbital plot, and manually (below – Manual Orbital Plot). A clear similarity can be seen between the orbital plots constructed by the two different methods. (A) Frequent uniform wavefronts are predominantly confined to a single direction of activation, indicating a highly organised region of the atrium. (B) Uniform activation occurs in two predominant directions. (C) Uniform activation becomes more spread out, and tends to occur mainly in three different directions. (D) In this orbital plot there are relatively few uniform wavefronts that occur. Furthermore, these wavefronts are spread out in all directions with no particular directional preference.

3.4 Discussion

In this chapter, the development and validation of a new technique to map activation during AF without the need for a time window is presented. This technique shows comparable accuracy (mean difference $<5^\circ$) to that of conventional isochronal mapping with careful manual adjustment of LAT.

In the past, observational data from humans has been critical to the mechanistic understanding of atrial fibrillation. Electrogram recordings allowed focal activity within the pulmonary veins to be observed, which then provided the underpinning for pulmonary vein isolation.⁶ Subsequently, over decades, multipolar catheters have routinely been used during ablation procedures. However, validated methods for assessing wavefront propagation across the field of these multipolar catheters have not been described. Instead, many investigators have attempted to infer mechanisms from analyses of electrograms 'point-by-

point' (for example using 'fractionation' or dominant frequency analysis). The observation of human atrial fibrillatory wavefronts is an important step in developing a better mechanistic understanding of atrial fibrillation. RETRO-Mapping provides an accurate, and practical solution to this mapping problem.

A variety of different techniques to track uniform activation were initially tested. Data collected during AF was initially tested on these different techniques in order to identify their strengths and weaknesses before any time consuming and extensive validation steps had been undertaken. It was possible to track activation using the voltage-time relationship of bipolar electrograms in Ripple Mapping, however the constant low-level movement of dynamic bars was distracting. Additionally, there were not enough moving ripple bars to be able to easily identify activation patterns. Overlaying the dynamic mesh to create a dynamic landscape was helpful to determine the direction of uniform wavefronts, but required a second map of dots moving constantly in the direction of the majority of uniform wavefronts to be produced. The direction in which the dots moved was determined by the operator, and therefore highly subjective. Furthermore, it was not possible to display multiple uniform wavefronts from a single location on one map.

Windowed cross-correlation enabled a propagation map to be created of the activating wavefront. Triangulation of electrodes further assisted by increasing the density of points from cross-correlating electrograms with multiple neighbouring electrograms. This technique was selected and underwent a series of validation steps, initially starting with sinus rhythm and atrial tachycardia, and subsequently AF.

Sinus rhythm and atrial tachycardia data has been used to confirm that this method is able to track uniform activation. Following this, the technique has been applied to data collected during AF. This has shown that it is possible to achieve comparable results to those of manual isochronal mapping. Qualitative comparison of the automated and manual isochronal maps in some instances demonstrate that very little manual adjustment in annotation of LAT could result in a dramatic change to a map (Figure 3-9). The electrogram annotation algorithms in current mapping systems have not been specifically designed for mapping AF, and therefore it is understandable why they might be less accurate than manual annotation. Importantly, RETRO-Mapping allows human interpretation of mapped locations after they have been analysed. Wavefront propagation can be viewed by playing the data

segments back at different speeds while simultaneously displaying electrograms to ensure that the user is in agreement with the RETRO-AD results.

These findings are in agreement with prior mapping studies that have identified uniform wavefronts interspersed with disorganised activation¹¹⁴, focal activation^{30, 120, 121} and rotational activation.¹²² Some patients appear to have more organised AF with a greater number of uniform wavefronts concentrated in a single direction.²⁷ By mapping different locations within the LA, it was evident that some locations within the same patient express different degrees of organisation/disorganisation. This may be the result of the mechanisms underlying AF, or possibly a manifestation of the underlying structural anatomy. However, at present much of the interpretation of orbital plots is qualitative, and lacks a robust method to classify and quantify activation patterns. Despite this, orbital plots provide a method of displaying multiple different directions of uniform wavefront summarised on a single plot for a single location.

Previous mapping studies have shown that uniform wavefronts occur in multiple different directions in the same location.¹¹³ Therefore, constructing a single isochronal map of a wavefront is of limited value if we are to better understand activation patterns. Despite this, it is possible to produce isochronal maps for individual wavefronts during AF, using current 3D electroanatomical mapping systems. A variety of automated settings can be used to annotate the LAT of electrograms once a time window has been set to include only the electrograms from a single wavefront. These include annotation of the first deflection, and maxima or minima of the voltage or its gradient with time. The first deflection setting appeared to be the most reliable setting for signal annotation to identify uniform wavefronts during AF, although all methods have their strengths and weaknesses.

Other groups have characterised the complex activation patterns during AF^{23, 25, 27, 113-115, 123} but, due to practical difficulties of the laborious analysis techniques, mapping is restricted to short recording durations from limited regions. The resultant activation maps are also difficult to interpret, even for those with experience in this type of mapping. More conventional, automated techniques such as isochronal activation mapping have been available on clinical systems for several years. However, the cycle length variability precludes their use for mapping activation during AF. Even in instances of regular cycle length tachycardia, the technique can be challenging: relatively few incorrectly annotated electrograms can render an isochronal map completely inaccurate.¹¹⁸

The limited market release of CARTOFINDER™ has been used to map uniform wavefronts during atrial tachycardia and pacing¹²⁴, and subsequently during AF¹²⁵ to map potential drivers using a 64-pole basket catheter. The algorithm for this technique is proprietary, and raises questions as to how electrogram annotation and data processing are carried out. Additionally, both electrode contact and an even coverage of data points can be challenging when using the basket catheter.

More recently, AcQMap, a dipole mapping system that exploits electrostatic field theory has been developed. Through application of this system with a specially designed basket catheter, global continuous maps of AF have been obtained.¹²⁶ Using AcQMap, results of a recent trial have identified non-PV drivers in patients with persistent AF. In addition to PVI, ablation of these localised sources was undertaken. However, only 30% (38/125 patients) with persistent AF were ablated to sinus rhythm with mapping guided ablation, and the additional ablation time of non-PV targets was similar to the ablation time for PVI; 23.8 ± 17.7 and 30.5 ± 11.8 respectively. Moreover, AF was induced in some of these patients as they presented in sinus rhythm.

During AF, mapping is complicated by constant electrogram amplitude and cycle length variation, as well as double potentials and fractionated electrograms. This hampers the correct annotation of LAT and prevents setting of a fixed time window.

3.5 Limitations

As this is a feasibility study aimed at validation of a new activation mapping algorithm, mapping was limited to only a small area of the left atrium in a small number of patients. The emphasis has therefore been to develop a tool that can go on to be used in a larger, prospective dataset by mapping more extensive regions of the atria to further validate the observed activation patterns. Orbital plots are qualitatively analysed for their activation direction and degree of organisation. This is subjective and can make comparison of some orbital plots challenging. Tools are required that can be applied to these data that enable data analysis to be more quantitative. Automated mapping is currently limited to uniform wavefronts, with manual identification of other patterns. Developing techniques for automated identification of the different activation patterns observed is required.

3.6 Conclusion

In this chapter, a systematic approach has been applied to the development of a technique for mapping wavefronts during AF. This has been done by considering the ideal requirements of a mapping system capable of mapping AF, which include: (i) correctly identify the relative timings between electrodes on a multipolar catheter without the need for manual adjustment; (ii) not require setting of a single, fixed time window; (iii) be at least comparable to the accuracy of carefully adjusted manual isochronal mapping, and; (iv) display mapping data in a manageable way for the user to interpret. RETRO-Mapping has been developed with these specific considerations in mind. The uniform wavefronts can be mapped with this automated algorithm, however it is not clear if the direction of these organised wavefronts are random, or possess reproducible and stable vectors over prolonged periods of time.

4 Mechanistic Insights from Mapping Persistent Atrial Fibrillation

4.1	Introduction.....	94
4.2	Methods	94
4.2.1	Patient selection	95
4.2.2	Design modifications of RETRO-Mapping.....	97
4.2.3	Optimal mapping duration	98
4.2.4	Developing Analysis Techniques.....	98
4.2.5	Statistical analysis	101
4.3	Results	102
4.3.1	Optimal mapping duration	102
4.3.2	Percentage match in activation patterns during persistent AF	103
4.3.3	Temporal stability of CFAEmean	107
4.3.4	Temporal stability of mean bipolar voltage	108
4.3.5	Relationship between low percentage match and CFAEmean stability 109	
4.3.6	Correlation between CFAEmean and mean bipolar voltage	110
4.3.7	The Effect of Amiodarone on CFAEmean and Mean Voltage: A Sub-analysis 112	
4.3.8	Organisation characteristics of persistent AF.....	114
4.3.9	Correlation between CFAEmean and R50	118
4.3.10	Correlation between CFAEmean and Shannon entropy	119
4.4	Discussion	119
4.5	Limitations	124
4.6	Conclusion	125

4.1 Introduction

AF is widely regarded as a disorganised atrial arrhythmia, with random activation patterns. This was originally supported by the multiple wavelet theory^{17, 53, 127}, and additionally from studies that have attempted to map LAT during AF.^{23, 27, 34, 113-115} These laborious manual mapping techniques have prevented longer durations of AF being mapped over larger atrial areas. The initial validation of RETRO-Mapping in the previous chapter (Chapter 3) was a proof-of-concept, aimed at developing an automated tool to map activation during AF and overcome the problem of manual analysis.

Mapping techniques have focused attention on global simultaneous mapping of the atrium, both invasively and non-invasively.^{49, 128} These techniques are hampered by their incomplete mapping of the atrium. A roving endocardial multipolar catheter to sequentially map the entire atrium could overcome this problem. However, this type of mapping means that each location has been mapped at a different time. Consequently, direct comparison between the activation patterns of sequentially mapped locations would be considered illogical by current literature and mechanistic theory.

Despite concerns about sequential activation mapping during AF, it is surprising that many operators are accepting of bipolar voltage and CFAE maps that have been collected in a similar fashion during AF. An inverse relationship between areas of fractionation and atrial fibrosis has been demonstrated using MRI.⁶⁹ Little is known about the relationship of these components with activation patterns during AF when data are sequentially collected, and whether all of these parameters remain spatially stable over time.

In this chapter, the updated software version of RETRO-Mapping has been used to study atrial activation patterns during persistent AF in greater detail. The purpose of this was to ascertain the spatiotemporal dynamics of persistent AF, and whether a sequential mapping technique is justifiable. If a particular location has electrophysiological features which are stable in time, then comparison with an adjacent area is justified. On this background, we tested the hypothesis that there are stable characteristics during persistent AF at given locations.

4.2 Methods

Significant changes were made to the software which allowed the speed of analysis to be improved. The GUI was also completely rebuilt to allow orbital plots from multiple locations

to be simultaneously displayed in relation to one another. This can be manipulated by the user in a moveable 3-dimensional model. Techniques for data analysis were also developed and incorporated with this software update. This was important, as analysis of orbital plots was solely qualitative. Application of quantitative tests enables data to be analysed more objectively.

4.2.1 Patient selection

Patients with symptomatic persistent AF that were undergoing clinically indicated catheter ablation procedures were prospectively recruited. All patients were spontaneously in AF on the day of their procedure. Patients with previous left atrial ablation were excluded. Procedures were conducted in the post-absorptive state under general anaesthesia. Anticoagulation regimens were maintained, and unfractionated heparin administered after trans-septal puncture. All antiarrhythmic medications were discontinued at least five half-lives before the procedure with the exception of amiodarone. Eight patients (8/18) were established on amiodarone and continued to take this until that day of their procedure to investigate its effects on atrial activation patterns.

All procedures were performed by a single operator using Ensite Precision and the AFocusII catheter. Left atrial and pulmonary venous geometry were collected at the start of each case (See Methods Chapter, section 3.3.1). Following this, the AFocusII was held in a stable position on the left atrial endocardium for collection of a 30 second data segment; 'dataset A'. Immediately following this a further 30 second data segment was recorded in the same location; 'dataset B'. The AFocusII was subsequently moved to multiple different stable recording locations, and the process repeated. Each recording location was shadowed on the Precision LA geometry (Figure 4-1). Overall, 322 data segments were recorded from 161 different locations in 18 patients. Patient demographics and characteristics are displayed in Table 4-1.

Case	Gender	Age (yr)	Duration in persistent AF	LA dimension (mm)	LVEF (%)	Amiodarone	Number of data segments
*1	F	69	9	44	30	N	4
*2	M	53	11	46	45	Y	4
*3	M	45	14	42	55	N	8
*4	M	58	11	49	40	Y	4
*5	F	45	20	42	50	Y	5
*6	M	64	16	54	55	N	7
*7	M	65	14	35	40	N	6
*8	M	68	21	39	55	N	12
*9	M	62	18	40	55	N	9
10	M	58	51	38	60	N	10
11	M	75	23	43	55	N	17
12	M	56	34	43	50	Y	6
13	M	65	29	51	55	Y	15
14	F	65	8	43	30	Y	15
15	M	64	15	56	55	Y	17
16	F	75	21	41	55	N	8
17	M	76	9	46	40	N	8
18	M	47	44	47	55	Y	6

Table 4-1. Patient demographics and characteristics. *Delayed interval mapping was undertaken in 9/18 patients.

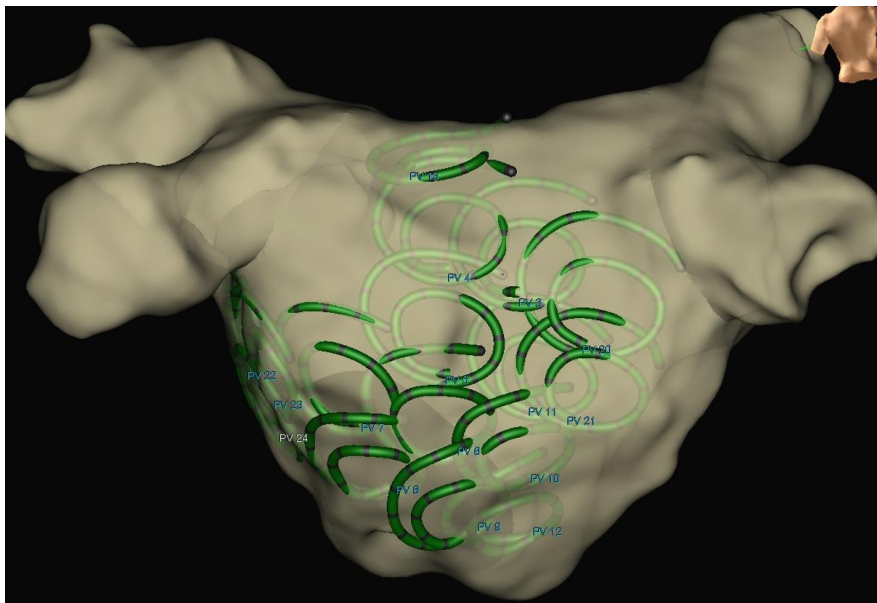


Figure 4-1. AFocusII catheter shadows from multiple locations of the posterior left atrium and floor. Data segments (30 seconds each) were collected from each location to generate two datasets; ‘A’ and ‘B’. In instances of delayed interval mapping (described below), the catheter was returned to the shadow of the first mapped location for collection of two further datasets; ‘C’ and ‘D’.

Delayed interval mapping was undertaken in the initial 9/18 patients. After completing data collection for dataset A and B, the AFocusII was returned to the first catheter location at least 10 minutes later. Two further datasets ('dataset C' and 'dataset D') were acquired in this location to investigate the temporal effect on activation patterns from the same location during persistent AF over an extended time period.

4.2.2 Design modifications of RETRO-Mapping

The updated GUI allows all data segments that have been collected from a patient to be simultaneously displayed. The exported matrix of x , y , and z coordinates from the AFocusII catheter provides the electrode and data segment positions relative to one another within the matrix. Data segments can be selected or deselected, determined by the user. A dropdown menu allows the user to display the catheter positions alone, orbital plots alone, or both together for each data segment. Once loaded, the model can be manipulated by rotation so that all data segments can be viewed (Figure 4-2). If the user highlights any of the data segments from the list, the original GUI displaying the RETRO-Propagation Map and corresponding electrograms can be viewed.

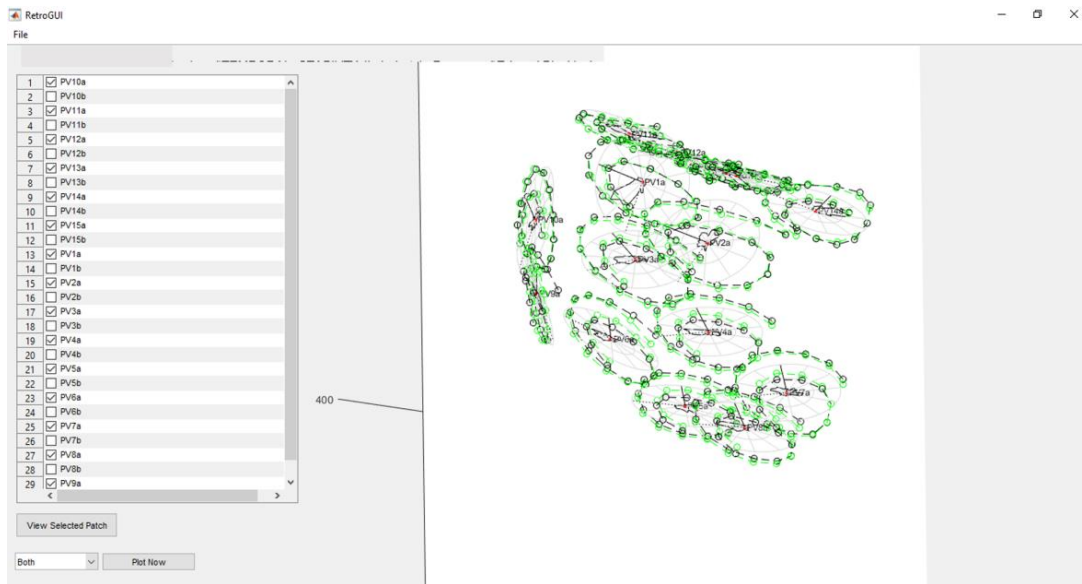


Figure 4-2. GUI for the updated software version of RETRO-Mapping. A list of data segments are displayed in a window (left). Data segments can be displayed by clicking each box. A drop down menu (lower left) allows the user to display the catheter positions alone, the orbital plots alone, or both. The catheter positions with their orbital plots are displayed in the main window in this example, and can be manipulated by the user.

4.2.3 Optimal mapping duration

Data was collected from patients during persistent AF to identify the optimal mapping duration. The AFocusII catheter was held in a stable position on the left atrial endocardial surface for 60 seconds. Data segments were divided into incremental sampling times increasing by 10 seconds each time, ranging 10 to 60 seconds. These data were analysed to identify the time at which activation patterns stabilised, thereby indicating sufficient data collection. Orbital plots for each 10 second increment were compared with the orbital plot at 60 seconds to identify the point at which there is no significant change in percentage match.

4.2.4 Developing Analysis Techniques

Quantifying similarity of activation patterns

Initial comparison of datasets from the same patient was qualitative. This was a crude method of analysis which prevented statistical testing, and was open to subjective interpretation. To overcome this, location matched datasets (datasets A and B, and delayed mapping, datasets C and D) all underwent analysis to assess the similarity of activation patterns over time. Data

was collected carefully to ensure that all location matched datasets were within ≤ 5 mm of one another.

Orbital plots were converted to histograms for analysis, with vector direction in degrees on the x-axis categorised in to 36 bins (10° per bin), and quantity of activation on the y-axis. The custom analysis code automatically loads up each folder of data which contains the histogram data, i.e. the probability distribution of the activation directions at each catheter location. The percentage match for each selected pair of datasets are evaluated using this probability data. The percentage match provides a quantitative measure of the similarity in activation directions between two datasets from the same mapping location. This is calculated by dividing the probability/frequency in each bin at a selected location in comparison to a second dataset. This is evaluated for all 36 bins and summed up to give the overall percentage match between the two datasets (Figure 4-3).

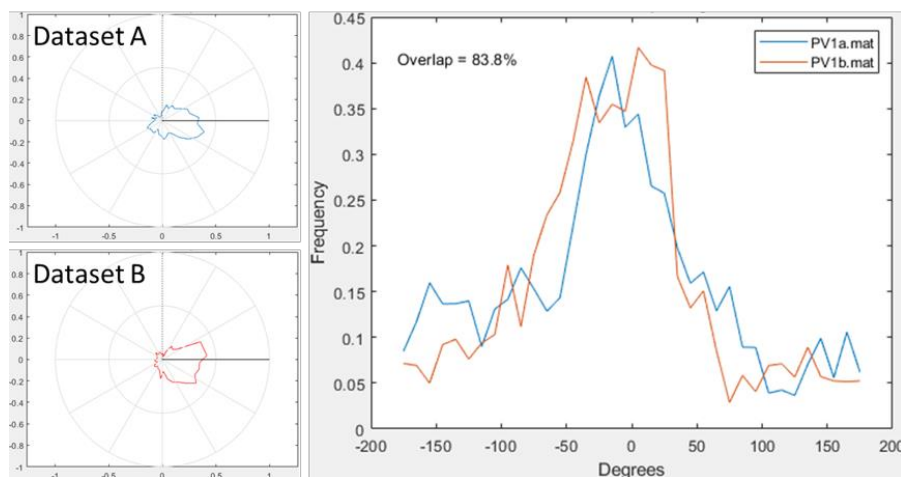


Figure 4-3. Datasets A and B have been collected sequentially from the same location of the left atrium during persistent AF. Post-processing with RETRO-Mapping has produced orbital plots of activation for each 30 second data segment (left, Dataset A and B). The orbital plots are displayed to the right as a histogram (x-axis, degrees; y-axis, frequency of activation). The overlapping area for the two datasets is calculated to quantify the degree of similarity when the same location is mapped at different times (83.8% in this example).

Organisation characteristics: Shannon Entropy and R50

Percentage match can be used to determine whether activation patterns remain stable over time, but does not provide an objective measure of organisation. Activation patterns during

AF are frequently referred to as being disorganised. Two different methods to assess the organisation characteristics of AF were tested. In the first method, Shannon entropy of each data segment was calculated. Shannon entropy can be used as a statistical measure for the degree of organisation of all wavefront vectors in a mapped location. The following equation is used to perform the calculation:

$$H = - \sum_{i=1}^N P_i \log_2 (P_i)$$

Where i is the bin number, N is the number of populated bins, and P_i is the proportion of data falling into the i th populated bin, subject to the condition $\sum_i P_i = 1$. In our calculation, the number of bins is 36, as we divide the 360° orbital plot in to 36 bins, each being 10°. If a wavefront vector occurs for 100% of the samples in a single bin, it is completely predictable, and will have an entropy of 0. The maximum entropy for 36 bins is 5.17 ($\log_2(36)$), and would represent an equal chance of all vectors occurring. This would be expected to occur in disorganised regions, where activation is completely unpredictable; i.e. random activation. We can therefore use entropy to assess the degree of organisation, and compare entropy values of repeat mapping on a per location basis. If activation for a specific location is completely random, one would expect the entropy of that location to be significantly different when mapped repeatedly at different times.

A novel technique was developed in the second method. The spread of activation directions on each orbital plot was used to determine how organised a mapped location was in a particular direction. Orbital plots for each location from datasets A and B were represented as histograms. This range is calculated by first sorting the probabilities into descending order per 10° bin (36 bins), and then evaluating at which angle the cumulative sum of these sorted probabilities is greater than or equal to 50% of the total sum of probabilities. This will be referred to as the 'R50' – the range in degrees in which 50% of the activation is contained. Data segments with a high degree of organisation in a particular direction would be expected to show a smaller range/spread of activation; a low R50. With completely random activation patterns, one would expect to have a theoretical R50 maxima of 180°.

CFAE_{mean} and mean peak-to-peak bipolar voltage over 8 seconds

Ensite Precision was used for CFAE analysis using the standard algorithm available on the clinical workstation. CFAE_{mean} was calculated for each data segment from an 8 second sampling time. For each data segment, percentage area of CFAE_{mean} >120ms (areas without CFAE), 80-120ms (conventional CFAE range), and <80ms (rapid CFAE/near continuous activation) was calculated, based on recognised criteria.^{81, 84} The following settings were applied to the CFAE_{mean} tool: CL 80-120ms; EGM width <10ms; EGM refractory period 50ms; peak-to-peak sensitivity 0.08mV; interpolation set to 10mm and interior projection 5mm.

An 8 second mean peak-to-peak bipolar voltage map was created for each data segment using the same 8 seconds used for CFAE_{mean} map construction. A lower cut-off of 0.35mV was set to define areas of low voltage based on its correlation with regions of fibrosis seen on MRI with late gadolinium enhancement.⁷³ An upper cut-off was set at 0.50mV to define areas that were not likely to represent fibrosis. The following settings were also applied to the mean peak-to-peak bipolar tool: EGM width <10ms; EGM refractory period 50ms; peak-to-peak sensitivity 0.08mV; interpolation set to 10mm and interior projection 5mm. For each data segment, percentage area of mean peak-to-peak bipolar voltage >0.50mV, 0.35-0.50mV, and <0.35mV was calculated.

Where delayed mapping was undertaken (datasets C and D), CFAE_{mean} and mean peak-to-peak bipolar voltage maps were created using the same method.

4.2.5 Statistical analysis

Results were expressed as mean +/- SD. Bland-Altman analysis was used to visualise the reproducibility of measurements between datasets A and B, and this was quantified by the limits of agreement. The two-way ANOVA was used for comparison for delayed mapping analysis (datasets A, B, C and D) with Dunnett's post hoc test performed for any significant analyses, including those with significant qualitative differences.

Hierarchical statistics were used to quantify whether the outcome variables differed (a) across patients and (b) across locations within patients. In summary, mixed effects models were used to see if the variance across repeat measurements was reduced significantly when (a) patients were allowed to vary as a random effect, and (b) locations within patients were allowed to vary as a random effect. Significance testing was performed using a Chi square test

of the $-2 \log$ likelihood. The clustering at each level of hierarchy was calculated and reported as an intraclass correlation (ICC).

Correlation statistics were used to identify relationships between mapping parameters. A value of $P < 0.05$ was considered statistically significant.

4.3 Results

4.3.1 Optimal mapping duration

Initially orbital plots were visually assessed to identify the point at which activation patterns no longer changed. This method suggested that at around 20-30 seconds, most orbital plots seemed to look similar to orbital plots at 60 seconds. In order to provide a more objective measure for optimal mapping time, percentage match was applied.

Each 10 second time increment for a data segment was displayed simultaneously as an orbital plot, superimposed on one another based upon the electrode x , y , and z coordinates. This ensured that adequate catheter stability had been achieved in each location. Displaying the 5 orbital plots from the same location as a histogram allowed the similarity in activation pattern to be more clearly appreciated (Figure 4-4). For each location, percentage match was calculated for every 10 second time increment, using 60 seconds as the comparator (Table 4-2). Activation patterns for 10/12 locations stabilised with no significant change at 30 seconds of data collection compared to 60 seconds of data collection ($P < 0.05$). The remaining 2/12 locations reached stability with no significant change at 40 seconds of data collection. It was important to achieve an appropriate balance between the amount of time required for mapping, and adequate data collection. Therefore, 30 seconds per data segment was used as the mapping duration for each location.

Location	Percentage Match with 60 second Data Segment (%)				
	10 sec	20 sec	30 sec	40 sec	50 sec
1	75.5*	82.5*	87.3	90.1	96
2	78.1*	80.2*	84.1*	92.7	96.6
3	84.7*	88.2*	90	92.1	95.1
4	80*	87.9*	92.5	93.7	97
5	84.1*	90.4*	93.6	93.8	96.4
6	71.9*	79.3*	81*	93.8	94.3
7	76.4*	82.1*	88.4	91.4	95.1
8	83.1*	84*	92.4	94.5	96.3
9	74.9*	81.9*	88.1	91.8	94.7
10	82.6*	87.6*	90.6	91.4	93.7
11	67.2*	77*	89.2	92.1	95.8
12	76*	80.8*	87	88.7	93.1

Table 4-2. Percentage match to identify the optimal mapping duration in each location. The percentage match between each 10 second time increment is calculated against 60 second of data collection for each location. *Significant difference in activation pattern compared with 60 second of data collection (P <0.05).

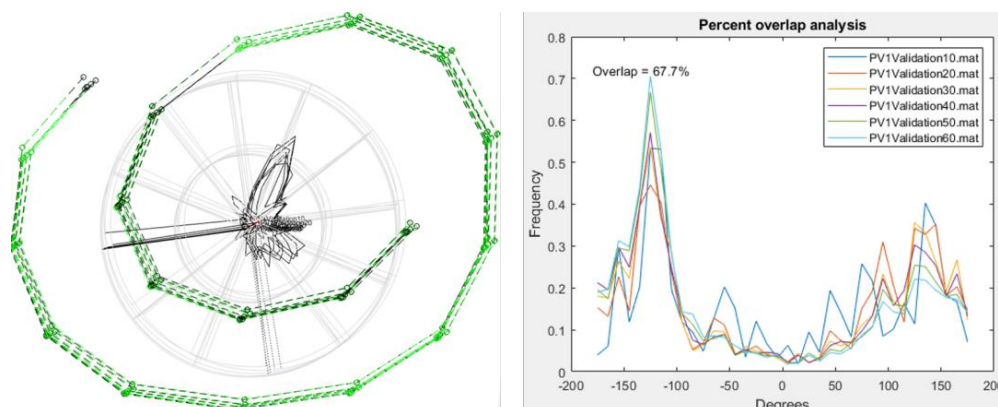


Figure 4-4. (Left) Five orbital plots and AFocusII catheter position are displayed for 10 second incremental mapping durations in a single location, ranging 10 to 60 seconds. (Right) The same 5 orbital plots are displayed as a histogram allowing the activation pattern of each 10 second incremental mapping duration to be clearly appreciated.

4.3.2 Percentage match in activation patterns during persistent AF

During persistent AF, the overall histogram percentage match (mean \pm SD, percent, n=161) between dataset A and dataset B was 79.5 ± 7.7 (95% CI 78 to 80.5). (Figure 4-5).

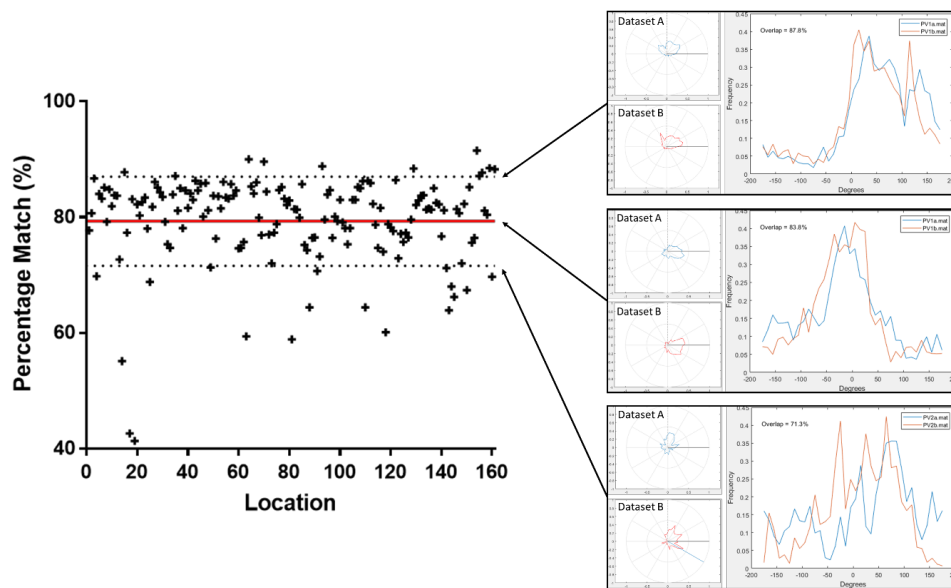


Figure 4-5. Percentage match between dataset A and B for each mapped location (n=161). Datasets A and B have been collected sequentially from the same location of the left atrium during persistent AF. Post-processing with RETRO-Mapping has produced orbital plots of activation over each 30 second mapping period. (Left) Graph showing percentage match between dataset A and B for each mapped location (n=161). The overall percentage match (mean, \pm SD, percent) was 79.5 ± 7.7 (95% CI 78.3 to 80.7). The overall mean percentage match is displayed on the graph with a red line, with a dotted black line for standard deviation. (Right) Orbital plots are represented alongside as a histogram (degrees, x-axis; frequency of activation, y-axis). For three different locations, the overlapping area for the two datasets is calculated to quantify the degree of similarity when the same location is mapped at different times.

In 9/18 patients, two further datasets (dataset C and dataset D) were collected from the first location mapped, at least 10 minutes later (mean time delay, min:sec, between dataset A and C was 20:34, range 11:05 to 36:35). The percentage match in activation patterns from datasets A and B was defined as the ‘control group’ for each location. The control group mean percentage match (\pm SD, percent) was 79.6 ± 3.6 (95% CI 76.9 to 82.4) for these 9 patients (Table 4-3). Percentage match between dataset A and C (Delayed 1), and dataset A and D (Delayed 2) was calculated for each location. There was no overall significant difference in activation pattern percentage match for Delayed 1 or Delayed 2 compared to the control group (P = 0.08).

Case	Control (%)	Delayed 1 (%)	Delayed 2 (%)	Time between A-C (min:sec)
1	83.3	87.3	74.7	17:37
2	74.7	74.8	77.1	22:39
3	81.1	67.0	72.7	27:52
4	84.6	81.3	76.6	17:55
5	76.9	71.7	79.9	17:24
6	76.5	45.3	38.6	21:25
7	81.5	78.0	81.4	36:35
8	81.2	74.1	67.6	19:40
9	76.4	77.7	78.6	11:05

Table 4-3. Details of percentage match for each patient undergoing delayed mapping of a single location.

Qualitatively, the activation pattern did not remain stable on delayed mapping in Patient 6 for either delayed mapping period (Figure 4-6). On this basis, despite no overall significant difference in activation pattern (n=9), post hoc analysis was done. This showed a significant difference in activation pattern for Delayed 1 and 2 compared to the control group. The control percentage match in this patient was 76.5%, and decreased to 45.3% in Delayed 1 (P = 0.01), and 38.6% in Delayed 2 (P = 0.004). There was no significant difference in activation patterns for the remaining 8 patients that underwent delayed mapping on post hoc analysis.

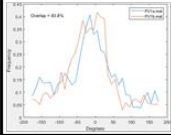
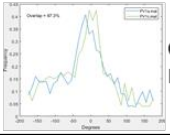

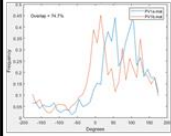
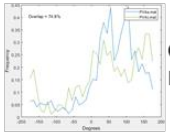
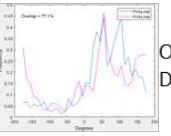
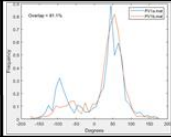
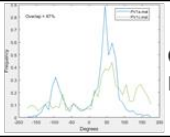
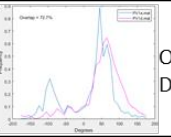
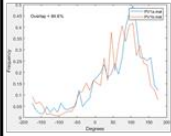
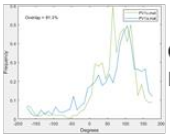
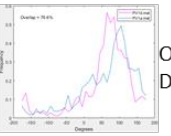
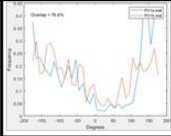
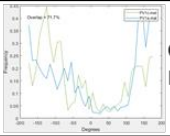
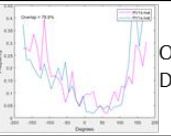
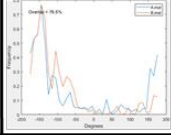
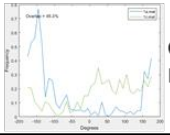
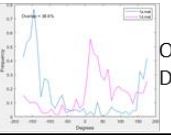
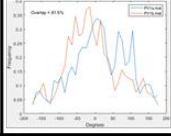
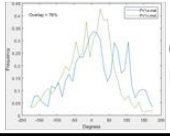
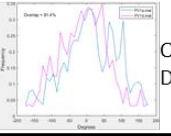
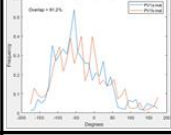
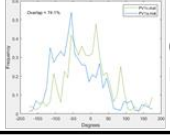
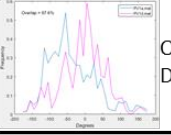
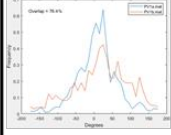
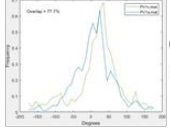
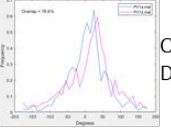
Patient	Control (0-30 sec)	Delayed 1 (min:sec)	Delayed 2 (min:sec)
1	 Overlap 83.3% Delay +0:30	 Overlap 87.3% Delay +17:37	 Overlap 74.7% Delay +18:07
2	 Overlap 74.7% Delay +0:30	 Overlap 74.8% Delay +22:39	 Overlap 74.7% Delay +23:09
3	 Overlap 81.1% Delay +0:30	 Overlap 67.0% Delay +27:52	 Overlap 72.7% Delay +28:22
4	 Overlap 84.6% Delay +0:30	 Overlap 81.3% Delay +17:55	 Overlap 76.6% Delay +18:25
5	 Overlap 76.9% Delay +0:30	 Overlap 71.7% Delay +17:24	 Overlap 79.9% Delay +17:54
6	 Overlap 76.5% Delay +0:30	 Overlap 45.3% Delay +21:25	 Overlap 38.6% Delay +21:55
7	 Overlap 81.5% Delay +0:30	 Overlap 78.0% Delay +36:35	 Overlap 81.4% Delay +37:05
8	 Overlap 81.2% Delay +0:30	 Overlap 74.1% Delay +19:40	 Overlap 67.6% Delay +20:10
9	 Overlap 76.4% Delay +0:30	 Overlap 77.7% Delay +11:05	 Overlap 78.6% Delay +11:35

Figure 4-6. Percentage match in activation between the control group (datasets A and B), Delayed 1 (datasets A and C), and Delayed 2 (datasets A and D) are displayed for the 9/18 patients that underwent delayed interval mapping. After completing data collection for dataset A and B, the AFocusII™ was returned to the first catheter location, at least 10 minutes later. Two further datasets (dataset C and D) were acquired in this location to investigate the temporal effect on activation patterns during persistent AF over an extended time period. The percentage match in activation is displayed, along with the mapping time delay in each comparison.

4.3.3 Temporal stability of CFAE_{mean}

For each location mapped in datasets A and B (n=161), the percentage area of CFAE_{mean} was calculated within the following three ranges using Ensite Precision: 1. CFAE_{mean} >120ms (area without CFAE); 2. CFAE_{mean} 80-120ms (conventional CFAE range), and; 3. CFAE_{mean} <80ms (rapid/near continuous fractionation).

There was no significant difference in CFAE_{mean} area (%) between dataset A and B for each CFAE_{mean} range: 1. CFAE_{mean} >120ms, Bland-Altman mean difference 0.98, limits of agreement -20.0 to 18.0, $r = 0.016$, $P = 0.84$; 2. CFAE_{mean} 80-120ms, Bland-Altman mean difference 1.0, limits of agreement -19.0 to 21.0, $r = 0.06$, $P = 0.46$; 3. CFAE_{mean} <80ms, Bland-Altman mean difference -0.01, limits of agreement -13.0 to 13.0, $r = 0.04$, $P = 0.61$ (Figure 4-7). However, there was variability across different patients and different locations. The variance of CFAE_{mean} in all three ranges, was greater between different patients than the variance within patients: CFAE_{mean} >120ms, ICC 0.43 ($P = <0.0001$); CFAE_{mean} 80-120ms, ICC 0.32 ($P = <0.0001$), and; CFAE_{mean} <80ms, ICC 0.45 ($P = <0.0001$). The variance of CFAE_{mean} was also greater for different locations within the same patient than the variance within the same locations for the same patient: CFAE_{mean} >120ms, ICC 0.92 ($P = <0.0001$); CFAE_{mean} 80-120ms, ICC 0.86 ($P = <0.0001$), and; CFAE_{mean} <80ms, ICC 0.86 ($P = <0.0001$).

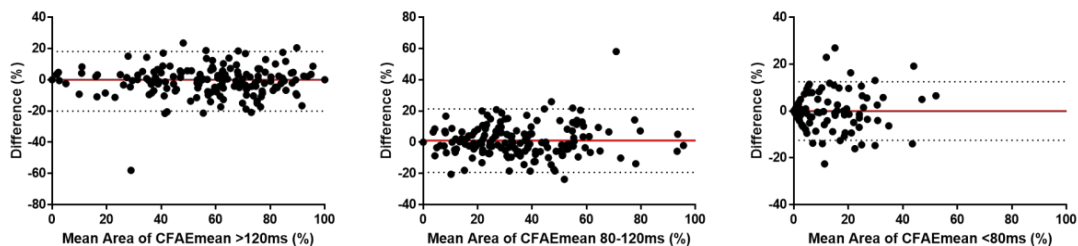


Figure 4-7. Bland-Altman plot showing agreement between CFAE_{mean} area (datasets A and B) represented by CFAE_{mean} >120ms (no CFAE), 80-120ms (conventional CFAE range), and <80ms (rapid CFAE/near continuous activity) for each data segment.

Delayed interval mapping (datasets C and D) in 9/18 patients was used to determine the stability of CFAE_{mean} over longer time periods (>10 minutes) in the same location. Dataset A was defined as the control group for each location. Dataset C and D were defined as Delayed 1 and Delayed 2, respectively. There was no overall difference between Delayed 1

and Delayed 2 compared to the control group across the three CFAE mean ranges: CFAE mean >120ms, $P = 0.85$; CFAE mean 80-120ms, $P = 0.47$; CFAE mean <80ms, $P = 0.27$. However, Patient 6 showed a significant difference in both Delayed 1 and 2 compared to the control group for CFAE mean 80-120ms ($P = 0.03$, Delayed 1 and 2 vs. Control) and CFAE mean >120ms ($P = 0.02$ Delayed 1 vs. Control, $P = 0.04$ Delayed 2 vs. Control) with Dunnett's post hoc test.

4.3.4 Temporal stability of mean bipolar voltage

Datasets A and B underwent analysis to identify the mean peak-to-peak bipolar voltage within three voltage ranges: 1. Mean voltage >0.5mV; 2. Mean voltage 0.35-0.5mV; 3. Mean voltage <0.35mV. For each location, the percentage area of these three voltage ranges was calculated.

Mean voltage area (%) remained stable between dataset A and B for each voltage range: 1. Mean voltage >0.5mV, Bland-Altman mean difference 0.68, limits of agreement -13.0 to 14.0, $r = 0.03$, $P = 0.71$; 2. Mean voltage 0.35-0.5mV, Bland-Altman mean difference 0.08, limits of agreement -18.0 to 18.15, $r = 0.03$, $P = 0.68$; 3. Mean voltage <0.35mV, Bland-Altman mean difference -0.72, limits of agreement -19.55 to 18.11, $r = 0.007$, $P = 0.93$ (Figure 4-8).

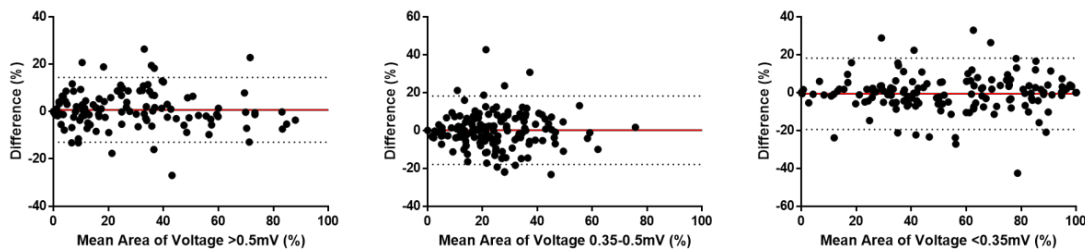


Figure 4-8. Bland-Altman plot showing agreement between peak-to-peak voltage area (datasets A and B) represented by voltage >0.5mV, 0.35-0.5mV, and <0.35mV for each data segment.

Similar to CFAE mean, there was a greater variance between patients than there was within patients: mean voltage >0.5mV, ICC 0.50 ($P < 0.0001$); mean voltage 0.35-0.5mV, ICC 0.16 ($P < 0.0001$); mean voltage <0.35mV, ICC 0.53, $P < 0.0001$. Variance was also greater for different locations within the same patient than the variance within the same locations for the same patient: mean voltage >0.5mV, ICC 0.95 ($P < 0.0001$); mean voltage 0.35-0.5mV, ICC 0.81 ($P < 0.0001$); mean voltage <0.35mV, ICC 0.94, $P < 0.0001$.

Using dataset A as a control group, delayed interval mapping (datasets C and D) was used to determine the stability of mean voltage over longer time periods (>10 minutes) in the same location. There was no overall difference between Delayed 1 and Delayed 2 compared to the control group across the three mean voltage ranges: mean voltage <0.35mV, P = 0.14; mean voltage 0.35-0.5mV, P = 0.15; mean voltage >0.5mV, P = 0.74.

4.3.5 Relationship between low percentage match and CFAEmean stability

A low percentage match suggests random activation as it is changing over time, rather than remaining stable. Locations with low percentage match were investigated to identify whether these locations also had unstable CFAE maps. This might assist in determining CFAEs that are drivers and those due to passive effect of fibrillatory conduction. Percentage match between datasets A and B was greater than one standard deviation below the mean in 18/161 data segments (mean 79.5% ± 7.7%). These locations were further analysed to see if they displayed variability in CFAEmean spatiotemporal stability, as well as percentage match in activation pattern.

The CFAEmean characteristics of datasets A and B for these 18 locations were reviewed. These data segments were identified on the Bland-Altman plots shown in Figure 4-8 to see if they were beyond the upper or lower limits of agreement, signifying variability between dataset A and B. There was no relationship between locations with a low percentage match and significant variability in CFAEmean for the three CFAEmean ranges (Figure 4-9).

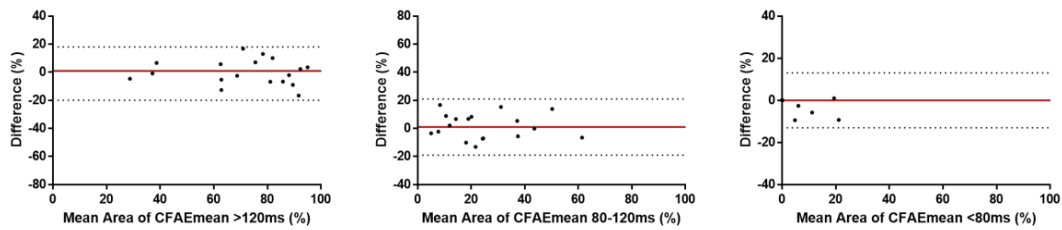


Figure 4-9. Eighteen data segments were identified with a percentage match more than one standard deviation below the mean (mean $79.5\% \pm 7.7\%$). These data segments were identified on the Bland-Altman plots showing the agreement between CFAEmean (datasets A and B) from Figure 4-8. There is no relationship between data segments that have a low percentage match and those with a variable CFAEmean (left to right): 1. CFAEmean $>120\text{ms}$, Bland-Altman mean difference 0.98, LOA -20.0 to 18.0, $r = 0.016$, $P = 0.84$; 2. CFAEmean 80-120ms, Bland-Altman mean difference 1.0, LOA -19.0 to 21.0, $r = 0.06$, $P = 0.46$; 3. CFAEmean $<80\text{ms}$, Bland-Altman mean difference -0.01, LOA -13.0 to 13.0, $r = 0.04$, $P = 0.61$.

4.3.6 Correlation between CFAEmean and mean bipolar voltage

Quantitative analysis of the area of peak-to-peak bipolar voltage and CFAEmean during persistent AF was performed for all data segments. This demonstrated a positive correlation, i.e. sites with a large area of fractionation (conventional CFAE range 80-120ms) had larger areas of high voltage: correlation between voltage $>0.5\text{mV}$ and CFAEmean 80-120ms ($r = 0.41$, $P < 0.0001$); correlation between voltage 0.35-0.5mV and CFAEmean 80-120ms ($r = 0.47$, $P < 0.0001$). However, there was no correlation between voltage and areas of rapid/near continuous fractionation (CFAEmean $<80\text{ms}$): voltage $>0.5\text{mV}$ and CFAEmean $<80\text{ms}$ ($r = 0.06$, $P = 0.42$); voltage 0.35-0.5mV and CFAEmean $<80\text{ms}$ ($r = 0.09$, $P = 0.25$); voltage $<0.35\text{mV}$ and CFAEmean $<80\text{ms}$ ($r = 0.09$, $P = 0.26$). (Figure 4-10).

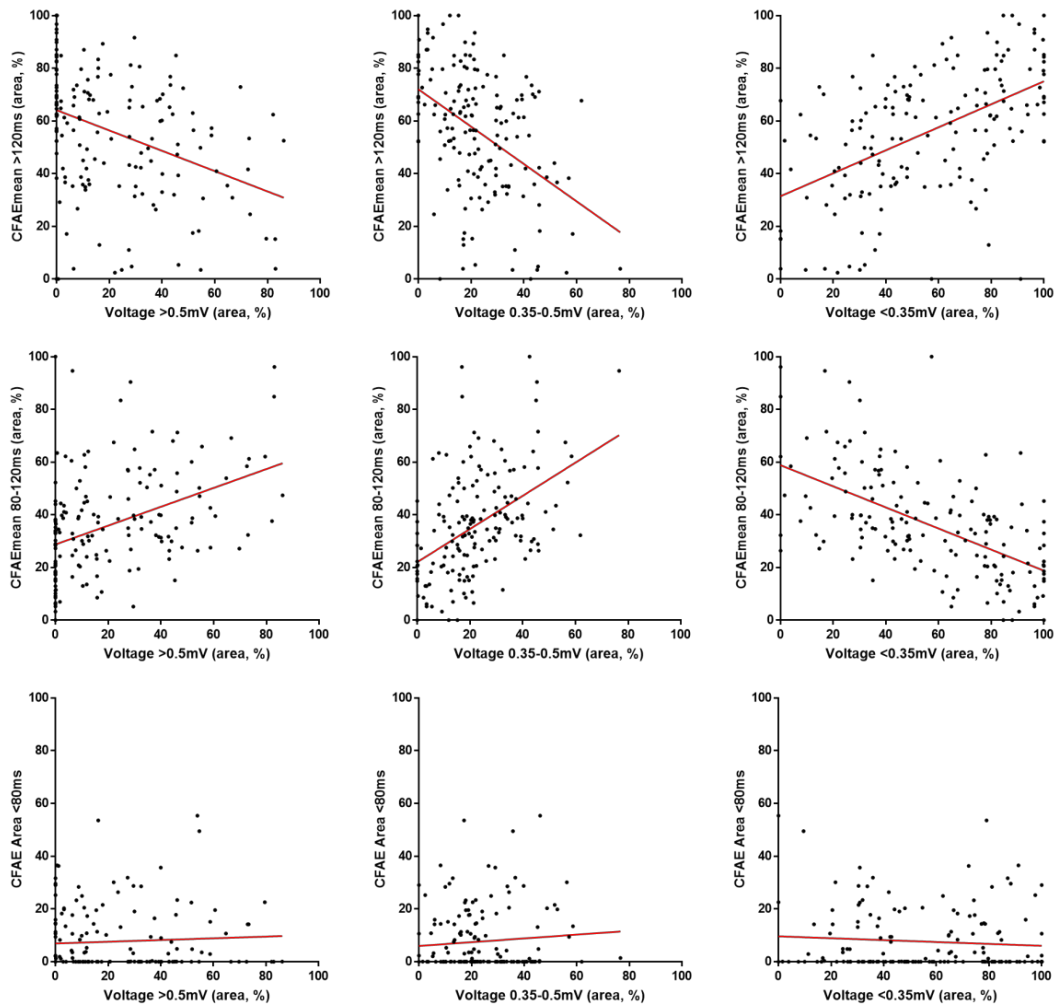


Figure 4-10. (Left to right, top row) Correlation between CFAE_{mean} >120ms (no CFAE) and: Voltage >0.5mV ($r = -0.37$, $P < 0.0001$); Voltage 0.35-0.5mV ($r = -0.44$, $P < 0.0001$); Voltage <0.35mV ($r = 0.52$, $P < 0.0001$). (Left to right, middle row) Correlation between CFAE_{mean} 80-120ms (conventional CFAE range) and: Voltage >0.5mV ($r = 0.41$, $P < 0.0001$); Voltage 0.35-0.5mV ($r = 0.47$, $P < 0.0001$); Voltage <0.35mV ($r = -0.58$, $P < 0.0001$). (Left to right, lower row) Correlation between CFAE_{mean} <80ms and: Voltage >0.5mV ($r = 0.06$, $P = 0.42$); Voltage 0.35-0.5mV ($r = 0.09$, $P = 0.25$); Voltage <0.35mV ($r = 0.09$, $P = 0.26$).

Excluding the effects of Amiodarone

The patient group that were not taking amiodarone were analysed again separately to investigate the relationship between CFAE_{mean} and mean bipolar voltage without the effects of amiodarone. This resulted in a stronger correlation between CFAE_{mean} >120ms and

CFAE_{mean} 80-120ms and all voltage groups. There remained no correlation between CFAE_{mean} <80ms in all voltage groups (Table 4-4).

CFAE _{mean} (ms)	Voltage (mV)	Correlation Overall (r)	Correlation Not on Amiodarone (r)
>120	>0.5	-0.37	-0.45
	0.35-0.5	-0.44	-0.46
	<0.35	0.52	0.60
80-120	>0.5	0.41	0.52
	0.35-0.5	0.47	0.51
	<0.35	-0.58	-0.69

Table 4-4. Table showing the strength of correlation between CFAE_{mean} and mean voltage for the overall patient population (combination of patient on amiodarone and not on amiodarone), and for only those patient not taking amiodarone. Correlation strength increases for all voltage groups when analysing patients not taking amiodarone separately.

4.3.7 The Effect of Amiodarone on CFAE_{mean} and Mean Voltage: A Sub-analysis

Eight patients were taking amiodarone at the time of data collection. These patients remained on amiodarone due to poor rate and symptom control when not taking this medication. A sub-study was carried out to identify the effects of amiodarone on CFAE_{mean} and mean bipolar voltage. Its effects were not studied on percentage match or R50 in this chapter, but have been studied in chapter 6.

Mean Voltage

The area (mean \pm SD, %) of voltage >0.5mV was significantly higher in patients that were not taking amiodarone compared to those taking amiodarone (24.5 ± 25.0 vs 16.08 ± 18.68 , respectively, $P = 0.015$). There was no significant difference in percentage area for atrial voltages of 0.35-0.5mV or <0.35mV ($P = 0.71$ and $P = 0.09$, respectively), although there was a trend towards patients that were taking amiodarone having a larger percentage area in these two lower voltage ranges. Mean percentage area of voltage 0.35-0.5mV: On amiodarone 23.23 ± 15.9 ; No amiodarone 22.31 ± 14.27 . Mean percentage area of voltage <0.35mV: On amiodarone 60.88 ± 27.2 ; No amiodarone 53.18 ± 29.31 (Figure 4-11).

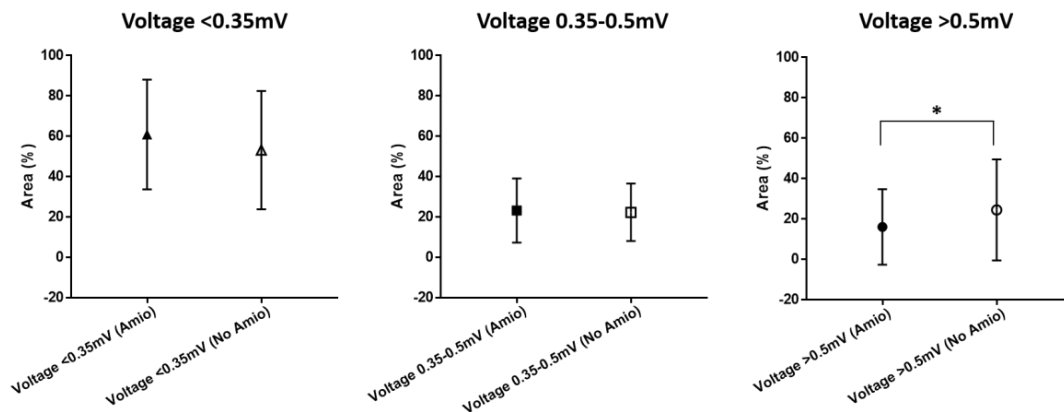


Figure 4-11. Effect of amiodarone on endocardial bipolar voltage area (mean \pm SD, %). Mean area of voltage $>0.5\text{mV}$ was significantly higher in patients that were not taking amiodarone (* $P = 0.015$).

CFAE_{mean}

The area (mean \pm SD, %) of CFAE_{mean} $<80\text{ms}$ (rapid/near continuous fractionation) was significantly higher in patients taking amiodarone compared to those not taking amiodarone (10.56 ± 13.92 vs 5.67 ± 9.46 , respectively, $P = 0.015$). The area of CFAE_{mean} $>120\text{ms}$ (not containing CFAE) was significantly lower in patients taking amiodarone compared to those not taking amiodarone (50.53 ± 25.02 vs 59.6 ± 22.38 , respectively, $P = 0.02$). There was no significant difference in the area of CFAE_{mean} $80\text{-}120\text{ms}$ (conventional CFAE range) between the two groups (38.67 ± 19.44 vs 34.69 ± 20.11 , respectively, $P = 0.21$). (Figure 4-12).

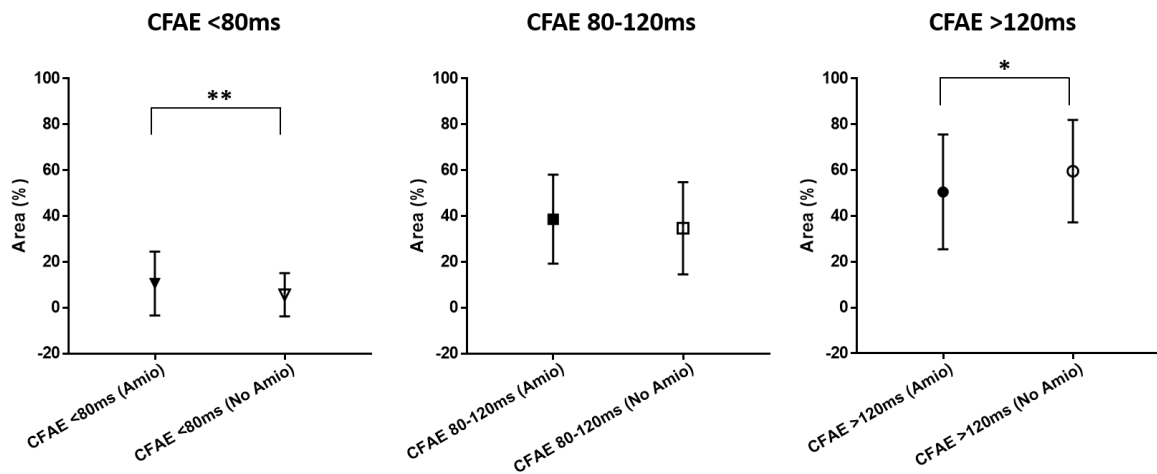


Figure 4-12. Effect of amiodarone on CFAE mean area (mean \pm SD, %). Area of CFAE mean >120ms was significantly higher in patients that were not taking amiodarone (* $P = 0.02$). Area of CFAE mean <80ms was significantly higher in patients that were taking amiodarone (** $P = 0.015$).

4.3.8 Organisation characteristics of persistent AF

Shannon entropy

Shannon entropy was calculated for each data segment during AF ($n=161$). A Bland-Altman plot was used to identify the level of agreement between data segments collected for dataset A and B (Figure 4-13). There was no significant difference in Shannon entropy between the two datasets (Bland-Altman mean difference: 0.003; limits of agreement: -0.37 to 0.37; $r = 0.13$; $P = 0.11$).

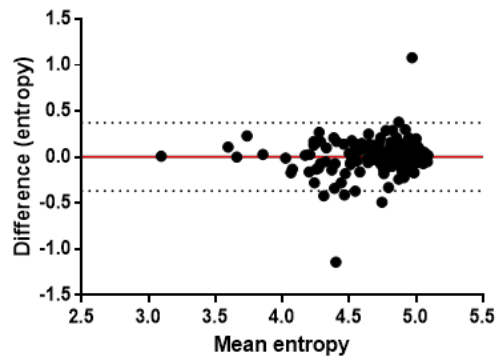


Figure 4-13. Bland-Altman plot showing agreement between Shannon entropy for each data segment (mean difference: 0.003; limits of agreement: -0.37 to 0.37; $r = 0.13$; $P = 0.11$).

Qualitative analysis of Shannon entropy in relation to the orbital plot highlighted some difficulties with its use. Entropy of datasets collected from a single location but at a different time could be compared with this method, however in some instances there was a disparity between the orbital plot activation patterns and the corresponding entropy. In situations of discrepancy, locations visually appeared to display organised activation in a single direction, but had a high entropy. One would expect entropy to be low with this type of orbital plot. This observation was related to orbital plots with a small amount of activation in all directions. Despite the majority of activation being in one ‘dominant’ direction, the low levels of activation in other directions resulted in a dramatic change in entropy. An example of this is shown below in Figure 4-14. This prevents comparisons being made between different mapping locations, although comparisons can be made between repeated measures from the same location.

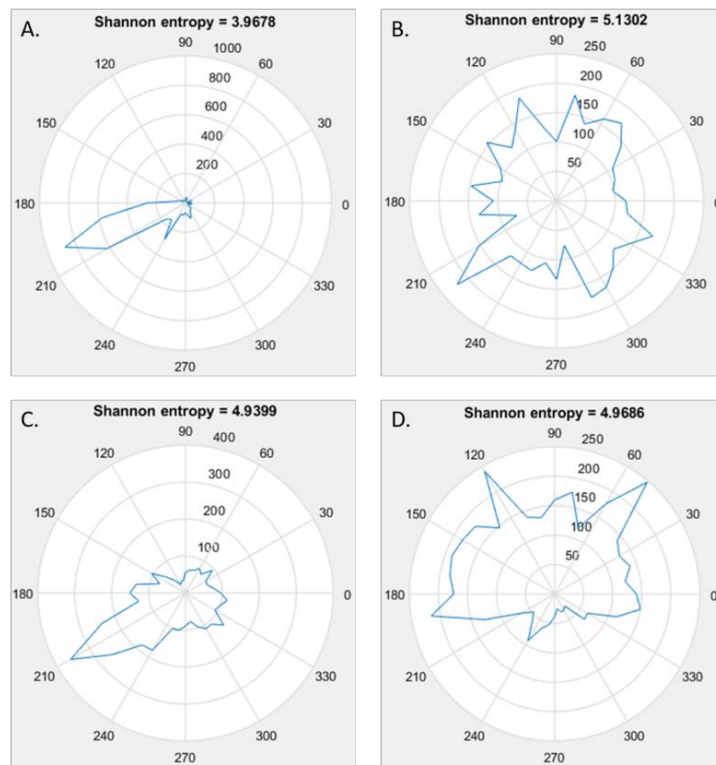


Figure 4-14. Orbital plots of four different data segments from different locations. The orbital plot of ‘A’ shows activation that had occurred in a single direction of activation, and corresponds to a low entropy. ‘B’ shows activation that has occurred in all directions, and has an appropriately high entropy. Orbital plot ‘C’ shows activation that is predominantly in a single direction, but a disproportionately high entropy due to low levels of activation in all directions. ‘D’ shows activation spread in multiple directions, but a similar entropy to ‘C’.

R50

The R50 is the range in degrees containing 50% of all activation for a location. For each data segment during AF, R50 remained stable in the same location between datasets A and B, with no significant difference (Bland-Altman mean difference: 0.87 degrees; limits of agreement: - 34.0 to 36.0; $r = 0.005$; $P = 0.95$). (Figure 4-15). Comparison between orbital plots and R50 showed visual consistency, where locations with a high R50 showed activation to be spread out in more different directions than locations with a low R50. Unlike Shannon entropy, R50 was unaffected by low levels of activation in different directions.

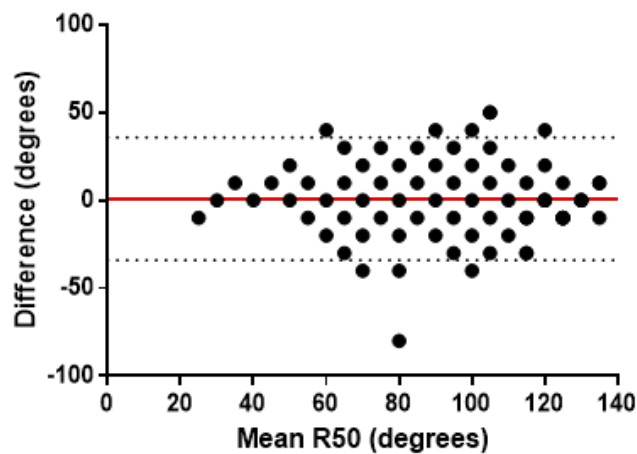


Figure 4-15. Bland-Altman plot showing R50 agreement between datasets A and B for each data segments (mean difference: 0.87 degrees; limits of agreement: -34.0 to 36.0; $r = 0.005$; $P = 0.95$)

Although R50 remained stable in the same location, the variance of R50 between patients was greater than the variance within patients (ICC 0.281; $P < 0.0001$). A greater variance in R50 was also observed between different locations within the same patient than the variance within the same locations for the same patient (ICC 0.765; $P < 0.0001$).

Using dataset A as a control group, delayed interval mapping (datasets C and D) was used to determine the stability of R50 over longer time periods (>10 minutes) in the same location. There was no overall difference between Delayed 1 and Delayed 2 compared to the control group ($P = 0.34$).

Comparison of Shannon entropy and R50

Comparative assessment was made between Shannon entropy and R50. The agreement between datasets A and B for these parameters were demonstrated with Bland-Altman analysis. Therefore, dataset A was used to identify the correlation between Shannon entropy and R50 (Figure 4-16). There was a weak positive correlation between entropy and R50 ($r = 0.32$, $P < 0.0001$).

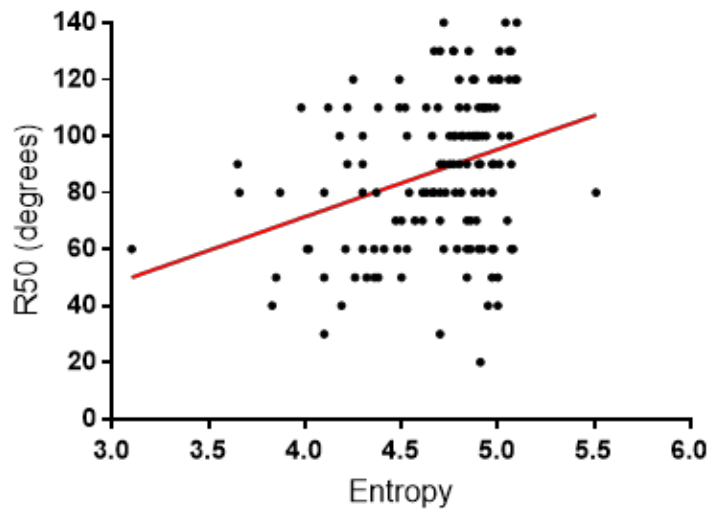


Figure 4-16. There was a weak positive correlation between Shannon entropy and R50 ($r = 0.32$, $P < 0.0001$).

4.3.9 Correlation between CFAE_{mean} and R50

Areas that did not contain CFAEs were defined as those with a CFAE_{mean} >120ms. There was a weak negative correlation between area of CFAE_{mean} >120ms and increasing R50 ($r = -0.27$, $P < 0.0001$). Areas containing CFAEs in the typical range of 80-120ms, showed a slightly stronger positive correlation between area of CFAE_{mean} and increasing R50 ($r = 0.36$, $P < 0.0001$). Highly fractionated areas, with a CFAE_{mean} <80ms, did not show any correlation with R50 ($r = -0.05$, $P = 0.55$). (Figure 4-17).

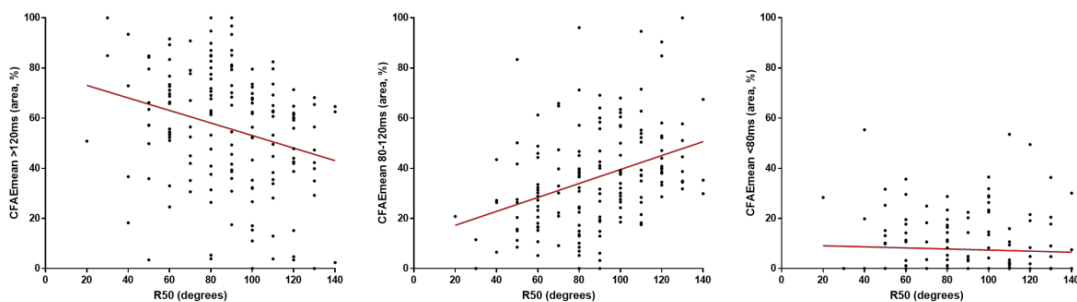


Figure 4-17. (Left to right) Correlation between CFAE_{mean} >120ms and R50 ($r = -0.27$, $P < 0.0001$); CFAE_{mean} 80-120ms and R50 ($r = 0.36$, $P < 0.0001$); and, CFAE_{mean} <80ms and R50 ($r = -0.05$, $P = 0.55$).

4.3.10 Correlation between CFAE_{mean} and Shannon entropy

There was no correlation between Shannon entropy and CFAE_{mean}: CFAE_{mean} >120ms ($r = -0.08$, $P = 0.30$); CFAE_{mean} 80-120ms ($r = 0.10$, $P = 0.22$); CFAE_{mean} <80ms ($r = 0.01$, $P = 0.88$). (Figure 4-18).

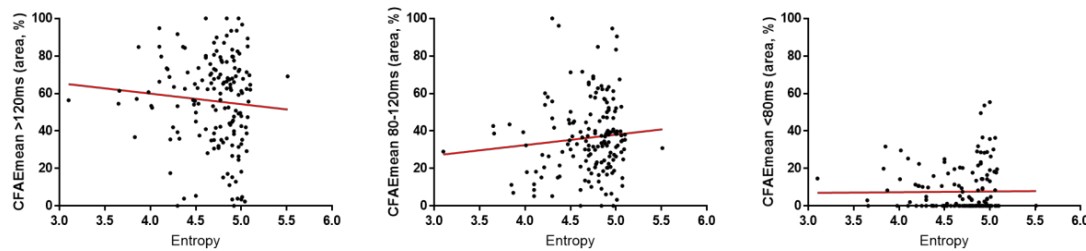


Figure 4-18. No correlation between Shannon entropy and CFAE_{mean} (above) or mean peak-to-peak voltage (below).

This finding is important, as it suggests that entropy cannot be used to assess the degree of organisation during AF. One would expect there to be a relationship between the amount of organisation in a particular direction, and the presence or absence of fractionation.

4.4 Discussion

These data demonstrate that there is evidence of spatiotemporal stability of a number of parameters during persistent AF. Although activation patterns appear chaotic, they are not random, and show consistency at anatomical locations. RETRO-Mapping has the advantage that there is no requirement for setting a window of interest, and the user does not need to manually assign LAT to electrograms. The automation of this process enables longer durations of AF to be mapped, over larger atrial surface areas compared to manual analysis. Therefore, sequential mapping is justified provided analysed segments are of sufficient durations.

A mapping duration of 30 seconds for each data segment was chosen, as utilised by others using CARTOFINDER.¹²⁵ This mapping duration was chosen because a balance between optimal mapping duration for sufficient data collection, and procedural efficiency was required. At this duration of data collection, the majority of activation patterns were not significantly different to those obtained from 60 seconds of mapping. This implies that in the majority of cases, collection of 30 seconds is sufficient.

Percentage match was used as a method to determine the similarity of activation patterns for a given location that has been mapped at a different time. During atrial tachycardia, one would expect a theoretical percentage match of 100% if the same location was mapped at different times. This of course would be unlikely given that very minor catheter movements will occur over the course of data collection for each 30 second data segment. The overall mean percentage match for datasets A and B was 79.5% across 161 different locations from 18 patients. Therefore, it is unlikely that this has occurred by chance alone. This high percentage match results from multiple wavefronts occurring in the same direction but at different times. Transient linking has been described by others, and the probability of such an event being reported as unlikely to have occurred by chance.^{113, 129} Although this in itself is important, datasets A and B have been collected sequentially from each location. It was not clear if this phenomena was only present over short periods of time, or whether stability was maintained for longer periods of time.

The notion of spatiotemporal stability was further supported with data from delayed mapping of a single location, carried out in 9/18 patients. Using percentage match between dataset A and B as a control group, two delayed interval mapping groups were created by returning to the same location at least 10 minutes later (mean delay between dataset A and C; 20mins 34secs), and collecting two further datasets (C and D). Even with delayed interval mapping, percentage match in activation pattern remained unchanged compared to the control group. In part, small differences in percentage match are contributed to by the minor differences in catheter position when trying to orientate the AFocusII with the exact shadow position of the control datasets. The remainder may represent a degree of variability in local activation at different times due to cardiac anisotropy.

Recently, CARTOFINDER has been used to target intermittent but repetitive focal activation during AF, resulting in high rates of AF termination or AF cycle length prolongation.¹²⁵ High rates of freedom from atrial arrhythmia recurrence at 12 months have been observed using a novel dipole density mapping technique to target localised, non-PV regions in the atrium in addition to PVI.¹²⁶ The success of these techniques suggests that the localised regions that were targeted have stable characteristics, otherwise neither AF termination or increased arrhythmia free survival should have resulted. Spatiotemporal stability of atrial activation patterns may be the result of localised mechanisms maintaining AF, and explain the success in the aforementioned studies using CARTOFINDER¹²⁵ and dipole

density¹²⁶ mapping. Similarly, the inconsistency in determining spatiotemporal stability of rotors may explain the challenges of reproducibility in ablation outcome.^{44, 130, 131}

Qualitative analysis of the orbital plots for delayed interval mapping highlighted a clear difference between the activation patterns observed in the control group compared to both delayed interval mapping groups in only one patient (Patient 6). Interestingly, there was no difference in percentage match when comparing the two delayed interval mapping datasets, and the two control group datasets with one another. This shows that there may be periodicity to spatiotemporal stability in some locations. Kuklik *et al.* observed transient linking of wavefronts, and the occurrence of multiple different uniform wavefront directions and different wavefront sequences (i.e. rotational, collision, conduction block) occurring in the same locations at different times.¹²⁹ A mapping duration of 30 seconds for each dataset may have important implications if spatiotemporal periodicity occurs over prolonged periods of time, and might explain the changes observed in Patient 6. Support for this argument comes from epicardial wave mapping of persistent AF by Lee *et al.* in which activation patterns were described as heterogeneous and unstable when using a mapping duration of 10 seconds.¹³² This is contrary to the findings of our data, and might be explained by the use of a mapping duration that is of insufficient duration.

Alongside activation mapping of persistent AF with RETRO-Mapping, more conventional parameters were investigated to see if these also displayed spatiotemporal stability. It is debatable whether CFAE spatiotemporal stability exists. Using a 64-electrode basket catheter for simultaneous data acquisition over a continuous 5 minute period during AF, Habel *et al.* reported spatiotemporal variability in characteristics of CFAE.¹³³ In contrast to this, Kogawa *et al.* used the same basket catheter, identifying the presence of spatiotemporal stability over a 10 minute period in both paroxysmal and persistent AF.¹³⁴ More recently, mean bipolar voltage has been shown to stabilise with a mapping duration >4 seconds when comparing consecutive maps during AF.¹³⁵ Our data supports the spatiotemporal stability of both 8-second CFAE mean and mean peak-to-peak bipolar voltage maps collected sequentially with a roving catheter. More importantly we have demonstrated with delayed interval mapping that spatiotemporal stability remains present. Interestingly, Patient 6 also showed a significant difference when comparing CFAE mean 80-120ms (P = 0.03, Delayed 1 and 2 vs. Control) and CFAE mean >120ms (P = 0.02 Delayed 1 vs. Control, P = 0.04 Delayed 2 vs. Control) to the control group. This again highlights that there may be something mechanistically

different about this patient or atrial location, or that CFAE spatiotemporal periodicity may occur at some locations.

Analysis of data segments showing variability in activation patterns was undertaken to ascertain whether these locations also contained variability in CFAE mean maps over time, as was observed with delayed interval mapping for Patient 6. Data segments with a mean percentage match greater than one standard deviation below the mean were identified. These 18 data segments were identified on the Bland-Altman plots assessing CFAE mean agreement between datasets A and B. All of these data segments were within the limits of agreement on the Bland-Altman plots. This is interesting, as it suggests that although activation patterns displayed less spatiotemporal stability, CFAE mean remained stable in these locations. This goes against observations that have shown electrogram fractionation to be highly dependent on direction of activation.¹³⁶ However, these differences were based on comparing CFAE locations identified during AF, CS pacing and sinus rhythm. Analysis in our study was unfortunately offline, however understanding the effect of ablation at these locations may be valuable.

Further analysis of CFAE mean, mean bipolar voltage and percentage match was undertaken using intra-class correlation coefficient (ICC) statistics. We observed that all three of these parameters expressed a greater variability between patients than between different locations within the same patient. This is logical, as the underlying structural consequences and pathological processes are likely to express greater heterogeneity between patients, than within different atrial areas of the same patient. Furthermore, the underlying mechanism may also be a contributory factor, particularly if different mechanisms exist in different patients.

Comparative assessment was made between mean bipolar voltage and CFAE mean. This showed a positive correlation, i.e. sites with a large area of fractionation (conventional CFAE range 80-120ms) had larger areas of high voltage (voltage >0.5mV and 0.35-0.5mV). These findings are in keeping with the observations of others, where an inverse relationship has been found between areas of gadolinium enhancement on MRI, and CFAE. Jadidi *et al.* suggest that atrial fibrosis (i.e. low voltage) is associated with slower and more organised conduction, while more healthy regions of the atrium (i.e. higher voltage) is associated with CFAE.⁶⁹ In contrast to the findings of Jadidi *et al.* there was no relationship between bipolar voltage and areas of rapid/near continuous fractionation (CFAE mean <80ms), despite using very similar mapping parameters. In this study bipolar contact electrograms were used to

determine voltage directly. Jadidi *et al.* used gadolinium enhancement from atrial MRI to determine locations of fibrosis. The anisotropic properties of the atrium with the contact electrogram will provide a more functional assessment of the atrium, and is likely to represent significant differences to the more anatomical and static information obtained with gadolinium enhancement. These two different methods for determining 'healthy' and 'unhealthy' areas in the atrium may therefore be responsible for the different observations in the relationship between bipolar voltage and CFAEmean <80ms.

Eight of the patients studied remained on amiodarone during the time of data acquisition due poor rate and/or symptom control without its use. A subgroup analysis was carried out to separate the patients that were taking amiodarone from those not taking amiodarone, to investigate its effects on endocardial mean voltage and CFAEmean. Patients taking amiodarone were found to have significantly smaller areas where the voltage was >0.5mV. Amiodarone has multiple effects on a wide variety of voltage gated ion channels.¹³⁷ These effects are frequently inhibitory or down-regulatory. There is no literature to suggest that amiodarone results in a decreased endocardial bipolar voltage, but it is understandable why it might. Alternatively, the patient group that were taking amiodarone may simply reflect patients with a higher underlying burden of fibrosis/disease substrate. Hence, these patients required powerful antiarrhythmic drugs like amiodarone for rate and symptom control. Similarly, patients that were not taking amiodarone has a significantly smaller area of CFAEmean <80ms (rapid/near continuous fractionation), and significantly larger area of CFAEmean >120ms (no CFAE). In contrast to this, Miwa *et al.* showed that patients taking amiodarone had fewer areas of CFAE requiring ablation than patients not taking amiodarone.¹³⁸ It is likely that our result represents healthier atria in patients not requiring amiodarone for symptom control rather than a direct amiodarone effect.

AF cycle length is often used to quantify extent of organisation during AF. The AF cycle length is determined either from the LAA or sometimes the mid-CS. However, this measurement is crude and represents an overall summary from the entire chamber rather than the subtle differences at different locations. Longer AF cycle lengths are associated with fewer regions containing CFAE.¹³⁸ The degree of fractionation is commonly used to comment on how 'organised' or 'disorganised' a location is during AF. The degree of fractionation can vary for different locations in the atria. When an orbital plot is produced for a mapped location, it is a summary of the data acquired from all electrodes of the AFocusII catheter over

the duration of the mapping period. Spatiotemporal dispersion of fractionation has been described, where a highly fractionated bipolar electrogram can neighbour an organised and unfractionated bipolar electrogram.⁹¹ Orbital plots do not allow spatiotemporal dispersion to be appreciated. R50 was developed as a novel tool to quantify organisation of a mapped location by summarising the orbital plot data acquired from each catheter location.

R50 is the range in degrees containing 50% of the total activation for an orbital plot. A high R50 represents a location in which activation is spread out and occurs in multiple different directions. A low R50 represents a location in which activation directions are less variable. A positive correlation between increasing area of CFAE 80-120ms and increasing R50, was observed. This is in agreement with what one might expect, and aligned with shorter AF cycle lengths in instances of greater fractionation. Locations with large areas of fractionation are more likely to show activation in multiple directions (higher R50), indicating that these areas are more disorganised. R50 also displays the same characteristics as CFAE_{mean} with variability in the degree of organisation within different locations in the same patient, but greater variability when comparing different patients. This is in agreement with clinical observations, where some patients appear to have more 'organised' AF than others.

The changing wavefront direction near the pivot point of rotational sites results in a broad distribution of bipolar electrogram amplitudes in close proximity to it. Shannon entropy has been used to demonstrate that locations with a high entropy co-localise with the pivot point of rotational sources.¹³⁹ It would therefore be expected that locations with frequent uniform wavefronts might have a low Shannon entropy, however our results did not reflect this. A falsely high entropy, indicating 'less organised' activation occurred in certain situations. If low levels of activation occurred in multiple directions, and despite the majority of activation being highly organised in a narrow and single direction, a high entropy was assigned. Although mapping of the same location at a different time resulted in entropy reproducibility locally, they were not always visually reflective of orbital plots. This prevented comparison of different locations which could contain a similarly high entropy, but clear visual differences in orbital plot organisation.

4.5 Limitations

Mapping was restricted to limited regions of the left atrium. This was because of the time required to collect data from each location twice. Having demonstrated stability of activation

patterns, a larger left atrial area can be mapped within the same time period as only a single data segment from each location is required. It is likely that percentage match in activation patterns for locations is higher than those observed. Small movements in the catheter will affect the percentage match, especially with delayed mapping which involves returning to a previous location several minutes later.

One of the consequences of offline analysis was the requirement for a fixed data collection time period to be adhered to. Some patients have more 'organised' AF, and therefore it is likely that these patients do not require data collection for such long periods of time. A stable atrial tachycardia technically requires only a single wavefront in each location. As such, online data export and analysis would enable the operator to identify the optimal mapping period with a patient tailored approach.

4.6 Conclusion

RETRO-Mapping has been developed to further investigate activation patterns during AF to advance our mechanistic understanding. This chapter presents the important novel discovery that during sequential mapping, atrial activation patterns during persistent AF do not appear to be random, but show distinct stability over prolonged periods of time. This is important because it validates a sequential mapping technique, suggesting that it is feasible to compare sequentially mapped locations. Established metrics, including CFAE_{mean} and mean bipolar voltage, were also investigated. These also expressed spatiotemporal stability. A novel tool has also been developed – R50 – for quantitative analysis of the degree of organisation in mapped locations, and can be used to compare different locations in the same or different patients. The relationship between an increasing R50 and areas containing larger areas of fractionation, which supports R50 as a method to determine organisational characteristics of AF. One would expect that larger areas of fractionation would result in a greater degree of disorganisation. Further work is required to develop a method to display sequentially mapped locations so that they can be easily interpreted. It is also important to establish the underlying cause of the observed stable activation patterns. This may assist with identifying the mechanisms responsible for the observed activation patterns, and ultimately targets or strategies for ablation.

5 Focal Activation during Persistent Atrial Fibrillation

5.1	Introduction.....	127
5.2	Methods	128
5.2.1	Patient selection	128
5.2.2	Characterising Atrial Activation Patterns	129
5.2.3	Additional tools for analysis	130
5.2.4	Myofiber Architecture	131
5.2.5	Statistical analysis.....	131
5.3	Results	132
5.3.1	Wavefront characteristics during persistent AF.....	132
5.3.2	Focal Activations and Conventional Markers of Atrial Substrate ...	135
5.3.3	Focal Activations and Novel Markers of Atrial Substrate.....	137
5.3.4	Choropleth Maps.....	139
5.3.5	Effect of Amiodarone on Focal Activation.....	141
5.3.6	Effect of Duration of Persistent Atrial Fibrillation on Focal Activation	141
5.3.7	Atlas of Myofiber Architecture with Choropleth Maps.....	143
5.4	Discussion	144
5.5	Limitations	146
5.6	Conclusion	146

5.1 Introduction

In the previous chapter, the feasibility of a sequential activation mapping technique for persistent AF has been demonstrated. This is based on the premise that atrial activation patterns during persistent AF are not random but remain stable over time, despite their chaotic appearance. It is therefore possible to compare activation patterns of locations that have not been simultaneously acquired. This is a major change in our thinking of AF mechanism, and goes against the multiple wavelet hypothesis, which describes random re-entry of multiple wavelets. However, it does not directly explain the underlying mechanism responsible.

Focal drivers from the pulmonary veins remain the only consistently demonstrated mechanism driving human AF, irrespective of mapping techniques. PVI has produced consistent and reproducible results between different centres and technologies, confirming the importance of PV drivers in AF.^{7, 140} Patients in whom PVI does not prevent AF are assumed to have other perpetuators such as non-PV focal drivers, spiral waves, localised re-entry or macro-reentry.^{49, 141} This has motivated adjunctive ablation techniques, but these remain inconsistent in outcome studies.^{83, 142, 143}

Atrial delayed enhanced MRI has identified that the majority of CFAEs reside in locations either without fibrosis or with only patchy fibrosis, while atrial fibrosis is associated with slower and more organised conduction.⁶⁹ This is supported by data showing a correlation between fractionation and higher bipolar voltages in the previous chapter, and in agreement with data from other groups.¹³⁶ In this chapter, the relationship between focal activation and spatiotemporally stable characteristics including CFAE and bipolar voltage are studied. Subsequently, RETRO-Mapping is used to further characterise and map atrial activation patterns during persistent AF. A focal driver hypothesis, where focal activation beyond the pulmonary veins drives fibrillation, may offer an explanation for atrial activation patterns. It is based upon the assumption that the perpetuators of AF are competing and intermittent, but have characteristic activation patterns and anatomical stability. Therefore, activation close to a perpetuator comprises: wavefronts characteristic to that perpetuator; wavefronts characteristic to other perpetuators; and meandering wavefronts. Importantly, activation is not random. To illustrate this concept, consider the idealised case of two focal sources. Figure 5-1 illustrates the effect of using a multi-electrode mapping catheter on the myocardium in

between two stable drivers that are competing to activate the myocardium. Using this simple theoretical model of AF, it is immediately apparent from sequential wavefronts in the region of the catheter, that there are two alternating directions of activation. With data collection from multiple locations, it would be possible to locate the anatomical regions where the AF perpetuators are situated.

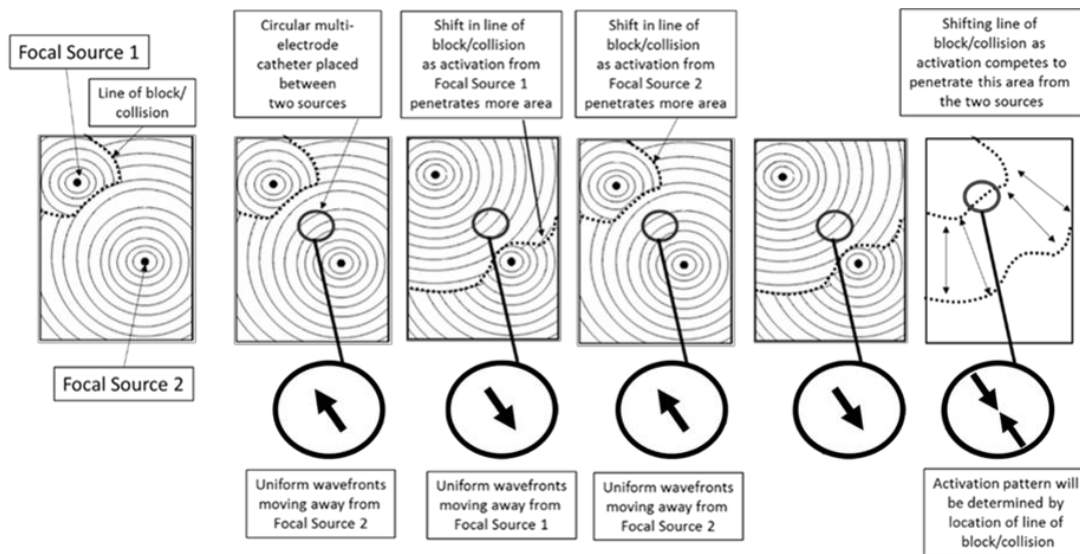


Figure 5-1. Theoretical model of a ‘focal driver’ mechanism for atrial fibrillation. Two focal sources are shown. A line of conduction block/collision occurs where the two focal sources interact with one another. This line of block/collision will shift over the course of time depending on the cycle lengths of the respective focal sources, and the refractory properties of the myocardium. A multi-electrode mapping catheter held in a stable position between these two focal sources can be used to identify the activation direction. Due to the shifting line of block/collision as the focal sources compete with one another, the activation direction will change.

5.2 Methods

5.2.1 Patient selection

One hundred and fourteen data segments were collected from 18 patients with persistent AF. All patients were undergoing clinically indicated procedures, and were prospectively recruited. Procedures were carried out using the same technique described previously (see Section 2.2.2). Antiarrhythmic drugs were stopped at least 5 half-lives before the day of the procedure, with the exception of amiodarone. Six patients were established on this medication, and continued to take it up to the day of their procedure. Five patients had

previously undergone left atrial ablation with PVI only, but no linear left atrial ablation. Two patients were in sinus rhythm on the day of their procedure as they had undergone electrical cardioversion for symptom control while awaiting catheter ablation. Table 5-1 shows details of patient characteristics.

Case	Age (yr)	Gender	Previous AF ablation	Duration in persistent AF	LA dimension (mm)	Amiodarone
1*	56	M	No	36	45	Y
2	58	M	No	5	43	N
3	35	M	Yes	6	32	N
4	53	M	Yes	24	47	N
5	67	M	No	48	41	N
6	59	M	Yes	8	46	N
7	63	F	No	10	34	N
8	64	M	No	3	41	N
9	66	F	No	18	51	Y
10*	78	F	No	12	49	N
11	70	M	No	10	41	Y
12	53	M	No	12	42	N
13	60	M	No	22	42	N
14	83	F	No	19	38	N
15	66	F	No	14	45	Y
16	53	F	Yes	22	32	Y
17	55	F	Yes	16	30	N
18	56	M	No	12	54	Y

Table 5-1. Patient demographics and characteristics. *Patients induced on the day of their procedure.

5.2.2 Characterising Atrial Activation Patterns

Mapping was performed using the AFocusII catheter to collect 30 second data segments. Mapping was restricted to the posterior wall and floor of the left atrium because of the relative ease of obtaining good contact with all electrodes of the AFocusII catheter. It is appreciated that there may be local differences in atrial activation patterns. The number of data segments collected varied between patients as some patients had extensive regions where no atrial electrograms could be collected. These data were exported for offline processing with RETRO-Mapping.

Manual Data Analysis using RETRO-Mapping

Data segments were manually reviewed with RETRO-PM to characterise and document the types of wavefront that occur during persistent AF. Bipolar electrograms were simultaneously reviewed to ensure that the RETRO-PM was an accurate representation.

Analysis of Choropleth Maps

A choropleth map was produced for each patient. Focal activations identified during manual analysis were placed on the choropleth map in the location where earliest activation had been observed. A focal activation was defined as activation in which a wavefront starts from a point within the catheter mapping area, and eccentrically propagating outwards towards the periphery of the catheter in all directions. Qualitative analysis was undertaken to identify the relationship of dominant activation directions in relation to the location of focal activations. Based on the theoretical model shown in Figure 5-1, the dominant direction of activation would be expected to move away from focal sources in all directions.

Surrogate Markers of Atrial Substrate

Using the method described in the previous chapter, 8 second CFAE_{mean} and mean peak-to-peak bipolar voltage area of each data segment was calculated. The area of CFAE_{mean} >120ms (not containing CFAE), 80-120ms (conventional CFAE range), and <80ms (rapid/near continuous fractionation); and voltage >0.5mV, 0.35-0.5mV and <0.35mV was calculated for each data segment. This was done to identify the relationship between atrial activation patterns and focal activations with the underlying atrial substrate.

R50 and Number of Dominant Directions

RETRO-Mapping was used to calculate R50 (the range in degrees containing 50% of activation in an orbital plot), and number of dominant directions (see below, Section 5.3.3) for each data segment to determine organisation characteristics. These data were also analysed to study the relationship between organisation and focal activations.

5.2.3 Additional tools for analysis

Dominant Directions of Activation

A qualitative approach was initially taken for identification of the number of dominant directions. In situations where there was a clear single dominant direction, observational analysis was possible. However, analysis was extremely difficult for all other situations. Custom software was therefore written to assign dominant directions of activation in order to overcome this problem, and provide a more objective measure.

The dominant direction of activation is determined by firstly smoothing the probability distribution from the orbital plot using a Savitzky-Golay filter with 5th order polynomial and

frame width of 7 samples. A Savitzky-Golay filter is a digital filter that can be applied to a set of digital data points in order to smooth the data, and increase the signal-to-noise ratio. This is followed by a local peak detection which is used to locate the dominant peaks in the data to identify the angles at which the highest probability of activation occurs. A high number of dominant directions relates to a data segment that has uniform activation in multiple different directions. Orbital plots with a lower number of dominant directions are representative of locations containing a greater amount of its total activation in fewer different directions. This information is different to that gained using R50. R50 will only provide information on the spread of activation in different directions. It does not tell you how that activation is directed. Identification of the number of dominant directions will help to identify the direction, or directions that activation is occurring. For example, R50 may be the same for two different locations. However, activation in one location might all be going in a single direction, whereas the activation for the other location may be split in two different directions. If atrial activation patterns are determined by focal drivers, it is important to be able to define the relationship of these drivers with dominant directions of activation.

5.2.4 Myofiber Architecture

An atlas of myofiber orientation⁷⁸ was merged with the choropleth map for each patient. Following analysis of each data segment, the orbital plot for each location was analysed with respect to its corresponding location on the myofiber orientation atlas. Activation direction was assessed qualitatively for each data segment with respect to myofiber orientation. Activation was reported as either 'related' (similar direction, within 30 degrees either side) or 'unrelated' (different direction, >30 degrees either side) to myofiber orientation. This was done to identify whether atrial activation patterns during persistent AF are determined by the underlying myofiber orientation, or if activation patterns are independent of the underlying structural architecture.

5.2.5 Statistical analysis

Results were expressed as mean +/- SD. Welch's t-test and correlation statistics were used to identify relationships between mapping parameters. A value of $P < 0.05$ was considered statistically significant.

5.3 Results

5.3.1 Wavefront characteristics during persistent AF

A total of 114 data segments were recorded from the posterior wall and floor of the left atrium in 18 patients. Qualitative assessment of RETRO-PM and RETRO-AD demonstrated the presence of uniform wavefronts in all data segments. These were interspersed with disorganised activity and a variety of activation patterns that have been described in the AF mapping literature (Figure 5-2, A). These include (See Movie 5-1):

- Uniform wavefronts – Activation showing directional uniformity moving across the catheter from one side to the other
- Focal activation – activation of a wavefront starting from a point within the catheter contact area, and eccentrically propagating outwards towards the periphery of the catheter
- Rotational waves – rotational movement of a wavefront through $\geq 360^\circ$ to that of its origin
- Turning waves – movement of a propagating wavefront through $>45^\circ$ but $<360^\circ$ to that of its origin
- Wavefront collision – two or more uniform wavefronts propagating across, and colliding within, the catheter mapping area

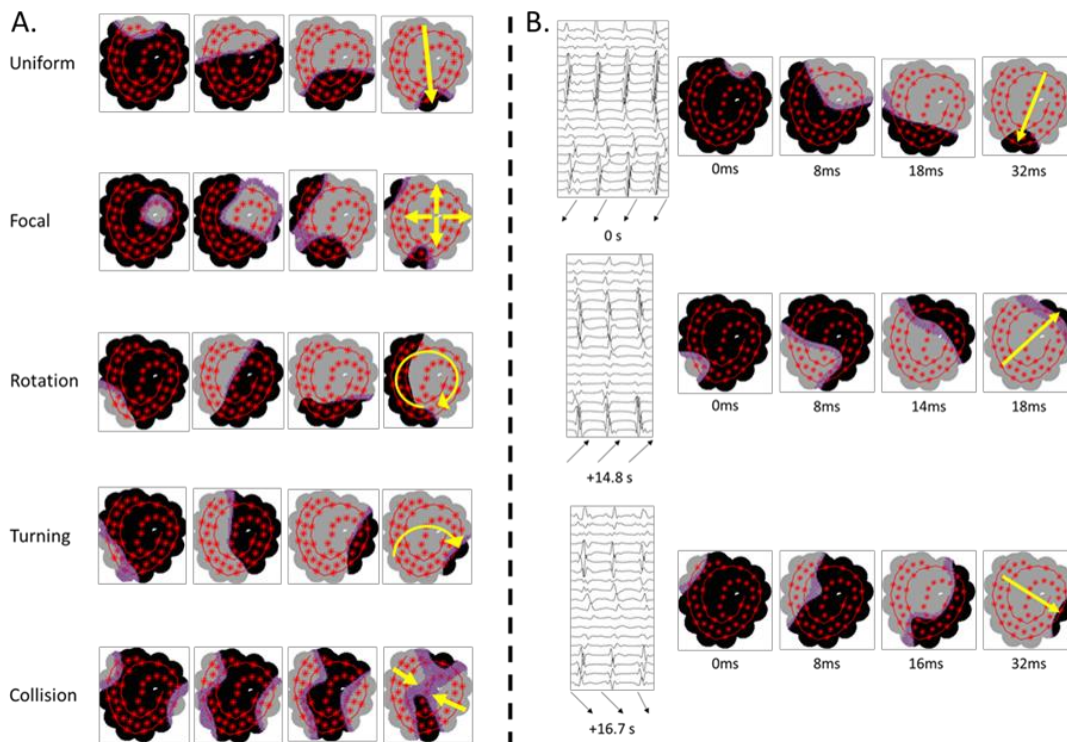


Figure 5-2. (A. Top to bottom panel) Examples of a uniform wavefront, focal activation, rotational activation, turning wavefront, and wavefront collision identified during manual analysis. The activating wavefront can be seen to progress across the face of the catheter in grey (moving from left-to-right across each row), and the direction of activation manually assigned (yellow arrow). (B.) Example of ‘transient linking’ of wavefronts in the same data segment at different time points. Below the electrograms of each wavefront, an arrow shows the wavefront activation direction. There are only small differences in the activating directions of successive wavefronts. Three different directions of activation are shown (top to bottom). The activating wavefront is shown in grey to progress across the catheter and the manual direction is assigned (yellow arrow).

After uniform wavefronts, a similar direction of uniform wavefront could then re-appear several seconds later at the same catheter location (Figure 5.2, B). On some occasions repetitive uniform wavefronts were seen to follow one another consecutively - ‘transient linking’.¹¹³ Multiple different directions of transient linking sometimes occurred in the same location at different time points. Transition between directions of activation was observed during episodes of disorganisation, spontaneously, or following episodes of wavefront collision. When wavefront collision occurred, transition between activation directions often matched the directions of the colliding wavefront directions involved.

Focal Activations

Thirteen (13/18) patients showed evidence of focal activations from 32 (32/114) data segments. In total, 111 focal activations were observed. When focal activations were identified, they could either occur as a single focal activation, or as multiple focal activations sequentially, where one immediately follows another. Further information about the number of focal activations in each patient is provided in Table 5-2.

Case	Total number of focal activations	Data segments with focal	Total number of data segments	Mean focal activation number	Duration in persistent AF	Amiodarone
1*	11	2	6	1.8	36	Y
2	4	2	8	0.5	5	N
3	17	4	7	2.4	6	N
4	7	1	3	2.3	24	N
5	0	0	4	0	48	N
6	6	1	6	1	8	N
7	12	2	7	1.7	10	N
8	9	2	4	2.3	3	N
9	20	4	4	5	18	Y
10*	5	3	3	1.7	12	N
11	4	4	8	0.5	10	Y
12	0	0	8	0	12	N
13	6	3	11	0.6	22	N
14	6	3	7	0.9	19	N
15	0	0	6	0	14	Y
16	0	0	5	0	22	Y
17	0	0	7	0	16	N
18	4	1	10	0.4	12	Y

Table 5-2. Frequency of focal activations in each patient. All patients were spontaneously in persistent AF on the day of the procedure with the exception of two patients (*AF induced on the day of the procedure). Mean number of focal activations is calculated by dividing the total number of focal activations by the total number of data segments.

Single focal activations were the most common, and occurred a total of 69 times in 30/32 data segments. Episodes of repetitive non-sequential single focal activations occurred in 16 of these data segments. This is where a single focal activation was observed, interspersed with other activation patterns, followed by recurrence of a further single focal activation in the same location at a later time.

Sequential focal activations were less commonly observed. Two sequential focal activations were identified 14 times in 11/32 data segments, three sequential focal activations 2 times in 2/32 data segments, and four sequential focal activations 2 times in 2/32 data segments. There was no evidence on sustained focal activations lasting longer than 4 sequential activations (Figure 5-3).

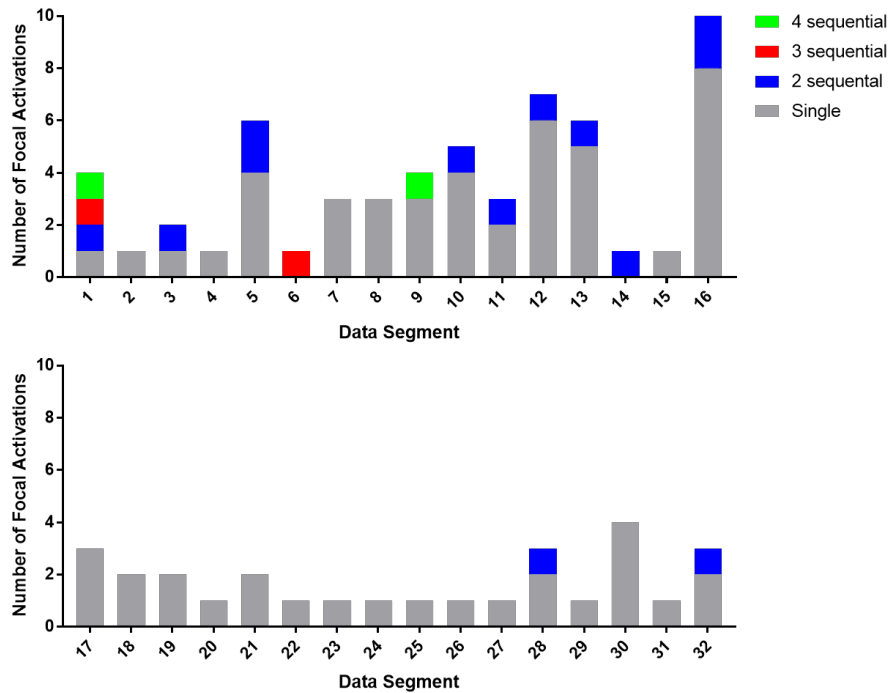


Figure 5-3. Frequency and pattern of focal activation is displayed for each data segment where focal activation was identified.

5.3.2 Focal Activations and Conventional Markers of Atrial Substrate

CFAEmean and mean peak-to-peak bipolar voltage area (%) were calculated for each data segment over an 8 second period. The CFAEmean and mean peak-to-peak bipolar voltage of data segments with and without focal activations were compared. In total, 32/114 data segments contained focal activations.

CFAEmean

There was no significant difference in CFAEmean area between data segments with and without focal activation, although a trend towards focal activation presence being associated with a larger area of CFAEmean 80-120ms (conventional CFAE range) and <80ms (rapid/near continuous fractionation) was observed: CFAEmean >120ms (no CFAE), mean difference -11.42 ± 6.043 (95% CI -23.51 to 0.67), $P = 0.06$; CFAEmean 80-120ms, mean difference 5.77 ± 4.33 (95% CI -2.86 to 14.41), $P = 0.19$; CFAEmean <80ms, mean difference 5.67 ± 4.04 (95% CI -2.49 to 13.83), $P = 0.17$. (Figure 5-4).

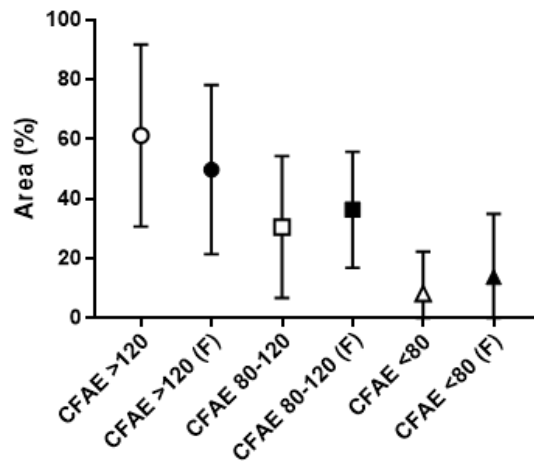


Figure 5-4. CFAE_{mean} was calculated over 8 seconds for each data segment. There was no overall significant difference in CFAE_{mean} area for data segments with focal activations (F), and those without focal activation.

Mean peak-to-peak Bipolar Voltage

Mean peak-to-peak bipolar voltage area <0.35mV was significantly smaller in data segments containing focal activations compared to those without; mean difference -11.62 ± 5.77 (95% CI -23.16 to -0.084), $P = 0.048$. A trend was observed towards the presence of focal activation and data segments containing a larger area of higher voltage; for voltage 0.35-0.5mV (mean difference 4.15 ± 3.44 ; 95% CI -2.77 to 11.07 ; $P = 0.23$), and voltage >0.5mV (mean difference 7.48 ± 6.231 ; 95% CI -5.03 to 20.0 ; $P = 0.24$). (Figure 5-5).

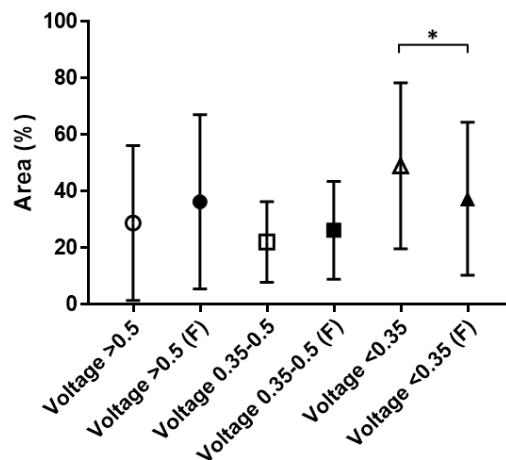


Figure 5-5. Mean peak-to-peak bipolar voltage was calculated over 8 seconds for each data segment. Overall, data segments with focal activations had a significantly smaller area of very low voltage myocardium (<0.35mV, *P = 0.048). There was no overall significant difference in voltage area for data segments with (F), and without the presence of focal activation in for >0.5mV or 0.35-0.5mV.

5.3.3 Focal Activations and Novel Markers of Atrial Substrate

R50

R50 was calculated for each data segment. The mean R50 (degrees, \pm SD) was not significantly different between data segments containing focal activations (90.31 ± 23.07 ; 95% CI 82 to 98.6) and without focal activations (88.66 ± 27.02 ; 95% CI 82.72 to 94.6): mean difference 1.65 ± 5.05 ; 95% CI -8.44 to 11.74; P = 0.74.

There was no correlation between R50 and number of focal activations ($r = 0.03$, P = 0.73). (Figure 5-6).

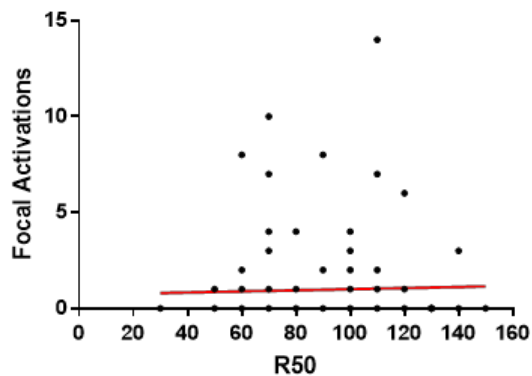


Figure 5-6. There was no correlation between R50 and focal activation.

Dominant Directions of Activation

Data segments were analysed with custom software to identify the number of dominant directions in each location ($n = 114$). The number of dominant directions ranged from 1 (organised activation) to 8 (activation spread in multiple directions). The mean number of dominant directions was 2.9 ± 1.8 .

There was no significant difference in the number of dominant directions when comparing data segments with focal activations (2.8 ± 1.5 ; $n = 32$) to those without focal activations (3.0 ± 2.0 ; $n = 82$): mean difference -0.3 ± 0.3 ; 95% CI -0.9 to 0.4 ; $P = 0.43$ (Figure 5-7).

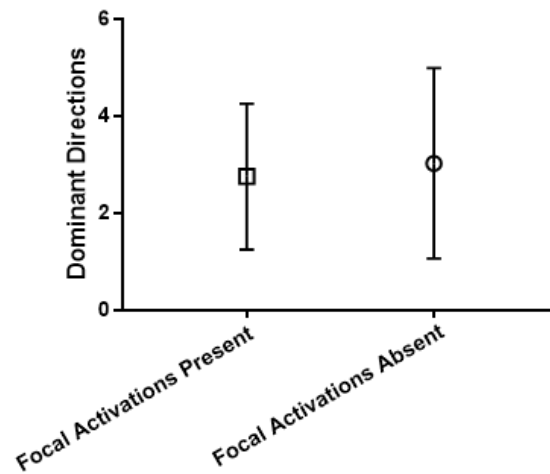


Figure 5-7. There was no significant difference in the number of dominant directions when comparing data segments with focal activations to those without focal activations.

5.3.4 Choropleth Maps

Focal Activations

The locations in which focal activations had been observed were projected on to the choropleth map, without the geometry shell. Qualitative analysis was undertaken to identify the relationship of focal activations to orbital plots on the choropleth map. Specifically, they were evaluated to see if the general dominant direction of activation moved away from locations where focal activation had been observed. The dominant direction of activation spread away from locations of focal activation in 21/32 orbital plots (Figure 5-8).

The choropleth map was then evaluated to assess the effect of focal activation on neighbouring orbital plots. In 13 locations where focal activation had been identified, the dominant direction of a neighbouring orbital plot moved towards the focal activation.

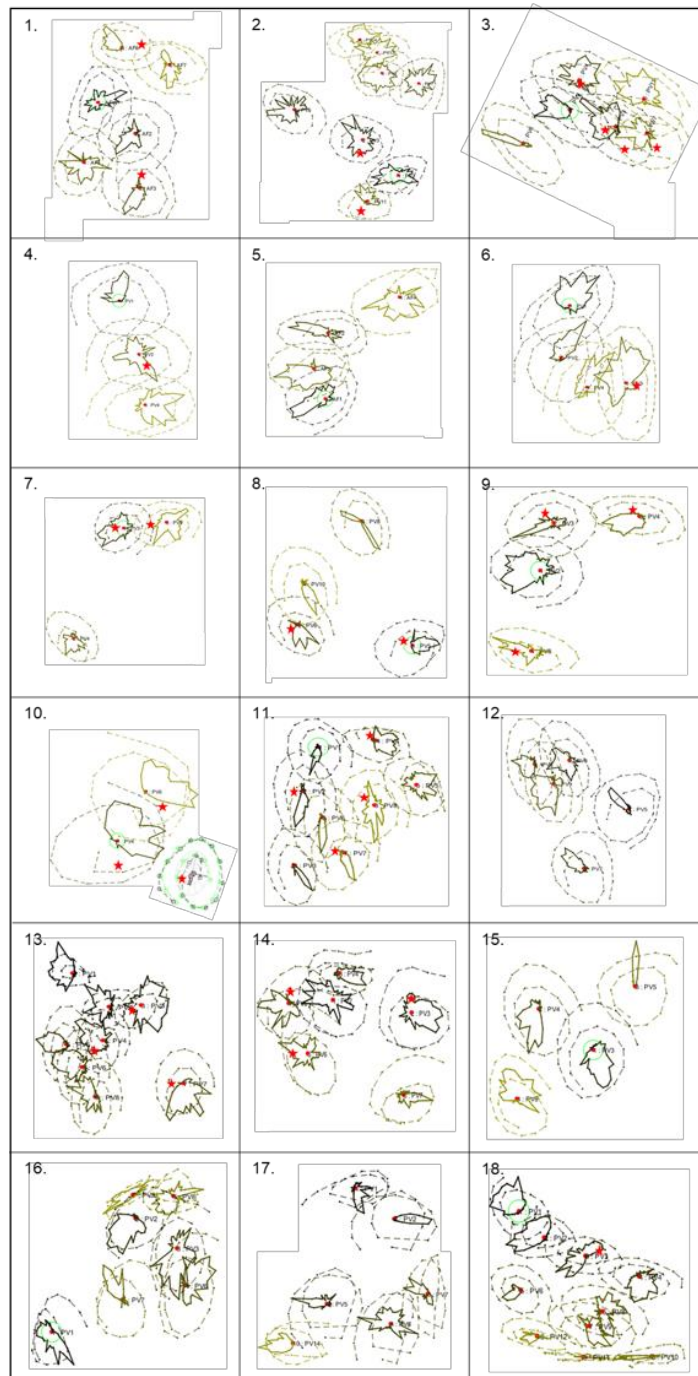


Figure 5-8. Choropleth maps for 18 patients are displayed. The location in which focal activation was identified has been annotated with a red star. The red dot in each orbital plot marks the centre of the AFocusII catheter and is a reference point only. The dominant direction of activation in some locations appears to move away from locations of focal activation, however activation in neighbouring locations is frequently seen to move towards focal activation.

5.3.5 Effect of Amiodarone on Focal Activation

Six patients were taking amiodarone up to the day of data collection, while the remaining 12 patients were not on amiodarone. Data was analysed to identify the effect of amiodarone on focal activation.

The mean number of focal activations was calculated for each patient. The mean number of focal activations identified in patients not taking amiodarone was 1.1 ± 0.9 (95% CI 0.5 to 1.7), and 1.3 ± 1.9 (95% CI -0.7 to 3.3) in patients taking amiodarone (Figure 5-9). There was no significant difference between the two patient groups: mean difference -0.2 ± 0.8 (95% CI -2.2 to 1.9), $P = 0.85$. This is important, as one might expect amiodarone to be associated with suppression of any automatic focal ectopy. The absence of any effect on suppression of focal activation from amiodarone may suggest epicardial-endocardial activation or re-entry.

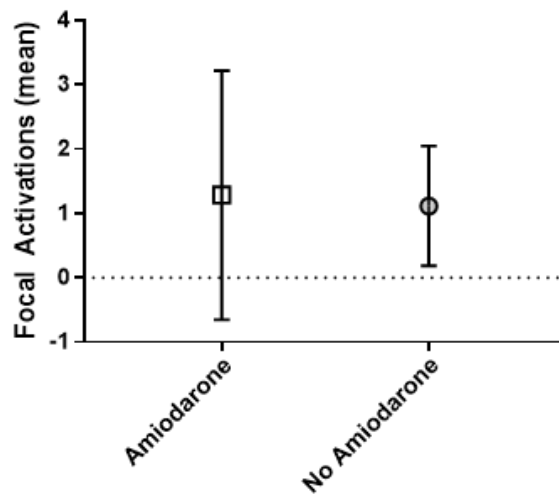


Figure 5-9. Mean number of focal activations per data segment is displayed for patients taking amiodarone, and patients not taking amiodarone. There was no significant difference between the two groups: mean difference 0.2 ± 0.8 (95% CI -2.2 to 1.9), $P = 0.85$.

5.3.6 Effect of Duration of Persistent Atrial Fibrillation on Focal Activation

Twelve patients had been in persistent AF for ≥ 12 months at the time of data collection, and 6 patients < 12 months. Data was analysed to identify the effect of AF duration on focal activation.

The mean number of focal activations identified in patients with a persistent AF duration ≥ 12 months was 1.1 ± 1.5 (95% CI 0.1 to 2.0), and 1.4 ± 0.9 (95% CI 0.5 to 2.3) in patients with a duration < 12 months (Figure 5-10). There was no significant difference between the two patient groups: mean difference 0.3 ± 0.6 (95% CI -0.8 to 1.5), $P = 0.55$.

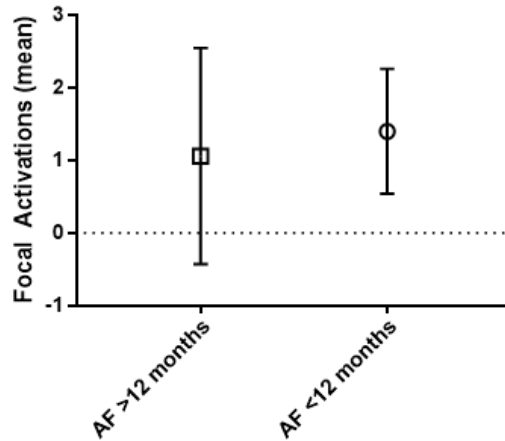


Figure 5-10. Mean number of focal activations per data segment is displayed for patients with a persistent AF duration ≥ 12 months, and < 12 months. There was no significant difference between the two groups: mean difference 0.3 ± 0.6 (95% CI -0.8 to 1.5), $P = 0.55$.

There was also no correlation between the mean number of focal activations and duration of persistent AF ($r = -0.12$; 95% CI -0.55 to 0.37; $P = 0.64$). (Figure 5-11).

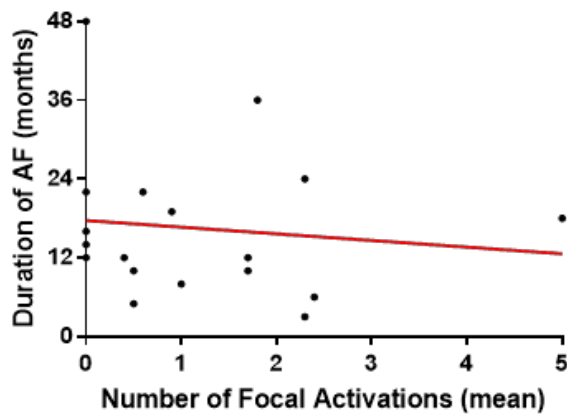


Figure 5-11. There was no correlation between the mean number of focal activations and duration of persistent AF ($r = -0.12$; 95% CI -0.55 to 0.37 ; $P = 0.64$).

5.3.7 Atlas of Myofiber Architecture with Choropleth Maps

It is important to recognise that the use of an ‘atlas’ of myofiber orientation from a small study on fibre orientation makes many assumptions about fibre orientation between patients, particularly in conditions where an underlying atrio-myopathy may be present.

An atlas of myofiber orientation⁷⁸ was merged with the choropleth map for each patient. Activation direction was assessed qualitatively for each data segment with respect to myofiber orientation. Activation was reported as either ‘related’ (same or similar direction; within 30 degrees either side of myofiber orientation) or ‘unrelated’ (different direction) to myofiber orientation.

The dominant direction of activation appeared to be related to myofiber orientation in 27/114 data segments, and was unrelated in 87/114 data segments. Patient 11 had the highest number of data segments in which the dominant direction of activation appeared to be related to myofiber orientation. Five data segments were related, while 2 data segments were not related to myofiber orientation in this patient (Figure 5-12).

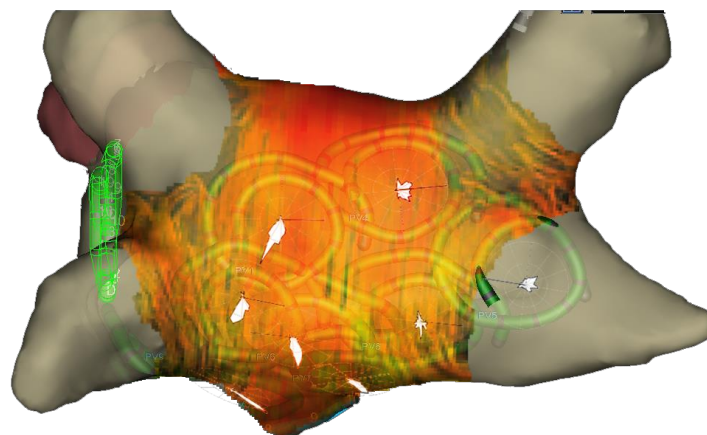


Figure 5-12. The posterior view of the left atrial geometry of Patient 11 is displayed, with the AFocusII shadows and choropleth map. Myofiber orientation has been projected over the top of the choropleth map so that the dominant direction of activation can be appreciated, relative to fibre orientation. Five orbital plots show the dominant activation direction to be similar to that of myofiber orientation.

5.4 Discussion

In this chapter, the relationship between focal activation and conventional markers of atrial substrate has been studied during persistent AF. RETRO-Mapping has been used to test the hypothesis that focal activation within the left atrium is responsible for the observed choropleth map atrial activation patterns. An approach that focuses upon organised wavefronts has been adopted. These are not subject to the difficulties inherent in trying to characterise complex patterns of activation, and do not require ultra-high resolution recordings.

In the previous chapter (Chapter 4), the spatiotemporal stability of atrial activation patterns during persistent AF has been demonstrated. Doing so has allowed locations mapped sequentially to be displayed simultaneously on a single map – a choropleth map. Each orbital plot provides a 'footprint' of each area that is mapped. Choropleth maps, which are comprised of multiple orbital plots, summarise these activation patterns spatially. The choropleth map displays data relating to the uniform activation patterns only, and does not display information relating to focal activation directly. It is the uniform activation that was hypothesised to be a surrogate of focal activation.

Other mapping studies have demonstrated intermittent periods of regular and repetitive activation.^{34, 144, 145} Using a commercially available spiral multipolar catheter and 3D cardiac mapping system, RETRO-Mapping can be used to show the dominant direction of organised wavefronts during AF.

The custom-made mapping software was originally designed to detect wavefronts with directional uniformity, and therefore can only be expected to identify uniform wavefronts. During manual analysis, focal activation patterns were infrequently observed, with the point of earliest activation centrally within the mapping catheter spreading eccentrically outwards toward the periphery. These sites of activation may represent a true focal trigger, micro-reentry or epi-endocardial breakthrough. All focal activation patterns were identified from manual analysis rather than an automated algorithm. Other groups undertaking epicardial mapping have also observed focal activation, with 2-4 foci in the majority of patients.¹¹⁵ Interestingly a remarkably high proportion of focal-origin wavefronts have been reported by some studies, accounting for over 10% of fibrillation waves in patients with persistent AF.¹³² We did not observe such frequent occurrences, possibly due to the limited region of atria that

was mapped. Similar to our observations, episodes were short lived, rather than continuous sequential focal activations occurring for long periods of time. It is therefore not surprising that the activation direction on choropleth maps could not be attributed to the location in which focal activation was identified.

Simultaneous endo-epicardial mapping would be required to definitively differentiate between true focal activation and epi-endocardial breakthrough. It is therefore not possible to determine the true origin of the focal activation that was identified from these data. Using high density mapping, de Groot *et al.*³¹ observed marked differences in the endo- and epicardial atrial activation patterns during AF with simultaneous mapping of a limited region of the right atrium. They also identified episodes of focal activation, the majority of which were the result of endo-epicardial breakthrough, however a small number of simultaneous endo-epicardial focal activations were also observed. We found that in instances where multiple focal activations were seen in a single data segment, they occurred in the same location each time. If these were epicardial-endocardial breakthrough episodes, it would not make sense for activations to occur in the same location each time. The caveat to this is that epicardial-endocardial breakthrough occurs due to the underlying local myofiber architecture.

Endocardial mapping with basket catheters has reported the presence of atrial rotors in almost all cases.⁴⁴ By contrast, epicardial contact mapping has not demonstrated rotors at all¹⁴⁶, or observed them infrequently and for no more than a couple of cycles.^{27, 132} While these findings were in agreement with the presence of organised wavefronts, focal activity was not detected with such frequency, and there was no evidence of the existence of stable rotors.

The orbital plots demonstrate that there is a strong bias to wavefront direction in atrial fibrillation. The challenge is whether AF mechanisms and targets for ablation can be inferred from this information. It is feasible that the recurrent uniform activations of transient linking may be the product of a focal source. Due to the complex electrophysiological milieu of AF it is likely that these episodes would occur in close proximity to their sources before they interact with other wavefronts, refractory myocardium, or areas of scar. However, despite focal activation being identified, we could not determine if it is a driving mechanism.

Focal activations have been identified at pulmonary veins and within sites of CFAE by Yamabe *et al.* but not in the non-CFAE sites.¹⁴⁷ We observed a trend towards focal activation

being associated with locations containing a larger area of fractionation. Furthermore, focal activation was also associated with a trend towards locations containing a larger area of high (>0.5mV) and intermediate (0.35-0.5mV) voltage, and a significantly smaller area of low voltage (<0.35mV). It has previously been reported that CFAE and more healthy atrial voltages tend to co-localise. This suggests that there might be a relationship between focal activation, CFAE and voltage. This could assist in identifying active drivers that are critical to AF maintenance. Data analysis was offline, however the effect of ablation at sites containing CFAE, focal activation and voltage >0.35mV would help to determine their role in maintenance of AF.

It has previously been shown that amiodarone can suppress atrial tachycardia.¹⁴⁸ A sub-study was undertaken to identify the effects of amiodarone on the frequency of focal activation. It is logical that amiodarone should also suppress focal activation during AF. However, there was no significant difference in the frequency of focal activation for patients that were, and were not taking amiodarone. The absence of an effect raises the question of whether the episodes of focal activation that were observed were the result of epicardial-endocardial breakthrough or re-entry.

5.5 Limitations

The data are analysed 'off-line' after the procedure, so mapping could not be guided by the areas of 'interest' identified. Mapping has been confined to a limited region of the atrium. The labour intensive nature of manual analysis for focal activation precludes mapping of the entire atrium. Automation of the process to identify focal activation would facilitate mapping of larger regions of the atrium. Given the observations of other research groups, mapping of both atria would be advantageous. A definite mechanism has not been demonstrated, nor a clear ablation target for the patients in whom mapping was performed. It is possible that the frequency of focal activation is higher, and is still responsible for the chorepleth activation patterns, but the mapping resolution is not sufficiently high enough. Nevertheless, a practical and feasible method for approaching the mapping of fibrillatory wavefronts has been demonstrated, that has so far been elusive.

5.6 Conclusion

These data cannot determine focal activation as the driver for the activation patterns seen in chorepleth maps, although it is possible that the mapping resolution is not sufficient to detect

all focal activation. With higher resolution mapping, the frequency of focal activation may be higher.

The heterogeneity in observations of activation patterns and the proposed mechanisms of AF has a number of causes: the arrhythmia is complex; activation has to be inferred from electrograms that are an imperfect indicator of transmembrane potential; and even if activation is known, the underlying mechanism may not be obvious. Detailed characterisation of the dominant direction of activation and the presence or absence of focal activation is achievable with multipolar catheters that are in clinical use. This could help to improve our understanding of the mechanisms that perpetuate AF, on a patient-specific basis, and ultimately lead to a more robust framework for identifying ablation targets.

6 The Effect of Ablation on Atrial Activation Patterns during Persistent Atrial Fibrillation

6.1	Introduction.....	149
6.2	Methods	151
6.2.1	Patient selection	151
6.2.2	Live Data Export.....	152
6.2.3	Choropleth Maps.....	153
6.2.4	Data analysis techniques	153
6.2.5	Statistical Analysis	154
6.3	Results	154
6.3.1	Baseline Percentage Match	154
6.3.2	Organising effects of ablation	155
6.3.3	Correlation between R50 and dominant directions.....	164
6.3.4	Differences between induced and spontaneous persistent AF	165
6.3.5	Effect of previous ablation	168
6.3.6	Workflow for online RETRO-Mapping	170
6.4	Discussion	171
6.5	Limitations	175
6.6	Conclusion	175

6.1 Introduction

The observation of focal activations in patient with persistent AF using RETRO-Mapping is consistent with the findings of other groups.^{31, 125, 149} The creation of choropleth maps is an important step towards better understanding the global activation patterns of sequentially acquired data segments on a single map.

During conventional antral PVI procedures, it is commonplace for operators to anecdotally describe more 'organised' AF after isolation of the pulmonary veins. The mid-CS, and more commonly the LAA are recording locations for LA cycle length but are crude measurements, usually calculated over the course of 30 cycle lengths. Prolongation of the AF cycle length resulting from PVI has been demonstrated¹⁵⁰, and is frequently used in the AF literature to quantify the organising effect of ablation.¹⁵¹ Seminal literature report prolongation of LAA cycle length by 5-6ms following ablation being considered to have resulted in a significant effect.^{83, 87, 116} If R50 can be used as a marker for determining organisational characteristics of AF it would be expected to decrease following PVI, while LAA cycle length increases. Importantly, R50 might provide more detailed information regarding local characteristics of organisation. LAA cycle length is a summary of organisational characteristics for the entire LA. While local AF cycle lengths can be calculated, collision from wavefronts and fractionated electrograms can make their interpretation in the body of the atrium challenging. Much of the current justification for increased organisation relates to LAA cycle length prolongation. This may be an oversimplification for such a complex electrophysiological milieu.

There are no data to describe the effects of PVI on atrial activation patterns, in part due to the significant challenges of mapping activation during AF. CARTOFINDER is a proprietary algorithm and has been used to identify focal drivers before and after PVI¹²⁵, although the atrial activation patterns themselves are not described. Focal ectopy from the pulmonary veins is an accepted mechanism associated with AF⁶. Exclusion of these focal drivers offers a plausible reason for why AF becomes more organised following PVI. Having demonstrating spatiotemporal stability during persistent AF, it might be possible to attribute the changes in activation pattern after ablation to the effects of catheter ablation, despite not proving that atrial activation patterns on RETRO-Choropleth Maps directly result from focal activations.

This of course assumes that stability persists over even longer periods of time than demonstrated with delayed interval mapping in chapter 4.

In this chapter, RETRO-Mapping has been used, with the validated tools for data analysis previously discussed, to study the effects of PVI on atrial activation patterns during persistent AF. We used RETRO-Mapping to test the hypothesis that PVI leads to more 'organised' atrial activation patterns. A workflow for live data export and analysis during a catheter ablation procedure has also been developed and described.

6.2 Methods

6.2.1 Patient selection

Patients with symptomatic persistent AF that were undergoing clinically indicated catheter ablation procedures were prospectively recruited. Three patients were in sinus rhythm on the day of the procedure, one of which had converted to sinus rhythm on amiodarone, and the other two had undergone DC cardioversion while awaiting ablation. Three patients with previous PVI only, and no linear or CFAE ablation were also included. Procedures were conducted in the post-absorptive state under general anaesthetic. Anticoagulation regimens were maintained, and unfractionated heparin administered after trans-septal puncture. All antiarrhythmic medications were discontinued at least five half-lives before the procedure with the exception of amiodarone. Patients established on amiodarone continued to take this up to the day of the procedure.

All procedures were performed by a single operator using Ensite Precision and the AFocusII catheter for data collection. Left atrial and pulmonary venous geometry were collected at the start of each case. Following this, the AFocusII was held in a stable position on the left atrial endocardium for collection of 30 second data segments in multiple different locations. A shadow of the AFocusII catheter was projected on to the LA geometry for each recording location. PVI was undertaken in ipsilateral pairs with antral circumferential ablation using the TactiCath ablation catheter at 25-30W. Isolation of each pulmonary vein was confirmed. Isolation was defined as the absence of PV signals on the AFocusII catheter during AF. Once isolation of all veins was confirmed, catheter shadows for each data segment were displayed, one at a time. The AFocusII catheter was returned to the same location and catheter orientation for collection of a further 30 second data segment in each location after PVI.

Overall, 554 data segments were collected from 23 patients. Data was collected from 277 different locations before and after PVI. Patient characteristics are displayed in Table 6-1. Twenty-four patients were recruited, however one patient terminated to sinus rhythm during catheter ablation of the right sided pulmonary veins, and was therefore excluded. Patient characteristics and demographics are displayed in Table 6-1.

Case	Gender	Age (yr)	Duration in persistent AF (months)	Previous AF ablation	LA size (mm)	LVEF (%)	Induced persistent AF	Amiodarone	Data segments
1	M	58	51	N	38	60	N	N	11
2	F	69	9	N	44	30	N	N	12
3	M	75	23	N	43	55	N	N	17
4	M	53	11	N	46	45	N	Y	14
5	M	58	11	N	49	40	N	Y	9
6	M	56	34	N	43	50	N	Y	5
7	M	65	29	N	51	55	N	Y	6
8	M	60	9	N	43	50	N	N	20
9	M	66	13	N	54	50	Y	N	10
10	M	64	16	N	54	55	N	N	10
11	M	54	26	N	51	50	N	N	7
12	F	75	21	N	41	55	N	N	9
13	M	62	28	Y	50	55	N	N	21
14	M	53	13	N	45	35	Y	Y	15
15	M	65	12	N	34	60	Y	N	16
16	M	56	18	N	51	35	N	Y	8
17	M	69	48	N	56	40	N	Y	6
18	M	55	30	N	49	45	N	Y	21
19	M	76	9	Y	46	40	N	N	11
20	M	47	44	Y	47	55	N	Y	6
21	F	74	12	N	42	55	N	N	14
22	M	65	14	N	35	40	N	N	16
23	F	71	15	N	50	45	N	N	13
*24	F	45	20	N	42	50	N	Y	N/A

Table 6-1. Patient characteristics. Details of previous ablation procedures are provided in the Appendix section. *Patient 24 terminated to sinus rhythm during catheter ablation of the right sided pulmonary veins, after the left sided veins had been isolated.

6.2.2 Live Data Export

All data analysis up to, and including this point has been conducted offline. If activation mapping of AF is to be used to guide ablation strategy, it is a requirement that live data export and analysis can be achieved. A sub-study later in this chapter (See 6.3.6) involves online 'live' data export and analysis of 43 data segments in 3 further patients.

Ensite Precision does not allow data to be exported during a case. Data export for offline analysis purposes is done by ending the active study and entering a case review mode. Software was provided from Abbott that would permit rights to export data during an 'open' Ensite Precision case. This software has not previously been used by Abbott, but allows the potential for access to live data only, and is not a means to analyse these data. Custom software was written to identify electrode location and bipolar electrogram data from the AFocusII catheter while data is being acquired for each data segment. Recognition of the

AFocusII catheter was achieved, however obtaining electrogram data was more challenging. Initial problems with 50Hz noise on all bipoles of the AFocusII catheter were resolved by applying a notch filter within the custom software. Despite this, no electrogram data could be streamed live from the catheter despite a 6 month endeavour. The software rights from Abbott were authorised with a limited license duration. Prior to this license expiring, an application for a license extension was made. The issuing of this is awaited, however the current license lapsed during this period.

To overcome this obstacle, a protocol was devised so that data could be exported during the case. Prior to PVI, data was collected in the method previously described. Following data collection before PVI, the case was ended so that data could be exported. The case was re-opened following data export, and PVI undertaken. This process took around 3-5 minutes. Data analysis was undertaken using RETRO-Mapping during the time that catheter ablation was being undertaken to isolate the pulmonary veins.

6.2.3 Choropleth Maps

Choropleth maps were constructed in the method previously described.

6.2.4 Data analysis techniques

All data segments underwent analysis to identify percentage match at baseline, and R50 and number of dominant directions of activation before and after PVI in the methods previously described (See 4.2.4).

All patients underwent collection of two consecutive data segments from the first location mapped; datasets A and B. This was used to calculate a baseline percentage match for each patient and ensure spatiotemporal stability was present. Data segments were collected from multiple different locations before ablation with PVI; dataset A pre-PVI. Following confirmed pulmonary vein isolation, the AFocusII catheter was returned to each location mapped in dataset A pre-PVI for collection of a further 30 second data segment; dataset A post-PVI.

Mean LAA cycle length was calculated over 30 AF cycle lengths before and after PVI. A significant change in LAA cycle length was defined as >6ms prolongation following ablation, as per established criteria.^{87, 116}

6.2.5 Statistical Analysis

Results were expressed as mean \pm SD. Significance testing was performed using Welch's t-test for unequal variance. The Wilcoxon signed-rank test was calculated for paired groups. Correlation statistics were used to identify relationships between mapping parameters. A value of $P < 0.05$ was considered statistically significant. Changes in ≥ 6 ms change LAA cycle length were considered significant in accordance with established data.

6.3 Results

6.3.1 Baseline Percentage Match

Before PVI, the baseline percentage match was calculated at the first location mapped to ensure atrial activation pattern stability. Mean baseline percentage match (%) was 78.0 ± 10 (95% CI 74.0 to 84.0). This is similar to the mean baseline percentage match observed in chapter 4 ($79.5\% \pm 7.7\%$, $n=161$).

Spatiotemporal stability was defined as being present at the start of the case if percentage match was no greater than one standard deviation below the overall mean percentage match at baseline from chapter 4 (see 4.4.2); $79.5\% \pm 7.7\%$. This will be referred to as the 'standardised percentage match'. Activation was stable in 19/23 patients in accordance with this criteria (Figure 6-1).

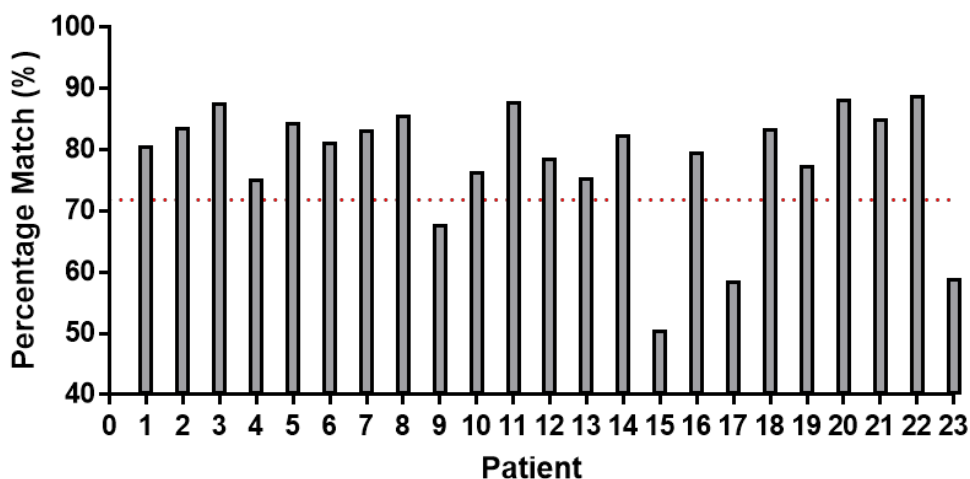


Figure 6-1. Baseline percentage match for the first location mapped in each patient is displayed in this graph. One standard deviation below the standardised percentage match ($79.5\% \pm 7.7\%$) is represented by the broken red line. Baseline percentage match falls below this value in 4 patients.

6.3.2 Organising effects of ablation

Left Atrial Appendage Cycle Length

LAA cycle length was calculated before and after PVI for all 23 patients. There was a significant increase in LAA cycle length (mean \pm SD, milliseconds) of 17.74 ± 15.95 ($P < 0.0001$) after PVI compared to before PVI (Figure 6-2). Mean LAA cycle length before PVI was 192.2 ± 20.63 , and after PVI was 209.9 ± 29.31 . The LAA cycle length increased in all patients following PVI. A significant prolongation in LAA cycle length was identified (>6 ms) in 18/23 patients.

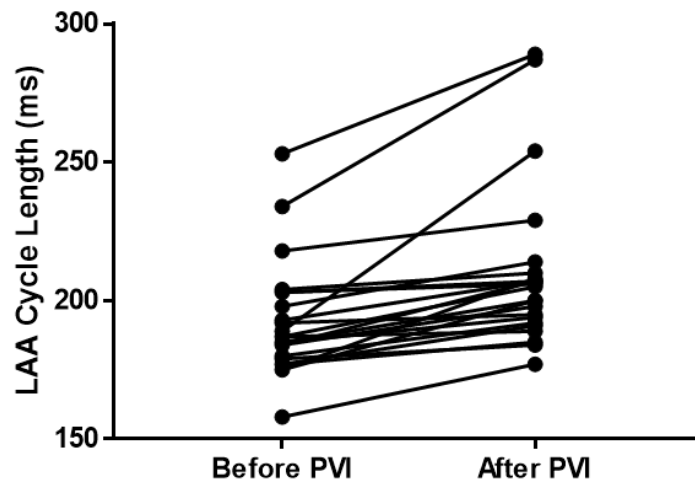


Figure 6-2. Graph showing the LAA cycle length (ms) before and after PVI. LAA cycle length increased in all patients after PVI.

R50

R50 was calculated before and after PVI for all locations mapped ($n=277$). This showed (mean, \pm SD, degrees): R50 before PVI of 87.36 ± 30.88 (95% CI 83.71 to 91.02); R50 of 65.74 ± 32.6 (95% CI 61.88 to 69.6) after PVI. Overall, there was a significant decrease in R50 following PVI (mean difference -21.62 ; 95% CI -25.49 to -17.76 ; $P < 0.0001$); i.e. activation became more organised in a particular direction after isolation of the pulmonary veins. The mean R50 was calculated for each patient before and after PVI. Although the overall R50 had decreased, a variable response to PVI was identified between different patients (Figure 6-3).

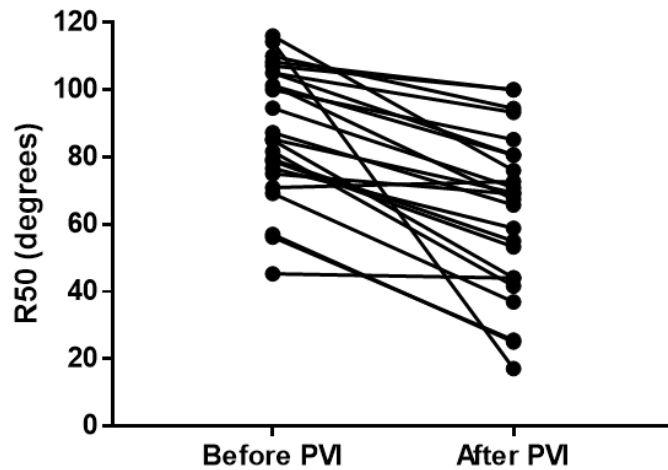


Figure 6-3. Graph displaying the difference in mean R50 for each patient before and after PVI.

Further analysis of the mean R50 for each patient showed that 16/23 patients had a significant decrease in R50 following PVI; i.e. PVI resulted in AF becoming more organised in a particular direction (Figure 6-4). There was a trend towards an increase in R50 in 1/23 patients. The remaining 6/23 patients showed a trend towards a decreased R50 following PVI. Four of the 7 patients with no significant effect on R50 from PVI were on amiodarone while the remaining 3 patients were not.

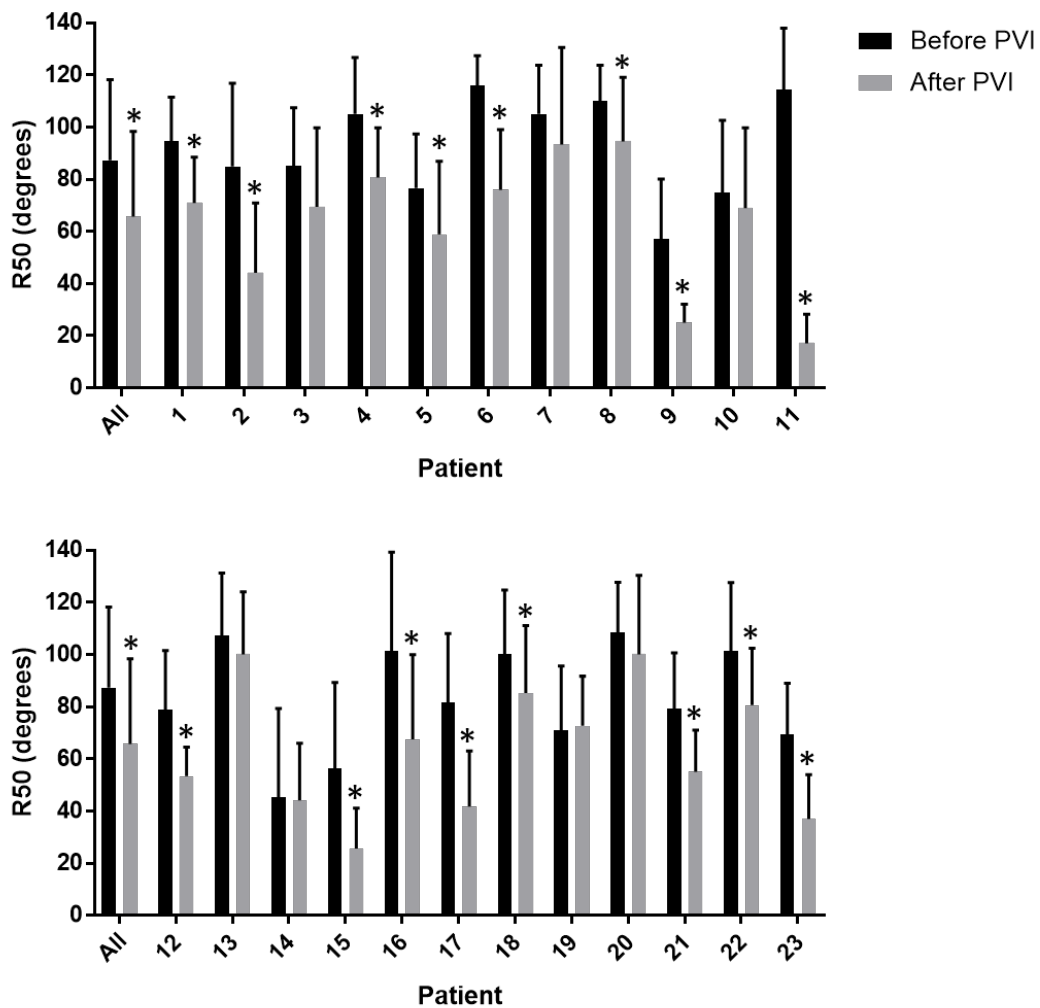


Figure 6-4. Histograms showing significant decrease (*P < 0.05) in mean R50 overall, and for 16/23 patients after PVI.

Correlation between LAA Cycle Length and R50

The change in LAA cycle length and R50 was calculated following ablation with PVI. The correlation between the change in LAA cycle length and mean R50 following ablation with PVI for each patient was investigated. There is a negative correlation between increasing LAA cycle length and decreasing R50; $r = -0.48$ (95% CI -0.75 to -0.072), $P=0.02$ i.e. PVI results in an increase in LAA cycle length and a decrease in R50, signifying atrial activation in more organised after PVI (Fig 6-5).

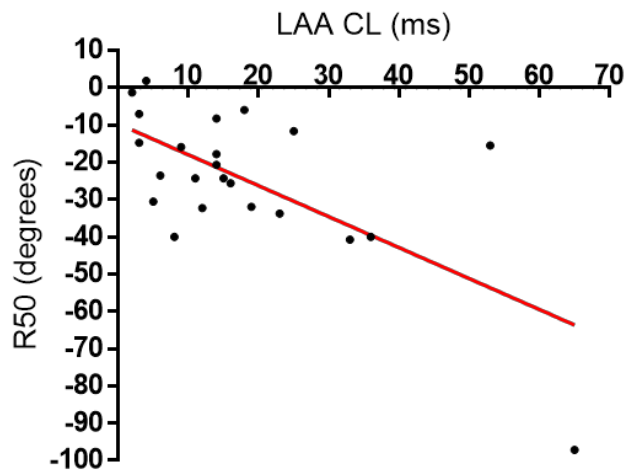


Figure 6-5. The difference between R50 and LAA cycle length before and after PVI is displayed in this graph. There is a negative correlation between increasing LAA cycle length and decreasing R50 following PVI; $r = -0.48$ (95% CI -0.75 to -0.072), $P=0.02$.

Of the 18/23 patients in whom a significant increase in LAA cycle length was demonstrated after PVI, 14/23 also demonstrated a significant decrease in R50. LAA cycle length significantly increased in 4/23 patients without an accompanying significant decrease in R50. There were 2/23 patients that showed a significantly decreased R50 without an accompanying significant increase in LAA cycle length (Table 6-2).

Case	Change in LAA CL After – Before PVI (ms)	Change in R50 After – Before PVI (degrees)
1	6*	-23.6*
2	33*	-40.8*
3	9*	-15.9
4	11*	-24.3*
5	14*	-17.8*
6	36*	-40*
7	25*	-11.7
8	53*	-15.5*
9	19*	-32*
10	18*	-6
11	65*	-97.2*
12	16*	-25.6*
13	3	-7.1
14	2	-1.3
15	5	-30.6*
16	23*	-33.8*
17	8*	-40*
18	3	-14.8*
19	4	1.8
20	14*	-8.3
21	15*	-24.3*
22	14*	-20.7*
23	12*	-32.3*

Table 6-2. The change in LAA cycle length and R50 after ablation with PVI compared to before PVI is displayed for each patient (*P <0.05 for R50, *≥6ms CL increase).

Patient 11 had the greatest increase in LAA cycle length and the greatest decrease in R50 following PVI; mean decrease in R50 was $-97.14^\circ \pm 22.89^\circ$ (95%CI -118.3° to -75.98° , P <0.0001) after PVI, compared to R50 before PVI. Data collected during persistent AF (before PVI) was used to produce a choropleth map. Before PVI, the mean R50 was $114.3^\circ \pm 23.7^\circ$ (95% CI 92.36° to 136.2°). This is consistent with activation that is not organised in any particular direction, and is reflected by the choropleth map. Orbital plots show activation to be spread out in multiple different directions (Figure 6-6).

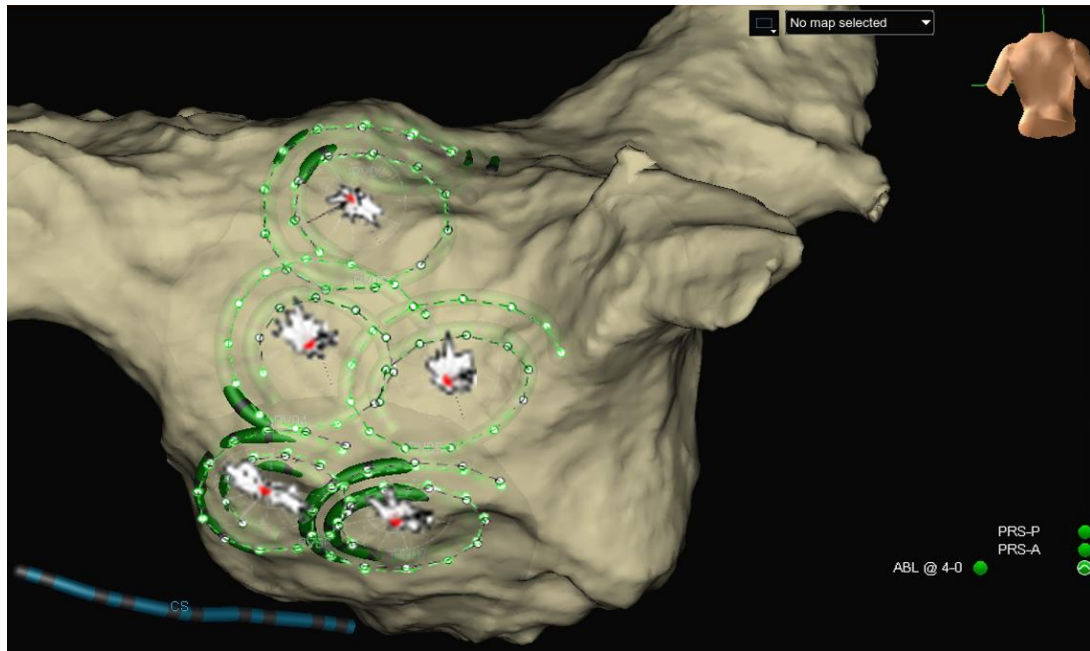


Figure 6-6. Choropleth map for Patient 11 during persistent AF, prior to PVI. Orbital plots for 5 data segments are projected on to the LA geometry in Ensite Precision. Activation is spread out in multiple directions, and is consistent with the high mean R50 $114.3^\circ \pm 23.7^\circ$ (95% CI 92.36° to 136.2°).

The left sided pulmonary veins were isolated first. Upon isolation of the right sided pulmonary veins, activation in the CS became regular with distal to proximal activation; CL 254ms (189ms before PVI). This tachycardia was mapped conventionally using Ensite Precision to produce a LAT map which was consistent with a dual circuit of activation moving clockwise around the mitral annulus, and roof dependent left atrial macro re-entry (Figure 6-7). This tachycardia terminated during linear ablation at the roof.

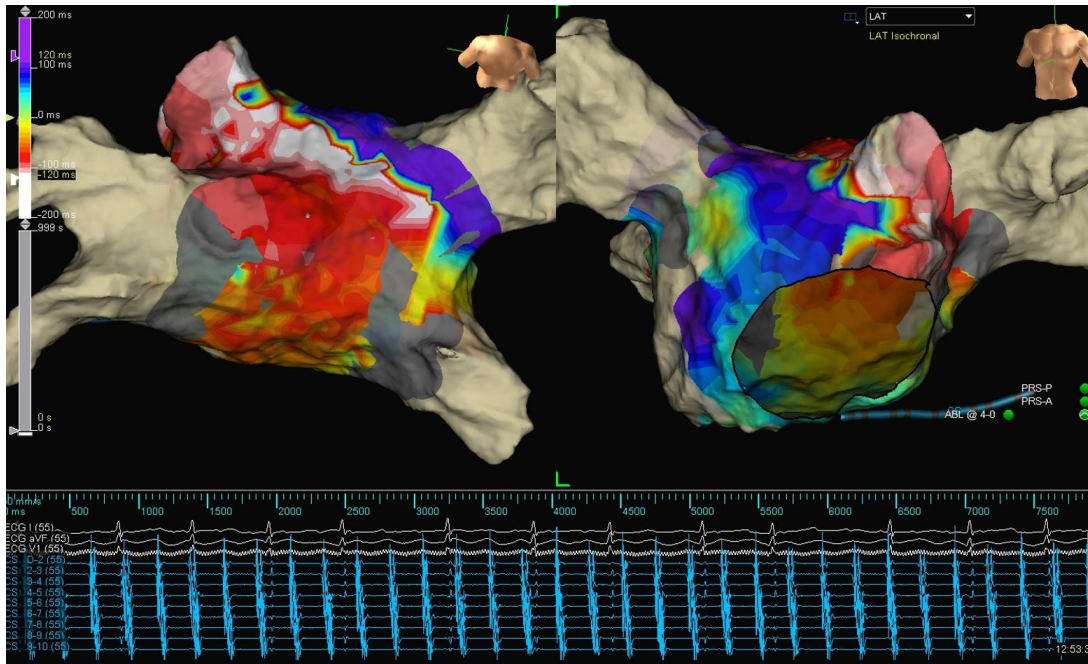


Figure 6-7. LAT map for Patient 11 after PVI. CS activation is distal to proximal. Earliest activation (white) meets latest activation (purple) in a line extending from the mitral annulus and across the roof.

A choropleth map using data collected after PVI was created for Patient 11 using RETRO-Mapping (Figure 6-8). There was a significant decrease in mean R50 after PVI; R50 mean $17.14^\circ \pm 11.13^\circ$ (95% CI 6.85° to 11.13°) after PVI. The activation direction from each orbital plot was consistent with that of the LAT map created using Ensite Precision. The low R50 reflects activation that is highly organised in a single direction of activation.

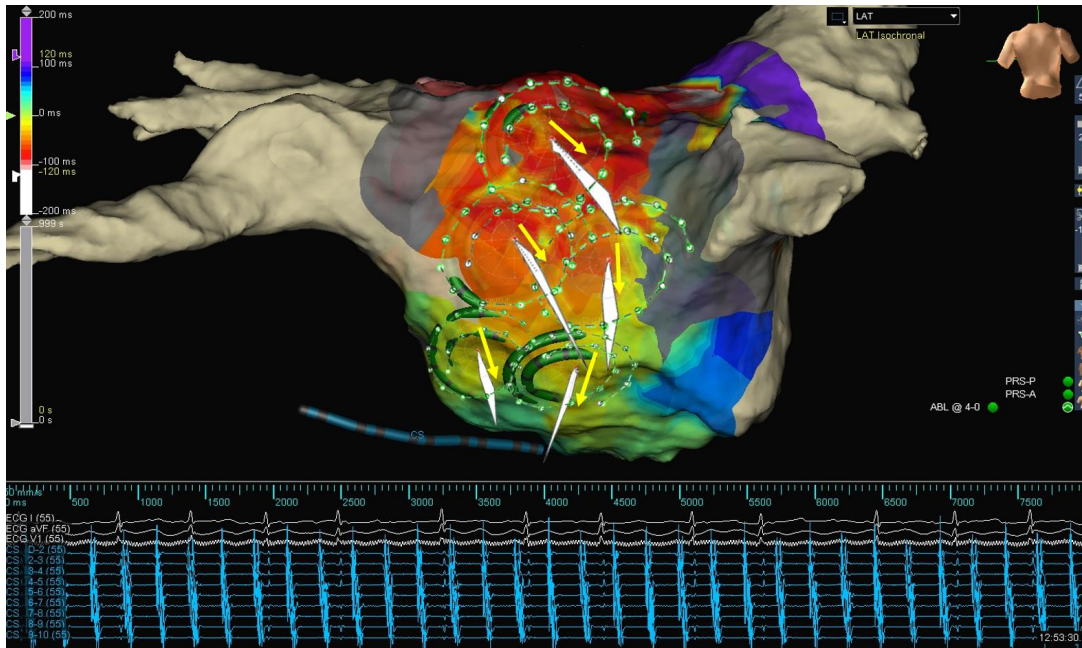


Figure 6-8. Choropleth map of Patient 11 after PVI. Orbital plots for 5 data segments are projected on to the LA geometry in Ensite Precision, with the LAT map simultaneously displayed. Yellow arrows have been added to aid with visual interpretation of activation direction only, and would not usually be part of a choropleth map. Activation in each location is highly organised, and is reflected by the low mean R50 $17.14^\circ \pm 11.13^\circ$ (95% CI 6.85° to 11.13°). Choropleth map activation is consistent with that of the conventional LAT map.

Dominant directions

The same data segments were also analysed to identify the number of dominant directions before and after PVI. The number of dominant directions ranged from 1 (most organised) to 8 (least organised). PVI resulted in a significant decrease in the number of dominant directions (mean difference -0.74 ; 95% CI -0.96 to -0.51 ; $P < 0.0001$); i.e. activation becomes confined to fewer different directions after PVI. The mean number of dominant directions before PVI was 2.8 ± 1.7 (95% CI 2.6 to 3.0). Following PVI there was a decrease in the mean number of dominant directions, to 2.1 ± 1.4 (95% CI 1.9 to 2.2).

The mean number of dominant directions was calculated for each patient. Ablation with PVI showed that there was a reduction in the number of dominant directions in 22/23 patients (Figure 6-9).

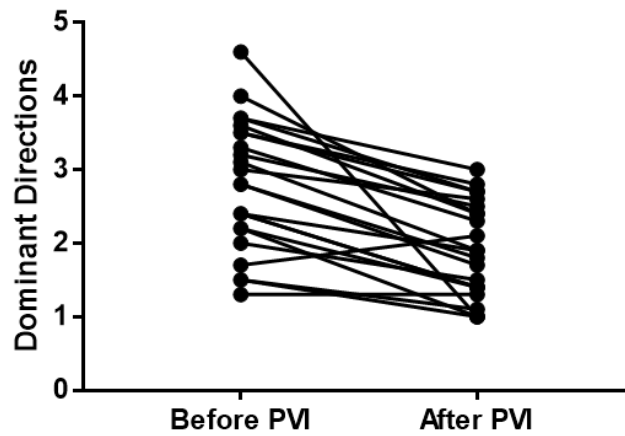


Figure 6-9. Graph displaying the difference in mean number of dominant directions for each patient before and after PVI (mean difference -0.74; 95% CI -0.96 to -0.51; P <0.0001).

There was a significant reduction in the mean number of dominant directions for 5/23 patients following PVI. Patient 19 showed a trend towards an increased number of dominant directions of activation. This patient also showed in trend towards increased R50. There was a trend towards a reduced number of dominant directions after ablation compared with before ablation in the remaining 17/23 patients (Figure 6-10).

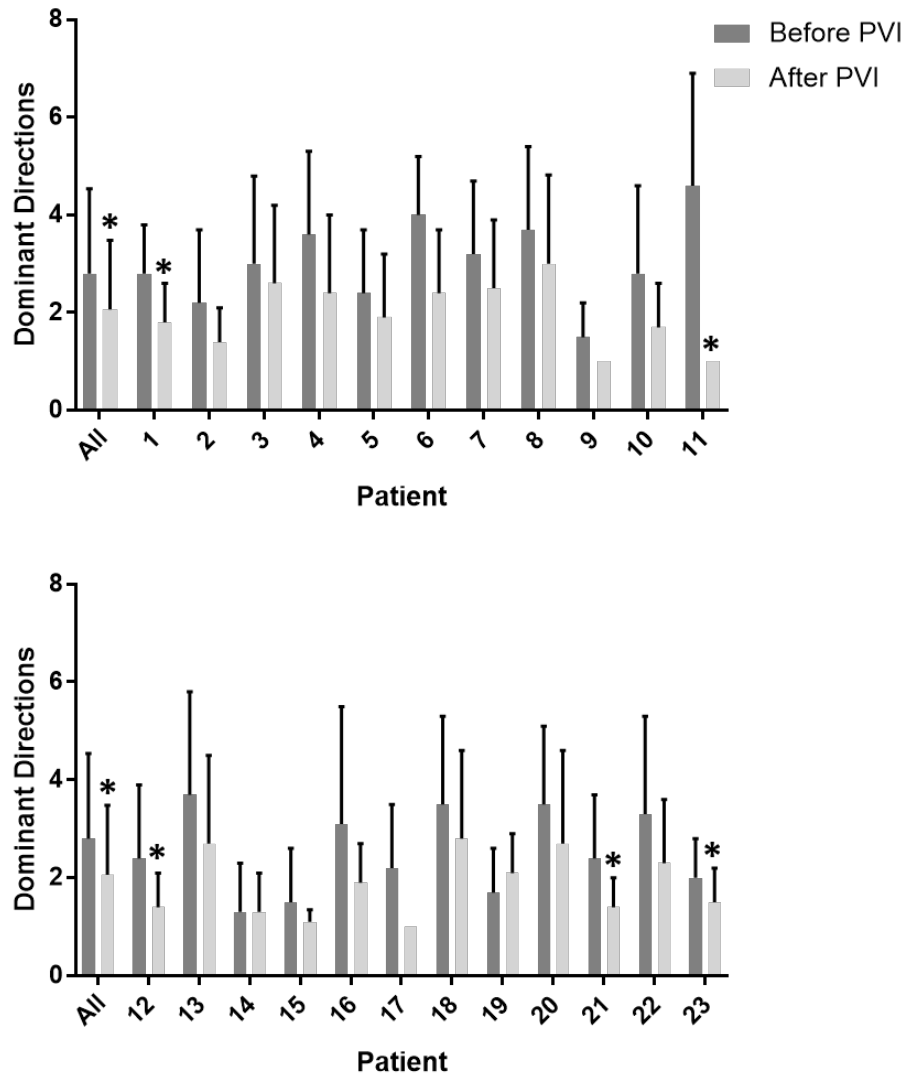


Figure 6-10. Histogram showing significant decreases (* $P < 0.05$) in the number of dominant directions following PVI overall, and for 5/23 patients.

6.3.3 Correlation between R50 and dominant directions

The relationship between R50 and number of dominant directions was investigated. One would expect that as R50 decreases, showing more organised activation in a particular direction, the number of dominant directions might also decrease. Analysis showed an overall positive correlation between R50 and number of dominant directions before ($r=0.72$, 95% CI 0.66 to 0.77, $P < 0.0001$) and after PVI ($r=0.74$, 95% CI 0.69 to 0.79, $P < 0.0001$). (Figure 6-11).

A sub-analysis showed that the positive correlation between R50 and number of dominant directions was present in all patients, before and after PVI.

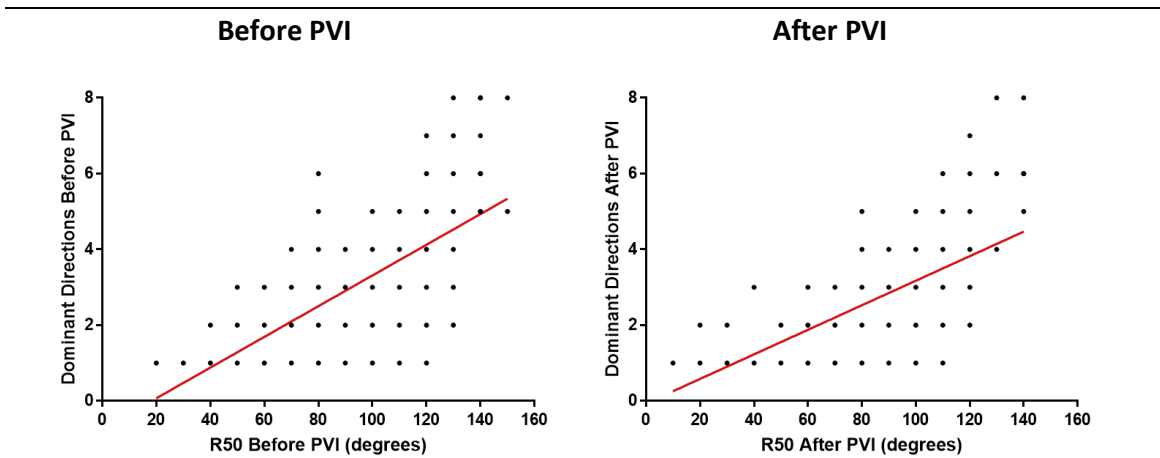


Figure 6-11. Correlation between R50 and number of dominant directions before (left) and after (right) PVI. There is a positive correlation between R50 and number of dominant directions: Before PVI $r=0.72$, 95% CI 0.66 to 0.77, $P < 0.0001$; After PVI $r=0.74$, 95% CI 0.69 to 0.79, $P < 0.0001$.

6.3.4 Differences between induced and spontaneous persistent AF

Three patients with persistent AF presented in sinus rhythm on the day of their procedure. Two of these patients had undergone electrical cardioversion for symptomatic control while awaiting their catheter ablation procedure, and one had reverted to sinus rhythm while on amiodarone. AF was induced with burst pacing from the CS as previously described (See 3.3.2), allowing 2 minutes before mapping. Comparison was made between the 3/23 patients with induced persistent AF, and 20/23 patients with spontaneous persistent AF.

R50

Before PVI, the mean R50 (degrees) for patients with: Induced persistent AF was 52 ± 31 (95% CI 43 to 62); Spontaneous persistent AF was 93 ± 27 (95% CI 90 to 97). Patients with induced persistent AF had a significantly lower mean R50, indicating that these patients have more organised AF; mean difference -41 ± 5.1 (95% CI -51 to -31), $P < 0.0001$ (Figure 6-12).

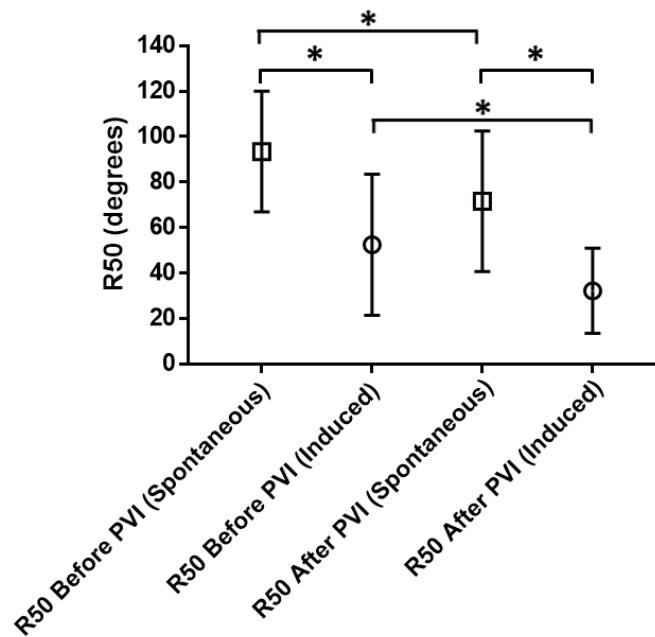


Figure 6-12. The effect of ablation with PVI on R50 for patients with induced and spontaneous persistent AF are displayed (*P < 0.0001).

After PVI, the mean R50 for patients with: Induced persistent AF was 32.2 ± 18.8 (95% CI 26.3 to 38.1); Spontaneous persistent AF was 71.6 ± 30.95 (95% CI 67.6 to 75.5). Patients with induced persistent AF also had a significantly lower mean R50 after PVI compared to spontaneous persistent AF after PVI; mean difference -39.37 ± 3.56 (95% CI -46.45 to -32.3), $P < 0.0001$. Mean R50 significantly decreased following PVI in both patient groups: Induced persistent AF -20 ± 30 (95% CI -30 to -11), $P < 0.0001$; Spontaneous persistent AF -22 ± 33 (95% CI -26 to -18), $P < 0.0001$ (Figure 6-12).

LAA Cycle Length

Mean LAA cycle length for patients with induced persistent AF was shorter than for patients with spontaneous persistent AF, both before and after PVI. The mean LAA cycle length for patients with induced persistent AF before PVI was 182.7 ± 22.81 (95% CI 126.0 to 239.3), and spontaneous persistent AF before PVI was 193.6 ± 20.54 (95% CI 194.0 to 203.2). After PVI the mean LAA cycle length for induced persistent AF was $190.7 \pm$ (95% CI 154.5 to 226.9), and spontaneous persistent AF was $212.8 \pm$ (95% CI 198.7 to 226.9).

Dominant Directions

Before PVI, the mean number of dominant directions for patients with: Induced persistent AF was 1.44 ± 0.98 (95% CI 1.13 to 1.75); Spontaneous persistent AF was 3.04 ± 1.73 (95% CI 2.82 to 3.26). Patients with induced persistent AF had a significantly lower mean number of dominant directions, indicating that these patients have more organised AF; mean difference -1.60 ± 0.19 (95% CI -1.98 to -1.22), $P < 0.0001$ (Figure 6-13). This finding is consistent with patients with induced persistent AF also having a low R50.

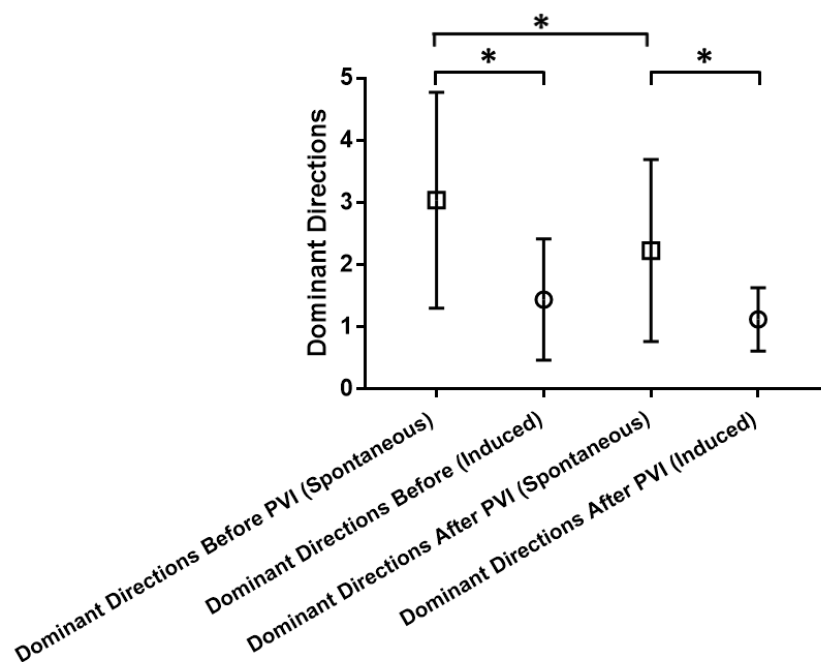


Figure 6-13. The effect of ablation with PVI on the number of dominant directions for patients with induced and spontaneous persistent AF are displayed (* $P < 0.0001$).

After PVI, the mean number of dominant directions for patients with: Induced persistent AF was 1.12 ± 0.51 (95% CI 0.96 to 1.28); Spontaneous persistent AF was 2.23 ± 1.46 (95% CI 2.04 to 2.42). Patients with induced persistent AF also had a significantly lower mean number of dominant directions after PVI compared to spontaneous persistent AF; mean difference -1.11 ± 0.12 (95% CI -1.35 to -0.86), $P < 0.0001$. Within both induced and spontaneous persistent AF patients, following PVI there was a decrease in mean number of dominant directions: Induced persistent AF mean difference -0.32 ± 1.06 (95% CI -0.65 to 0.017), $P = 0.06$; Spontaneous

persistent AF mean difference was -0.81 ± 1.98 (95% CI -1.06 to -0.56), $P < 0.0001$ (Figure 6-13). There was a significant decrease in mean number of dominant directions for spontaneous, but only a trend towards decreased number of dominant directions for patients with induced persistent AF.

Percentage Match

Baseline percentage match (%) to assess for spatiotemporal stability for the two groups was: Induced persistent AF – mean 67 ± 16 (95% CI 27 to 107); Spontaneous persistent AF – mean 80 ± 8.4 (95% CI 76 to 84). There was a trend toward lower baseline percentage match with induced persistent AF; mean difference -13 ± 9.4 (95% CI -51 to 24), $P = 0.29$ (Figure 6-14). The baseline percentage match for patients with induced persistent AF was greater than one standard deviation below the standardised mean percentage match ($79.5\% \pm 7.7\%$) indicating that activation patterns were not stable before PVI in patients with induced persistent AF.

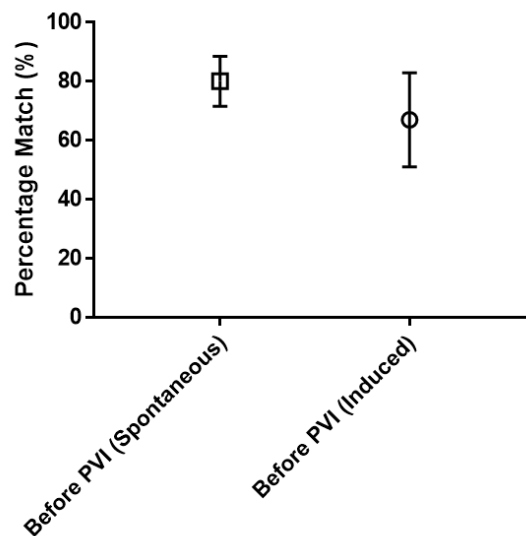


Figure 6-14. The difference in baseline percentage match (mean, \pm SD, %) in patients with spontaneous and induced persistent AF are displayed.

6.3.5 Effect of previous ablation

Three patients (3/23) had undergone previous ablation with PVI for persistent AF. Patient 13 had undergone 2 previous ablations for AF, however the LUPV remained connected. Patients 19 and 20 had undergone a single ablation for AF. The LLPV and RLPV had reconnected in

Patient 19, and the RLPV had reconnected in Patient 20. For these 3 patients, the first dataset was collected before any ablation. Reconnected PVs were then re-isolated, and a repeat dataset collected after isolation.

Data was initially analysed for the 20/23 patients with no previous left atrial ablation. When comparing datasets collected before and after PVI in this group, there was a significant decrease (mean difference \pm SD) in R50 ($-24.21 \pm 32.75^\circ$; 95% CI -28.48 to -20.14 ; $P < 0.0001$), number of dominant direction (-0.85 ± 1.87 ; 95% CI -1.09 to -0.62 ; $P < 0.0001$), and percentage match ($-38.23 \pm 21.28\%$; 95% CI -48.18 to -28.27 ; $P < 0.0001$) following PVI.

Data was analysed for the 3/23 patients with a history of previous ablation, in whom between 1 and 2 PVs required re-isolation. When comparing datasets collected before and after completion of PVI in this group, there was no significant decrease in R50 ($-4.74 \pm 27.19^\circ$; 95% CI -13.67 to 4.2 ; $P = 0.29$), number of dominant directions (-0.03 ± 1.82 ; 95% CI -0.63 to 0.57 ; $P = 0.93$), or percentage match ($-26.27 \pm 15.04\%$; 95% CI -63.64 to 11.1 ; $P = 0.09$) following re-isolation of the reconnected veins (Figure 6-15). LAA cycle length in patients 13 and 19 did not show any significant increase after PVI, while there was a significant increase in LAA cycle length in patient 20.

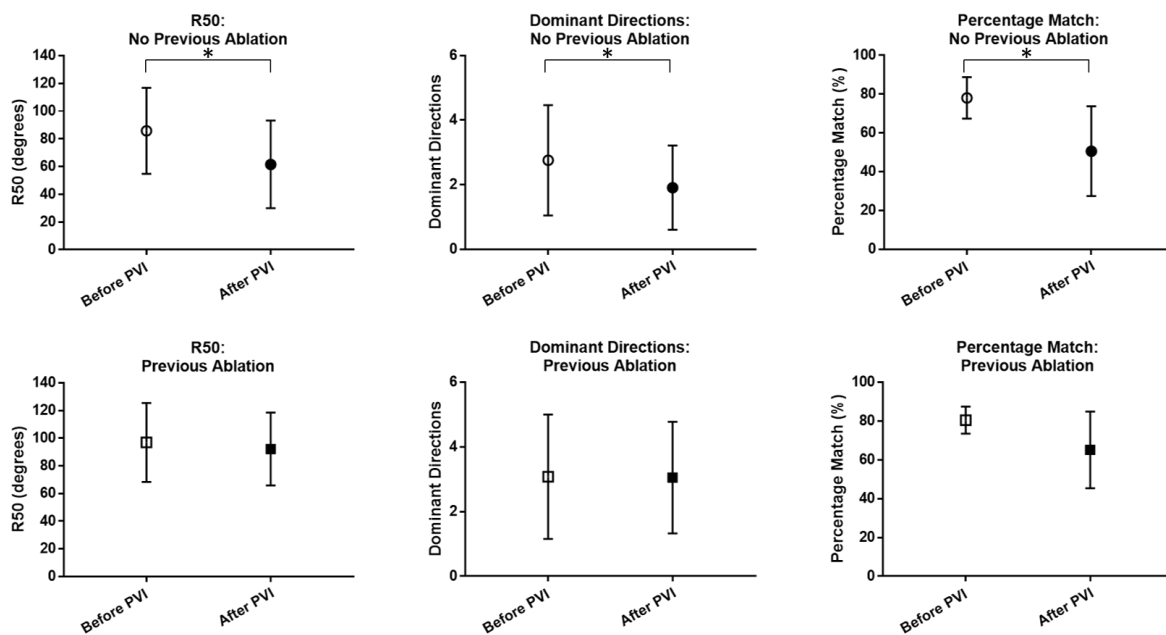


Figure 6-15. Differences between patient that have undergone previous PVI for persistent AF and those with no previous ablation. There was a significant decrease in R50, number of dominant directions, and percentage match following PVI in patients with no previous history of AF ablation (* $P < 0.0001$). There was no significant difference for these parameters in patients that had undergone previous AF ablation procedures.

6.3.6 Workflow for online RETRO-Mapping

In addition to the patients recruited in this chapter, three patients were recruited to develop a workflow that allowed data to be analysed during a procedure. Difficulties with accessing live data from Ensite Precision forced an alternative approach to be sought.

Forty three data segments were collected from 3 patients before PVI. All patients had undergone two or more previous catheter ablation procedures for persistent AF. Prior to data collection, the PVs were assessed for isolation. All 4 veins in each patient were isolated at the start of the case. Following data collection, the active case in Ensite Precision was closed to allow the whole case to be exported to an external hard drive. Immediately following this, the case was re-opened to enable catheter ablation to be undertaken at the discretion of the operator. This process takes approximately 3-5 minutes.

It is not possible to run the entire export file from Ensite Precision for analysis with RETRO-Mapping, and requires selection of the precise data for analysis manually. During the

time that catheter ablation was being undertaken, the case was imported to a laptop supplied by Abbott/St Jude which runs the clinical version of Ensite Precision. In order to obtain the data required for analysis with RETRO-Mapping, each recorded data segment has to be individually selected and stored as an export file containing the raw bipolar electrogram and electrode location data from the AFocusII catheter. These files are subsequently exported on to an external hard drive, and are ready for importing to RETRO-Mapping. This process takes approximately 10 minutes. RETRO-Mapping undertakes the analysis process to identify the activation patterns for each data segment and displays them in the GUI for the user. The data analysis phase takes 30-40 minutes, depending on the number of data segments that have been acquired.

Using the method described, approximately 45-55 minutes is required for analysis of data from the time that data collection has been completed. Although this method allows data to be exported and analysed during a case, it is not currently at a stage that it can be relied upon for clinical use.

6.4 Discussion

It is common for clinical electrophysiologists to describe “more organised” AF following ablation. However, the way that this statement is qualified is subjective and based upon CS activation patterns, or based on crude measurement of LAA cycle length over 30 cycle. This chapter uses RETRO-Mapping to quantify the effect of catheter ablation with PVI on persistent AF with regard to a number of novel parameters, and their correlation with the established marker of LAA cycle length. Specifically, these novel parameters include; R50, number of dominant directions, and percentage match. Sub-group analyses have also been undertaken to investigate the difference between induced and spontaneous persistent AF, and patients with previous PVI to gain further mechanistic insight.

Besides termination of AF, the LAA cycle length is commonly used to determine response to catheter ablation. As AF becomes more organised, the LAA cycle length prolongs, and when it reaches a critical cycle length it is associated with termination of AF.⁸³ An increase of just 5-6ms in mean LAA cycle length over 30 cycles is considered to represent a significant response to ablation.^{83, 87, 116} Our observations were consistent with this. Following PVI, there was prolongation of LAA cycle length in all patients to some degree, reaching significance in 18/23 patients. Of the 5/23 patients that showed a trend towards increased LAA cycle length,

each patient had one or more of the following characteristics; previous PVI (with 1 reconnected PV), induced persistent AF, or taking amiodarone. It is understandable why a greater number of isolated PVs at baseline might result in a lesser increase in LAA cycle length on completion of their isolation to those with all PVs electrically connected at baseline. Similarly, possible suppression of focal drivers with amiodarone might explain why a more significant effect from PVI was not seen in patients on this drug. However, other groups have described differences between patients with induced and spontaneous AF, with longer LAA cycle lengths recorded during induced compared to spontaneous AF in a canine atria.¹⁰⁰ We observed the opposite, however there was a much greater increase in LAA cycle length following ablation for patients with spontaneous compared to induced persistent AF. This does suggest that mechanistic differences likely exist between the two, and that the pulmonary veins might play a more important role in spontaneous compared to induced AF.

Although LAA cycle length can be used to assess the response to catheter ablation, it reflects electrical information pertaining to the entire LA. There is interest in ablation beyond the PVs, which demands a more detailed and localised understanding of activation within the atria. It is possible to create maps showing the local AF cycle length throughout the atria. Similar to CFAE maps, wavefront collision and electrogram fractionation can make signal annotation challenging. Uniform wavefronts occurring during AF are used to produce orbital plots in RETRO-Mapping. R50 is the range in degrees in which 50% of this activation is contained and is calculated from orbital plots. There are local differences in R50 between different patients, and also within different locations in the same patient.

Isolation of the pulmonary veins has previously been shown to result in prolongation of the LAA cycle length.^{83, 151} This effect was also identified in this study. Following PVI, R50 decreased in all except 1 patient. This suggests that activation became more organised after PVI, as activation became restricted to a narrower spread of directions. Analysis of individual patients showed a significant reduction in R50 in the majority of patients (16/23). There was a trend towards decreased R50 following PVI in a further 6/23 patients, however one patient showed a trend towards increased R50. It is possible that patients that did not show a significant reduction in R50 following PVI may be the result of inadequate data collection, or identify patients in whom the predominant mechanism is non-PV driven AF. Importantly, there is a correlation between increased LAA cycle length and decreased R50 in response to

PVI, validating R50 as a tool to quantify 'organisation' of AF, and a tool to determine the effects of catheter ablation.

Sih *et al.* have shown differences in AF cycle length between patients with induced and spontaneous AF, identifying induced AF to have a longer cycle length than persistent AF in a canine model, indicating that induced AF is more organised.¹⁰⁰ In this study, patients with induced AF had a significantly lower R50 than those with spontaneous persistent AF, both before and after PVI. The demonstration of a lower R50 in patients with induced R50 is consistent with AF being more organised in this group of patients compared to spontaneous persistent AF.

We identified that the mean LAA cycle length in patients with induced AF was shorter than for patients with spontaneous persistent AF, and contradicts the findings of Sih *et al.*¹⁰⁰ This might be explained by the methods used for measuring the cycle length following AF induction by the researchers. They measured the AF cycle length over a 10 second period of AF beginning 2 seconds after AF induction and at least 2 seconds before spontaneous AF termination. It is common that the AF cycle length varies significantly until it becomes stable following induction. Similarly, AF cycle length usually gradually prolongs just before AF terminates.⁸³ Bearing this in mind, it is unlikely that the mean AF cycle length that they used can be relied upon, based on their measurement criteria by the researchers.

Konings *et al.* characterised the atrial activation patterns that occur during in AF, showing different degrees of disorganisation.²⁷ Gerstenfeld *et al.* showed that multiple uniform wavefront can intermittently occur in the same or multiple different directions in the same location.¹¹³ Focal drivers within the PVs have previously been documented, and remain the only consistently proven mechanism for AF.⁶ Increased organisation was shown following ablation with PVI in this study, determined by an increased LAA cycle length, and decrease in R50. The exclusion of focal drivers within the PVs, together with exclusion of any focal drivers within the confines of the circumferential antral ablation offers a plausible explanation for the increased organisation demonstrated.

Following PVI, there was a significant decrease in the number of dominant directions compared to before PVI; i.e. activation becomes confined to fewer different directions after PVI. In agreement with the observations of differences between induced and spontaneous persistent AF, patients with induced persistent AF also had a lower number of dominant directions than patients with spontaneous persistent AF. It was also demonstrated that there

is a strong positive correlation between an increasing number of dominant directions and increasing R50. This might provide additional indirect evidence that as focal drivers are excluded within the confines of the antral circumferential ablation lesion sets, there are fewer directions in which the uniform wavefronts originate. Strengthening of this indirect evidence comes from the patients that had undergone previous PVI only procedure. Although these three patients did have some very limited PV reconnection, the PVs were largely isolated. Re-isolation did not result in any significant change in R50, number of dominant directions, or percentage match. This suggests that there is an alternative mechanism responsible for maintenance of AF in these patients, and the PVs are not implicated.

An alternative explanation for the change in activation pattern relates to the functional effect of introducing obstacles that alter the potential pathway that activation can take. The posterior wall between the antral PVI lesions effectively becomes a 'corridor' in which activation is restricted. The relationship between left atrial structural pathways and electrical function during persistent AF has not been fully characterised. Wavefronts with preferential activation direction have been demonstrated during re-entrant arrhythmias, and structural determinants suggested to be implicated.⁷⁵ Electrical conduction from the PVs has also been correlated with anatomic features in canine atria.⁷⁶ A recent technique has been developed which allows the myofiber architecture of the human left atrium to be imaged using diffusion tensor magnetic resonance imaging (DTMRI) at the submillimetre level.⁷⁸ If the mechanism of change in activation pattern was the functional effect of ablation boundaries, one might expect activation to either move 'up' or 'down' the posterior wall only. We did not observe this, and identified activation to move in directions that are not consistent with the atlas of myofiber orientation, and goes against activation patterns solely being determined by myofiber orientation.

RETRO-Mapping has also been demonstrated to be effective at mapping regular cycle length tachycardias. All electroanatomical mapping systems have the capability of producing conventional isochronal maps, however it has been demonstrated that incorrect annotation of only a few points can result in a map that does not reflect the underlying tachycardia mechanism.¹¹⁸ The benefit of RETRO-Mapping is that it does not require a window of interest to be set or any manual adjustment of signal annotation. One particular group of atrial tachycardias that might benefit from this type of mapping are those with a variable cycle

length. It is not possible to map these tachycardias using conventional methods, but would be possible using RETRO-Mapping.

Finally, a workflow has been developed that allows data to be analysed during a catheter ablation procedure. The significant problems with developing a live data export in real time has limited the rate at which data can be analysed. Furthermore, the speed at which the data is analysed through RETRO-Mapping is not fast enough at present, and requires refinement to improve the analysis speed. As a result, it is not possible to undertake ablation within the acceptable time constraints of a clinical procedure at present.

6.5 Limitations

In order to assess the change in R50 and dominant directions between datasets collected before and after PVI, the catheter had to be returned to the same location and in the same catheter orientation. There were some problems with interference with the magnetic data location in Ensite Precision prevented its use during procedures in our catheterisation laboratory. Reliance was therefore upon the impedance based system which can suffer from 'map shifts' due to changes in impedance throughout the case. To minimise errors of incorrect mapping position, the CS catheter was shadowed, along with the AFocusII position in all 4 veins so that any changes could be identified and corrected.

A large amount of time was spent attempting to develop a live data export and analysis method. It was underestimated how challenging this would be, and has prevented live data export and analysis. This is a requirement if the analysed data is to be used during a clinical procedure to guide ablation.

6.6 Conclusion

Catheter ablation of persistent AF with PVI results in significant organisation of fibrillatory activity. This is evidenced by decreased R50 and number of dominant directions, and an increase in LAA cycle length. It is not clear if these effects are purely down to isolation of the PVs, or if it is a combination of the functional effects and also inadvertent isolation of focal drivers during PVI. It is clear that differences exist between induced and spontaneous persistent AF, and between those patients that have undergone PVI only procedures but have the existence of minor PV re-connections at baseline. It might be possible to use RETRO-Mapping to quantify the effect of catheter ablation which may provide prognostic information for recurrence rates and modes of AF.

7 Conclusions and Future Work

7.1	Introduction.....	177
7.2	Original Contributions	177
	7.2.1 Activation Mapping of Atrial Fibrillation	177
	7.2.2 Spatiotemporal Stability of Atrial Fibrillation.....	178
	7.2.3 Tools to Quantify Activation Characteristics	179
7.3	Implications of the research.....	180
7.4	Future directions	181
7.5	Conclusion	182

7.1 Introduction

Mapping to determine arrhythmia mechanism is crucial to successful catheter ablation. Development of techniques to map regular cycle length tachycardias have resulted in greatly improved procedural outcome¹¹⁸, however such advances have not been observed with atrial fibrillation. As a result, ablation beyond pulmonary vein isolation has not consistently been shown to improve long term outcomes.¹⁵²

The population of patients suffering from AF is expected to significantly increase over the coming years. Therefore, the number of patients requiring catheter ablation will substantially grow. Although mapping of AF may not be required for an initial ablation procedure, it is likely to benefit patients in whom PVI does not result in maintenance of sinus rhythm.

A literature review, in Chapter 1, has identified some of the significant challenges that exist when attempting to map AF and some of the existing techniques that have caused great controversy. It is interesting that despite around 100 years of attempts to understand the underlying mechanisms of AF, several mechanisms have been suggested but evidence to confirm or disprove them is still lacking. The intention of this thesis was to develop a new automated technique which enables AF to be mapped in order to understand the mechanisms that maintain persistent AF. The eventual goal is to utilise this understanding to improve catheter ablation outcome with a patient tailored approach.

7.2 Original Contributions

7.2.1 Activation Mapping of Atrial Fibrillation

In Chapter 3, the development and validation of a technique for activation mapping of AF was presented. This involved the development of a novel computational algorithm to track uniform activation during AF and display the data in a manageable way for the user to interpret. Importantly, this technique had to be able to operate without the use of either a fiducial signal, or a fixed time window. The algorithm underwent extensive validation to ensure that activation maps were consistent with isochronal mapping, which was defined as the 'gold standard'. It is accepted that there is no true gold standard.

The technique for mapping AF was further developed in Chapters 3 and 4, with automated techniques to quantify organisational characteristics of mapped locations. Large

volumes of AF data underwent initial manual analysis, with subsequent analysis using RETRO-Mapping, as well as a novel method to display these data in the form of a choropleth map. The user interface was further developed in these chapters, to allow multiple different locations to be simultaneously displayed, determined by the user. Importantly, this user interface also allows the user to review the raw electrogram data that has been used to generate maps for corroboration of results.

7.2.2 Spatiotemporal Stability of Atrial Fibrillation

In Chapter 4, RETRO-Mapping was used to demonstrate that atrial activation patterns during persistent AF are not random. This is an extremely important discovery, as it implies that an ablation target may exist, and that a sequential mapping technique using a roving multipolar catheter is feasible.

Qualitative assessment of orbital plots was initially applied. This identified that activation pattern of the majority of orbital plots stabilises at around 20-30 seconds. Development of 'Percentage Match' also provided evidence that activation patterns tend to become stable at 30 seconds of data collection. The same technique was used to show that atrial activation patterns during persistent AF remain stable over time periods of at least 10 minutes. In addition to showing stability of atrial activation during persistent AF, more conventional markers of atrial substrate have also been shown to remain stable over time. This includes both endocardial mean peak-to-peak bipolar voltage and CFAE_{mean}, measured over 8 seconds.

An explanation for the stability of these activation patterns was explored in Chapter 5. This was based on the previously described theory of a focal driver hypothesis, and a simplified hypothetical model of AF. Manual analysis of data segments for focal activation was compared with the activation patterns and the novel tools for analysis of data segments, such as R50 and number of dominant directions (described in Chapters 4 and 5). Although focal activation was identified, it was not possible to demonstrate that they were responsible for the observed activation patterns.

Finally, the effect of pulmonary vein isolation on atrial activation patterns has been characterised, in Chapter 6. Until now, crude markers such as LAA cycle length measured over 30 AF cycle lengths, and activation sequences on the CS catheter have been used to 'prove' that AF becomes more organised with PVI. This is an oversimplification of such a complex

electrophysiological process. RETRO-Mapping has provided insight in to the effect of PVI on atrial activation patterns. Novel tools for analysis, including R50 and number of dominant directions have been studied alongside LAA cycle length to show that there is a quantifiable relationship between them all.

7.2.3 Tools to Quantify Activation Characteristics

RETRO-Mapping was developed for activation mapping of persistent AF, as at the time of embarking on this research, there were no commercially available platforms that currently exist. Since this research, CARTOFINDER and more recently a novel method using dipole mapping have been developed, but are not available on general commercial release. As a result, there are no established tools available for activation mapping of AF. In Chapters 3, 4 and 5 of this thesis, new tools were developed and tested. In addition, some established analysis techniques, such as Shannon entropy, fractionation, and voltage were also applied.

The rationale behind development of these tools was because qualitative comparison of data was subjective and prevented statistical testing. It was quickly noticed that although Shannon entropy could be used to compare repeated mapping of a location, it could not be used to compare different locations mapped in the same patient, or different patients with regard to the degree of AF organisation. Development of new tools (R50 and number of dominant directions) provided a method to compare locations within, and between locations. In Chapter 4, R50 provided a method to define the directional spread of activation, in which different locations could be compared. Additional analysis with the development of dominant direction assignment, in Chapter 5, assisted in determination of how activation was directed. In Chapter 6, the relationship between R50, dominant directions and the more established marker of LAA cycle length were studied in response to ablation. The correlations between R50, number of dominant directions, and LAA cycle length helps to validate these tools as markers of organisation during AF.

The new tools that were developed in this thesis have allowed detailed characterisation of activation patterns. Furthermore, the effect of ablation can be measured quantitatively. These parameters may assist operators to identify the appropriate ablation strategy for patients to improve procedural outcomes.

7.3 Implications of the research

Since the discovery of focal ectopy from the pulmonary veins initiating AF⁶, adjunctive ablation techniques have failed to result in significant incremental benefit from catheter ablation. Attempts at improving success rates have frequently involved the use of surrogate markers of activation to infer mechanisms. It is well accepted that an understanding of atrial activation patterns during atrial tachycardia enables the underlying mechanism to be identified, leading to successful ablations. It is therefore understandable why mapping activation during AF might lead to the same success.

RETRO-Mapping is a technique that tracks uniform wavefronts that occur during AF in order gain mechanistic information. The automation of data analysis allows larger regions of the atrium to be mapped, as this technique is not reliant on manual analysis. Furthermore, this technique maps activation without a time window. This may have important implications in mapping other arrhythmias, such as variable cycle length atrial tachycardias. Conventional mapping techniques are reliant on a fixed time window or fiducial signal. If there is a significant variability in cycle length, it is not possible to map the arrhythmia. RETRO-Mapping is not reliant on a fixed time window, or fiducial signal and should therefore be able to map the arrhythmia.

In this thesis, some patients were found to have multiple neighbouring data segments with very similar activation directions and patterns. In these situations, this might represent patients that are able to support macro re-entry. These patients may benefit from additional linear ablation, which has previously not been shown to provide additional benefit over PVI alone.

In the research presented in this thesis, it has been shown that there are differences between patients in terms of the effect of PVI, and the stability of activation patterns. RETRO-Mapping may help to classify the different 'types' or mechanisms of AF that exist in different patients. This has two important implications. Firstly, ablation techniques could be tailored to the requirements of each patient. Secondly, it may assist in providing prognostic data on the success of catheter ablation in certain patients. Importantly, data collection can be done with conventional multipolar catheters and a commercially available mapping system.

7.4 Future directions

This thesis involves the development of a computational method to map atrial activation during atrial fibrillation with the aim of improving the procedural outcome of catheter ablation by understanding the mechanisms that maintain AF. The ultimate aim would be to incorporate this technique in to established mapping systems for its widespread use in hospitals around the world.

In this thesis, mapping and data analysis was conducted off-line. Ensite Precision does not allow the user to export data from the platform during the clinical case. Although licensed software was provided from Abbott to enable export of data during the procedure, it was not possible to achieve this. The alternative method did allow data to be exported and analysed during the case. However, if this mapping technique is to be used during a clinical procedure it is a requirement that the procedure would not need to be interrupted for data export. This has been the major obstacle to progression of this research, however work is ongoing to overcome this problem.

The speed of data analysis has also prevented the use of RETRO-Mapping during a clinical procedure. The nature of development of a computational system means that new developments are added to the existing platform. This can produce inefficiencies in the way that data is analysed and stored. The work in this thesis has shown that the mapping technique is effective. The next step to improve the computational efficiency will involve review of the algorithms in order to maximise analysis efficiency.

To date, data collection has been intentionally confined to a limited region of the atrium. The extensive validation steps that have been undertaken have involved labour intensive manual analysis of large volumes of data. Furthermore, the computational efficiency has also prevented larger amounts of data to be collected due to the speed of automated analysis. Having validated RETRO-Mapping, future research will be directed towards data collection from the entire left and right atrium. The development of a live data export platform will also assist in optimising the amount of data that needs to be collected from each location. Some patients appear to have more organised AF than others, and it is therefore likely that 30 seconds of data collection in some patients is not required.

Data collection from the entire left and right atrium will also be important to understand the modes of arrhythmia recurrence in patients following ablation. It is recognised that some

patients remain in sinus rhythm following PVI, while others recur with either AF or atrial tachycardia. RETRO-Mapping may be useful for predicting the mode of arrhythmia recurrence. This is important, as it may help to identify specific characteristics of patients that have a tendency to have post ablation atrial tachycardia due to either roof or mitral macro re-entry. If this is determined at the time of the initial procedure, empirical linear ablation may assist in preventing this mode of recurrence.

Towards the end of this research, Abbott released a new multipolar mapping catheter; the HD Grid. This catheter has smaller electrodes with a dense electrode configuration. Development and validation of RETRO-Mapping is required to allow data to be collected and analysed with this catheter. One of the concerns with the AFocusII catheter was that the electrode density was not sufficient for detection of focal activation. The improved central coverage of electrodes in the catheter mapping area of the HD Grid will provide superior resolution.

Incorporation of this mapping technique has been discussed with Biosense Webster. There is an ongoing working relationship, however Biosense Webster have recently developed CARTOFINDER as a tool for mapping AF. An important step moving forwards is to compare data analysed using CARTOFINDER with that of RETRO-Mapping to ascertain any similarities or differences between the mapping techniques.

7.5 Conclusion

The research presented in this thesis has involved the development of a new method for mapping atrial activation during persistent AF, and new tools for both qualitative and quantitative analysis of AF. This has resulted in the novel discovery that persistent AF is not random, and shows stability of activation patterns in addition to established surrogate markers of atrial substrate. It is hoped that this contribution will help to advance the quality of treatment that patients receive in the future.

8 References

1. Ezekowitz MD. Atrial fibrillation: the epidemic of the new millennium. *Ann Intern Med.* 1999;131:537-8.
2. Majeed A, Moser K and Carroll K. Trends in the prevalence and management of atrial fibrillation in general practice in England and Wales, 1994-1998: analysis of data from the general practice research database. *Heart.* 2001;86:284-8.
3. Benjamin EJ, Wolf PA, D'Agostino RB, Silbershatz H, Kannel WB and Levy D. Impact of atrial fibrillation on the risk of death: the Framingham Heart Study. *Circulation.* 1998;98:946-52.
4. Stewart S, Hart CL, Hole DJ and McMurray JJ. A population-based study of the long-term risks associated with atrial fibrillation: 20-year follow-up of the Renfrew/Paisley study. *Am J Med.* 2002;113:359-64.
5. Kotecha D, Holmes J, Krum H, Altman DG, Manzano L, Cleland JG, Lip GY, Coats AJ, Andersson B, Kirchhof P, von Lueder TG, Wedel H, Rosano G, Shibata MC, Rigby A, Flather MD and Beta-Blockers in Heart Failure Collaborative G. Efficacy of beta blockers in patients with heart failure plus atrial fibrillation: an individual-patient data meta-analysis. *Lancet.* 2014;384:2235-43.
6. Haïssaguerre M, Jaïs P, Shah DC, Takahashi A, Hocini M, Quiniou G, Garrigue S, Le Mouroux A, Le Métayer P and Clémenty J. Spontaneous Initiation of Atrial Fibrillation by Ectopic Beats Originating in the Pulmonary Veins. *N Engl J Med.* 1998;339:659-66.
7. Atul Verma CyJ, Timothy R. Betts, Jian Chen, Isabel Deisenhofer, Roberto Mantovan, Laurent Macle, Carlos A. Morillo, Wilhelm Haverkamp, Rukshen Weerasooriya, Jean-Paul Albenque, Stefano Nardi, Endrj Menardi, Paul Novak, Prashanthan Sanders. Approaches to Catheter Ablation for Persistent Atrial Fibrillation. *NEJM.* 2015;372:1812-1822.
8. Steinberg JS, Shah Y, Bhatt A, Sichrovsky T, Arshad A, Hansinger E and Musat D. Focal impulse and rotor modulation: Acute procedural observations and extended clinical follow-up. *Heart rhythm : the official journal of the Heart Rhythm Society.* 2017;14:192-197.
9. WE G. The nature of fibrillary contraction of the heart - Its relation to tissue mass and form. *Am J Physiol.* 1914;33:397-414.
10. Mayer A. Rhythmical pulsation in Scyphomedusae. *Carnegie Inst Wash Pub.* 1906;47:1-62.
11. WE G. Auricular Fibrillation. *Physiological Reviews.* 1924;4:215-250.
12. Mines R. On dynamic equilibrium in the heart. *The Journal of Physiology.* 1913;46:349-383.

13. Lewis T DA, Iliescu CC. Further observations upon the state of rapid re-excitation of the auricles. *Heart*. 1921;8:311-340.
14. Lewis T. The Nature of Flutter and Fibrillation of the Auricle. *BMJ*. 1921:590-593.
15. Lewis T. Observations upon flutter and fibrillation. Part IV. Impure flutter; theory of circus movement. *Heart*. 1918;7:1918-1920.
16. Moe GK AJ. Atrial fibrillation as a self-sustaining arrhythmia independent of focal discharge. *American heart journal*. 1959;58:59-70.
17. Moe GK, Rheinboldt WC and Abildskov JA. A computer model of atrial fibrillation. *American heart journal*. 1964;67:200-20.
18. Lee S, Sahadevan J, Khrestian CM, Durand DM and Waldo AL. High density mapping of atrial fibrillation during vagal nerve stimulation in the canine heart: restudying the Moe hypothesis. *J Cardiovasc Electrophysiol*. 2013;24:328-35.
19. Allesie MA, Bonke FI and Schopman FJ. Circus movement in rabbit atrial muscle as a mechanism of tachycardia. III. The "leading circle" concept: a new model of circus movement in cardiac tissue without the involvement of an anatomical obstacle. *Circ Res*. 1977;41:9-18.
20. Allesie MA, Bonke FI and Schopman FJ. Circus movement in rabbit atrial muscle as a mechanism of tachycardia. II. The role of nonuniform recovery of excitability in the occurrence of unidirectional block, as studied with multiple microelectrodes. *Circ Res*. 1976;39:168-77.
21. Allesie MA, Bonke FI and Schopman FJ. The mechanism of supraventricular tachycardia induced by a single premature beat in the isolated left atrium of the rabbit. I. Circus movement as a consequence of unidirectional block of the premature impulse. *Recent Adv Stud Cardiac Struct Metab*. 1975;5:303-8.
22. Allesie MA, Bonke FI and Schopman FJ. Circus movement in atrial muscle as a mechanism of supraventricular tachycardia. *J Physiol (Paris)*. 1972;65:Suppl:324A.
23. M. A. Allesie WJEPL, F. I. M. Bonke, J. Hollen. Experimental evaluation of Moe's multiple wavelet hypothesis of atrial fibrillation. In: Zipes DP, Jalife J, editors *Cardiac Electrophysiology and Arrhythmias* New York, NY. 1985:265-275.
24. Canavan; TE, Schuessler; RB, Boineau; JP, Con; PB, Cain; ME and Cox JL. Computerized Global Electrophysiological Mapping of the Atrium in Patients with Wolff-Parkinson-White Syndrome. *Ann Thorac Surg*. 1988;46:223-231.
25. Cox JL CT, Schuessler RB, Cain ME, Lindsay BD, Stone C, Smith PK, Corr PB, Boineau JP. The surgical treatment of atrial fibrillation. II. Intraoperative electrophysiologic mapping and description of the electrophysiologic basis of atrial flutter and atrial fibrillation. *J Thorac Cardiovasc Surg*. 1991;101:406-426.

26. Konings KT, Smeets JL, Penn OC, Wellens HJ and Allessie MA. Configuration of unipolar atrial electrograms during electrically induced atrial fibrillation in humans. *Circulation*. 1997;95:1231-41.
27. Konings; KTS, Kirchhof; CJHJ, Smeets; JRLM, Wellens; HJJ, Penn; OC and Allessie MA. High-Density Mapping of Electrically Induced Atrial Fibrillation in Humans. *Circulation*. 1994;89:1665-1680.
28. Schuessler RB, Grayson TM, Bromberg BI, Cox JL and Boineau JP. Cholinergically mediated tachyarrhythmias induced by a single extrastimulus in the isolated canine right atrium. *Circ Res*. 1992;71:1254-67.
29. Schuessler RB, Kawamoto T, Hand DE, Mitsuno M, Bromberg BI, Cox JL and Boineau JP. Simultaneous epicardial and endocardial activation sequence mapping in the isolated canine right atrium. *Circulation*. 1993;88:250-63.
30. Natasja M. S. de Groot RPMH, Joep L. Smeets, Eric Boersma, Ulrich Schotten, Martin J. Schalij, Harry Crijns, Maurits A. Allessie. Electropathological Substrate of Longstanding Persistent Atrial Fibrillation in Patients With Structural Heart Disease Clinical Perspective. *Circulation*. 2010;122:1674-1682.
31. de Groot N, van der Does L, Yaksh A, Lanters E, Teuwen C, Knops P, van de Woestijne P, Bekkers J, Kik C, Bogers A and Allessie M. Direct Proof of Endo-Epicardial Asynchrony of the Atrial Wall During Atrial Fibrillation in Humans. *Circulation Arrhythmia and electrophysiology*. 2016;9e:e003648.
32. Rothberger CJ WH. Vorhofflimmern und Arrhythmia perpetua (Atrial fibrillation and perpetuating arrhythmia). *Wien Klin Wochenschr*. 1909:839-844.
33. Scherf D, Romano FJ and Terranova R. Experimental studies on auricular flutter and auricular fibrillation. *American heart journal*. 1948;36:241-51.
34. Harada; A, Sasaki; K, Fukushima; T, Ikeshita; M, Asano; T, Yamauchi; S, Tanaka; S and Shoji T. Atrial Activation During Chronic Atrial Fibrillation in Patients With Isolated Mitral Valve Disease. *Ann Thorac Surg*. 1996;61:104-112.
35. Jais P, Haissaguerre M, Shah DC, Chouairi S, Gencel L, Hocini M and Clementy J. A focal source of atrial fibrillation treated by discrete radiofrequency ablation. *Circulation*. 1997;95:572-6.
36. Quintanilla JG, Perez-Villacastin J, Perez-Castellano N, Pandit SV, Berenfeld O, Jalife J and Filgueiras-Rama D. Mechanistic Approaches to Detect, Target, and Ablate the Drivers of Atrial Fibrillation. *Circulation Arrhythmia and electrophysiology*. 2016;9:e002481.
37. Pandit SV and Jalife J. Rotors and the Dynamics of Cardiac Fibrillation. *Circ Res*. 2013;112:849-862.
38. Winfree AT. Electrical instability in cardiac muscle: phase singularities and rotors. *J Theor Biol*. 1989;138:353-405.

39. Davidenko JM, Pertsov AV, Salomonsz R, Baxter W and Jalife J. Stationary and drifting spiral waves of excitation in isolated cardiac muscle. *Nature*. 1992;355:349-51.
40. Skanes AC, Mandapati R, Berenfeld O, Davidenko JM and Jalife J. Spatiotemporal periodicity during atrial fibrillation in the isolated sheep heart. *Circulation*. 1998;98:1236-48.
41. Chen J, Mandapati R, Berenfeld O, Skanes AC, Gray RA and Jalife J. Dynamics of wavelets and their role in atrial fibrillation in the isolated sheep heart. *Cardiovasc Res*. 2000;48:220-32.
42. Mandapati R, Skanes A, Chen J, Berenfeld O and Jalife J. Stable microreentrant sources as a mechanism of atrial fibrillation in the isolated sheep heart. *Circulation*. 2000;101:194-9.
43. Salama G and Morad M. Merocyanine 540 as an optical probe of transmembrane electrical activity in the heart. *Science*. 1976;191:485-7.
44. Narayan SM KD, Shivkumar K, Clopton P, Rappel W-J, Miller JM. Treatment of atrial fibrillation by the ablation of localized sources: CONFIRM (Conventional Ablation for Atrial Fibrillation With or Without Focal Impulse and Rotor Modulation) trial. *J Am Coll Cardiol*. 2012;60:628–636.
45. Narayan SM, Krummen DE, Shivkumar K, Clopton P, Rappel WJ and Miller JM. Treatment of atrial fibrillation by the ablation of localized sources: CONFIRM (Conventional Ablation for Atrial Fibrillation With or Without Focal Impulse and Rotor Modulation) trial. *J Am Coll Cardiol*. 2012;60:628-36.
46. Haissaguerre M, Shah AJ, Cochet H, Hocini M, Dubois R, Efimov I, Vigmond E, Bernus O and Trayanova N. Intermittent drivers anchoring to structural heterogeneities as a major pathophysiological mechanism of human persistent atrial fibrillation. *J Physiol*. 2016;594:2387-98.
47. Haissaguerre M, Hocini M, Denis A, Shah AJ, Komatsu Y, Yamashita S, Daly M, Amraoui S, Zellerhoff S, Picat MQ, Quotb A, Jesel L, Lim H, Ploux S, Bordachar P, Attuel G, Meillet V, Ritter P, Derval N, Sacher F, Bernus O, Cochet H, Jais P and Dubois R. Driver domains in persistent atrial fibrillation. *Circulation*. 2014;130:530-8.
48. Knecht S, Sohal M, Deisenhofer I, Albenque JP, Arentz T, Neumann T, Cauchemez B, Duytschaever M, Ramoul K, Verbeet T, Thorsten S, Jadidi A, Combes S, Tavernier R, Vandekerckhove Y, Ernst S, Packer D and Rostock T. Multicentre evaluation of non-invasive biatrial mapping for persistent atrial fibrillation ablation: the AFACART study. *Europace*. 2017;19(8):1302-1309.
49. Narayan SM, Krummen DE and Rappel WJ. Clinical Mapping Approach To Diagnose Electrical Rotors and Focal Impulse Sources for Human Atrial Fibrillation. *Journal of Cardiovascular Electrophysiology*. 2012;23:447-454.
50. Miller JM, Kalra V, Das MK, Jain R, Garlie JB, Brewster JA and Dandamudi G. Clinical Benefit of Ablating Localized Sources for Human Atrial Fibrillation: The Indiana University FIRM Registry. *J Am Coll Cardiol*. 2017;69:1247-1256.

51. Rappel WJ, Zaman JA and Narayan SM. Mechanisms for the Termination of Atrial Fibrillation by Localized Ablation: Computational and Clinical Studies. *Circulation Arrhythmia and electrophysiology*. 2015;8:1325-33.
52. Hansen BJ, Zhao J, Csepe TA, Moore BT, Li N, Jayne LA, Kalyanasundaram A, Lim P, Bratasz A, Powell KA, Simonetti OP, Higgins RS, Kilic A, Mohler PJ, Janssen PM, Weiss R, Hummel JD and Fedorov VV. Atrial fibrillation driven by micro-anatomic intramural re-entry revealed by simultaneous sub-epicardial and sub-endocardial optical mapping in explanted human hearts. *Eur Heart J*. 2015;36:2390-401.
53. Moe GK. On the multiple wavelet hypothesis of atrial fibrillation. *Arch Int Pharmacodyn Ther*. 1962;140:183-188.
54. Armour JA, Murphy DA, Yuan BX, Macdonald S and Hopkins DA. Gross and microscopic anatomy of the human intrinsic cardiac nervous system. *Anat Rec*. 1997;247:289-98.
55. Takahashi Y, Jais P, Hocini M, Sanders P, Rotter M, Rostock T, Hsu LF, Sacher F, Clementy J and Haissaguerre M. Shortening of fibrillatory cycle length in the pulmonary vein during vagal excitation. *J Am Coll Cardiol*. 2006;47:774-80.
56. Lim PB, Malcolme-Lawes LC, Stuber T, Kojodjojo P, Wright IJ, Francis DP, Wyn Davies D, Peters NS and Kanagaratnam P. Stimulation of the intrinsic cardiac autonomic nervous system results in a gradient of fibrillatory cycle length shortening across the atria during atrial fibrillation in humans. *J Cardiovasc Electrophysiol*. 2011;22:1224-31.
57. Patterson E, Po SS, Scherlag BJ and Lazzara R. Triggered firing in pulmonary veins initiated by in vitro autonomic nerve stimulation. *Heart rhythm : the official journal of the Heart Rhythm Society*. 2005;2:624-31.
58. Schauerte P, Scherlag BJ, Pitha J, Scherlag MA, Reynolds D, Lazzara R and Jackman WM. Catheter ablation of cardiac autonomic nerves for prevention of vagal atrial fibrillation. *Circulation*. 2000;102:2774-80.
59. Katritsis DG, Giazitzoglou E, Zografos T, Pokushalov E, Po SS and Camm AJ. Rapid pulmonary vein isolation combined with autonomic ganglia modification: a randomized study. *Heart rhythm : the official journal of the Heart Rhythm Society*. 2011;8:672-8.
60. Katritsis DG, Pokushalov E, Romanov A, Giazitzoglou E, Siontis GC, Po SS, Camm AJ and Ioannidis JP. Autonomic denervation added to pulmonary vein isolation for paroxysmal atrial fibrillation: a randomized clinical trial. *J Am Coll Cardiol*. 2013;62:2318-25.
61. Lim PB, Malcolme-Lawes LC, Stuber T, Wright I, Francis DP, Davies DW, Peters NS and Kanagaratnam P. Intrinsic cardiac autonomic stimulation induces pulmonary vein ectopy and triggers atrial fibrillation in humans. *J Cardiovasc Electrophysiol*. 2011;22:638-46.
62. Baykaner T, Zografos TA, Zaman JAB, Pantos I, Alhousseini M, Navara R, Krummen DE, Narayan SM and Katritsis DG. Spatial relationship of organized rotational and focal sources in human atrial fibrillation to autonomic ganglionated plexi. *Int J Cardiol*. 2017;240:234-239.

63. Marrouche NF, Wilber D, Hindricks G, Jais P, Akoum N, Marchlinski F, Kholmovski E, Burgon N, Hu N, Mont L, Deneke T, Duytschaever M, Neumann T, Mansour M, Mahnkopf C, Herweg B, Daoud E, Wissner E, Bansmann P and Brachmann J. Association of atrial tissue fibrosis identified by delayed enhancement MRI and atrial fibrillation catheter ablation: the DECAAF study. *JAMA*. 2014;311:498-506.
64. Daccarett M, Badger TJ, Akoum N, Burgon NS, Mahnkopf C, Vergara G, Kholmovski E, McGann CJ, Parker D, Brachmann J, Macleod RS and Marrouche NF. Association of left atrial fibrosis detected by delayed-enhancement magnetic resonance imaging and the risk of stroke in patients with atrial fibrillation. *J Am Coll Cardiol*. 2011;57:831-8.
65. Chang CJ, Lin YJ, Higa S, Chang SL, Lo LW, Tuan TC, Hu YF, Udyavar AR, Tang WH, Tsai WC, Huang SY, Tung NH, Suenari K, Tsao HM and Chen SA. The disparities in the electrogram voltage measurement during atrial fibrillation and sinus rhythm. *J Cardiovasc Electrophysiol*. 2010;21:393-8.
66. Teh AW, Kistler PM, Lee G, Medi C, Heck PM, Spence SJ, Sparks PB, Morton JB, Sanders P and Kalman JM. The relationship between complex fractionated electrograms and atrial low-voltage zones during atrial fibrillation and paced rhythm. *Europace*. 2011;13:1709-16.
67. Hansen BJ, Csepe TA, Zhao J, Ignozzi AJ, Hummel JD and Fedorov VV. Maintenance of Atrial Fibrillation: Are Reentrant Drivers With Spatial Stability the Key? *Circulation Arrhythmia and electrophysiology*. 2016;9.
68. Rolf S, Kircher S, Arya A, Eitel C, Sommer P, Richter S, Gaspar T, Bollmann A, Altmann D, Piedra C, Hindricks G and Piorkowski C. Tailored atrial substrate modification based on low-voltage areas in catheter ablation of atrial fibrillation. *Circulation Arrhythmia and electrophysiology*. 2014;7:825-33.
69. Jadidi AS, Cochet H, Shah AJ, Kim SJ, Duncan E, Miyazaki S, Sermesant M, Lehrmann H, Lederlin M, Linton N, Forclaz A, Nault I, Rivard L, Wright M, Liu X, Scherr D, Wilton SB, Roten L, Pascale P, Derval N, Sacher F, Knecht S, Keyl C, Hocini M, Montaudon M, Laurent F, Haissaguerre M and Jais P. Inverse relationship between fractionated electrograms and atrial fibrosis in persistent atrial fibrillation: combined magnetic resonance imaging and high-density mapping. *J Am Coll Cardiol*. 2013;62:802-12.
70. Tanaka K, Zlochiver S, Vikstrom KL, Yamazaki M, Moreno J, Klos M, Zaitsev AV, Vaidyanathan R, Auerbach DS, Landas S, Guiraudon G, Jalife J, Berenfeld O and Kalifa J. Spatial distribution of fibrosis governs fibrillation wave dynamics in the posterior left atrium during heart failure. *Circ Res*. 2007;101:839-47.
71. Corradi D, Callegari S, Benussi S, Maestri R, Pastori P, Nascimbene S, Bosio S, Dorigo E, Grassani C, Rusconi R, Vettori MV, Alinovi R, Astorri E, Pappone C and Alfieri O. Myocyte changes and their left atrial distribution in patients with chronic atrial fibrillation related to mitral valve disease. *Hum Pathol*. 2005;36:1080-9.
72. Verma A, Wazni OM, Marrouche NF, Martin DO, Kilicaslan F, Minor S, Schweikert RA, Saliba W, Cummings J, Burkhardt JD, Bhargava M, Belden WA, Abdul-Karim A and Natale A. Pre-existent left atrial scarring in patients undergoing pulmonary vein antrum isolation: an independent predictor of procedural failure. *J Am Coll Cardiol*. 2005;45:285-92.

73. Qureshi N, Doherty D, Kim S, Bai W, Matthew S-S, Ng FS, Lefroy D, Linton N, Whinnett Z, Davies W, Kanagaratnam P, Peters NS and Lim PB. AF Voltage as a Functional Marker for Atrial Fibrosis: Assessing the spatio-temporal correlation of low voltage regions during AF vs SR with late-gadolinium enhanced CMRI defined fibrosis in patients with persistent AF. *Europace*. 2016;18(9): e003382.
74. Yagishita A, S DEO, Cakulev I, Gimbel JR, Sparano D, Manyam H, Manrique-Garcia A, Arredondo M, Mackall J and Arruda M. Correlation of Left Atrial Voltage Distribution Between Sinus Rhythm and Atrial Fibrillation: Identifying Structural Remodeling by 3-D Electroanatomic Mapping Irrespective of the Rhythm. *J Cardiovasc Electrophysiol*. 2016;27:905-12.
75. Spach MS. Anisotropic structural complexities in the genesis of reentrant arrhythmias. *Circulation*. 1991;84:1447-50.
76. Hocini M, Ho SY, Kawara T, Linnenbank AC, Potse M, Shah D, Jais P, Janse MJ, Haissaguerre M and De Bakker JM. Electrical conduction in canine pulmonary veins: electrophysiological and anatomic correlation. *Circulation*. 2002;105:2442-8.
77. Berenfeld O, Zaitsev AV, Mironov SF, Pertsov AM and Jalife J. Frequency-dependent breakdown of wave propagation into fibrillatory conduction across the pectinate muscle network in the isolated sheep right atrium. *Circ Res*. 2002;90:1173-80.
78. Pashakhanloo F, Herzka DA, Ashikaga H, Mori S, Gai N, Bluemke DA, Trayanova NA and McVeigh ER. Myofiber Architecture of the Human Atria as Revealed by Submillimeter Diffusion Tensor Imaging. *Circulation Arrhythmia and electrophysiology*. 2016;9:e004133.
79. Nathan H and Eliakim M. The junction between the left atrium and the pulmonary veins. An anatomic study of human hearts. *Circulation*. 1966;34:412-22.
80. Everett THT, Li H, Mangrum JM, McRury ID, Mitchell MA, Redick JA and Haines DE. Electrical, morphological, and ultrastructural remodeling and reverse remodeling in a canine model of chronic atrial fibrillation. *Circulation*. 2000;102:1454-60.
81. Hunter; RJ, Diab; I, Tayebjee; M, Richmond; L, Sporton; S, Earley; MJ and Schilling RJ. Characterization of Fractionated Atrial Electrograms Critical for Maintenance of Atrial Fibrillation: A Randomized, Controlled Trial of Ablation Strategies (The CFAE AF Trial). *Circulation Arrhythmia and electrophysiology*. 2011;4:622-629.
82. Jais MH, Matthew W, Méléze H and Pierre. The Substrate Maintaining Persistent Atrial Fibrillation. *Circ Arrhythmia Electrophysiol* 2008;1:2-5.
83. Haissaguerre M SP, Hocini M, Takahashi Y, Rotter M, Sacher F, Rostock T, Hsu LF, Bordachar P, Reuter S, Roudaut R, Clémenty J, Jais P. Catheter ablation of long-lasting persistent atrial fibrillation: critical structures for termination. *J Cardiovasc Electrophysiol*. 2005;16(11):1125-37.
84. Nademanee K, McKenzie J, Kosar E, Schwab M, Sunsaneewitayakul B, Vasavakul T, Khunnawat C and Ngarmukos T. A new approach for catheter ablation of atrial fibrillation: mapping of the electrophysiologic substrate. *J Am Coll Cardiol*. 2004;43:2044-53.

85. Oral H, Chugh A, Good E, Wimmer A, Dey S, Gadeela N, Sankaran S, Crawford T, Sarrazin JF, Kuhne M, Chalfoun N, Wells D, Frederick M, Fortino J, Benloucif-Moore S, Jongnarangsin K, Pelosi F, Jr., Bogun F and Morady F. Radiofrequency catheter ablation of chronic atrial fibrillation guided by complex electrograms. *Circulation*. 2007;115:2606-12.
86. Wong KC, Paisey JR, Sopher M, Balasubramaniam R, Jones M, Qureshi N, Hayes CR, Ginks MR, Rajappan K, Bashir Y and Betts TR. No Benefit of Complex Fractionated Atrial Electrogram Ablation in Addition to Circumferential Pulmonary Vein Ablation and Linear Ablation: Benefit of Complex Ablation Study. *Circulation Arrhythmia and electrophysiology*. 2015;8:1316-24.
87. Hunter RJ, Diab I, Tayebjee M, Richmond L, Sporton S, Earley MJ and Schilling RJ. Characterization of fractionated atrial electrograms critical for maintenance of atrial fibrillation: a randomized, controlled trial of ablation strategies (the CFAE AF trial). *Circulation Arrhythmia and electrophysiology*. 2011;4:622-9.
88. Stiles MK, Brooks AG, John B, Shashidhar, Wilson L, Kuklik P, Dimitri H, Lau DH, Roberts-Thomson RL, Mackenzie L, Willoughby S, Young GD and Sanders P. The effect of electrogram duration on quantification of complex fractionated atrial electrograms and dominant frequency. *J Cardiovasc Electrophysiol*. 2008;19:252-8.
89. Atienza F, Almendral J, Ormaetxe JM, Moya A, Martinez-Alday JD, Hernandez-Madrid A, Castellanos E, Arribas F, Arias MA, Tercedor L, Peinado R, Arcocha MF, Ortiz M, Martinez-Alzamora N, Arenal A, Fernandez-Aviles F, Jalife J and Investigators R-A. Comparison of radiofrequency catheter ablation of drivers and circumferential pulmonary vein isolation in atrial fibrillation: a noninferiority randomized multicenter RADAR-AF trial. *J Am Coll Cardiol*. 2014;64:2455-67.
90. Jadidi AS, Lehrmann H, Keyl C, Sorrel J, Markstein V, Minners J, Park CI, Denis A, Jais P, Hocini M, Potocnik C, Allgeier J, Hochholzer W, Herrera-Sidloky C, Kim S, Omri YE, Neumann FJ, Weber R, Haissaguerre M and Arentz T. Ablation of Persistent Atrial Fibrillation Targeting Low-Voltage Areas With Selective Activation Characteristics. *Circulation Arrhythmia and electrophysiology*. 2016;9 (3)pii: e002962.
91. Seitz J, Bars C, Theodore G, Beurtheret S, Lellouche N, Bremond M, Ferracci A, Faure J, Penaranda G, Yamazaki M, Avula UM, Curel L, Siame S, Berenfeld O, Pisapia A and Kalifa J. AF Ablation Guided by Spatiotemporal Electrogram Dispersion Without Pulmonary Vein Isolation: A Wholly Patient-Tailored Approach. *J Am Coll Cardiol*. 2017;69:303-321.
92. Lin YJ LM, Chang SL, et al. Benefits of atrial substrate modification guided by electrogram similarity and phase mapping techniques to eliminate rotors and focal sources versus conventional defragmentation in persistent atrial fibrillation. *JACC Clin Electrophysiol*. 2016;2:667-678.
93. Ng J and Goldberger JJ. Understanding and interpreting dominant frequency analysis of AF electrograms. *J Cardiovasc Electrophysiol*. 2007;18:680-5.
94. Atienza F, Almendral J, Moreno J, Vaidyanathan R, Talkachou A, Kalifa J, Arenal A, Villacastin JP, Torrecilla EG, Sanchez A, Ploutz-Snyder R, Jalife J and Berenfeld O. Activation of inward rectifier potassium channels accelerates atrial fibrillation in humans: evidence for a reentrant mechanism. *Circulation*. 2006;114:2434-42.

95. Atienza F, Almendral J, Jalife J, Zlochiver S, Ploutz-Snyder R, Torrecilla EG, Arenal A, Kalifa J, Fernandez-Aviles F and Berenfeld O. Real-time dominant frequency mapping and ablation of dominant frequency sites in atrial fibrillation with left-to-right frequency gradients predicts long-term maintenance of sinus rhythm. *Heart rhythm : the official journal of the Heart Rhythm Society*. 2009;6:33-40.
96. Verma A, Lakkireddy D, Wulffhart Z, Pillarisetti J, Farina D, Beardsall M, Whaley B, Giewercer D, Tsang B and Khaykin Y. Relationship between complex fractionated electrograms (CFE) and dominant frequency (DF) sites and prospective assessment of adding DF-guided ablation to pulmonary vein isolation in persistent atrial fibrillation (AF). *J Cardiovasc Electrophysiol*. 2011;22:1309-16.
97. Pantos I, Katritsis G, Zografos T, Camm AJ and Katritsis DG. Temporal stability of atrial electrogram fractionation in patients with paroxysmal atrial fibrillation. *Am J Cardiol*. 2013;111:863-8.
98. Morillo CA, Klein GJ, Jones DL and Guiraudon CM. Chronic rapid atrial pacing. Structural, functional, and electrophysiological characteristics of a new model of sustained atrial fibrillation. *Circulation*. 1995;91:1588-95.
99. Wijffels MC, Kirchhof CJ, Dorland R and Allessie MA. Atrial fibrillation begets atrial fibrillation. A study in awake chronically instrumented goats. *Circulation*. 1995;92:1954-68.
100. Sih HJ, Zipes DP, Berbari EJ, Adams DE and Olgin JE. Differences in organization between acute and chronic atrial fibrillation in dogs. *J Am Coll Cardiol*. 2000;36:924-31.
101. Saksena S, Prakash A, Krol RB and Shankar A. Regional endocardial mapping of spontaneous and induced atrial fibrillation in patients with heart disease and refractory atrial fibrillation. *Am J Cardiol*. 1999;84:880-9.
102. Stevenson WG and Soejima K. Recording techniques for clinical electrophysiology. *J Cardiovasc Electrophysiol*. 2005;16:1017-22.
103. Del Carpio Munoz F, Buescher TL and Asirvatham SJ. Three-dimensional mapping of cardiac arrhythmias: what do the colors really mean? *Circulation Arrhythmia and electrophysiology*. 2010;3:e6-11.
104. Delacretaz E, Soejima K, Gottipaty VK, Brunckhorst CB, Friedman PL and Stevenson WG. Single catheter determination of local electrogram prematurity using simultaneous unipolar and bipolar recordings to replace the surface ECG as a timing reference. *Pacing and clinical electrophysiology : PACE*. 2001;24:441-9.
105. de Bakker JM and Wittkamp FH. The pathophysiologic basis of fractionated and complex electrograms and the impact of recording techniques on their detection and interpretation. *Circulation Arrhythmia and electrophysiology*. 2010;3:204-13.
106. de Bakker JMT HR, Simmers TA. Activation mapping: Unipolar versus bipolar recording. In: Zipes DP, Jalife J, eds: *Cardiac Electrophysiology. From Cell to Bedside*. Second Edition. Philadelphia, PA: W.B. Saunders. 1995:1068.

107. Lorenz E. Deterministic Nonperiodic Flow. *Journal of the Atmospheric Sciences*. 1963;20:130-141.
108. Kaplan DT and Cohen RJ. Is fibrillation chaos? *Circ Res*. 1990;67:886-92.
109. Witkowski FX and Penkoske PA. Activation patterns during ventricular fibrillation. *Ann N Y Acad Sci*. 1990;591:219-31.
110. Garfinkel A, Spano ML, Ditto WL and Weiss JN. Controlling cardiac chaos. *Science*. 1992;257:1230-5.
111. Qureshi N S-SM, Kim S, Cantwell C, Ali R, Roney C, Sau A, Ng FS, Chowdhury R, Koa Wing M, Hayat S, Sohaib A, Lim E, Wright I, Lefroy D, Whinnett Z, Davies DW, Kanagaratnam P, Peters N, Lim PB. Assessment of the Spatio-Temporal Stability of Voltage During Atrial Fibrillation: Quantifying the Time Course of Mean Peak-to-Peak AF Voltage Allows for Meaningful Spatial Differentiation for the Persistent AF Substrate. *Heart rhythm : the official journal of the Heart Rhythm Society*. 2015;12(5):Suppl S275.
112. Mann I, Coyle C, Qureshi N, Nagy SZ, Koa-Wing M, Lim PB, Francis DP, Whinnett Z, Peters NS, Kanagaratnam P and Linton NWF. Evaluation of a new algorithm for tracking activation during atrial fibrillation using multipolar catheters in humans. *J Cardiovasc Electrophysiol*. 2019;30(9):1464-1474.
113. Gerstenfeld EP, Sahakian AV and Swiryn S. Evidence for transient linking of atrial excitation during atrial fibrillation in humans. *Circulation*. 1992;86:375-82.
114. Holm M, Johansson R, Brandt J, Luhrs C and Olsson SB. Epicardial right atrial free wall mapping in chronic atrial fibrillation. Documentation of repetitive activation with a focal spread--a hitherto unrecognised phenomenon in man. *Eur Heart J*. 1997;18:290-310.
115. Lee S, Sahadevan J, Khrestian CM, Cakulev I, Markowitz A and Waldo AL. Simultaneous Batrial High-Density (510-512 Electrodes) Epicardial Mapping of Persistent and Long-Standing Persistent Atrial Fibrillation in Patients: New Insights Into the Mechanism of Its Maintenance. *Circulation*. 2015;132:2108-17.
116. Sanders P, Berenfeld O, Hocini M, Jais P, Vaidyanathan R, Hsu LF, Garrigue S, Takahashi Y, Rotter M, Sacher F, Scavee C, Ploutz-Snyder R, Jalife J and Haissaguerre M. Spectral analysis identifies sites of high-frequency activity maintaining atrial fibrillation in humans. *Circulation*. 2005;112:789-97.
117. Narayan SM, Krummen DE and Rappel WJ. Clinical mapping approach to diagnose electrical rotors and focal impulse sources for human atrial fibrillation. *J Cardiovasc Electrophysiol*. 2012;23:447-54.
118. Linton NW, Koa-Wing M, Francis DP, Kojodjojo P, Lim PB, Salukhe TV, Whinnett Z, Davies DW, Peters NS, O'Neill MD and Kanagaratnam P. Cardiac ripple mapping: a novel three-dimensional visualization method for use with electroanatomic mapping of cardiac arrhythmias. *Heart Rhythm*. 2009;6:1754-62.

119. Takahashi Y, Iwai S, Yamashita S, Masumura M, Suzuki M, Yabe K, Sato Y, Hirao K and Isoabe M. Novel Mapping Technique for Localization of Focal and Reentrant Activation During Atrial Fibrillation. *J Cardiovasc Electrophysiol*. 2017;28:375-382.
120. Takahashi Y, Hocini M, O'Neill MD, Sanders P, Rotter M, Rostock T, Jonsson A, Sacher F, Clementy J, Jais P and Haissaguerre M. Sites of focal atrial activity characterized by endocardial mapping during atrial fibrillation. *J Am Coll Cardiol*. 2006;47:2005-12.
121. Natasja de Groot LvdD, Ameeta Yaksh, Eva Lanter, Christophe Teuwen, Paul Knops, Pieter van de Woestijne, and Jos Bekkers CK, Ad Bogers, Maurits Allessie. Direct Proof of Endo-Epicardial Asynchrony of the Atrial Wall During Atrial Fibrillation in Humans. *Circulation Arrhythmia and electrophysiology*. 2016;9(5). pii: e003648.
122. Narayan SM, Patel J, Mulpuru S and Krummen DE. Focal impulse and rotor modulation ablation of sustaining rotors abruptly terminates persistent atrial fibrillation to sinus rhythm with elimination on follow-up: a video case study. *Heart rhythm : the official journal of the Heart Rhythm Society*. 2012;9:1436-9.
123. Allessie MA, Hoeks AP, Schmitz GM and Reneman RS. On-line mapping system for the visualization of the electrical activation of the heart. *Int J Card Imaging*. 1986;2:59-63.
124. Honarbakhsh S, Hunter RJ, Dhillon G, Ullah W, Keating E, Providencia R, Chow A, Earley MJ and Schilling RJ. Validation of a novel mapping system and utility for mapping complex atrial tachycardias. *J Cardiovasc Electrophysiol*. 2018;29:395-403.
125. Honarbakhsh S, Schilling RJ, Dhillon G, Ullah W, Keating E, Providencia R, Chow A, Earley MJ and Hunter RJ. A Novel Mapping System for Panoramic Mapping of the Left Atrium: Application to Detect and Characterize Localized Sources Maintaining Atrial Fibrillation. *JACC Clin Electrophysiol*. 2018;4:124-134.
126. Willems S, Verma A, Betts TR, Murray S, Neuzil P, Ince H, Steven D, Sultan A, Heck PM, Hall MC, Tondo C, Pison L, Wong T, Boersma LV, Meyer C and Grace A. Targeting Nonpulmonary Vein Sources in Persistent Atrial Fibrillation Identified by Noncontact Charge Density Mapping. *Circulation Arrhythmia and electrophysiology*. 2019;12:e007233.
127. Moe GK and Abildskov JA. Atrial fibrillation as a self-sustaining arrhythmia independent of focal discharge. *American heart journal*. 1959;58:59-70.
128. Dubois R, Shah AJ, Hocini M, Denis A, Derval N, Cochet H, Sacher F, Bear L, Duchateau J, Jais P and Haissaguerre M. Non-invasive cardiac mapping in clinical practice: Application to the ablation of cardiac arrhythmias. *J Electrocardiol*. 2015;48:966-74.
129. Kuklik P, Lau DH, Ganesan AN, Brooks AG and Sanders P. High-density mapping of atrial fibrillation in a chronic substrate: evidence for distinct modes of repetitive wavefront propagation. *Int J Cardiol*. 2015;199:407-14.

130. Schade A, Nentwich K, Costello-Boerrigter LC, Halbfass P, Mueller P, Roos M, Barth S, Krug J, Szoelloesi GA, Lapp H and Deneke T. Spatial Relationship of Focal Impulses, Rotors and Low Voltage Zones in Patients With Persistent Atrial Fibrillation. *J Cardiovasc Electrophysiol*. 2016;27:507-14.
131. Gianni C, Mohanty S, Di Biase L, Metz T, Trivedi C, Gokoglan Y, Gunes MF, Bai R, Al-Ahmad A, Burkhardt JD, Gallingshouse GJ, Horton RP, Hranitzky PM, Sanchez JE, Halbfass P, Muller P, Schade A, Deneke T, Tomassoni GF and Natale A. Acute and early outcomes of focal impulse and rotor modulation (FIRM)-guided rotors-only ablation in patients with nonparoxysmal atrial fibrillation. *Heart rhythm : the official journal of the Heart Rhythm Society*. 2016;13:830-5.
132. Lee G, Kumar S, Teh A, Madry A, Spence S, Larobina M, Goldblatt J, Brown R, Atkinson V, Moten S, Morton JB, Sanders P, Kistler PM and Kalman JM. Epicardial wave mapping in human long-lasting persistent atrial fibrillation: transient rotational circuits, complex wavefronts, and disorganized activity. *Eur Heart J*. 2014;35:86-97.
133. Habel N, Znojkwicz P, Thompson N, Muller JG, Mason B, Calame J, Calame S, Sharma S, Mirchandani G, Janks D, Bates J, Noori A, Karnbach A, Lustgarten DL, Sobel BE and Spector P. The temporal variability of dominant frequency and complex fractionated atrial electrograms constrains the validity of sequential mapping in human atrial fibrillation. *Heart rhythm : the official journal of the Heart Rhythm Society*. 2010;7:586-93.
134. Kogawa R, Okumura Y, Watanabe I, Kofune M, Nagashima K, Mano H, Sonoda K, Sasaki N, Ohkubo K, Nakai T and Hirayama A. Spatial and temporal variability of the complex fractionated atrial electrogram activity and dominant frequency in human atrial fibrillation. *J Arrhythm*. 2015;31:101-7.
135. Qureshi NA, Kim SJ, Cantwell CD, Afonso VX, Bai W, Ali RL, Shun-Shin MJ, Malcolm-Lawes LC, Luther V, Leong KMW, Lim E, Wright I, Nagy S, Hayat S, Ng FS, Wing MK, Linton NWF, Lefroy DC, Whinnett ZI, Davies DW, Kanagaratnam P, Peters NS and Lim PB. Voltage during atrial fibrillation is superior to voltage during sinus rhythm in localizing areas of delayed enhancement on magnetic resonance imaging: An assessment of the posterior left atrium in patients with persistent atrial fibrillation. *Heart rhythm : the official journal of the Heart Rhythm Society*. 2019;16:1357-1367.
136. Jadidi AS, Duncan E, Miyazaki S, Lellouche N, Shah AJ, Forclaz A, Nault I, Wright M, Rivard L, Liu X, Scherr D, Wilton SB, Sacher F, Derval N, Knecht S, Kim SJ, Hocini M, Narayan S, Haissaguerre M and Jais P. Functional nature of electrogram fractionation demonstrated by left atrial high-density mapping. *Circulation Arrhythmia and electrophysiology*. 2012;5:32-42.
137. Kodama I, Kamiya K and Toyama J. Cellular electropharmacology of amiodarone. *Cardiovasc Res*. 1997;35:13-29.
138. Miwa Y, Minamiguchi H, Bhandari AK, Cannom DS and Ho IC. Amiodarone reduces the amount of ablation during catheter ablation for persistent atrial fibrillation. *Europace*. 2014;16:1007-14.
139. Ganesan AN, Kuklik P, Lau DH, Brooks AG, Baumert M, Lim WW, Thanigaimani S, Nayyar S, Mahajan R, Kalman JM, Roberts-Thomson KC and Sanders P. Bipolar electrogram shannon entropy at sites of rotational activation: implications for ablation of atrial fibrillation. *Circulation Arrhythmia and electrophysiology*. 2013;6:48-57.

140. Haïssaguerre M, Jais P, Shah DC, Takahashi A, Hocini M, Quiniou G, Garrigue S, Le Mouroux A, Le Métayer P and Clémenty J. Spontaneous Initiation of Atrial Fibrillation by Ectopic Beats Originating in the Pulmonary Veins. *N Engl J Med*. 1998 Sep 3;339(10):659-66.
141. Haissaguerre M, Hocini M, Shah AJ, Derval N, Sacher F, Jais P and Dubois R. Noninvasive panoramic mapping of human atrial fibrillation mechanisms: a feasibility report. *J Cardiovasc Electrophysiol*. 2013;24:711-7.
142. Hunter; RJ, Diab; I, Tayebjee; M, Richmond; L, Sporton; S, Earley; MJ and Schilling RJ. Characterization of Fractionated Atrial Electrograms Critical for Maintenance of Atrial Fibrillation: A Randomized, Controlled Trial of Ablation Strategies (The CFAE AF Trial). *Circ Arrhythm Electrophysiol*. 2011;4(5):622-9.
143. Haissaguerre M, Wright M, Hocini M, Jais P. The Substrate Maintaining Persistent Atrial Fibrillation. *Circ Arrhythm Electrophysiol*. 2008 Apr;1(1):2-5.
144. Holm; M, Johansson; R, Brandt; J, Luhrs; C and Olsson SB. Epicardial right atrial free wall mapping in chronic atrial fibrillation: Documentation of repetitive activation with a focal spread — a hitherto unrecognised phenomenon in man. *European Heart Journal*. 1997;18:290-310.
145. Kanagaratnam P, Cherian A, Stanbridge RD, Glenville B, Severs NJ and Peters NS. Relationship between connexins and atrial activation during human atrial fibrillation. *J Cardiovasc Electrophysiol*. 2004;15:206-16.
146. de Groot NM, Houben RP, Smeets JL, Boersma E, Schotten U, Schalij MJ, Crijns H, Allessie MA. Electropathological Substrate of Longstanding Persistent Atrial Fibrillation in Patients With Structural Heart Disease: epicardial breakthrough. *Circulation*. 2010 Oct 26;122(17):1674-82.
147. Yamabe H, Kanazawa H, Itoh M, Kaneko S and Ogawa H. Difference in the maintenance mechanism of atrial fibrillation perpetuated after pulmonary vein isolation between paroxysmal and persistent atrial fibrillation: Effects of subsequent stepwise ablation. *Int J Cardiol*. 2016;210:109-18.
148. Ge H, Li X, Zhang Y, Liu H and Jiang H. [Clinical course and treatment of ectopic atrial tachycardia in 144 children]. *Zhonghua Er Ke Za Zhi*. 2015;53:214-9.
149. Lanters EA, Allessie MA and NM DEG. Dynamics of Focal Fibrillation Waves during Persistent Atrial Fibrillation. *Pacing and clinical electrophysiology : PACE*. 2016;39:403-4.
150. Haissaguerre M, Sanders P, Hocini M, Hsu LF, Shah DC, Scavee C, Takahashi Y, Rotter M, Pasquie JL, Garrigue S, Clementy J and Jais P. Changes in atrial fibrillation cycle length and inducibility during catheter ablation and their relation to outcome. *Circulation*. 2004;109:3007-13.
151. O'Neill MD, Jais P, Takahashi Y, Jonsson A, Sacher F, Hocini M, Sanders P, Rostock T, Rotter M, Pernat A, Clementy J and Haissaguerre M. The stepwise ablation approach for chronic atrial fibrillation--evidence for a cumulative effect. *JICE*. 2006;16:153-67.

152. Verma A, Sanders P, Macle L, Deisenhofer I, Morillo CA, Chen J, Jiang CY, Ernst S and Mantovan R. Substrate and Trigger Ablation for Reduction of Atrial Fibrillation Trial-Part II (STAR AF II): design and rationale. *American heart journal*. 2012;164:1-6 e6.